School of Pharmacy

Laboratory of Biophysics and Surface Analysis

Application Of The Quality Control Methodologies To A Novel Solid Dosage Co-crystal Model System

Aalae Alkhalil

BSc, MSc in Pharmacy & Pharmaceutical Sciences

Thesis Submitted To The University Of Nottingham

For The Degree Of Doctor Of Philosophy

July 2013

"All The Praise and Most of The Love Go to The Ever Merciful, To You God (Allah) for All Your Blessings

my thesis is dedicated to my beloved family; my real mother (Mona Aldairi who passed away in 1988 when I was 5 years old), my maternal aunt "the angel" Safaa Aldairi (who became my second mother) for her ultimate caring which without her and my dad (Adel Alkhalil), I was not be able to be in such stage in my life. I am indebted to my beautiful brothers & sister-in-law; Maher, Bashar, Kenan, and Bassel & Rasha (his wife) for their pure love, affection, and encouragement.

Thank God for Being Next to Me Everywhere and All The Time in My Life and Surrounding Me with Such Wonderful Family"

Statement

"And say: My Lord! Increase me in Knowledge"

(Holy Qur'an, Surat Taha, Chapter 20, Verse 114).

There are few good habits which in my opinion can make our life wonderful if adopted;

- the habit of doing good deeds and contributing in charity expenditure to those who are in need,
- the habit of speaking the truth, and the habit of practice Knowledge. Knowledge is the life of the mind which without mind become idle. A person who acquires knowledge has to practice it in action as knowledge without action is futile.

Accordingly, I hereby declare that the information embodied in my thesis which entitled **"Application Of Quality Control Methodologies To A Novel Solid Dosage Co-crystal Model System"** is the result of hardworking and extreme passion to provide correct and true information.

September, 2012 **Aalae Alkhalil**

Acknowledgements

I would like to express my deep gratitude to Dr. Jonathan Burley my main academic supervisor, and other co-supervisors Dr. Jonathan Aylott and Prof. Clive Roberts for their inspiring guidance and constant encouragement throughout the course of my research work.

I thank as well my internal supervisor in Damascus Prof. M. Amer Al-Mardini, Head of Damascus University in Syria for his helpful academic suggestions and co-operation in providing a full support in Damascus University to keep this project fully funded.

I would like to thank Dr. Jagadeesh N. Babu, the research fellow in Burley group for his helpful discussions, moral support and encouragement during his working period in Nottingham.

I have to say that I learnt a great deal in this fascinating field of research through provoking discussions, and I consider my association with all my supervisors and the post-doctorate fellow a rewarding experience.

I thank as well people in School of Chemistry especially Prof. Sandy Blake, and Dr. William Lewis for collecting single crystal data of the flurbiprofen-nicotinamide co-crystal compound studied in this thesis.

I also thank people from Boots Science Building, School of pharmacy especially Mrs. Gail Atkinson and Mrs. Julia Crouch for their help in administrative paper work, everyone in LBSA division, Burley's group, and my colleagues in the office A03 for providing such a nice atmosphere for working.

Special thanks to my close friends and relatives; in the UK: Zahia, Rasha, Abdennour, Valeria, Andy, Adeyinka, Sarah, Klara, Romaissa, Nahed; friends in Syria: Kholoud, Lana, Assel, Baraa, Ghoson, Kinda, Ola, and Batool. In Dubai, my aunt Buthenia and her nice family.

Deep appreciation to my uncle's family in Nottingham for looking after me and considering me a one of their wonderful family; both uncle and his wife, and my three cousins (Khaled, Fadi, and Noor) and their own wonderful families. My prayers go to my paternal grandfather Abdul Hamed Al-khalil until he recovers from his sudden illness and to my maternal grandmother Qutona Aldairi to keep her well.

Lastly, I acknowledge the financial support which I received from Damascus University. Also my appreciation to Laboratory of Biophysics and Surface Analysis (LBSA) in School of Pharmacy, and Nottingham Nanotechnology and Nanoscience Centre (NNNC) in Nottingham University for providing the required facilities for my research work.

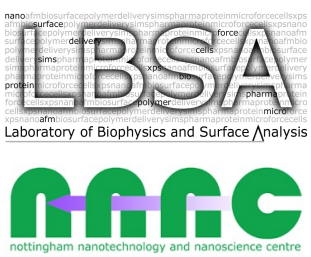

List of Publications

J. C. Burley, **A. Alkhalil**, M. Bloomfield, and P. Matousek. Transmission Raman spectroscopy for quality control in model cocrystal tablets. *Analyst*, 137(13):3052-3057, 2012.

A. Alkhalil, J. B. Nanubolu, and J. C. Burley. Analysis of phase transitions in molecular solids: quantitative assessment of phonon-mode *vs* intramolecular spectral data. *RSC Adv.*,2:209-216, 2012.

A. Alkhalil, J. B. Nanubolu, C. J. Roberts, J. W. Aylott, and J. C. Burley. Confocal Raman microscope mapping of a Kofer melt. *Crystal Growth & Design*, 11(2):422-430, 2011.

A. Alkhalil, J. B. Nanubolu, C. J. Roberts, J. W. Aylott, and J. C. Burley. *In-situ* phase screening of Kofler melt by confocal Raman mapping. Abstracts from the UK-PharmSci Conference, 1-3 September 2010, *Journal of Pharmacy and Pharmacology*, 62(10):1443-1444, 2010.

A. Al-Mardini, S. Al Hakeem, R. Akasha, and **A. Alkhalil**, Measuring transparency to improve good governance in the public pharmaceutical sector in the Syrian Arab Republic, World Health Organization, Regional Office for the Eastern Mediterranean. *WHO Library Cataloguing in Publication Data*, 2009, http://applications.emro.who.int/dsaf/dsa1003.pdf.

List of Abbreviations

Active Pharmaceutical Ingredients	APIs
Quality Control	QC
Flurbiprofen	FBP
Nicotinamide	NCT
Non Steroidal Anti-Inflammatory Drugs	NSAIDs
Biopharmaceutics Classification System	BCS
Generally Recognized As Safe	GRAS
Hot-stage Microscopy	HSM
Room Temperature	RT
Food and Drug Administration	FDA
Process Analytical Tool	PAT
Research and Development	R&D
New Molecular Entities	NMEs
Cambridge Structural Database	CSD
Three Dimension	3D
Relative Humidity	RH
Indomethacin	IND
Saccharine	SAC

Carbamazepine	CBZ
Ultraviolet–visible	UV-Vis
Infra-red	IR
Near Infra-red	NIR
Differential Scanning Calorimetry	DSC
Single Crystal X-Ray Diffraction	SXD
X-Ray Powder Diffraction	XRPD
Good Laboratory Practice	GLP
Modulated Differential Scanning Calorimetry	MDSC
Liquid Assisting Grinding	LAG
Direct Classical Least Square	DCLS
Principal Component Analysis	PCA
Hierarchical Agglomerative Clustering	HAC
Red Green Blue	RGB
Variable Temperature	VT
Transmission Raman Spectroscopy	TRS
Good Manufacturing Practices	GMPs

Abstract

Co-crystals are multi-component, single phase materials in which the co-crystal formers exist in an uncharged state. This interaction between components occurs without affecting the intra-molecular covalent bonding of the involved components or altering their chemical integrity. This class of materials has recently gained the interest in the pharmaceutical industry for modifying the physicochemical properties of some active pharmaceutical ingredients (APIs) such as solubility, hygroscopicity, and mechanical properties.

However like all multi-component systems, there are some analytical challenges associated with using traditional quality control (QC) tools that involve sample preparation steps prior to the analysis. This can sometimes have an impact on the physical state of such systems and therefore affect the outcomes of analysis correlated with the actual materials.

Flurbiprofen (FBP) and nicotinamide (NCT) in this work were selected to form a model co-crystal system. FBP falls in the carboxylated group of non steroidal anti-inflammatory drugs (NSAIDs), used herein as an API. It belongs to class II of the Biopharmaceutics Classification System (BCS), therefore its low aqueous solubility and dissolution rate affect its bioavailability. NCT is a vitamin B3 derivative and generally regarded as safe (GRAS) substance. It is used as co-crystallising agent due to its solubility enhancing property.

FBP-NCT co-crystal system was previously studied by Berry *et al.*, where a FBP-NCT co-crystal was prepared using Kofler method and screened

by means of the hot-stage microscopy (HSM). FBP-NCT co-crystal was recently prepared *via* rapid evaporation from ethanol solution, and screened for its physicochemical and mechanical properties by Shing *et al.* who found an improvement in such properties compared to the pure API (FBP).

There is a wide range of methods for preparing co-crystals, of which methodologies with minimal environment impact were mainly adopted in this work i.e., Kofler fusion and co-grinding methods. Within the Kofler fusion method, it was feasible to identify and screen simultaneously parent components as well as the emerging material at room temperature (RT) by means of confocal Raman microscopy. Detailed information from Raman mapping on the investigated phases were achieved using statistical analysis. The analysis resulted in a refinement regarding the traditional assumption about the binary phase diagram. It also revealed the presence of two forms of FBP-NCT co-crystals which were consequently explored by coupling thermal analysis with Raman spectroscopy and X-ray diffraction.

Using co-grinding preparation, FBP-NCT co-crystals were prepared on a large scale; enough for solid dosage formulation. Subsequent crystallisation of the resulting compound using a solution method generated single crystals suitable for x-ray crystal structure determination.

Moreover in this work, a solid-state dosage form of FBP-NCT co-crystal was prepared for the first time, then investigated using transmission Raman spectroscopy. The investigation included the presence of drug and excipient, and their composition in tablets. This procedure can be considered as a platform for studying the QC of drug preparation, using a reliable, non-destructive, non-invasive, and very rapid analytical tool. Such type of study complied well with the food and drug administrative (FDA) outlines on employing process analytical technology (PAT) protocol for analysing and controlling pharmaceutical manufacturing processes.

Contents

Page

List of Figures

Page

CHAPTER 1

General Introduction

1.1 Pharmaceutical Drug Development

World research and development (R&D) expenditure reached over $120 billion annually in the areas of pharmaceutical and biotechnology, and general industries[1]. Pharmaceutical research-based investment has vastly increased compared to other innovation **(fig 1.1 a)**. It has proved to be the lead advancing sector in global healthcare since 1950[2]. This is in part due to the interest in using the state-of-art technology to understand the mechanism of complex disease and most importantly find the right medication. Developing a new medicine is very challenging involving long and complex procedures. Part of this challenge relates to the regulatory authorities only approving few drugs out of the many candidates entered into clinical trials **(fig 1.1 b)**. Drug development hence takes a very long time (10 to 15 years) and is an expensive process **(fig 1.1 b, c)**. R&D investments increased by $35 billion in 5 year period since 1995 as reported by the Pharmaceutical Research and Manufacturers of America (PhRMA)[3] **(fig 1.1 c)**. According to PharmSource®, the global R&D investment share in the pharmaceutical industry is divided almost equally on preparation methods, characterisation, and drug formulation **(fig 1.1 d)**[4–6]. Despite such huge investment,

the productivity of R&D has fallen in the last 10 years[7,8]. There has been a decrease in the number of new drug approvals of priority or standard need **(fig 1.1 c)**, and this has led to filing more applications to patent new commercial products of comparable characteristics to existing products of expired patents[9–11].

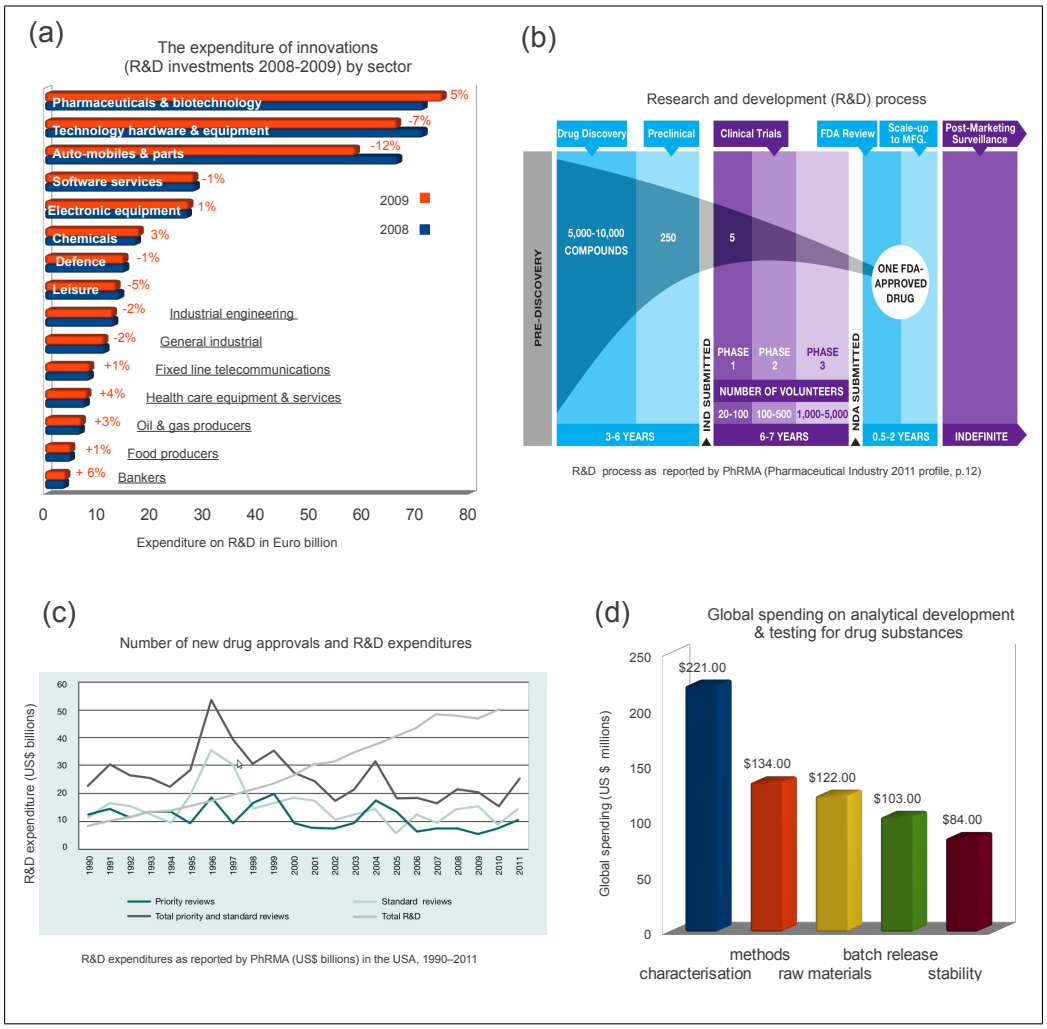

Figure 1.1: R&D expenditures and drug approval process. The industrial world investment on R&D (2008-2009) is shown in (a) the plot was generated after the international federation of pharmaceutical manufacturers & associations (IFPMA)[1]. Being more interested in the R&D process within the pharmaceutical field, the process drug development is shown in (b) "as reported by PhRMA (Pharmaceutical Industry 2011 profile, p.12)"[1]. The number of new drug approvals and R&D expenditures in US$ billions over the last 11 years are shown in (c) "as reported by FDA and PhRMA (1990 - 2011)[11]". The global spending (US $ millions) on analytical development & testing processes of drug substance is in (d), the plot was generated after PharmSource® report[4].

1.2 Molecular Properties of Drug Substances

While the focus in research units and organisations or even the pharmaceutical companies is to introduce new molecular entities (NMEs) with improved properties, other options can be taken based on the existing products such as using alternative solid-state forms. Pharmaceutical substances range from a single component (crystalline or amorphous) to multi-component systems such as hydrates/solvates, clathrates, salts, and co-crystals.

The reason for having such variation in pharmaceutical solid-state materials is due to drug chemistry and the need to introduce medications with desired physicochemical properties. Drug molecules may contain different functionalities which with the surrounding environment contribute to the ionization degree of molecule. The ion class state of the APIs varies from a non-ionisable (neutral) to an ionisable (acidic or basic) state. This compound status plays a key role in the ADME biopharmaceutical properties (absorption, distribution, metabolism, and excretion) of the drug. This is because the degree of ionisation (acidity/basicity, $pK_{a/b}$) can affect the solubility (LogS), drug distribution (LogD), and lipophilicity (LogP) profile of the compound[12–14].

The effect of ion class compounds on the molecular properties of 10,270 drugs, which belong to 12 large pharmaceutical companies* **(fig 1.2 a)**, was studied by Lesson *et al.*[14]. The study showed that the majority of substances belong to basic and neutral classes **(fig 1.2 b)** and that bases have a higher lipophilicity profile compared to acids and neutrals[14]. However, the increase level of lipophilicity in ion class compounds (LogP $>$ 3) holds a risk of producing drugs of a high toxicity[15–17]. Regarding drug

*AstraZeneca (1337 compounds), GlaxoSmithKline (1402 compounds), Merck (1519 compounds), Pfizer (1222 compounds), Abbott (392 compounds), Bristol-Myers Squibb (689 compounds), Janssen (581 compounds), Lilly (406 compounds), Novartis (615 compounds), Roche (784 compounds), Sanofi-Aventis (856 compounds), and Wyeth (467 compounds).

distribution, the cLogD value decreases among ion class compounds in the following order neutrals > bases > acids, due to their increased plasma protein binding[18–21]. Hence, neutral pharmaceuticals can be advantageous over ionic substances in terms of toxicity and efficacy. However, ionised compounds (acids or bases) are generally more soluble than neutrals (non-ionised). The poor solubility of neutral molecules can be improved when molecules are complexed with other solubility enhancing agents under a condition of choosing the right complementary agents, which is the case of designing multi-component systems. Multi-component systems not only offer the chance of improving the solubility but they can also modify the mechanochemical and physicochemical properties of substances such as the compressibility, hygroscopicity, and stability[22–32].

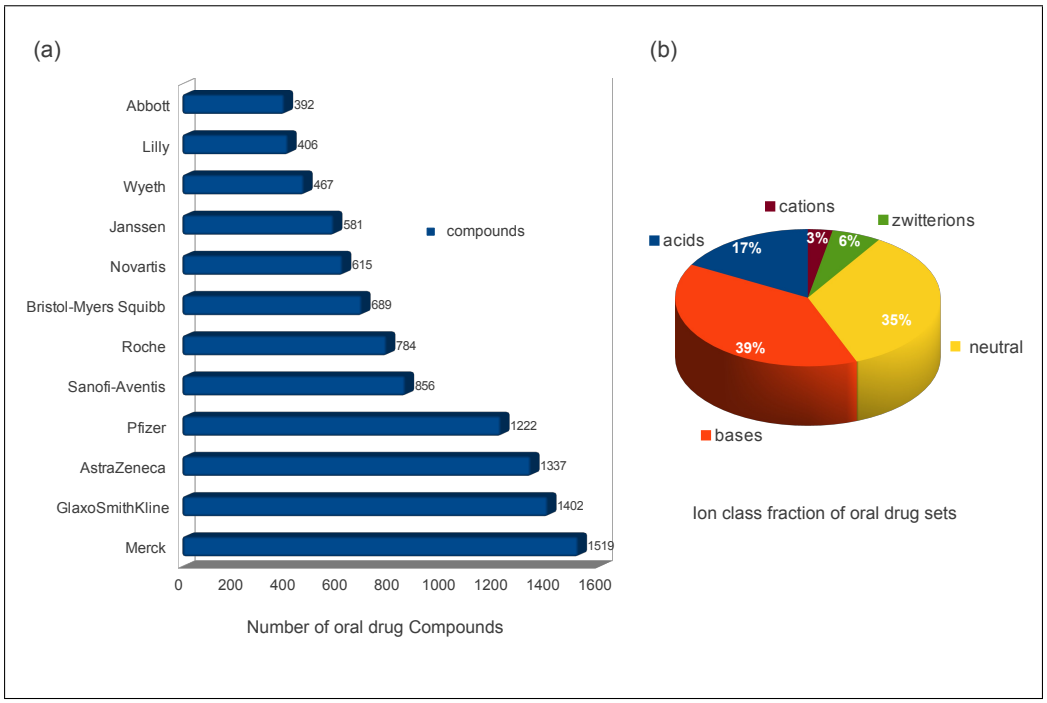

Figure 1.2: Ion class fraction of 10,270 oral drug compounds from of 12 pharmaceutical companies (a). The ionic composition of such compounds is shown in (b). The plot was generated after Lesson *et al.*[14].

1.3 Solid-State Materials

The physicochemical properties of substances is affected by the crystalline diversity of materials. Richard P. Feynman (a theoretical physicist) did once anticipate a change in the properties of substances if their structures have been rearranged*, *"What could we do with layered structures with just the right layers? What would the properties of materials be if we could really arrange the atoms the way we want them? ..... we will get an enormously greater range of possible properties that substances can have, and of different things that we can do."*[33].

The design of solid-state forms varies according to the requirement of usages such as in the agriculture, nutrition, pharmaceutical, chemical, or material science (applies physics, and forensic engineering) field[34,35]. Solid-state materials range from a single component with different polymorphic forms **(fig 1.3)** to molecular complexes **(fig 1.4, 1.5)**, depending on the number of components in the crystal lattice. In multi-component systems, the second component can be water, solvent, ion, or a co-crystal former. If there is a proper periodic arrangement between molecules (crystalline), then the resulting compounds are hydrates, solvates, clathrates, salts, or co-crystals **(fig 1.4, 1.5)**. However, if there is a randomness in the molecular arrangements then amorphous forms (non-crystalline) result, a phenomenon not only observed in single components but also in molecular complexes.

Molecules which adopt crystalline structure, whether single or multi-component systems, can sometimes adopt different conformation and packing forms, and this leads to so called polymorphism. Polymorphism and allotropism are related, the first term is used to describe the diversity in the structure of molecular compounds while the second one is related to the

*Feynman's talk was given on the 29th December 1959 at the California Institute of Technology (Caltech) in the annual meeting of the American Physical Society[33].

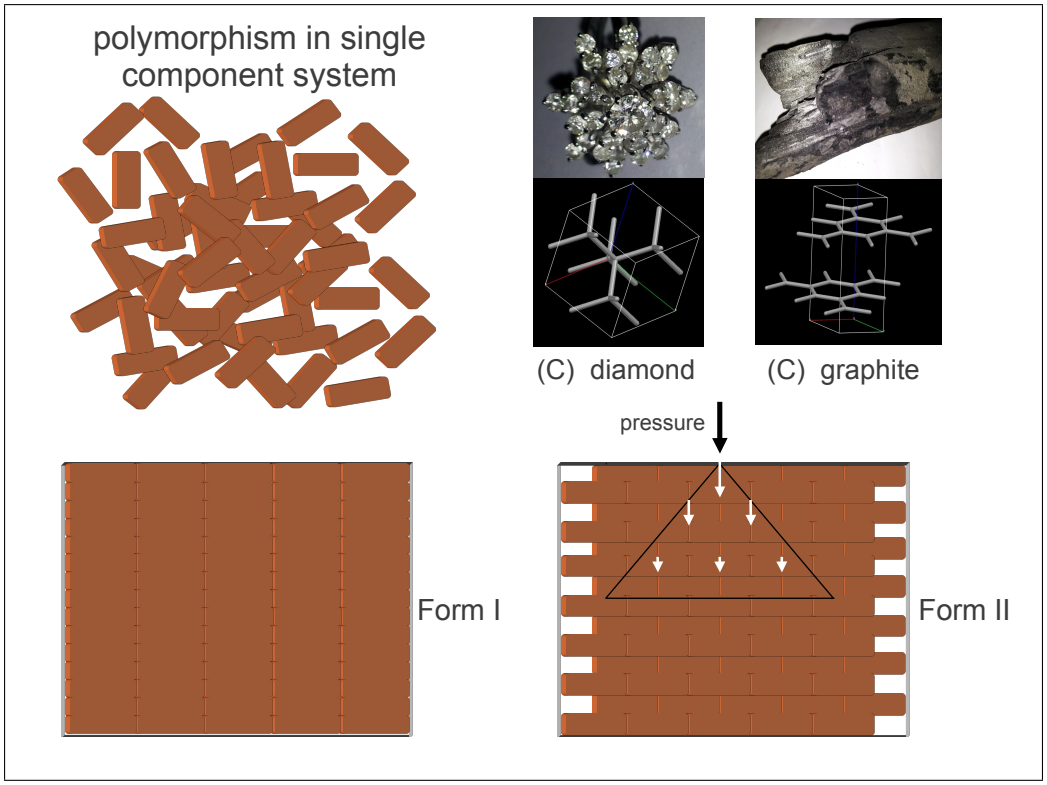

Figure 1.3: Schematic of single component polymorph. The figure is very comparable to wall brick whereas the brick units can be arranged in different forms. The more the block units are interlinked, the stronger the building becomes. The polymorphism phenomena resulted to materials with different physicochemical properties such as the differences between carbon allotropes diamond and graphite.

diversity in the structure of elements. An example for allotropism is carbon (C). Carbon has few allotropes such as diamond and graphite whereas the arrangement of the atoms is different between different structures, and this accordingly leads to differences in the properties. Equally is the case of organic molecules which can exhibit differences in the packing or the conformational arrangements within polymorphic molecules and a change in properties can result.[36].

Polymorphism was reported for the first time by F. Wöhler and J. Liebig in 1832, who discovered polymorphism in benzamide[37]. Later on, F. Wöhler reported the first molecular complex quinhydrone (quinone-hydroquinone co-crystal) in 1844[38]. In 1931, J.S. Buck and W. Ide reported the formation of additional compounds during bezoin reaction. These compounds contained equimolar amounts of two different benzoin derivatives[39].

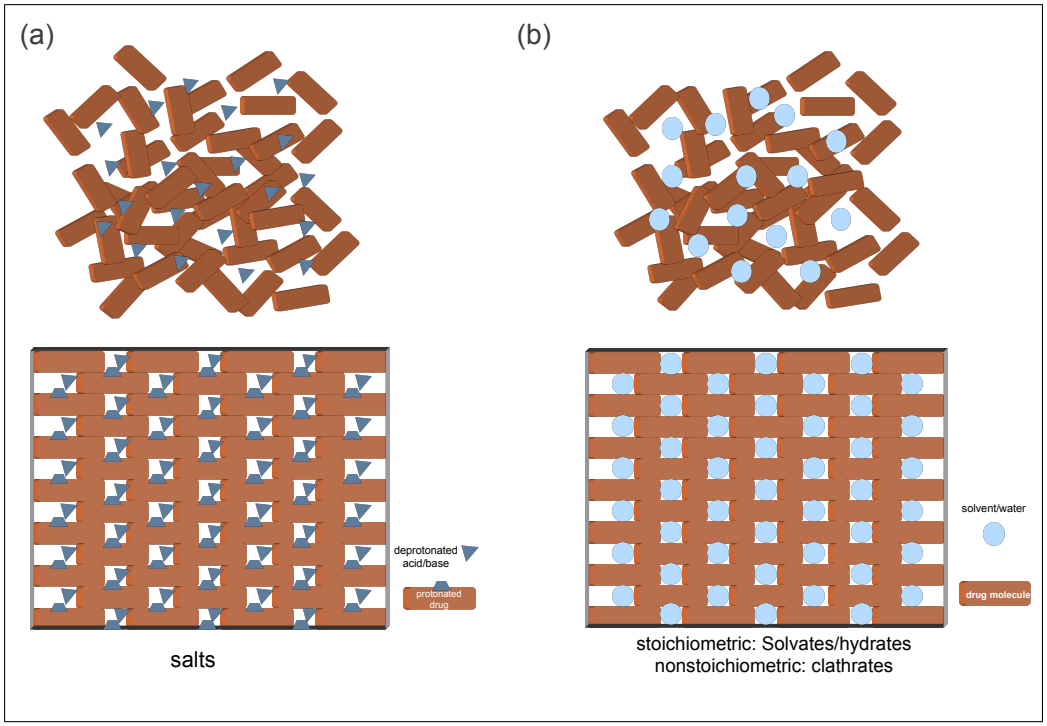

Figure 1.4: Schematic of molecular complexes. It shows in (a) the formation of salts in the presence of ions, while in (b) it resulted in solvates/hydrates in the presence of solvents/water.

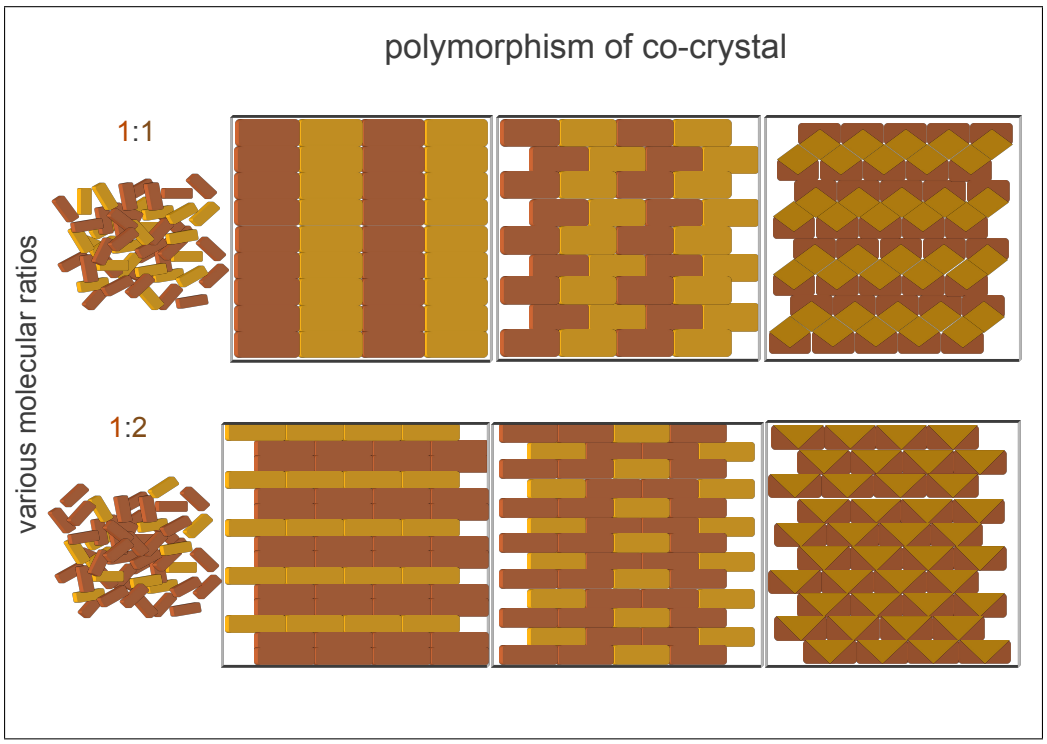

Figure 1.5: Schematic of co-crystal polymorphism. It shows the formation of co-crystal between one substance and a co-former in various packing and configuration manner between two ratios of linkage.

The formation of mixed crystals was found to occur by accident until the structures of organic molecules were rationally studied by S. J. Anderson in 1937[40] and then by Etter *et al.* in 1983[41] and A. I. Kitaigorodsky in 1984[42]. The latter published a book entitled "Mixed Crystals in Solid-State Sciences" describing the principle of close packing and the structure of solid-state materials[42]. Researchers have found that the formation process of molecular complexes does not occur randomly, but it rather requires studying the property of the crystal structural relationships and the possible packaging arrangement[43].

1.3.1 Crystal and Supramolecular Engineering

The concept of crystal engineering was introduced first by R. Pepinsky in 1955[44,45]. It has matured into preparing new compounds (molecular complexes) with enhanced physicochemical properties[46]. The main strategies in molecular complexes design focus on the structural compatibility and the energetic interactions between components[47].

The design of multi-component complexes follows the same protocols as crystal engineering, in terms of studying the crystal structural property relationships (the intermolecular interaction) and the possible packaging arrangements (the spatial arrangements), obtained through the Cambridge Structural Database (CSD)*[48].

According to Corey†, supramolecules are assembled from synthons which are basically formed *via* the intermolecular interaction between complementary functional groups of molecules[43]. This description is simplified

* CSD is a database repository of small molecules (organic and meta-organic compounds). It enables to visualise the chemical and crystallographic analysis of materials, and the determination of the three dimension (3D) structure calculated based on the diffraction of neutrons or x-rays.

† *"Supramolecular synthons are structural units within supermolecules which can be formed and/or assembled by known or conceivable synthetic operations involving intermolecular interactions"*[43].

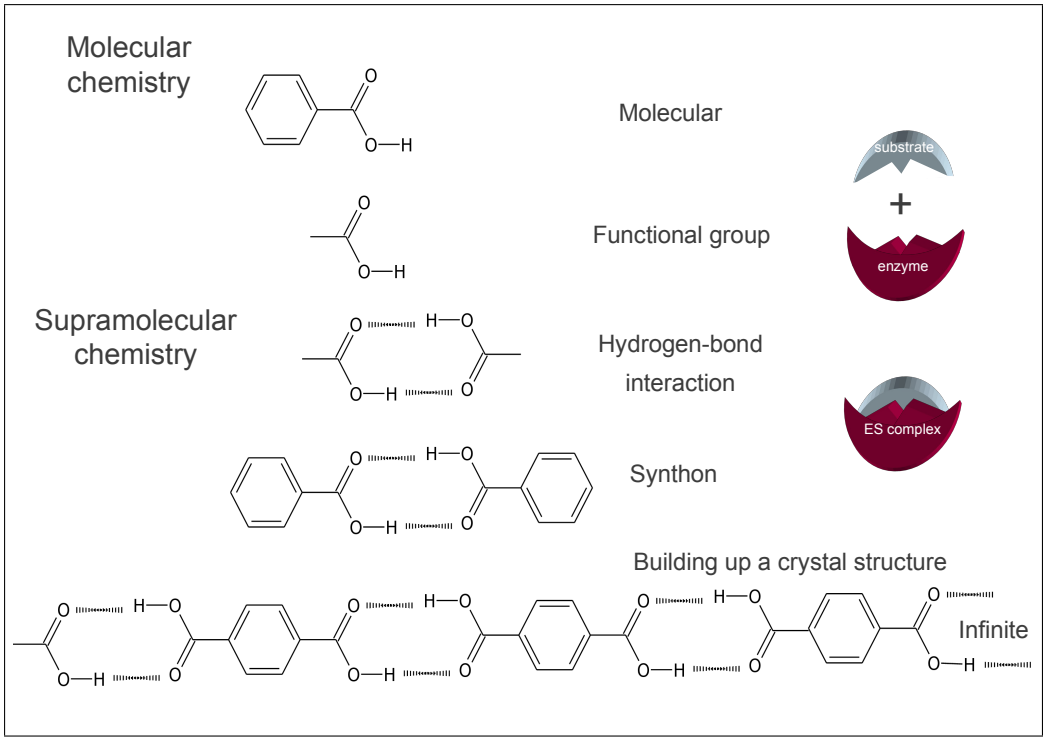

Figure 1.6: From molecular to supramolecular chemistry. It represents the self assembly of molecules into crystals, then supramolecular synthons.

in **fig 1.6** which displays the relationship between molecular and supramolecular chemistry. It shows that the crystalline structure is built up from molecules of complementary functional groups which intermolecularly interact to form a supramolecular synthon. The latter stands as the building blocks of supermolecules.

As mentioned previously, supramolecular synthons are constructed as a result of intermolecular interactions. Such interactions play an important role in supramolecular synthesis since they contribute in shaping molecules, defining their size and close packing. There are a number of such interactions, the most important type in the synthesis of molecular complexes is hydrogen bonds[43,48,49].

Bridging hydrogen bonds occurs between two moieties, usually complementary functional groups such as (H) connected to a donor and (O) as an acceptor **(fig 1.7)**. The most important aspects in hydrogen bonds are the length between acceptor...donor (i.e., O...H—donor) and acceptor...H (i.e., O...H), and the hydrogen bond angles φ (atom—acceptor...H) and θ

(acceptor...H—donor). It also requires a coordination between the angle θ (acceptor...H—donor) and the length of (acceptor...donor) bond[48]. The ideal distance between acceptor and donor falls within a range of 1.60 to 2.00 Å for bonds such as O...HN and O...HO. In addition, the preferable values for θ are around 150-160° and around 120-130° for φ[43].

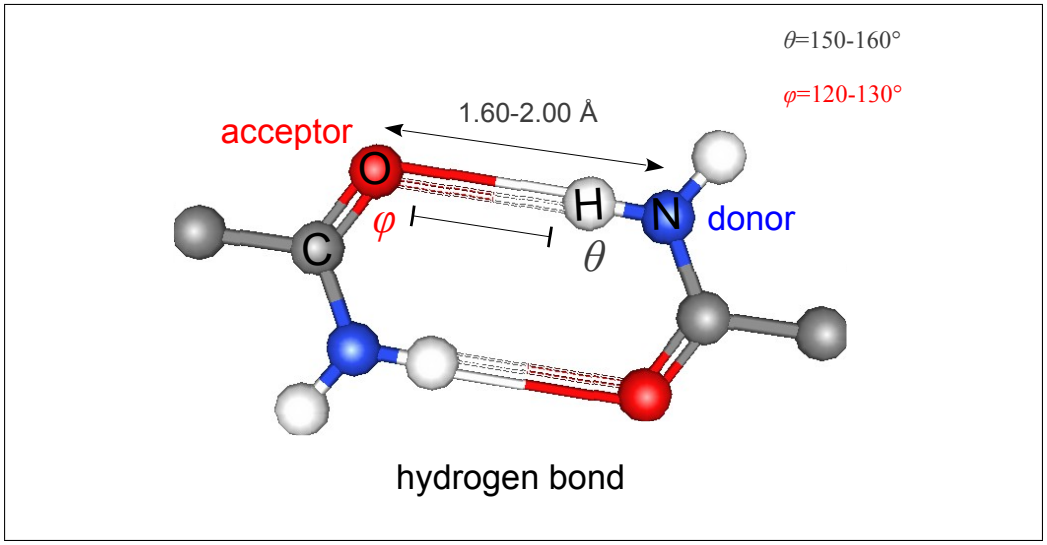

Figure 1.7: Hydrogen bond interaction between two complementary moieties. It shows the donor and the acceptor moieties, the complementary atoms (O, H), angle (θ, φ) and the (arrows) to indicate to the distance between (O, N) and (O, H).

Since the intermolecular interactions (hydrogen bonds type) are considered weak individually, the robustness of synthon, and spatial arrangement and conformation packaging become essential in the supermolecular design area. For instance, a carboxylic functionality is a common group that has been widely studied in crystal engineering. This group can form either supramolecular homosynthon or supramolecular heterosynthon, depending on the other complementary moiety. Interaction between similar functional groups yields homosynthon supramolecular structure but this is not energetically favourable. Alternatively, the interaction between different groups is more preferable. It produces supramolecular heterosynthon such as between carboxylic acid and amide, or carboxylic acid and pyridine*[34].

*"*In fact, carboxylic acid-pyridine interaction is more preferable than carboxylic acid-amide one"*[34].

Hence, it is not preferable from the crystal design point of view to have interactions between similar groups i.e., amide-amide or carboxylic-carboxylic, when compared to supramolecular heterosynthon such as carboxylic acid-pyridine, carboxylic acid-amide, alcohol-amine and alcohol-pyridine **(fig 1.8)**. Briefly, molecular complexes are likely to be thermodynamically favoured when two different components with complementary functional groups are capable of producing hydrogen bonds energetically stronger than those between molecules of each component.

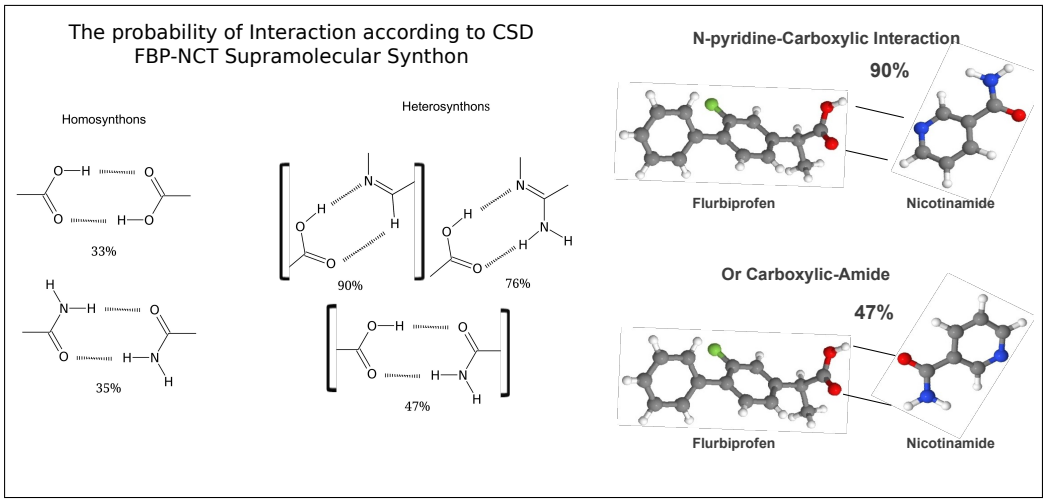

Figure 1.8: Probability of interactions between complexes according to CSD.

Molecular complex formation is governed by chemical and geometrical factors. Such phenomena can be illustrated through intermolecular interactions including, the non-covalent bonds hydrogen pattern and the recognition of crystal packing, an observation very comparable to enzyme-substrate interactions or the lock and key principle **fig 1.6**. However, for attenuating other influencing factors such as competition, cooperation and balance between intermolecular forces design, it is advisable to adopt strategies set by M. Etter and co-workers for co-crystal design. *"These rules reflect kinds of intermolecular association that are energetically favorable"*[49]:

- Good proton donors and acceptors are utilised in hydrogen bonds and only the best proton donors and acceptors remain.

- In the presence of the other functional groups and under the impact of various packing patterns, each functional group should retain its preferred interaction pattern.

Such rules are useful in avoiding many obstacles in co-crystal synthesis. For instance, the interference of competitive intra-molecular hydrogen bonds could be overcome by selecting other component "as a guest" that has the ability to conduct stronger hydrogen bond with the hosted molecule.

1.3.2 Pharmaceutical Co-crystals Background

Crystal engineering has addressed approaches to developing a new class of compounds (co-crystal) under a broad group of multi-component crystal structures (solvates, hydrates, clathrates, inclusion crystals)[50]. There is still a debate over finding a comprehensive definition for co-crystals[32,34,45,51–54]. One widely used definition is that co-crystals are multi-component crystals or molecular complexes, in which all molecules are solid at ambient conditions[48]. The molecules of co-crystal exist in different stoichiometric amounts through non-covalent bonds and are packed in a well defined order. The interaction in co-crystal compounds (hydrogen bonds) occur between complementary supramolecular synthons without breaking covalent bonds, or altering the chemical integrity of each molecule[48,55]. Hydrogen bonds are generally formed between active pharmaceutical ingredients and co-crystal agents. The latter should be non-toxic and pharmaceutically acceptable. There is a library for co-crystal agents[56] and it includes pharmaceutical excipients and compounds which are generally recognized as safe (GRAS) such as benzoic, succinic, fumaric acids, and nicotinamide[34].

The main difference between solvates and co-crystals is the physical state of parent pure components at room temperature. If one component is a liquid (water or solvent), then crystals are assigned as hydrate or solvates; but if they are solids then the resulting crystals are co-crystals. Alterna-

tively, the distinction between co-crystal and salts is based on the difference in the pK_a between base and acid ($\triangle pK_a$). If it is greater than 3.75 then a complete proton transfer is expected ending with the formation of salts likely. However, if the proton transfer is absent then a neutral compound (co-crystal) will be formed. There are some cases where the pK_a of both components is very similar, in this case the environment determines the extent of proton transfer[54,57,58].

Like other crystalline forms of the APIs, co-crystals can be designed by synthon strategies but that does not mean they are always formed as predicted. Therefore, pharmaceutical co-crystals can be considered as patentable inventions. For instance, S. Fox invented nicotinamide–ascorbic acid co-crystal system in 1947, vitamin C (ascorbic acid) in this compound will retain its stability and hence its potency will not be affected by surrounding environment[59]. H. Zellner invented a new co-crystal of α-naphthyl acetic acid with purine (caffeine or theophylline). The whole compound was found to be more soluble than individual purine substances, plus it has an antiphlogistic effect. This invention was accordingly disclosed in a US patent as an anti-Inflammatory compound in 1961[60]. S. Childs as well in 2008 disclosed a US patent to novel co-crystals and a protocol for co-crystallisation methodology[61]. He prepared three co-crystals of fluoxetine HCl with three different acids; succinic acid, fumaric acid, and benzioc acid. Based upon this he expanded the protocol to be applicable on the free base of the APIs, whereas the API should be prepared in salt form, such as NaCl, then co-crystallised with carboxylic acid for instance[61]. Therefore, co-crystals have an important place for further development in the pharmaceutical industry if a found compound exhibits improved physicochemical properties and clinical advantages over individual API.

1.3.3 Co-crystal Role in Drug Development

All solid-state state materials are important to the pharmaceutical industry, both single-component crystals and multi-component crystals (hydrates, solvates, salts and co-crystals) are used to modify the physicochemical properties of the drugs. There are however, some advantages of specific solid-state forms over others. Hydrates/solvates, for instance, are less likely to be useful when compared to salts and co-crystal. This is because the number of acceptable solvents are small compared to counter ions and co-crystal agents. The stability of hydrates/solvates is also an issue, as such compounds undergo dehydration/desolvation in the solid dosage forms under uncontrolled storage conditions. The loss of water or solvent might lead to unfavoured solid-state forms[62]. In contrast, salts and co-crystal are more stable as complexes with counter ions and co-crystal formers.*

The formation of salts is more rational compared to the formation of other molecular complexes (Hydrates/solvates), however it is mainly targeted to ionised molecules (basic or acidic). As a result, unionised APIs components which comprised nearly 40% of formulated drugs lack the ability of salts formation. Thus, the class of co-crystal compounds might offer the opportunity to modify the physical properties of APIs without altering their chemical identities *via* complexes formation with co-crystallising agents of complementary functional groups[32,65].

Pharmaceutical co-crystal synthesis has been implemented to improve the physiochemical properties (solubility, stability, and bioavailability) of some of APIs[47,66–70]. For instance, the stability of caffeine-dicarboxylic acid co-crystal in different relative humidity (RH) conditions was investigated and it has been found that this co-crystal exhibits better stability in various percentages of RH when compared to anhydrous caffeine[24]. The

* However, this does not exclude the chance of forming hydrates of salts or co-crystal under changed RH[63,64].

humidity contributes in the transformation of one specific crystal form to another[24]. Equally are polymorphs which may undergo a conversion to more stable crystalline form during storage and manufacturing process. For example, a change in carbamazepine (CBZ) form III has been noticed between batches[71]; form III was used to enhance the oral bioavailability of CBZ[71].

Hence, co-crystal engineering is driven by the need to improve the physiochemical properties of pharmaceutical active ingredient. For instance, Indomethacin (IND) was co-crystallised with saccharine (SAC) in order to improve drug solubility[26]. It was found that the IND—SAC co-crystal displayed faster dissolution rate than IND (γ-form). Caffeine—dicarboxylic acid co-crystal is another example[24]. The stability of this co-crystal was investigated at various RHs[24]. It has been found that this preparation exhibited better stability compared to anhydrous caffeine. Moreover, the pharmacokinetics of CBZ were screened when co-crystallised with SAC in dog models[71]. CBZ—SAC co-crystal exhibited a higher C_{max} (Maximum Plasma Concentrations) and T_{max} (Time to Maximum Plasma Concentration) compared to marketed CBZ (Tegretol®). In addition, it displayed an increase in the dissolution properties in regard to amorphous CBZ.

1.4 PAT & QC Analytical Drug Tools

As mentioned at the beginning of this chapter a lot of effort, time, and investment are devoted to develop NMEs or novel crystal forms which can be readily released into the market. Accordingly and because most of drugs are in a high demand, medicines becomes very expensive. As a result, an increasing number of counterfeit medicines have been reported[72]. Therefore, the regulatory authorities such as the FDA has strengthened the rules on drugs in development processes and product characterisation to minimise as much as possible the phenomenon of counterfeiting medicines.

There is a wide range of tools used for drug analysis. Traditional methods employ mostly chromatographies technique (i.e., high-performance liquid, gas, or thin-layer chromatography), and spectroscopies (i.e., Ultraviolet–visible (UV-Vis) and fluorescence spectroscopies). Employing such techniques requires sample preparation, including for instance dissolution, and calibration for each individual component within every sample. However, there are some challenging systems for which the traditional QC methods of screening and characterisation is not ideal such as some solid-state forms (polymorphs, salts, co-crystals and amorphous materials), and fake dosage forms (counterfeiting medicines).

Such systems are not amenable to be analysed using techniques which involve some sample preparation steps that affect the physical status of the drug. Most of the time the information needed in screening medications is not only about the chemistry but also about the physicochemical status of formulated APIs. For example, does the formulation contain pure APIs or it is accompanied by different state form i.e., different polymorphs or even a co-crystal accidently formed between the API and one of the excipients. In another word, the intermolecular or intra-molecular information has to be confirmed during the development and the formulation processes.

Finding robust techniques for drug analysis during drug development and manufacturing process has become an essential requirement within the pharmaceutical industry[73]. The emphasis is to find a reliable, non-destructive, non-invasive, and rapid analytical tool. All of which underlay within the protocols of employing a real-time QC tools to design and analyse manufacturing and production processes or so called PAT the process analytical technology[74,75].

Most of the vibrational spectroscopic techniques such as infra-red (IR)[76–79], terahertz and Raman spectroscopy can meet such criteria. They are considered as non-destructive tools of analysis mostly utilised with-

out major sample preparations. Within the pharmaceutical area, vibrational spectroscopic techniques are used for screening the physical and physicochemical-chemical properties of components. Some of these analytical tools are more advantageous over others and this is dependant on the type of information required to be achieved.

For instance, near infra-red (NIR) spectroscopic analysis is widely used for quality control purposes in the pharmaceutical field as it provides a specific fingerprint identification for each molecule[80]. Mid-IR is used to probe the structural information so it is well suited to probe the intramolecular interactions. Finally, terahertz spectroscopy is used to probe the intermolecular interactions and thus it is good for characterising solid-state forms of molecules such as polymorphs and multi-component systems. Terahertz spectroscopy can be used along with IR to provide a complete chemical information encompassing both intermolcular (phonon) and intramolecular regions[81]. Alternatively, such rich information is obtainable using different data acquisition instruments.

For instance using Raman spectroscopy such details can be simultaneously achieved from a full spectral range covering both phonon and molecular regions (30-2000 cm^{-1}). Raman spectroscopy is relatively easy to handle [82] and can be used in reflective and transmission modes. Raman is mainly used in a backscattering mode and in this way provides real chemical information about drug identification, distribution, and stability from the surface and near surface regions of a sample. In transmission mode, data can be gathered from the bulk of a sample[83–85].

1.5 Flurbiprofen:Nicotinamide Case Study

Flurbiprofen is a member of the carboxylated group non steroidal anti-inflammatory drugs. It belongs to class II of the Biopharmaceutics Classification System, therefore has a limited bioavailability due to its low aqueous

solubility and dissolution rate[86]. It is also known for its polymorphic behaviour[87]. It has been studied with nicotinamide in solid dispersion form in 2005 by Varma *et al.*, who showed that the dissolution and the solubility of Flurbiprofen-Nicotinamide solid dispersions were improved compared to those of Flurbiprofen[88]. Nicotinamide is listed as a generally regarded as safe substance and suitable for human use[56]. It serves as an enhancing solubility agent, for instance it was also found to hydrotropically increase the solubility of ibuprofen[89] and riboflavin[90].

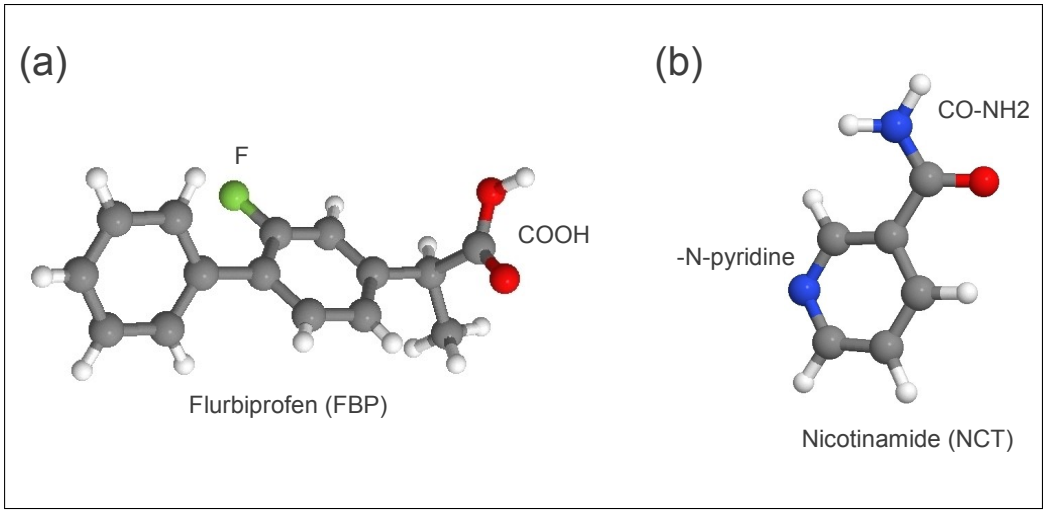

Figure 1.9: The chemical structure of the API (flurbiprofen) in (a), and the co-crystallising agent (nicotinamide) in (b). It shows the complementary functional groups (COOH) in (a) and (CONH2, N-pyridine) in (b).

In 2008, both FBP and NCT have been explored in a different solid-state system, they were studied in a Kofler melt* by Berry *et al.*[91] and Blagden *et al.*[92]. Kofler melt preparation has been adopted to overcome the effect on steric hindrance of FBP structure when co-crystallised with small molecules such as nicotinamide[91]. Flurbiprofen contains a carboxylic acid in its structure **(fig 1.9 a)**, which serves as a complementary functional group to nicotinamide amide group **(fig 1.9 b)**, and so can aid in the hydrogen bond interactions between FBP and NCT. Following such studies, in 2012,

*Kofler melt is a thermal technique based on a fusion between two components. Components are sandwiched between a side and coverslip which allows to form by melting a composition gradient and subsequently potential molecular complexes at the zone of melting.

the dissolution rate, moisture sorption, and the mechanical properties of FBP-NCT co-crystal, prepared from a rapid evaporation of ethanol solution of 1:1, FBP:NCT mixture, have been found to be improved over the pure FBP[86]. Hence, FBP-NCT co-crystal can be considered as a model co-crystal system to be explored starting from preparation to solid formulation using different methodologies.

1.6 Aims and Objectives

In this work, co-crystal was chosen as a solid-state system to be explored motivated by the recent interest of the pharmaceutical industry in multi-component systems. Co-crystals have became an increasingly attractive option for tailoring the physiochemical properties of drug substances. The study employed FBP-NCT co-crystal as a model system based on previous work done by Berry *et al.*[91] and Blagden *et al.*[92] using Kofler melt, and recently supported by Shing *et al.*[86].

During presented work, FBP-NCT co-crystal were prepared using environmentally friendly methodologies. The resulting compounds screened by means of a rapid and reliable analytical tool. The methods of co-crystallisation compromised not only the Kofler fusion method but also mechanochemical technique (liquid assisting grinding). The resulting compound was subsequently formulated in tablets as a solid dosage formulation. Such preparation methodologies and the resulting materials were evaluated for their effectiveness using various tools.

Traditional Screening Tools

- Differential Scanning Calorimetry (DSC) to identify the thermal behaviour of starting materials and resulting compound,
- HSM to optically clarify the thermal behaviour of studies materials,

- Single X-ray Diffraction (SXD) to identify the crystallographic chemical structure FBP-NCT co-crystal,
- X-Ray Powder Diffraction (XRPD) to investigate the structural behaviour of formed compounds. It was also used coupled with environment heating system.

Raman As A State-of-art Screening Tool

- Raman microscopy which was coupled with variable heating control system, to identify the chemical characteristics, and map the distribution of drug ingredients (both the chemistry and the composition) within sample preparations.

Therefore, the aim of this research project was to assemble a model co-crystal system using various methodologies and investigate the use of state of the art Raman and X-ray powder diffraction as the main analytical tools to study co-crystal preparations and co-crystal dosage formulation (tablets).

CHAPTER 2

Preparation Methods and Screening Techniques

2.1 Pharmaceutical Co-crystal Preparations

There is a range of methodologies for preparing pharmaceutical co-crystals. They fall under three main mechanisms; the dissolution, mechano-chemical grinding, and Kofler fusion contact method.

2.1.1 Growth from Solution

Co-crystals can potentially be achieved by slow evaporation of a solution containing stoichiometric amounts of components[93]. Solution evaporation leads to supersaturation phase which resulted in the precipitation of either new compounds or a mixture of components. Crystallisation from solution is traditionally used in the pharmaceutical industry for isolating single component crystals. This technique is exploited to generate pharmaceutical co-crystals from supersaturated solutions. This process is triggered by dissolving stoichiometric amounts from the API and the co-crystallising agent in a suitable solvent **(fig 2.1)**.

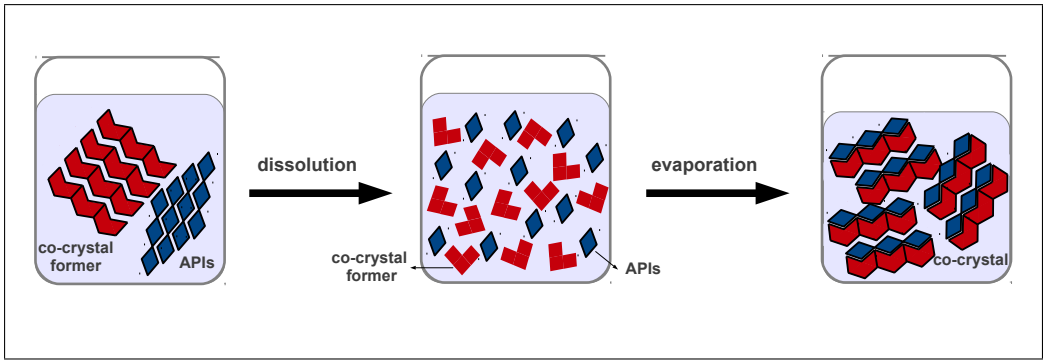

Figure 2.1: Co-crystal preparation from a solution.

However there are some considerations about this method: The first one is regarding the solubility of components in the chosen solvent. Both components have to exhibit similar solubility in the selected solvent **(fig 2.2 a)**, otherwise the least soluble material would precipitate before the completion of interaction. The mismatching in component solubility leads to a mixture of co-crystals and single component phases **(fig 2.2 b)**[92]. The other foible about this methodology is the existence of further layering of solvent as a ternary phase with the resulting compound[92,94]. Such impact can be leveled up by choosing components with similar solubilities in the selected solution, or dissolving components in a mixture of solvents[94].

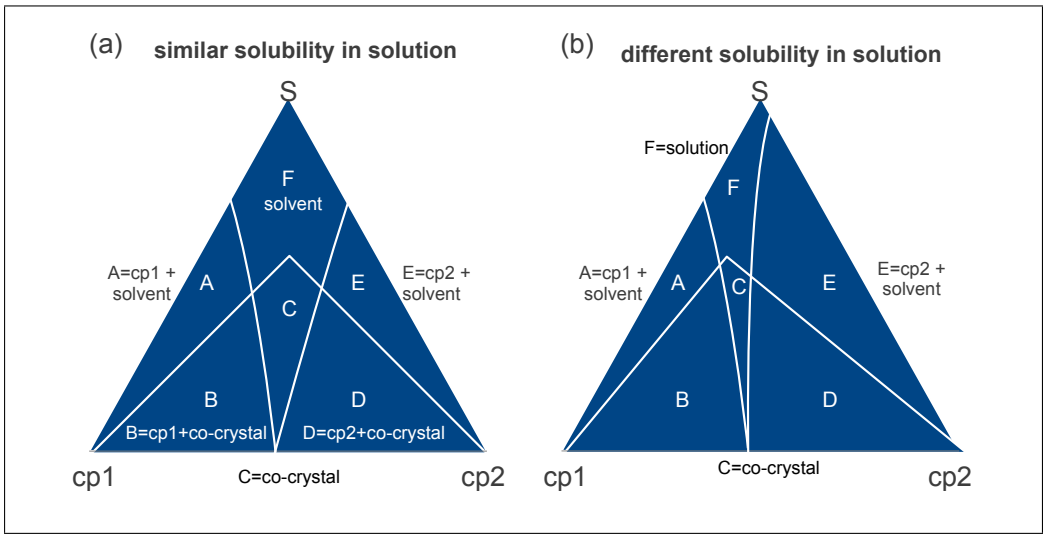

Figure 2.2: Ternary phase diagram of two components dissolved in a solution. (a) phase diagram of two components (cp1) and (cp2). (a) Similar solubilities and (b) different solubilities in solution where A=cp1+solvent, B=cp1+co-crystal, C=co-crystal, D=cp2+co-crystal, E=cp2+solvent and F=solvent. This figure is reproduced based on Blagden *et al.* work[92].

Many pharmaceutical co-crystals were generated using this method, such as caffeine co-crystals with oxalic acid, malonic acid and glutaric acid[24], CBZ co-crystals with NCT and SAC[95,96], and IND-SAC co-crystal[26]. The growth of co-crystal from solution can be performed in the presence of micro-crystals of the desired materials (seeding crystallisation). This approach is designed to ensure that the desired crystals are always obtained. Seeding often prevents the formation of kinetically preferable crystals and allows those thermodynamically favoured to form[97].

2.1.2 Slurry Preparation

This approach can generate co-crystal using small quantities of solvent. This process creates a localized surface of dissolution suitable for components to dissolve in, and form supersaturated phase which allows for co-crystal formation. Pharmaceutical co-crystals prepared using this technique include piroxicam with SAC and sulfamethazine with aspirin or benzoic acid[98].

2.1.3 Mechanochemical Grinding Technique

It has been noticed that co-crystals can be prepared simply by grinding the API with co-crystallising agents either dry (neat grinding) or in the presence of solvent (kneading or liquid assisting grinding)[99]. The effect of grinding on producing co-crystals can be attributed to the mechanical stress and the generated heat from the milling process. This mechanical process increases the surface area of interaction between materials due to fractured crystals, and enhances the interaction due to diffusion through such surfaces[100]. In addition, it can result in local melting at the interface area, similar to the eutectic phase i.e., the interaction between components occurs in a liquid phase[47,97,101].

The addition of small amounts of solvent during grinding (LAG) creates an atmosphere of vapour pressure of the solvent, which along with

the size of particles, and the length and the rate of milling contribute in the formation of co-crystal. It has been found that the co-crystal grinding method generates phases identical to those obtained by solution evaporation. This can be interpreted by the influence of strong intramolecular bonds on directing molecules to preferable crystalline form. However, solvent effects are still substantial in determining the rate of co-crystal formation, types and stability of crystalline forms[49]. In fact, adding solvents in which both components are dissolved enhances the kinetics process of grinding by opening the scope of interference between molecules; and thus increasing molecular collisions by means of adding additional degrees of orientation and conformational freedom[92,102]. Overall, it was suggested that co-crystal formation involves diffusion process through surface and this can be assisted

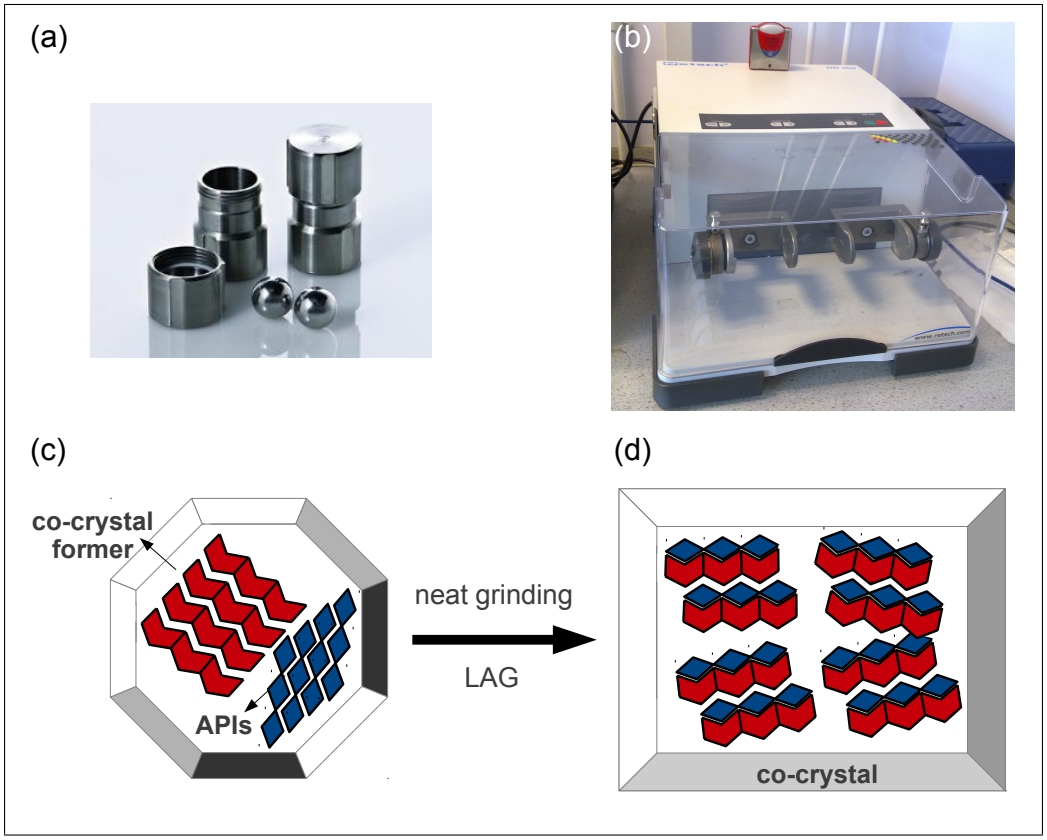

Figure 2.3: Mechanochemical grinding technique. It shows in (a) and (b) stainless steel jar with two balls used to contain the sample before mounted on Retsch® Ball Mill (mixer mill MM400). This machine is available in B27 Boos Science Building, School of Pharmacy, University of Nottingham. Grinding the API with co-crystal former (c) leads to the formation of co-crystal (d).

through another phase (solvent/gas) to various extent[103–105]. The role of mechanochemical grinding in molecular complexes is to activated the surfaces of reaction through defects or strains inducted by milling, and create new surfaces by the redistribution and the movement process of molecules and molecular products[106] It has been reported that the use of LAG can provide a control between the stoichiometric ratios and polymorphic forms of co-crystal[107,108]. Theophylline and caffeine (β-form) are examples of APIs co-crystallised with citric acid by neat grinding and in the presence of small quantities of water[63]. **Fig 2.3** shows the Ball Mill (mixer mill MM400) with two stainless steel grinding jars accompanied by a diagram of co-crystal formation using grinding approach.

2.1.4 Growth from the Melt

The principle behind this method is based on the fact that heating a mixture of two or more solid phases leads to a direct meeting in a liquid phase at their both lowest temperature. This temperature is called the eutectic point and the phase they meet in is the eutectic mixture. If the eutectic mixture of both components is capable to interact and exist in a distinct crystalline form with different properties, then a co-crystal is likely to seed from this emergent phase after cooling the preparation[109].

This concept was exploited in 1877 by M. W. Lehmann to prepare mixed complexes in a mixed–fusion experiment[109,110]. This experiment was refined in 1951, by L. Kofler and his wife A. Kofler, who investigated hundreds of organic molecules using Kofler melt technology[110,111] and it has later been used to prepare pharmaceutical co-crystals such as ibuprofen, FBP, fenbufen and salicylic acid with NCT by Berry *et al.*[91]. This approach involves placing a small amount of the higher melting component on a lid-covered slide, heated until melting occurs, and then allowing to solidify **(fig 2.4 I)**. The second component is then placed at the other edge

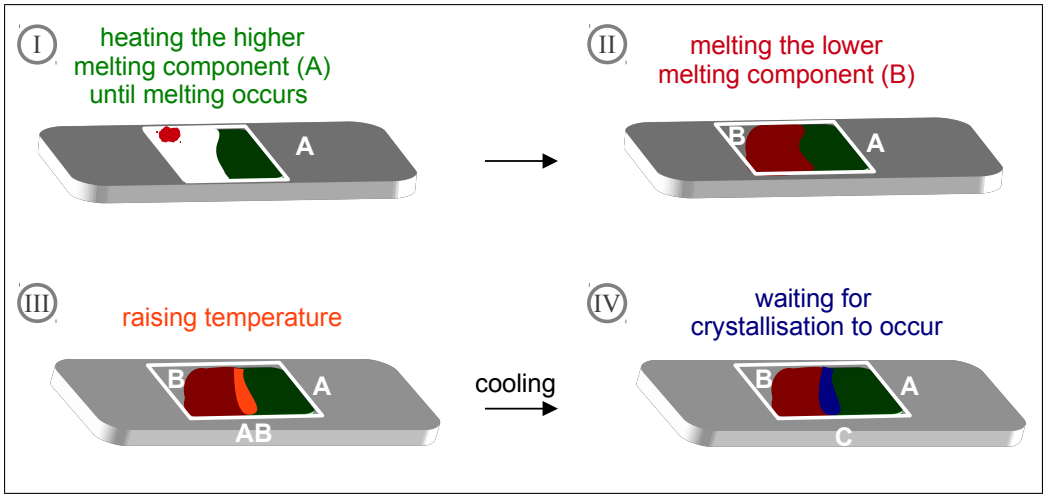

Figure 2.4: Schematic diagram of Kofler fusion preparation. It shows the consequential steps for preparing Kofler sample (I-IV) whereas the higher melting component is (A), the lower melting component (B), melted (AB) and the co-crystal is (C).

of the coverslip and melted. Once the second component melts, it slips under the coverslip and becomes in contact with the first component **(fig 2.4 II)**. Afterwards, the temperature is slightly raised to allow the second component to be at the juxtaposed parts of first component **(fig 2.4 III)**. Finally, the entire sample is cooled and awaiting time is given to help initiate the crystallisation of the new compound **(fig 2.4 IV)**. As a result, three distinct crystalline phases appear; both of the starting components and the new compound (co-crystal) along the zone of mixing.

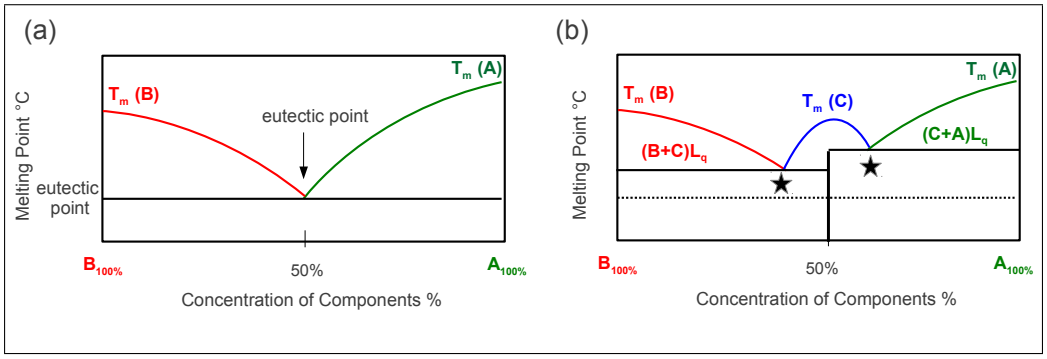

Figure 2.5: The binary phase-diagram of co-crystal formation. The temperature is plotted *vs* the molar fractions of components (A, B). It displays in (a) the melting of (A, B) at 100% of the starting components. Melting curves meet at the lowest temperature called eutectic point. When both components are able to recrystallise in a single crystalline phase, then a co-crystal (C) is formed as shown in (b).

This is explained in the binary phase diagram of this type of preparations **(fig 2.5)**. The curves in the phase diagram display the melting temperatures at each molar fraction from first and second components. These curves start from the melting points (T_m) of pure components on both sides and meet at the lowest temperature at a specific molar ratio, termed the eutectic temperature **(fig 2.5 a)**. If both components are able to recrystallise in a separated phase at this molar ratio, then another curve for the melting point of co-crystal appears **(fig 2.5 b)**.

The purpose of studying temperature-composition diagram is to ascertain whether or not a reaction takes place in molecular complex systems. Similar measurements were conducted in studying nicotinamide-ascorbic acid system[59,112]. However, not all of organic mixtures are capable to form molecular complexes when melted mixtures are cooled. More than half of organic compounds stay in a physical mixture form **(fig 2.6 blue)**, about 31.4% resulted in molecular complexes **(fig 2.6 red)**, while the rest belong to amorphous form or so called solid-solution **(fig 2.6 green)**[113].

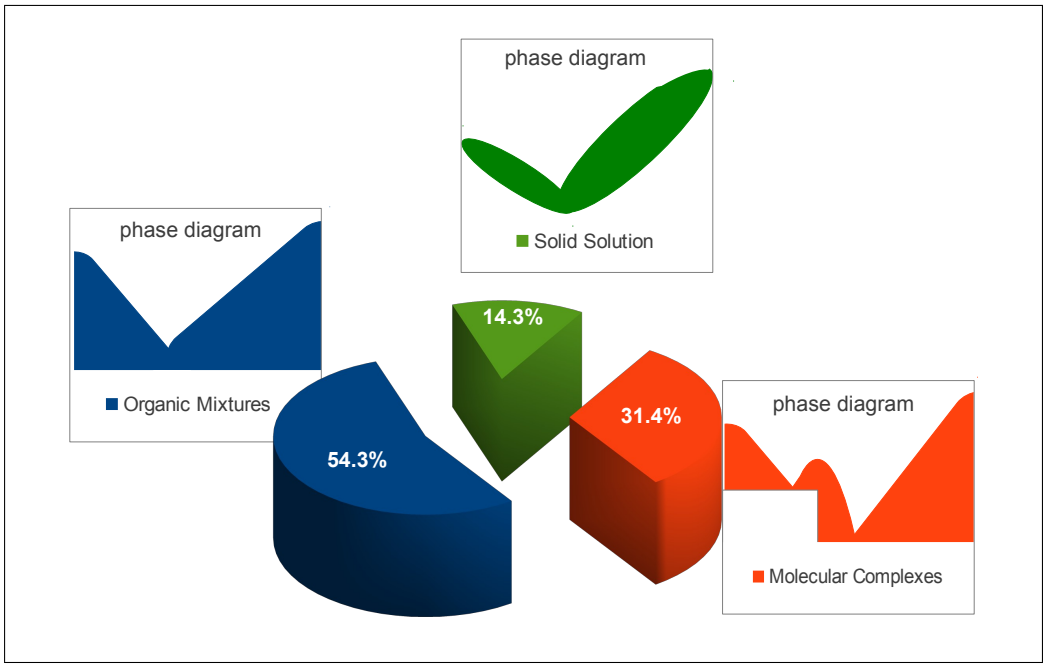

Figure 2.6: The phase diagrams and the fraction of binary systems. Physical mixtures are in (blue), molecular complexes are in (red), and solid-solution are in (green).

2.2 Pharmaceutical Co-crystal Screening

Co-crystals are generally investigated using different techniques such as conventional thermal analysis (differential scanning calorimetry and hot-stage microscopy), vibrational spectroscopic technique (Raman spectroscopy in its reflective and transmission modes), and crystallographic diffraction technique (x-ray powder diffraction and single x-ray diffraction). Since there is no one adequate technique capable alone of yielding a comprehensive identification for materials, it is important to collect data using more than one strategy. Therefore, a description about the principle of employed techniques and their commercial instruments will be explained in this section.

2.2.1 Differential Scanning Calorimetry

Conventional thermal analysis such as DSC is a widely common technique in the R&D laboratories. It is used to understand the change in the physical and chemical properties as a function of temperature or time. It is mostly the first step taken in the characterization studies of solid-state forms of an API[114]. DSC is used to measure the change in the energy as the sample is heated, cooled, or isothermally held. The main property measured by the DSC is the heat flow into the sample (endotherms) or out of the sample (exotherms) as a function of temperature or time. It is important to take into consideration the contribution of heat flow from DSC pans and the furnace. This is achieved by taking the difference in the heat flow between two pans; the first pan contains the sample and the other one is an empty pan used as a reference.

As heat is transferred to the pans, a thermocouple located underneath both stages monitors the differential heat flow **(fig 2.7)**. Consequently, the heat flow which reflects studied substances is referred to by $\triangle$H and this is usually plotted as a function of temperature or time. The

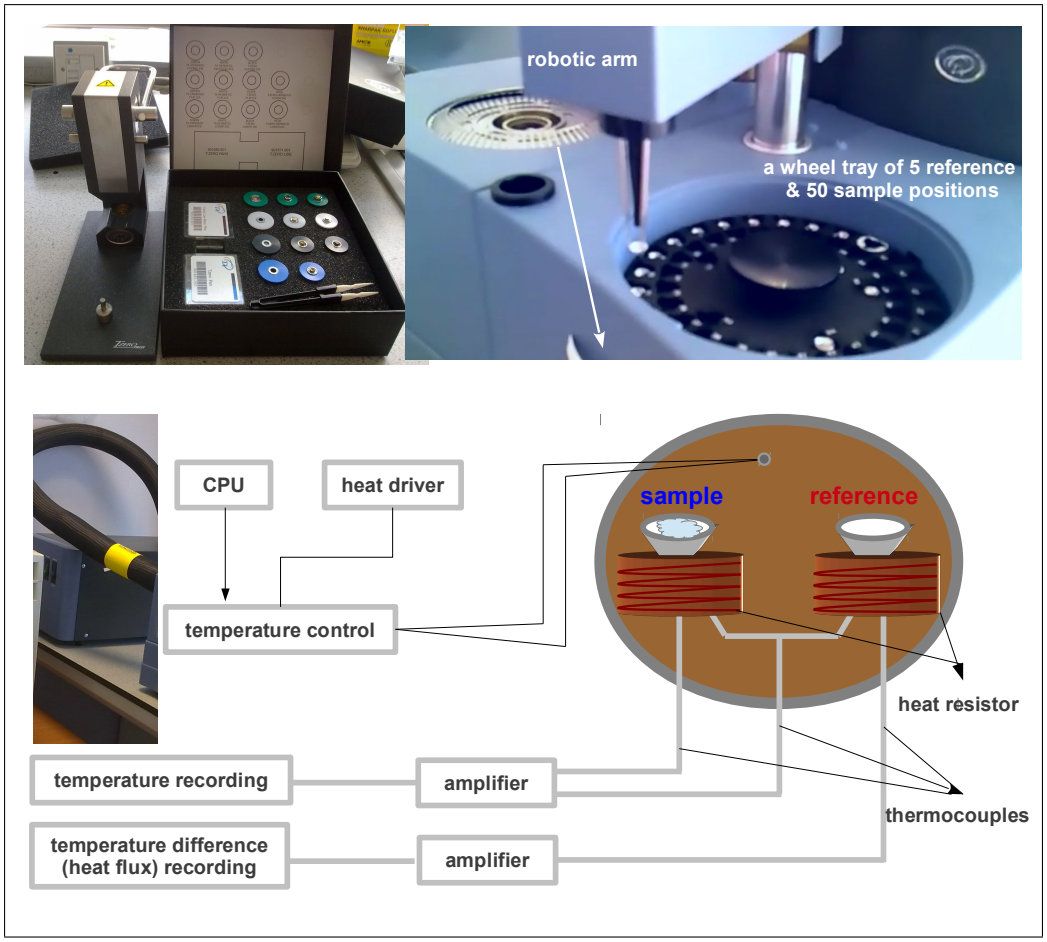

Figure 2.7: Differential scanning calorimetry DSC Q2000. The instrument exists in room C27 in Boots Science Building, School of Pharmacy, University of Nottingham. It is accompanied with T-zero® DSC Sample Encapsulation Press kit (top-left). The figure also shows the mechanisms of recoding thermal measurements at the bottom.

heat flow $\triangle$H is equivalent to the changes in the enthalpy hence, it can be used to measure the glass transition T_g event, crystallisation and phase transitions, melting, and heat of fusion events. All research equipments should undergo a regular calibration following the rules of good laboratory practice (GLP) or any other regulation set by research unit. DSC calibration is performed in relation to the melting temperature and the enthalpy of indium standard while the heat capacity is calibrated against sapphire.

TA Instruments DSC Q2000

TA Instruments DSC Q2000 (Crawley, United Kingdom) was employed to screen the starting materials and the resulting compounds. It is supplied

with 50-position auto-sampler which provides a flexibility in arranging more than one sample for measurement. It is equipped with DSC furnace with two uplifted stages for placing the sample and the empty reference pans. The furnace is provided with an auto-lid which works in coordination with the auto-sampler. Both sample and empty reference pans are transferred from the auto-sampler to the furnace by means of a robotic arm. Accordingly, the automation and the coordination between equipment's compartments enable for fast and efficient measurements. The operating heat range is (-40 to 400 °C). Sub-ambient operation is facilitated by a Refrigerated Cooling System (RCS40), which allows for DSC standard and modulated DSC (MDSC) operation over a temperature range of -40 to 400 °C. All measurements are scheduled and recorded automatically using Platinum™ software.

Samples are encapsulated using T-zero® DSC Sample Encapsulation Press, The press kit includes 4 die sets convenient for hermetic or non-hermetic sealing included in a black box kit with a tweezer and two boxes of DSC pans and lids. Dies are colour coded in green, white, black, blue which are compatible with T-zero or standard aluminum pans and lids; Black dies (suitable for non-hermetic sealing T-zero aluminum pans and lids) are the ones used in this research study **(fig 2.7)**.

2.2.2 Hot Stage Polarised Microscopy

Within the field of studying solid-state properties of pharmaceuticals, microscopic observation provides a rapid, and versatile, and often non-destructive method for analysing samples. The characterisation provides information regarding the physicochemical properties such as particle shape and size, optical properties, crystallisation, dissolution behaviour, and thermal behaviour when the microscopy is coupled with the hot-stage compartment[115]. Observing the thermal behaviour microscopically is obtainable using po-

larised light thermoscopy, which was a method of interest along the course of this research work. The principle behind polarised thermoscopy is depicted in **fig 2.8**.

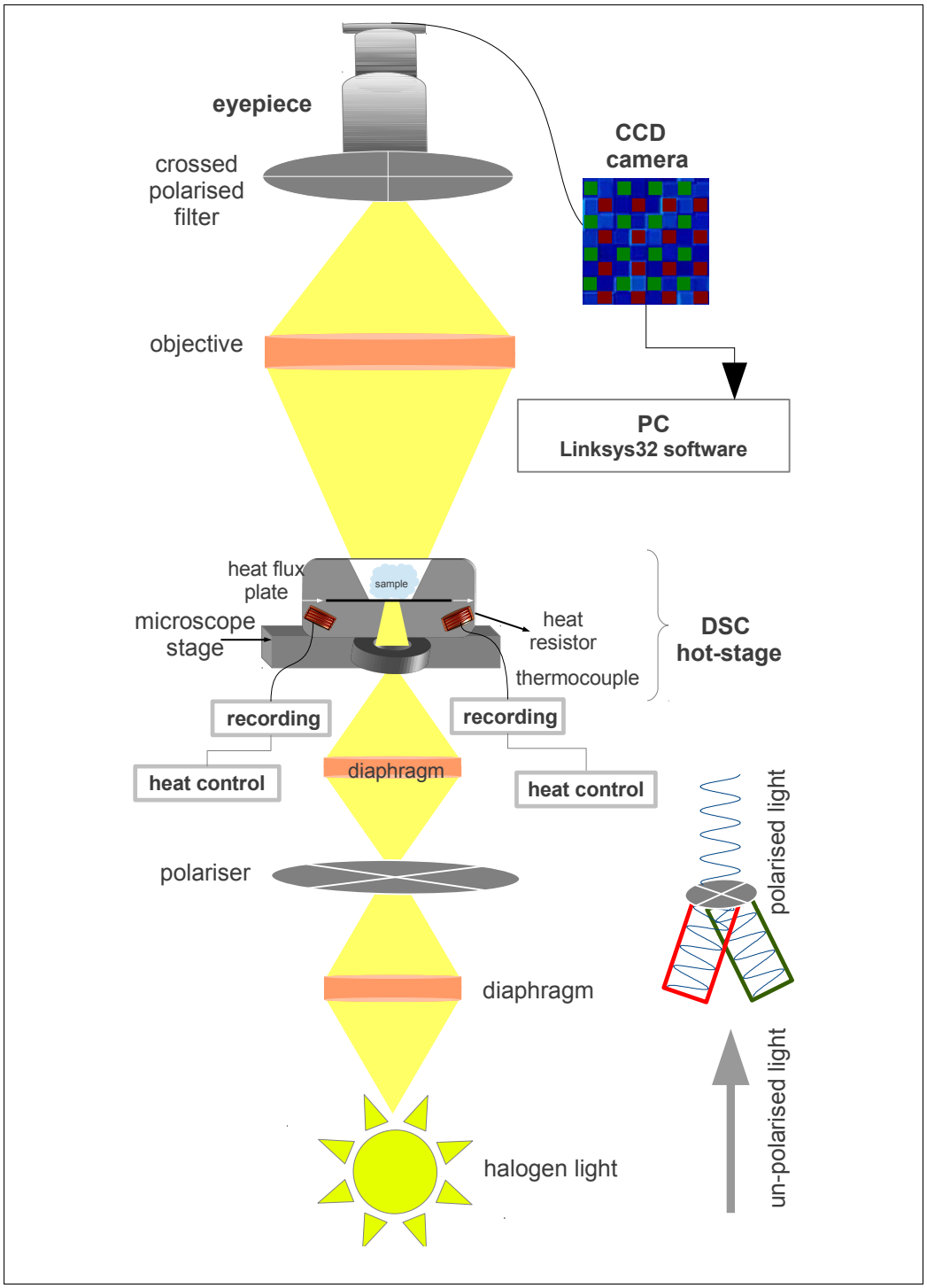

Figure 2.8: Sketched diagram showing the principle of polarised thermoscopy.

PriorLux Pol™ & Linkam DSC600

Thermoscopic investigation was observed using PriorLux Pol™ advanced polarised light microscope (PriorLux Pol™, Prior Scientific, Fulbourn, Cambridge, UK). PriorLux Pol™ **(fig 2.9)** is equipped with a mechanical stage of 360 degree rotation (1 degree increments) for placing sample. Samples are focused through the collaboration of focusing eyepieces of 10× magnification and 20 mm view field, and free objectives of either 4×, 10×, 20×, 40×, or 60× magnification. The focusing mechanisms (the co-axial and coarse adjustments) are controlled with a tension control focus stop. Samples are illuminated by a 12 V and 30 W halogen lamp with variable brightness control. Kohler illumination can be controlled using iris diaphragm with aperture size of 1.25 NA. The illuminated light can also be polarised using a rotating polariser which is scaled and controlled by means of Bertrand lens.

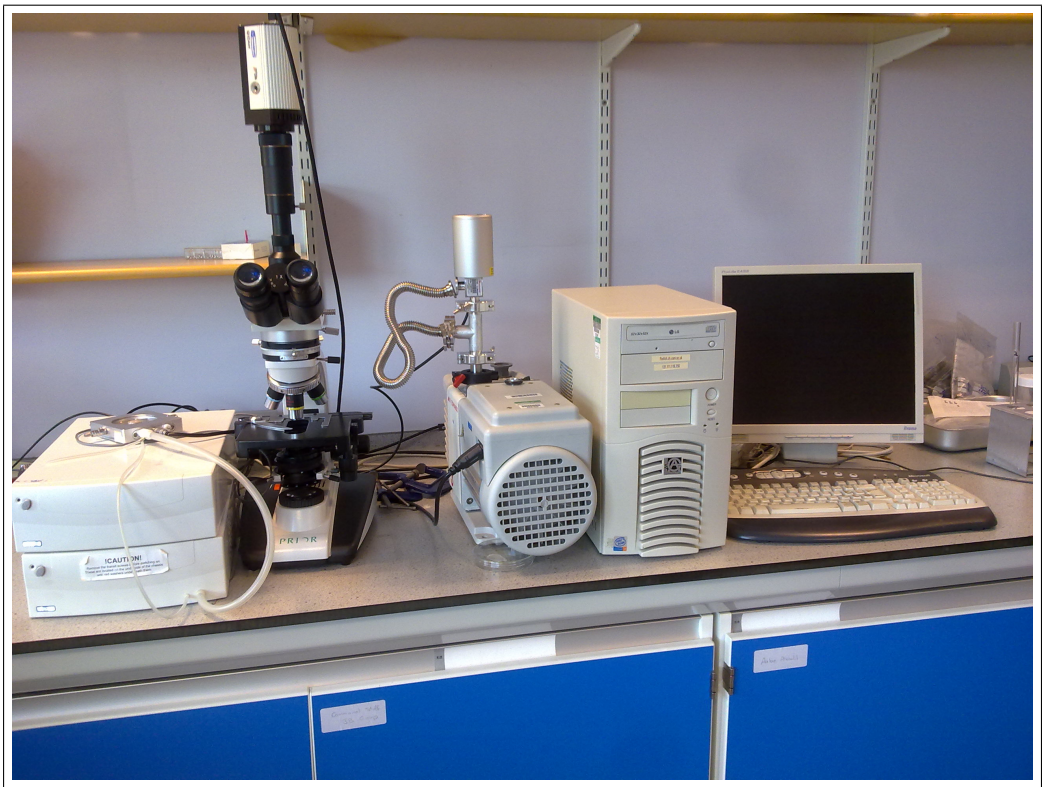

Figure 2.9: PriorLuxMET hot-stage polarised microscope exists in room C27 in Boots Science Building, School of Pharmacy, University of Nottingham.

Microscopic images are collected through a CCD camera attached to the microscope. CCD digital camera can be either used in its still mode for basic image capture, or in its advanced imaging mode for moving pictures. The videos can be generated from consequetive pictures collected at chosen time intervals using image capture software which is built within the Linksys32 package. PriorLux Pol™ is equipped with a Linkam DSC600 heating-freezing stage. The latter is controlled by T95-Linksys temperature programmer and Linksys32 software (Linkam Scientific Instruments Ltd., Tadworth, Surrey, UK) **(fig 2.9)**. Linksys32 package enables to control the hot-stage and the temperature programs i.e., the thermal scanning profile over selected temperature range and heating rate **(fig 2.9)**.

2.2.3 Raman Spectroscopy

Raman spectroscopy is useful for studying the chemical structure of different systems from simple chemicals and plastics to biological structures. It produces important information about physical properties such as crystal form, crystal size and molecular orientation. Raman spectroscopy has been recently combined with confocal microscopy and named confocal Raman spectroscopy. The latter technique yields chemical and other information about samples with a high spatial resolution. The high resolution was achieved due to the focality of laser on the sample by means of objectives, which collect and direct scattered light through a pinhole towards the detector. Since confocal Raman spectroscopy is the technique of choice for investigating heterogeneous systems on the micrometer scale, it is beneficial for studying co-crystalline forms.

Moreover, confocal Raman spectroscopy can also be attached to hot stage, which is useful for investigating co-crystal kinetics and formation. For instance, it was used for screening carbamazepine-nicotinamide synthesis[116]. Raman spectroscopy is very important in detecting polymorphic forms and

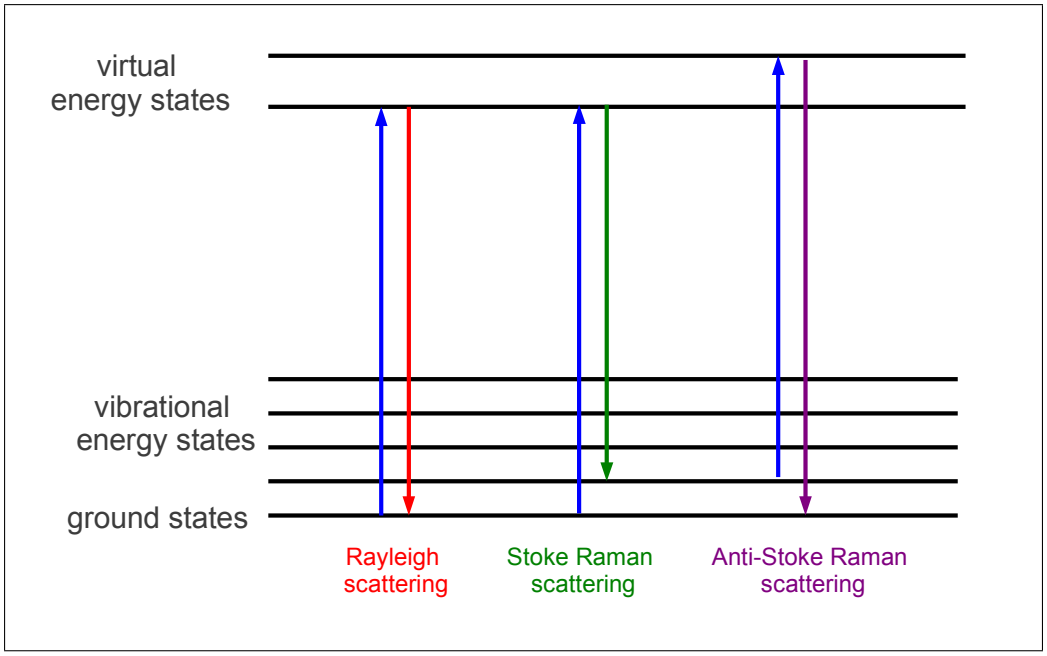

Figure 2.10: Schematic of the vibrational scattering showing the possible transitions between energy levels. It shows elastic scattering (Rayleigh scattering), inelastic Raman scattering (Stoke and Anti-Stoke scattering).

distinguishing between the presence of polymorphs[117].

Raman study involves the use of inelastic scattering of monochromatic radiation (photons) of energy sufficient to cause a distortion in the electron distribution cloud of covalent bonds. In all types of spectroscopic techniques, the instrument measures the changes in the energy of photon (either lost or gained) resulted from the interaction between photons and molecules within the sample. The nature of such change varies according to the nature of inter/intramolecular bonds within studied compound, the symmetry of its molecule, and the energy of incident light.[115]

Molecules are promoted to a virtual state when the distortion in the distribution of electronic clouds occurs. When molecules relaxes, they return back to the ground state releasing acquired energy either in the same frequency (Rayleigh scattering) or in a different frequency (Raman scattering). Hence, Raman scattering is an inelastic scattering which its frequency can be either less (Stoke scattering) or more (anti-Stoke scattering) than the frequency of incident light, depending on the original vibrational state of molecules. Most molecules exists in the ground state, this means that

when substance are subjected to a suitable radiation, they scatter light in Stoke mode. Such theory is simplified in **fig 2.10** which shows the electronic transition between energy levels.[118,119]

Confocal Raman Spectroscopy (LabRAM HR Horiba)

Raman spectrometer LabRAM HR from Horiba Jobin Yvon (Villeneuve d'Ascq, France) was utilised to screen and collect Raman spectra for samples and their co-crystal preparations. This system is provided with four laser lines 325 nm, 532 nm, 660 nm and 785 nm covering UV-VIS-NIR regions, optics for coupling laser to the samples and carrying back Raman signal through the spectroscopy. Raman signals are diffracted by the available gratings (1800, 1200, 600 lines/mm and 1200 lines/mm for UV). In this work 600 lines/mm gratings was employed. The dispersed signals were then detected by a large 1024 pixel CCD detector cooled at -70 °C.

This instrument is equipped with an Olympus BX41 microscope provided with; a white light illumination system working by reflection or transmission, a coloured camera to visualise the samples, XYZ motorized stage, and a variety of lenses 10×, 100× and 40× (UV) and 50× LWD, 100× LWD objectives. The ones used in this study were 10× and 50× LWD. It is also supplemented with standard XY manual cooling/heating stage (Linkam LTS350) with TMS94 temperature controlling programmer and LNP94 cooling system and a 2 litre dewar for liquid Nitrogen. These accessories allow to heat, cool, or isothermally hold the sample, and acquire Raman spectra as function of temperature. Hence, it enable to investigate the chemical changes accompanied studied materials while subjecting samples to heating environment. Hot-stage accessories were provided by Linkam Scientific Instruments Ltd (Surrey, UK).

There are other options to design the experiment using this instrument, encompassing a measurement as a function of a space. For instance,

Raman data can be acquired from a single point, or set up to record spectra from different sets of points which can be aligned in one line (line mapping), or many lines in a square or circle form (XY mapping), It is feasible also to run a 3D mapping by including the depth (XYZ mapping) **(fig 2.12)**. All these operations are set up and acquired through LabSpec 5 software,

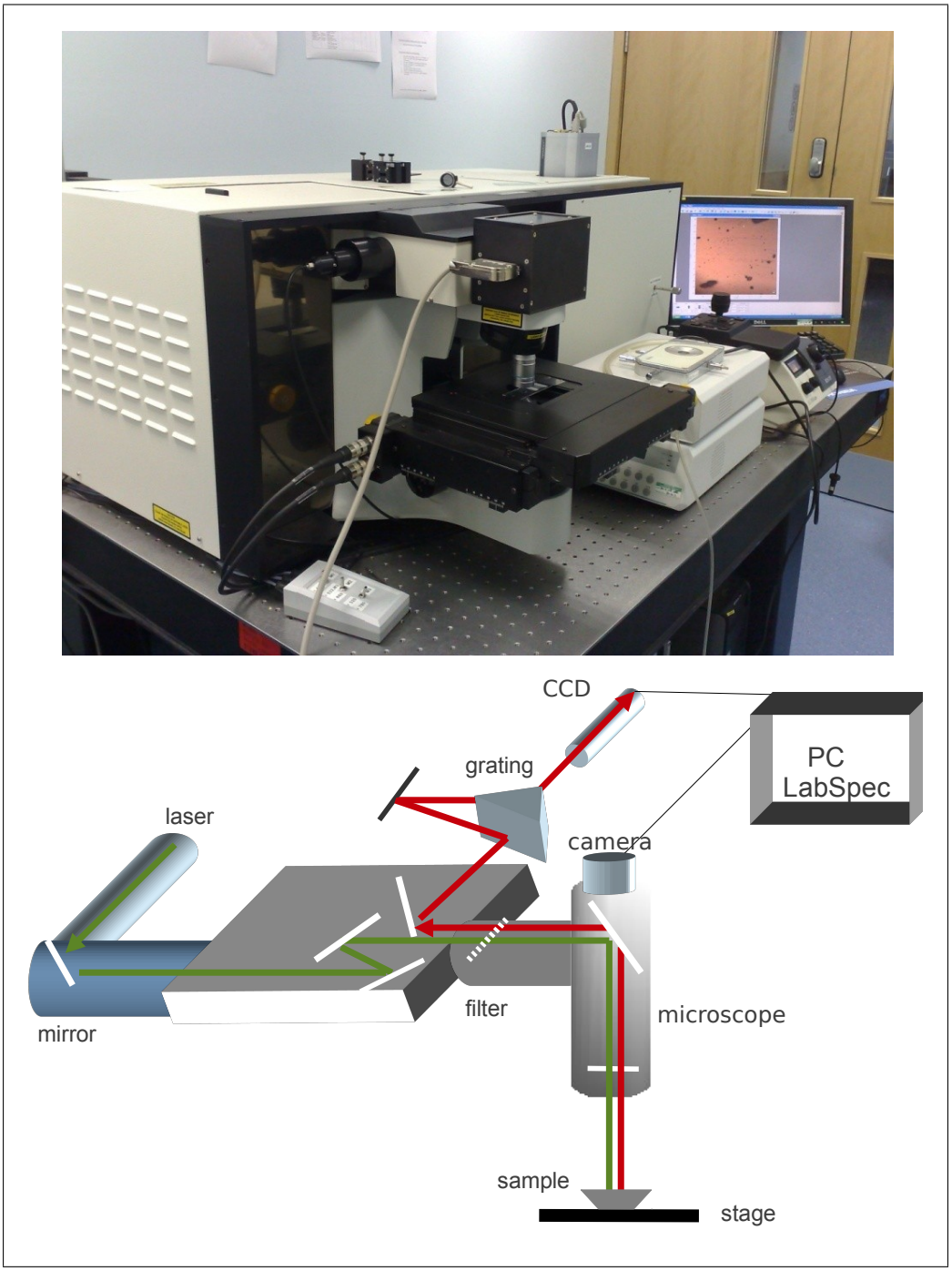

Figure 2.11: LabRAM HR Horiba confocal Raman instrument. The instrument is available in room B03 in the Nottingham Nanotechnology and Nanoscience Centre (NNNC), University of Nottingham.

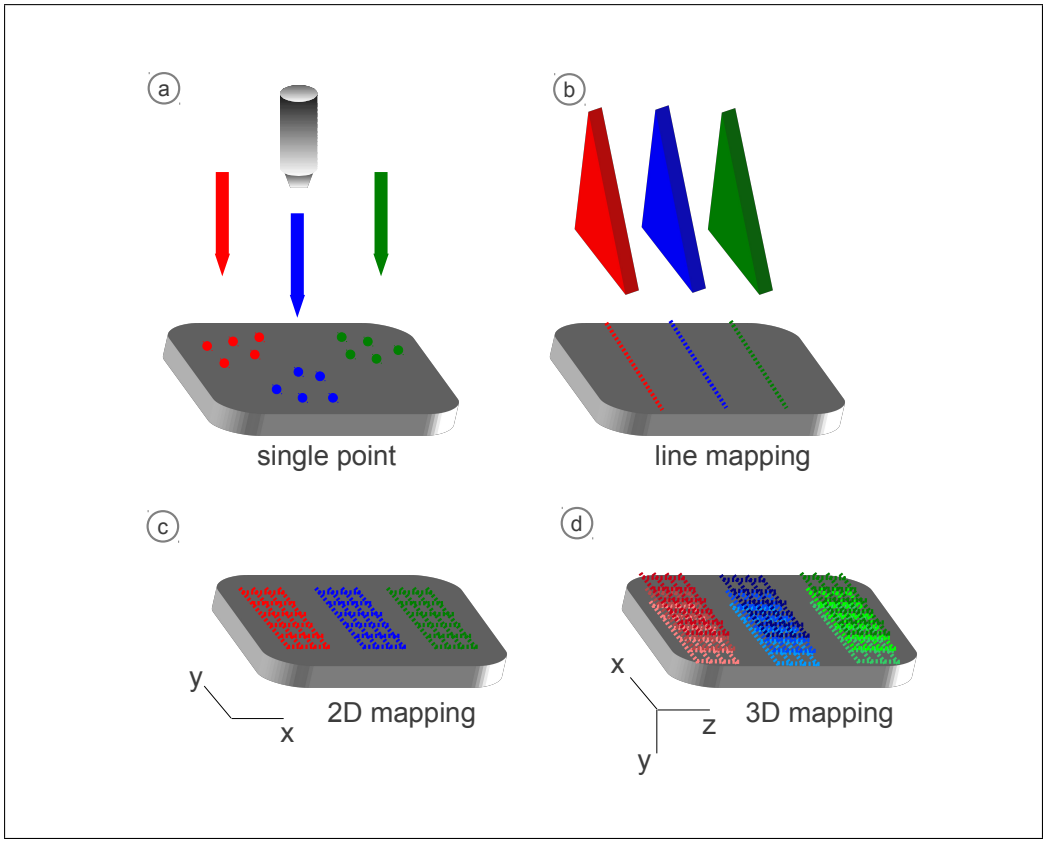

Figure 2.12: Schematic of Raman measurements as a function of space. Measurements can be recorded from different points (single point spectrum) as shown in (a), from a series of points aligned in a one line (line mapping) (b), many lines (XY mapping) (c), or in 3D form (XYZ mapping) (d).

which is designed to control Raman instrument. The Raman system was calibrated before acquiring measurements, on a standard silicon (Si) sample after adjusting the spectrograph zero position, the silicon Raman peak is within ± 1 pixel of 520.7 cm.

2.2.4 Raman Data Analysis

Matlab 7.6.0 (R2008a) Software Package

Matlab 7.6.0 (R2008a) is a separate licensed mathematical workspace written by the MathWorks, Inc. (MA, US). It was used in this work for principal component analysis on Raman mapping data of FBP-NCT Kofler system. Data were quantitatively simplified into sets of variables and linearly correlated with the original data.

R version 2.15.0

R is a separate free package designed by the R foundation for statistical computing, R version 2.15.0 (30-03-2012), which was downloaded in ubuntu 12.04 LTS. Scripts with suitable codes (routines) were written for analysing data using two statistical methods; principal component analysis and hierarchical agglomerative clustering.

Multivariate Data Analysis

Multivariate data analysis is one of the efficient algebraic approaches employed to simplify complex data, discriminate and classify between variables. In the current work, three protocols were mainly employed to analyse Raman and x-ray powder diffraction data.

1. **Direct Classical Least Square Analysis:** DCLS modeling allows image generation from large datasets based on a model parameter (i.e., spectrum). This model is predicted according to its similarity with a reference. Afterwards, the correlation between observations and a predicted model is calculated using the best-fit methodology based on minimising the sum of squared differences between observations and predicted model. Accordingly, observation with best fit with selected model are classified together and their degree of match is worked out[120]. This method was adopted in **chap 3**.

2. **Principal Component Analysis:** PCA is one of the fundamental methods in the statistical analysis of large datasets and it was employed in **chap 3, 4, 5** for analysing Raman mapping and VT-Raman data. PCA is a well established mathematical operation, through which large number of observations are transformed by rotation into a smaller number of orthogonal variables, known as principal components, each of which is characterised by a score (single vector variable)

and a loading (as many variables exist in a single original dataset)[121]. PCA can also be considered a clustering algorithm. It is useful for the analysis of phase transformations **chap 4**. PCA results can be presented as scores' plot (i.e., PC1 against PC2), and/or PC scores against number of observation (i.e., PC1 against temperature), and/or PCs loadings i.e., PC1 loadings against variable (wavenumber).

3. **Hierarchical Agglomerative Clustering:** In this method (HAC), the differences or the similarity between data variables are calculated and used to agglomerate and arrange datasets in a tree-like structure or dendrogram. The distance between datasets can be calculated in different methods but the one used in this research work was based on Euclidean method, afterwards the linkage between data was achieved using Ward's method as demonstrated in **chap 5**.[120]

2.2.5 X-ray Crystallography

X-ray crystallographic techniques have been described as a gold standard method to understand the crystal packaging, hydrogen bonding and structural conformation. When a sample is subjected to x-rays, each atom in its unit cell interacts with the incident radiation resulted in x-rays diffraction from all parts of the structure. Moreover, an interference similar to that between electrons in an atom occurred between scattered x-rays. Therefore, the overall diffracted x-rays represent the sum of individual unit cells.[115]

This perspective was visually simplified and mathematically valid by W. L. Bragg, who considered x-ray diffraction as a reflection from set of planes of different indices (h, k, l) and have intensity I_{hkl}. These indices are associated with atomic positions and other influencing factor of x-ray scattering. He added that diffraction does not occur until Bragg's law is satisfied **(eq 2.1)** which correlates between the wavelength of incident light (λ), its angle with respect to the planes (θ), and the distance between the

plane d_{hkl} **(fig 2.13)**.[115]

$$\lambda = 2 \times d_{hkl} \times sin\theta \tag{2.1}$$

Equation 2.1: Bragg's equation whereas the wavelength of incident beam is λ, the angle of incident light with respect to planes is θ, and the distance between the planes is d_{hkl}.

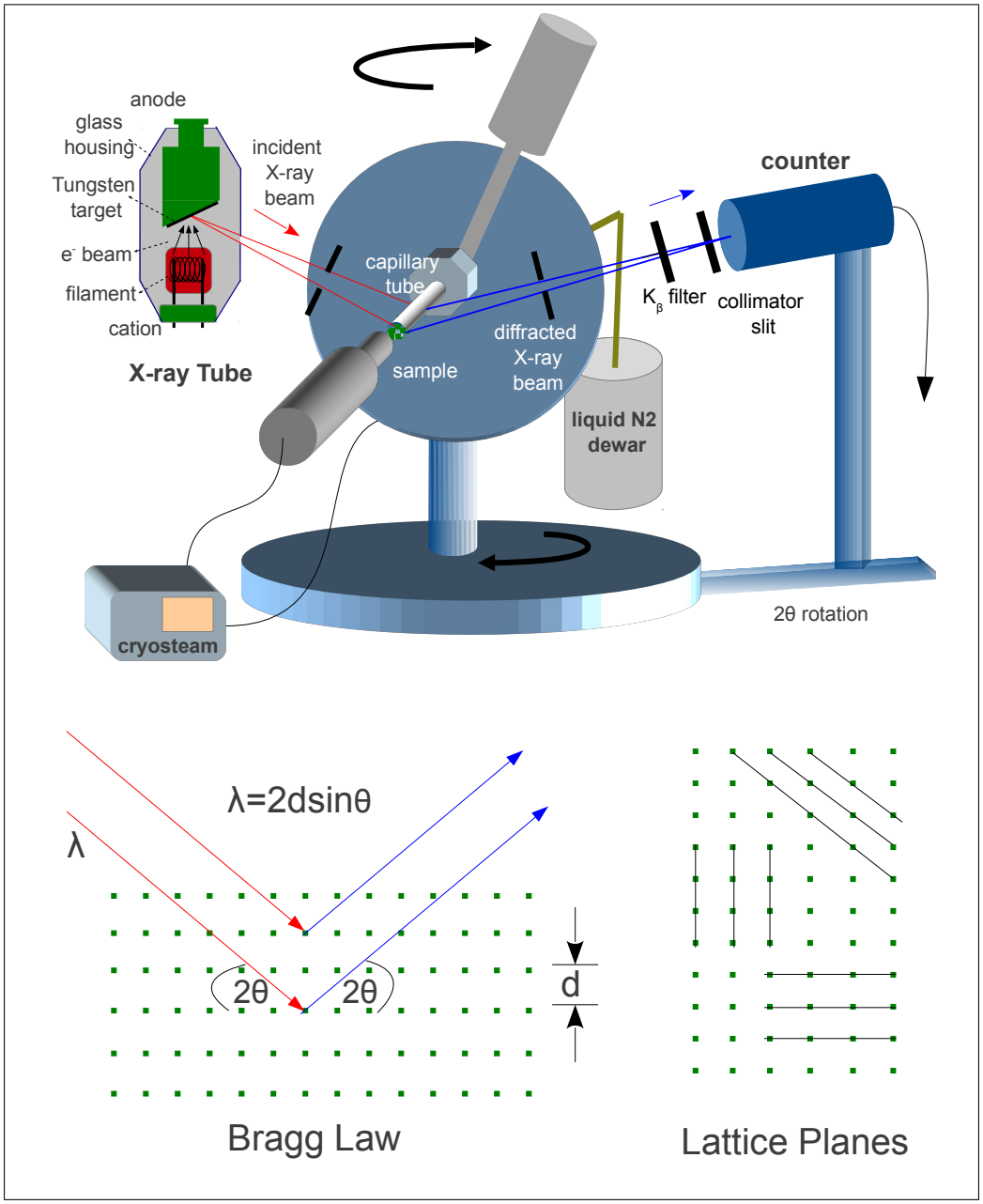

Figure 2.13: Sketched diagram showing the principle of XRPD and beam diffraction according to Bragg's law.

Bruker D8 Advance XRPD

X-ray powder diffraction (XRPD) is an analytical technique used for identifying crystalline phases and defining unit-cell dimensions. It is also widely used in the pharmaceutical industries as it provides a rapid mean for structural characterization. Thus, it can be used to determine co-crystals and detect their formations. For example, the formation of caffeine-salicylic co-crystal was confirmed by using XRPD when compared with the calculated patterns of pure components and co-crystal[122]. The formation of co-crystals can also be tracked using XRPD when a mixture of components is subjected to heating environment or so called variable temperatures (VT) resulting in VT-XRPD experiment. For instance, XRPD patterns of a mixture of caffeine and salicylic acid was taken at different temperature points. It was noticed that characteristic peaks appeared at 125 °C, 130 °C and 135 °C at (12.1° and 13.4° 2θ) for the caffeine-salicylic acid co-crystal, and vanished at 150 °C, around the melting point of co-crystal[122].

The principle of XRPD technique is based mainly on generating x-rays from evacuated tube, which is then collimated and filtered before hitting the sample. The loose powder of studied sample is filled in capillary tube and mounted on goniometer in the preferred orientation. Diffracted beam is then recoded by a suitable detector **(fig 2.13)**.

A Bruker D8 Advance powder diffractometer was the commercial equipment utilised to collect powder patterns in a Debye-Scherrer geometry. X-ray radiation was generated inside a ceramic x-ray tube from an anode made of copper Cu in Kα spectral line at wavelength λ= 1.54059 Å. The diffractometer is equipped with a scintillation detector and Bruker Kristalloflex generator set on voltage 40 kV and current 40 mA. Samples were loaded in borosilicate glass capillary tubes BGCT with 0.7 mm bore diameter, supplied by CTS Capillary Tube Supplies Ltd UK, and mounted on the goniometer in a preferable orientation. DIFFRACplus software pack-

age version 2.3 was used for data acquisition. Analysis was conducted using terminal window under Unix system, through which the raw data were processed to a format suitable for plotting.

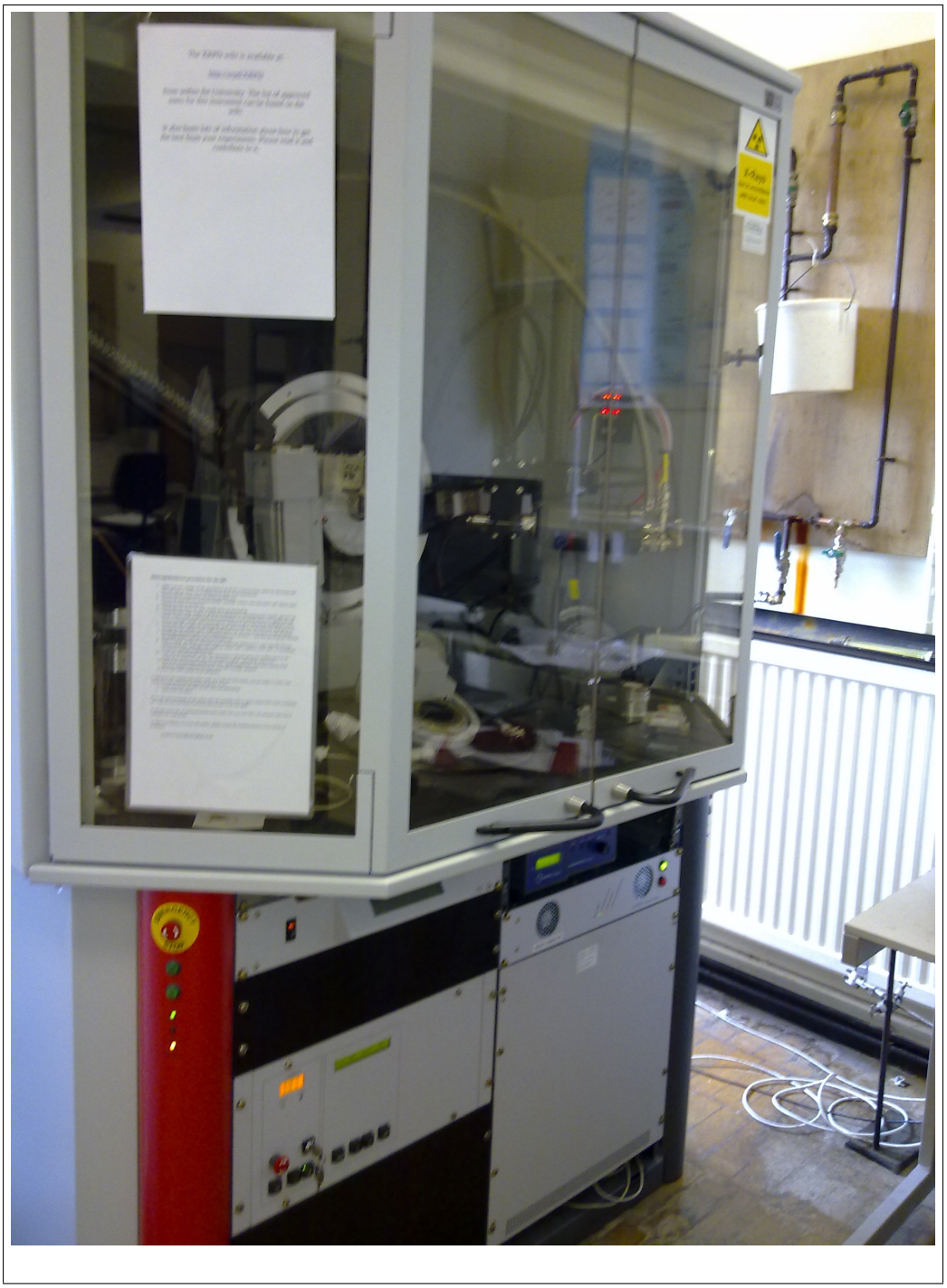

Figure 2.14: Bruker D8 Advance powder diffractometer. The instrument exists in room B15 at the School of Chemistry, University of Nottingham.

2.2.6 Single X-Ray Diffraction (Bruker AXS)

The principle of single x-ray diffraction (SXD) is very comparable to that of XRPD whereas x-rays are generated in a ceramic x-ray tube, then collimated and become monochromatic. The resulting x-ray beam is directed on the single crystal sample. Single crystal is mounted on the goniometer head which allows positioning the crystal in the centre of x-ray beam, and the rotation of goniometer enables collecting x-rays from different orientations. The cryo-cooling is often utilised to minimise crystal damage and reduce background noise in the measurements. In crystallographic structure determination, it is important to collect sets of diffracted beams of I_{hkl} intensities. Therefore, the intensities of diffracted beams are recored using suitable detector **(fig 2.15)**.

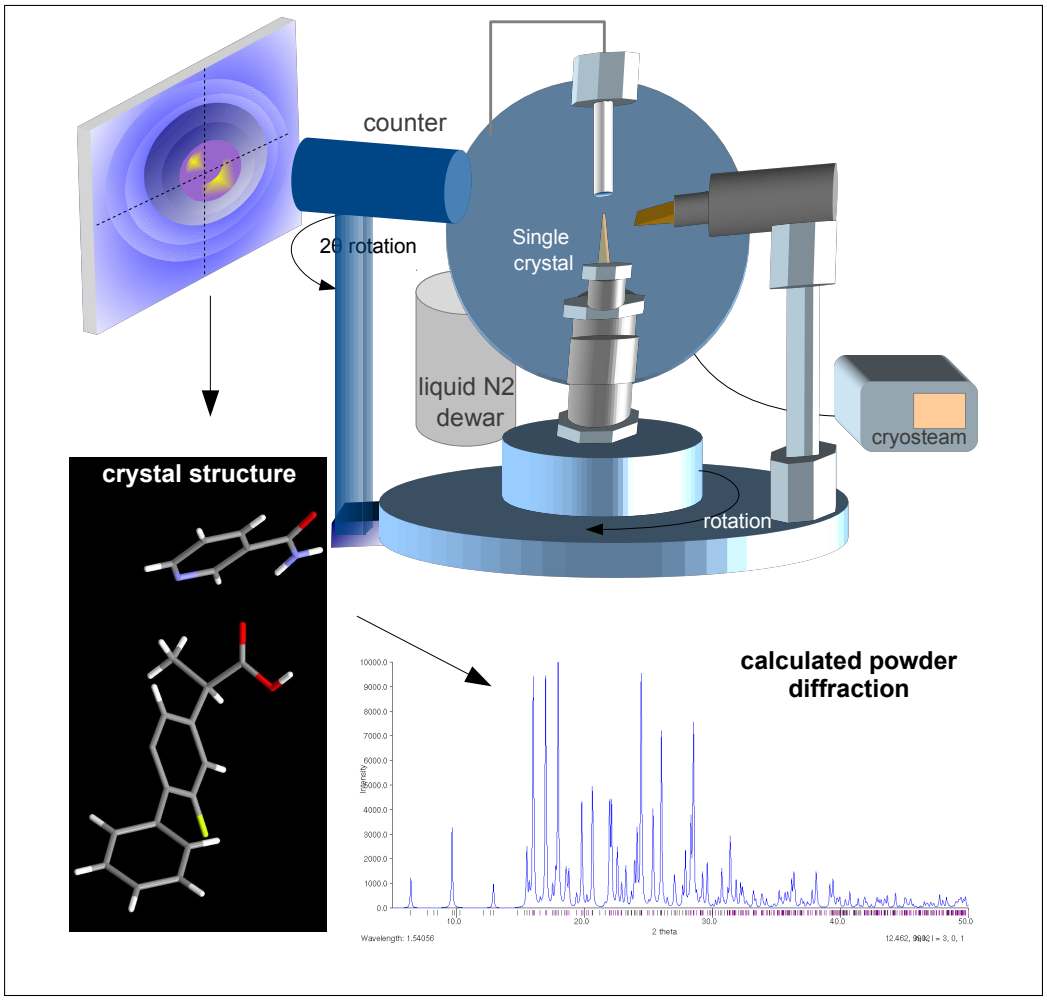

Figure 2.15: Sketched diagram showing the principle of single x-ray diffraction.

Bruker Nonius Smart Apex CCD diffractometer (Bruker AXS LTD., Coventry, UK) is a single x-ray instrument used to mount the single crystal of FBP-NCT co-crystal. X-ray radiation is generated inside a ceramic x-ray tube from an anode made of Mo in Kα spectral line at wavelength λ=0.71073 Å. The diffractometer is equipped with a Bruker Kristalloflex generator set on a voltage of 50 kV and a current of 40 mA, a graphite monochromator, and an Oxford Cryosystem Cryostream (Oxford Cryosystems Ltd., Long Hanborough, Oxford, UK).

2.2.7 Mercury 1.4.2 Package

Mercury package is a part of Cambridge Structural Database system. It was used to visualise the crystal structure of the starting material and calculate their powder diffraction data. Data were firstly obtained in a .CIF format from the Cambridge Crystallographic Data Centre (CCDC) *via* the CrystalWeb, then loaded in Mercury 1.4.2.

CHAPTER 3

Confocal Raman Mapping of Kofler Co-crystal Preparation

3.1 Abstract

The spatial distribution of molecular and crystalline entities in a model Kofler melt was for the first time characterised using confocal Raman microscopy/spectroscopy. Direct classical least squares and principal component analysis were used to generate hyperspectral maps. The long-standing view that the Kofler method is suitable for rapid and reliable mapping of a binary phase diagram is not supported from the results.

3.2 Introduction

Multicomponent solids are widely discussed in the context of a variety of applications in pharmaceutical, chemical and material fields[34,123]. Co-crystals, in particular, have recently gained a great deal of attention in pharmaceutical area[32,51]. They have been adopted as an approach to modify the properties of single-component materials, which have become a matter of importance in drug development and delivery fields[24,26,69–71]. Co-crystals can be defined as single-phase multi-component solid materials, where com-

ponents coexist in stoichiometric ratios and are linked through non-covalent bonds with the components remaining unionised[48].

Few techniques have been employed to generate co-crystals, of which solution screening is the dominant method of isolating new crystalline forms. However, this can be complex when applied to co-crystal formation, especially for components of differing solubilities[56,124]. This issue can be addressed by conducting the crystallisation from a melt, which avoids the use of any solvent. An example of this is the use of the fusion contact protocol by means of the hot-stage microscopy[125–127]. The concept of fusing mixed compounds, based on the contact method, was originally described by M. W. Lehmann in 1888[128], which was later refined by L. Kofler and A. Kofler[110] and called the contact method by W. C. McCrone[111]. In fact, the use of the fusion contact protocol for screening co-crystals is not particularly widespread and has remained unmodified since W. C. McCrone's work[111]. However, it has been recently revisited by a few researchers such as Davis *et al.*[109], McNamara *et al.*[129], and Berry *et al.*[91].

The basic premise of the Kofler mixed fusion method is to allow two components to meet between a glass microscope slide and a coverslip, and form (by melting) a composition gradient. Subsequently the potential formation of a co-crystal at this zone of melting is investigated by optical microscopy. The fusion method can also be used to generate small seeded crystals which can subsequently be used to grow larger crystals from solution (suitable for structure determination by single crystal X-ray diffraction)[56]. However, the main idea of using hot-stage microscopy in Kofler preparation is to screen the melting behaviour of two component systems in a single rapid and straightforward experiment, without the necessity to determine their full phase diagram*. The conventional theory of the observed phases

*McCrone, 1951[111]: *"the entire composition diagram is shown in the composition gradient"*; Berry *et al.*, 2008[91]: *"This zone is then comparable to the composition of the binary phase diagram for two components."*

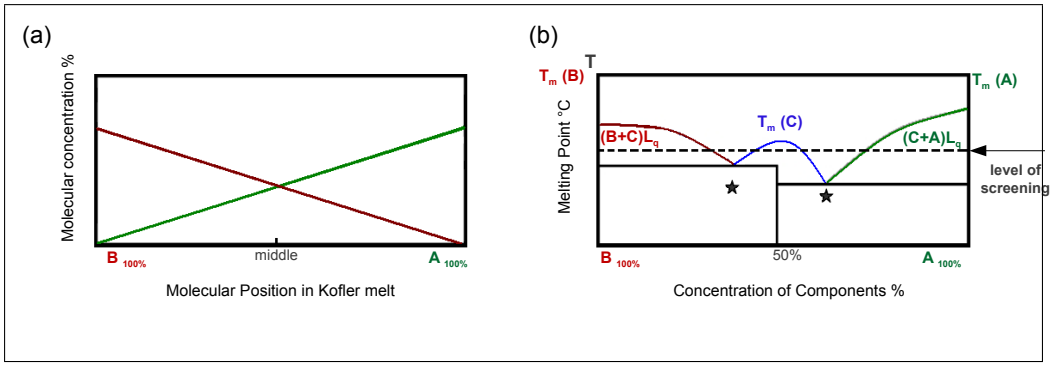

Figure 3.1: Schematics of the traditional component's position in Kofler melt preparation and its binary phase diagram. (a) is the plot of molecular fraction *vs* its position in Kofler melt slide, while (b) is the binary phase-diagram of the co-crystal formation. The temperature in the phase diagram is plotted *vs* the molar fractions of components (A and B, the higher and lower melting components, respectively). It shows the co-crystal formation (C) from stoichiometric (A and B) at 50%. It also displays the melting of (A, B) at 100% of each, Tm (A) and Tm (B) respectively. It indicates to the meeting in the liquid phase between component (A) and co-crystal (C), component (B) and the co-crystal (C) at the lowest temperature or eutectic temperature as indicated by asterisks where the intersection occurs in a wide and smooth style.

in an ideal Kofler experiment **(fig 3.1 a)** assumes a linear composition gradient across the zone of mixing after starting with 100% of the respective materials at the peripheral sides*[56,91,111].

The co-crystal formation is potentially achieved from the liquefied mixture at any area within the contact region, provided that the composition of components exists at a suitable molar ratio for the crystallisation of single-phase form (typically 1:1, 1:2, 2:1 or other commensurate ratio). This formation is separated from the components present at the peripheral sides with solidified eutectic mixtures existing at different ratios. Thus, Kofler melt preparation allows a rapid qualitative mapping of the phase diagram as outlined in **fig 3.1 b**.[56,110]

*Berry *et al.*, 2008[91]: *"with one side of the mixing zone representing 100% of one component and the other side 100 % of the other component, and with a concentration gradient across the zone."*; Davis *et al.*, 2004[109]: *"At some point in the mixing zone, there should be a 1:1 ratio of the two components. Moving from this point toward either pure component, the proportion of that component increases. Thus, a composition gradient exists across the mixing zone."*; and this was pictorially illustrated by Kuhnert-Brandstatter, Figs 6 and 7. Kuhnert-Brandstätter M., in "The status and future of chemical microscopy" from *Pure and Applied Chemistry*, 1965[130].

Despite all the benefits of traditional hot-stage microscopy in Kofler mixed fusion preparations, there are some serious limitations of this method in achieving full qualitative and quantitative characterisation. One severe limitation is that the hot-stage microphotographs often cannot unambiguously identify the phases present, as their interpretation depends on visual inspection. Therefore, such investigation is subjective and cannot be used for example to unequivocally identify phases. Therefore, it was proposed that such imperfections could be overcome by the use of spectroscopic mapping techniques for screening the Kofler melt.

Because the sample is held between a cover slip and a glass microscope slide, infra-red mapping methods such as contact method attenuated total reflectance IR (ATR-IR) are inappropriate as the Kofler melt is not directly accessible. Therefore confocal Raman microscopy was employed, which can be performed in a non-contact and confocal manner[118], in this study to investigate the spatial distribution of chemical and crystalline entities in a Kofler melt.

Raman spectroscopy/mapping is a well-established technique and is widely employed in many fields including pharmaceuticals[119,131]. It is typically used to provide information on the molecular nature of the sample by employing the spectral window 400 – 4000 cm^{-1}, which covers the energy range of intra-molecular vibrations. However by employing the lower energy phonon-mode bands (10 – 400 cm^{-1}), it is possible to probe the inter-molecular vibrations and thereby obtain detailed information about the solid-state characteristics of the sample, including polymorphism[132,133]. Phonon-mode data have recently been employed in generating Raman maps of spatially distributed polymorphs in molecular semiconductors[134], where they proved to be more sensitive to crystalline packing than the traditional intra-molecular bands.

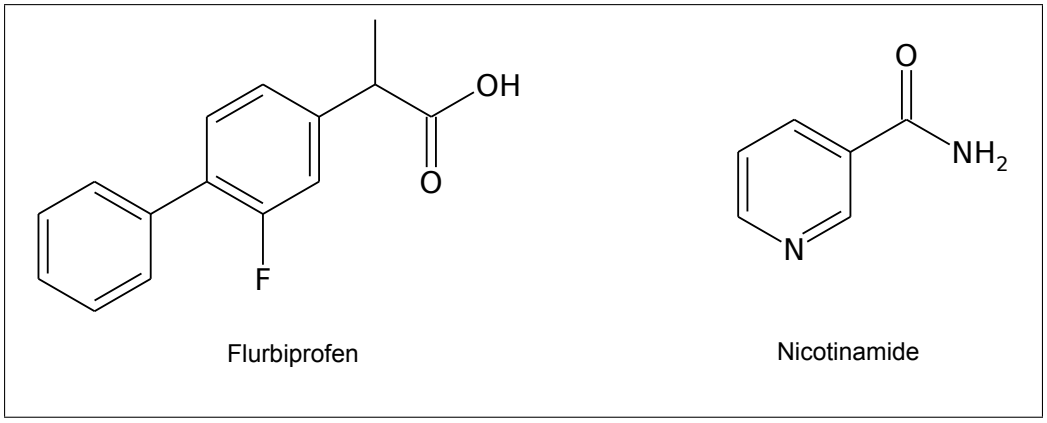

Figure 3.2: Schematic of chemical structure of flurbiprofen (left) and nicotinamide (right).

In the present study, confocal Raman spectroscopy/microscopy was employed to study the molecular and crystalline nature of a model Kofler melt system through both phonon-mode and intra-molecular bands. The study provides detailed insight into the applicability of the Kofler method for co-crystal screening and represents the first application of spectroscopic mapping method to a Kofler melt. The phonon-mode Raman data on the co-crystal are also the first example of the application of this emerging spectroscopic technique to characterising co-crystals.

The well-characterised model system flurbiprofen – nicotinamide, which was previously investigated by Berry *et al.* using standard hot-stage microscopy, was selected for this study. The characterisation in the Berry *et al.* study was based on standard hot-stage optical microscopy, which provided clear evidence for four separate phases in the FBP-NCT system; the co-crystal, FBP, and two NCT polymorphs[91]. Thus, the motivation was to use this system as a model in the spectroscopic mapping study. FBP is used as an active pharmaceutical ingredient and NCT is the co-crystallising agent. FBP **(fig 3.2, left)** possesses a carboxylated group in its structure while NCT **(fig 3.2, right)** has a pyridyl ring and amide group in its structure. Both groups allow NCT to serve as a complementary co-factor to FBP.

3.3 Experimental Section

3.3.1 Instruments

Raman spectral data were acquired using a LabRAM HR system (Horiba Jobin Yvon), a 600 lines/mm grating, a 532 nm laser source and a 50× objective lens and a Synapse thermo-electrically cooled CCD. Temperature control was achieved using a Linkam LTS350 hot-stage. The system was calibrated before acquiring measurements on a standard silicon, as well as the Rayleigh line. The silicon Raman peak was within ±1 pixel of 520.7 cm^{-1}. The grating was fixed to allow relatively rapid mapping, at the expense of a slightly restricted spectral range. Such combination improves the quality of data achieved through this instrument and allows for an access to the phonon-mode spectral window (30 – 400 cm^{-1}) as well as the higher wavenumber region (400 – 4000 cm^{-1}) which provides information on the traditional intra-molecular bands. Thereby, both the intramolecular and intermolecular spectral information could be obtained. The mapping was automated by an XY stage and set up to cover a grid of (1535 μm × 1619 μm) at 25 μm steps. 4030 Raman spectra were acquired based on an acquisition time of 3 sec/spectrum.

3.3.2 Materials

FBP and NCT were purchased from Sigma-Aldrich (Poole, UK) and were used as received. X-ray powder diffraction confirmed that they were of form I crystalline state when compared to patterns obtained from CSD (library Reference codes are "FLUBIP", and "NICOAM03", respectively)[135,136]. They were also found to melt as per literature by DSC (114.01 °C and 128.24 °C, respectively)[87,137].

3.3.3 Kofler Preparation

The process of Kofler melt preparation was carried out by placing a small amount of NCT on a glass microscopic slide under a coverslip. This was heated until melting occurred at around 130 °C, and then allowed to solidify. FBP was later placed at the opposite edge of the coverslip and melted at around 115 °C. Once melted, it was drawn by capillary action under the coverslip dissolving the juxtaposed part of the NCT. The temperature was slightly raised and the sample was held at which for 5 min. The whole preparation was then allowed to cool and kept at RT to solidify. All of these experiments were performed at room temperature. Therefore, the entire samples and the various interfaces identified are static.

As a pre-mapping procedure, Raman spectra were taken from the melted starting materials (FBP form I and NCT) and from their equimolar melted mixture. These Raman spectra were taken under the same conditions as for the Kofler preparation and therefore used as references. Raman spectra of the starting materials NCT and FBP form I, FBP form II, and co-crystal at the zone of mixing were acquired and used for assigning principal components' loadings to their original components.

3.3.4 Direct Classical Least Squares Analysis

Spectral data sets were subjected to baseline correction and mean normalization before carrying out DCLS analysis of the melted region. DCLS maps were generated by employing a limited number (n) of selected spectra to form a linear combination, which was then used to model all of the spectra in the Raman spectral image. The modelling is achieved through a best-fit methodology. The sum of the (n) components would not often be able to model 100% of a given spectral pixel in the image which is expressed by an error (ε) as shown **(eq 3.1)**. Both the molecular composition and

$$Y_{(v\times m)} = K \times X_{(c\times m)} + \varepsilon \tag{3.1}$$

Equation 3.1: Classical least square fitting model. Through this equation, a number of spectra (m) at a specific v-wavenumber of composition (c), arranged into Y matrix (v×m), are classified according to each representative spectrum (n) into a column of concentration matrix X (c×m) with a matrix of sensitivity K and an error of ε.

the crystalline form were of interest in a Kofler melt, and were investigated through employing the selected numbers (n) in particular spectral windows for the analysis. Setting n=2 would correspond to FBP and NCT molecules, whereas setting n=3 refers to the crystalline forms FBP, NCT, and a potential co-crystal. In addition to the number of spectra selection with which the DCLS model was created, there is also a choice of spectral window selection in which DCLS modeling was performed; in particular, the phonon-mode region (30 – 400 cm^{-1}), the molecular stretching region (400 – 1721.6 cm^{-1}), and the entire wavenumber region (30 – 1721.6 cm^{-1}).

3.3.5 Principal Component Analysis

Maps were also generated using PCA in the spectral regions mentioned previously in Matlab 7.6.0 (R2008a). Unlike DCLS which requires reference spectra for modeling experimental data, PCA predicts these models instead. PCA simplifies the data into sets of variables, which are linearly correlated with the original data. It characterises the variances in data by creating uncorrelated axes leading to transformation in the original coordinates. The axis that gives the highest variance between original data refers to the first score, the one with consequent variance is the following one, and so on[138]. Raman spectral profile data were split into individual spectra, baseline corrected under LabSpec 5 software and imported in text format into Matlab 7.6.0 (R2008a).

Each variable was divided by the standard deviation of its Raman spectrum, and all original data were mean normalized prior to PCA anal-

ysis. PCA scores were rescaled to represent their intensities and used afterwards to create red-green-blue (RGB) colour-map. Images areas with positive scores were assigned red derivative colour while negative ones were in blue. The first three principal components (PCs) were selected in this study having statistically significant values accounting for $> 93\%$ of variation. Loadings were compared with Raman spectra of NCT, FBP form I and II, and the spectrum extracted from the zone of mixing.

3.4 Results and Discussion

3.4.1 Kofler preparation

Several attempts were carried out in order to achieve the required Kofler preparation, involving the sample hold for a time above the eutectic temperature before being fully solidified. The formation of a suitable Kofler melt for later analysis was confirmed optically **(fig 3.3 a)**. The visual inspection shows clearly the existence of at least three crystalline phases in the Kofler melt, assigned as NCT, FBP, and co-crystal.

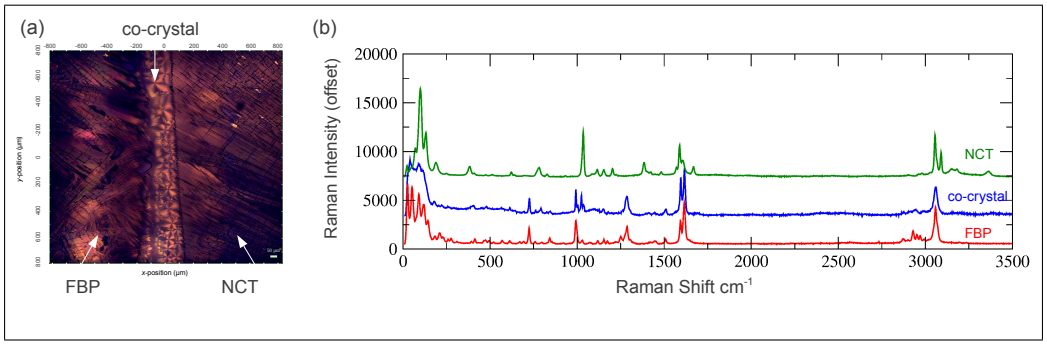

Figure 3.3: Fusion method preparation of FBP-NCT. Shown in (a) is Kofler preparation after cooling which includes in the peripheral regions, FBP (left) and NCT (right), and the zone of mixing at the centre in between, all are indicated by arrows, while (b) is Raman spectra extracted from the three optically distinct regions; NCT (green), co-crystal (blue), and FBP (red).

This was also chemically proven when investigating their Raman spectra acquired from the three optically different regions **(fig 3.3 b)**. Each of these spectra, referring to NCT, FBP, and co-crystal from Kofler preparation, was in a good agreement with the referenced samples prepared separately from a fusion procedure in which the composition gradient was not generated **(fig A.1)**.

3.4.2 Raman Mapping

Raman mapping of the NCT-FBP Kofler melt preparation was conducted following the optical and spectral confirmation of the preparation and its data were analysed by means of DCLS and PCA. For the DCLS analysis, a number (n) of representative spectra exhibiting similar features to the pure components were needed as an input for generation of the DCLS map. Such requirement was achieved by extracting spectra from the mapping data and comparing them to the reference samples of NCT, FBP and co-crystal prepared separately from the melt. **Fig 3.3 b** shows the possibility of using any of the spectra extracted from the three optically different regions as representative models. The point was made after confirming the similarity of extracted spectra to the referenced samples **(fig A.1, A.2)**.

Two (n) selections, n=2 and 3, were designated to probe the molecular and crystalline species, respectively. The selection n=2 refers to the starting (molecular) materials NCT and FBP, while n=3 alludes to the expected crystalline materials; the emerging phase (co-crystal) in addition to both crystalline starting materials.

In addition to the number of DCLS components selection and for the purpose of addressing the spatial distribution of molecular and crystalline entities, three selected spectral windows were employed in these analyses. The traditional intra-molecular spectral window (400 – 1721.6 cm^{-1}) is expected to be most sensitive to the molecular composition of the samples,

whereas the phonon-mode data (30 – 400 cm^{-1}) are expected to be more sensitive to the crystallographic nature of the samples. An analysis of the entire spectral range for comparison is also presented.

Direct Classical Least Square Analysis n=2:

Maps generated from a DCLS analysis with n=2 (i.e., maps achieved from reference spectra for NCT and FBP only) in the three spectral regions are indicated by two colours (green and red) along with their representative spectra as presented in **fig 3.4**. All three maps exhibit at least two well-defined regions which are separated by vertical boundaries **(fig 3.4**, top row**)**. The comparison of the optical image **(fig 3.3 a)** with the DCLS maps at n=2 indicates that the left-hand region in the DCLS maps corresponds to FBP plus co-crystal, and the right-hand to NCT only.

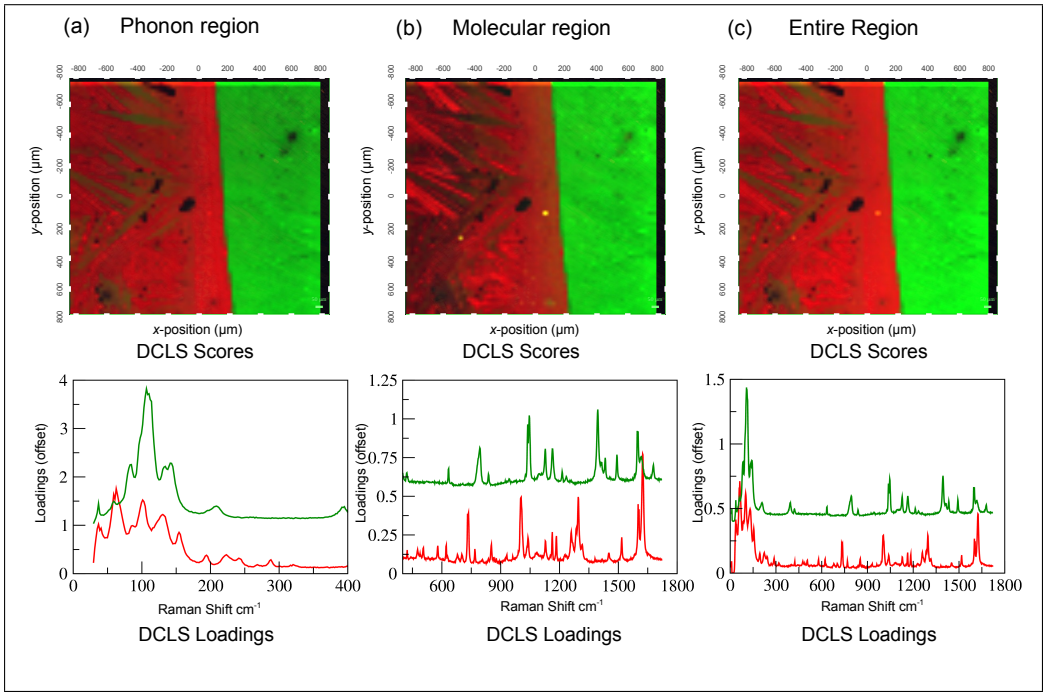

Figure 3.4: DCLS maps at two number of selection n=2. Two-component maps (scores and their corresponding models) are presented in three columns (a → c), each column consists of two rows (top row refers to scores while the bottom one is related to their corresponding models). Maps (scores & models) generated in the phonon-mode region 30 – 400 cm^{-1} are given in (a) column, the molecular region 400 – 1721.6 cm^{-1} in (b) column, and the entire spectral range in (c) column. The colours of scores and their models in the peripheral regions refer to the compositions of the higher (green) and lower melting components (red).

DCLS maps conducted at the three spectral regions are in general rather similar. However, some differences are apparent on closer inspection. For example, there is an evidence of a third region running vertically down the middle of the image in the map generated from the phonon-mode spectral window data **(fig 3.4 a)**, and to a lesser extent in the map generated from the molecular stretching and the entire spectral windows **(fig 3.4 b,c)**. This region corresponds to the co-crystal, which was again deducted from the comparison to the optical image in **(fig 3.3 a)**. Note that a reference spectrum for the co-crystal was not included into the input for map generation, and thus it is slightly surprising that the co-crystal can be identified from these maps.

In contrast to the phonon mode map, the co-crystal is not readily apparent from inspection of the map generated from the intra-molecular spectral range. Overall, for the n=2 DCLS map generation, the presence of the co-crystal is most clear in the phonon-mode data, and this is in accord with the phonon-mode data being more sensitive to the nature of the crystalline phase(s)[81,133].

Direct Classical Least Square Analysis n=3:

Similarly, DCLS maps were generated when n=3 using all spectral ranges (i.e., the input of spectra herein refers to FBP, co-crystal and NCT) **(fig 3.5)**. The three spectral ranges were similarly employed to generate separate maps **(fig 3.5 a,b,c)**. All three maps exhibit three distinct regions which correspond (from left to right) to FBP, co-crystal and NCT. Again the maps are similar in broad terms, but differences emerge on detailed inspection. In all three maps the interface co-crystal:NCT is very distinct, with the FBP:co-crystal interface being less discrete. This clearly indicates that the composition gradient is different in nature at these two interfaces. The FBP:co-crystal interface is less distinct in the map generated from

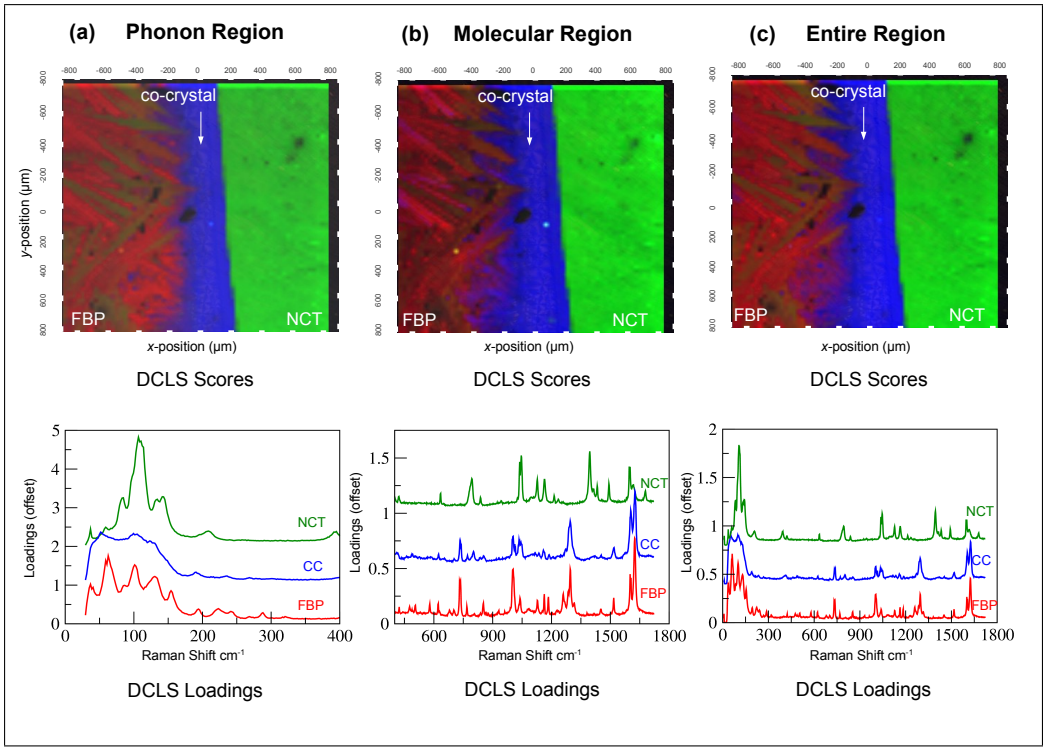

Figure 3.5: DCLS maps at three number of selection n=3. Three-component scores and their models are given in (a → c), each column consists of two rows (top row refers to scores while the bottom one is related to their corresponding models). Maps generated in the phonon-mode region 30 – 400 cm^{-1} are given in (a), the molecular stretching region 400 – 1721.6 cm^{-1} in (b), and the entire spectral range in (c). The colours of scores in the peripheral regions refer to the compositions of the higher and lower melting components (green and red, respectively) while the one at the zone of mixing (blue) refers to the co-crystal as shown also in their models.

the molecular data **(fig 3.5 b)** and the entire spectral region **(fig 3.5 c)** than in the phonon-mode data **(fig 3.5 a)**. The molecular conformation of FBP-NCT appears to be similar to those in both FBP and NCT unlike the differences in the holding intramolecular forces as manifested in the phonon region **(fig 3.5 a)**. The obvious interpretation of this is that the molecular composition gradient is relatively smooth, whereas the crystalline composition gradient is relatively sharp. This is expected for a Kofler melt, in which a molecular composition gradient is used to isolate a co-crystal of a particular composition. The co-crystal is expected only to form in a limited composition range, and the observed results are fully in accord with this.

Composition Gradient:

The differences in the nature of the interfaces in the FBP:co-crystal, and the co-crystal:NCT was commonly noticed in analyses generated for all spectral windows **(fig 3.5 a,b,c)**. This suggested the possibility of investigating the composition gradient across the Kofler melt preparation, an issue that has not been addressed in others' work[91,109,111]. **Fig 3.6** shows the averaged percentages of the existing components, taken from eight horizontal lines across the preparation, calculated from DCLS when n=3 at the phonon region, the molecular region, and the whole wavenumber window, respectively.

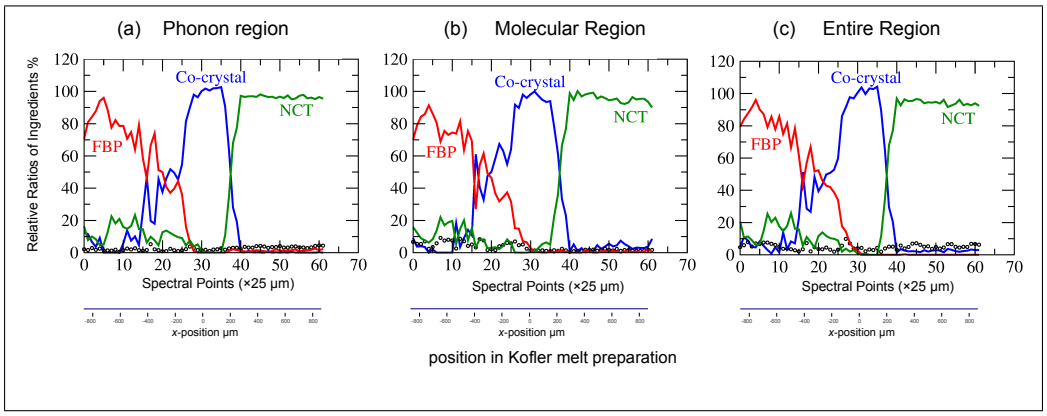

Figure 3.6: Composition gradient deduced from DCLS using three components selection n=3 in three spectral windows; phonon, molecular stretching and entire wavenumber region as shown in a, b, and c, respectively.

The relative amounts of material from such analysis do provide a good guide to the nature of the composition gradient if not the exact values of the composition. Analysis performed at the three spectral regions **(fig 3.6 a,b,c)** all show that the composition gradient of both starting components was not ideally linear, especially towards the higher-melting component (NCT). This is clearly noticed from the obvious sharp descent in NCT concentration and the sudden rise of co-crystal concentration. However, there is a gradual decrease/increase in components' concentration at the FBP/co-crystal interface. The reason for this can be deduced by considering the manner in which Kofler melt is prepared and studied. Conceptual perspective on such findings is proposed by taking into consideration the

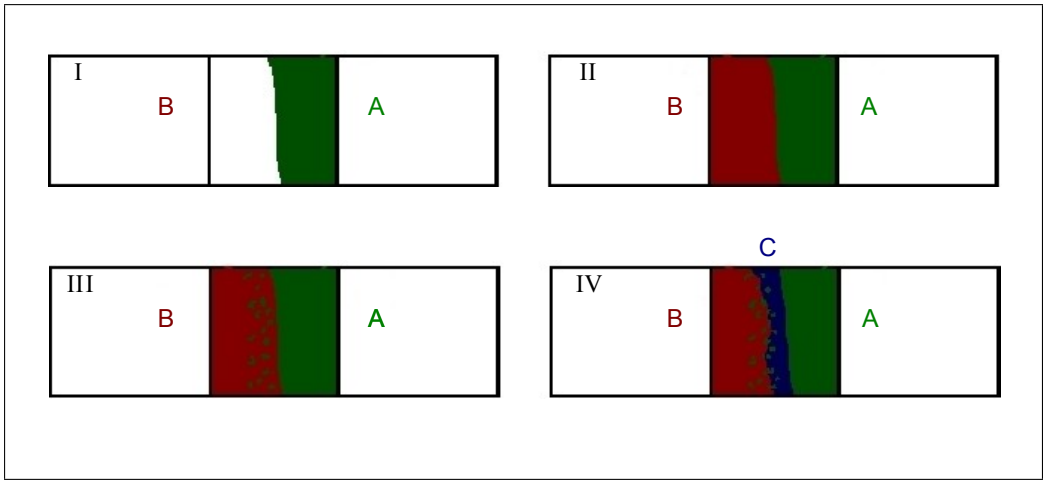

Figure 3.7: Schematic of proposed sequence of events in the formation of a Kofler melt in (I-IV). It shows the consequential steps for preparing Kofler sample, whereas the higher melting component is (A) shown in green, the lower melting component is (B) shown in red, and the co-crystal is (C) shown in blue.

sequential events of Kofler preparation **(fig 3.7 I-IV)**:

1. The highest melting material (NCT) was offset to one side, once it solidified after being melted **(fig 3.7 I)**;

2. Later on, the lower melting material (FBP) was melted when brought into contact with the juxtaposed part of the higher melting material (NCT) **(fig 3.7 II)**;

3. The lower melting material dissolved some solidified parts of the higher melting component (NCT) at the contact area, while the rest of parts remained inaccessible. This is analogous to the effect of tides on the seashore whereas the powerful sea waves erode only the facing coastal features, depositing the washed sands offshore **(fig 3.7 III)**. This phenomenon was clearly demonstrated from DCLS results, which revealed the discontinuity of the component distribution in NCT region. Thereby, the higher melting component forms an area with a very distinct border at the interface with the zone of mixing.

4. Finally, the higher melting material (NCT) portions already dissolved to saturation point in the liquefied lower melting component (FBP),

would crystallise forming a stripe of co-crystals along the contact area. Some detached NCT particles and unsolidified co-crystal might diffuse in the lower melting material (FBP), depending on how fast the lower melting component crystallises **(fig 3.7 IV)**.

The obviously different nature of the two interfaces observed in this work, refines the traditional vision of a linear composition gradient in Kofler preparation. Such results **(fig 3.6)** unambiguously demonstrate that a linear composition gradient does not form, and indeed on detailed consideration of the process of forming a Kofler melt, it is not expected to form. This is illustrated schematically in **fig 3.7**, in which the traditional vision of the Kofler melt preparation.

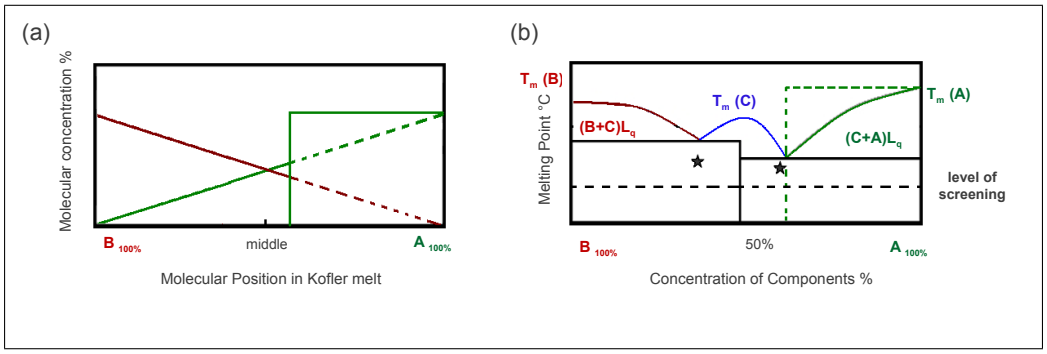

Figure 3.8: Schematics of new perspective about ingredient's position in Kofler melt preparation and its binary phase diagram. (a) is the plot of molecular fraction *vs* its position in Kofler melt slide, while (b) is the binary phase-diagram of the co-crystal formation. The temperature in the phase diagram is plotted *vs* the molar fractions of components (A and B, the higher and lower melting components, respectively while C is the co-crystal). The intersection occurs in a sharp form only in the melting component section (intermittent green line).

It shows the direct interface of the higher melting point solid with the rest of the preparation, instead of a linear composition gradient causing to a sharp change in the composition. This finding has important implications for the use of the Kofler melt as a screening method for co-crystal formation. In particular, the step change in the composition of the preparation by the highest melting component will restrict access to this part of the phase diagram (**fig 3.8**, intermittent line). Thus, any potential co-crystals

with compositions rich in the highest-melting component may not be experimentally accessible. The composition range which is rendered inaccessible will depend on a number of factors, the most important of which is likely to be the amount of time spent by the lower-melting liquid in contact with the higher-melting solid. The longer this time is, the more the chance is for the higher melting solid to dissolve into the lower melting liquid, and the more likely for the sharp change in composition at the interface to be reduced. Thus, DCLS findings represent an important step forwards in understanding the crystal growth in Kofler melts, which would be difficult to quantify without the use of Raman microscopy technique.

Principal Component Analysis:

Finally, the principal component analysis was the second chemometric method employed for Raman mapping analysis. Such an approach derives a number of independent linear combined variables that has sufficient information about the original chemical data without the interference of operators or the requirement for referenced spectra to model hyperspectral data on.

The first three principal components were selected for this study **(fig A.3)**, whose scores were heavily loaded by the presence of compounds in the three optically different regions, as shown in **fig 3.9**. These components displayed a homogeneous distribution of pure composition in the higher melting region, which forms a very distinct boundary once reaching the zone of mixing. In contrast to the higher melting region, PCA results highlighted the non-uniformity in the distribution of components in the lowest melting region and its unclear boundary with the zone of mixing region.* The homogeneous composition in the higher melting region was clearly confirmed by studying the first principal component (PC1) **(fig 3.9 a, scores)**. The

* PCA scores of the first three components were used to create red-green-blue (RGB) colour-map **(fig A.4)**, which shows similar feature to DCLS outcomes at n=3.

figure shows that PC1 was positively weighted only by NCT **(fig 3.9 a, loadings)**. Alternatively, the lower melting region displayed heterogeneity in components' composition. Such an issue was proven by investigating PCs' loadings. **Fig 3.9 b,c** show that components' weight on PC2 and PC3 refer to both FBP and co-crystal.

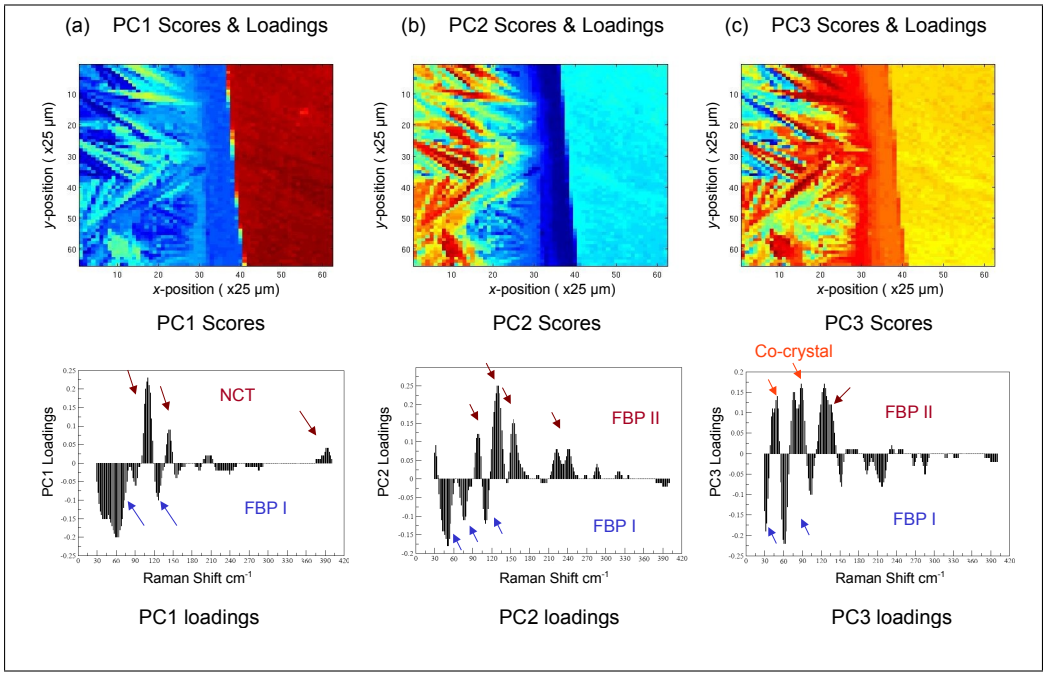

Figure 3.9: PCA analysis results. The first three PCs' scores and their corresponding loadings are shown in a, b, and c. Scores are in top row while bottom one refers to their corresponding loadings. Loadings comparability to Raman spectra of NCT, co-crystal, FBP I, and FBP II was checked in **Fig A.5**.

However, PCA loadings exhibited some positive weights specifically on PC2 which did not initially match with any of the referenced spectra **(fig A.5)**. These loadings, occurring strongly in the left-hand side of the images and do not correspond to FBP form I, alerted to the likelihood of polymorphism of this component. In this context, three different polymorphs of FBP have been reported in the literature; form I is the most stable form, form II could be induced by heteronucleation approaches with polymers and it could also be prepared from seed solutions. However, it is less stable than form I as it transforms to form I at around 90° C. The third form is the least stable, although it is stable between a slide and a coverslip. Moreover, it has been reported that the three forms can be simultaneously

crystallised from melt-quenched FBP form I.[87,139,140] **Fig A.6** confirms the similarity of reference spectra for FBP forms I and II* to those extracted from two different pixels in the Kofler melt preparation. It clearly indicates that polymorphism of FBP does indeed occur in prepared Kofler system.

Thus, PCA analysis was an effective exploratory tool for data interpretation especially when compared to DCLS. It revealed unexpectedly to the presence of polymorphism in FBP, which has not been noticed in DCLS approaches. The apparent lack of DCLS selectivity to the polymorphism of FBP is in fact purely an operator issue as the input of spectra for the two polymorphs of FBP into the DCLS map generation was not included, as such observation was not expected to occur.

With the benefit of hindsight, even the optical image **(fig 3.3 a)** presents some evidence of FBP polymorphism through the lower visual homogeneity of the FBP than the NCT, although this lower visual homogeneity is easy to mistake for larger differences in crystal habit and orientation when compared to NCT. Although NCT is well known to exhibit polymorphism[91], no evidence for the presence of more than one crystalline form of this molecule in such work was observed.

Overall, both multivariate approaches used in this study were invaluable. DCLS analysis was beneficial for yielding quantitative information. However, this needs to be preceded by a knowledge of all existent forms, which is not required for PCA analysis. Thus, both chemometric techniques yielded advantageous interpretation of the hyperspectral data as they could be served to quantify and characterise all crystal forms in the model Kofler melt.

*The single crystal structure of FBP form II was achieved in an attempt to prepare FBP-NCT co-crystal from solution **(fig A.7)**.

3.5 Conclusion

The work presented herein **(chap 3)** outlines the first use of confocal Raman microscopy to characterise Kofler melt preparations. This was shown to be valuable in generating detailed information on the investigated phases and providing qualitative information about the newly formed phases (co-crystal and component's polymorphs).

Detailed quantitative and qualitative information from Raman mapping were achieved with the use of chemometric approaches. In this work, two chemometric methods (DCLS and PCA) were explored to investigate the spatial distribution of the components, and restricted spectral ranges were employed to characterise the molecular and crystalline natures of the Kofler preparation.

The use of DCLS analysis provided a new perspective regarding the composition gradient present in Kofler melt preparations. It was shown that the composition gradient is not linear as a function of position as had been assumed until now. Rather, a sharp interface exists at the interface of the highest melting component and the co-crystal. This sharp interface restricts access to the binary phase diagram in Kofler preparation at compositions rich in the highest melting component. It is now advisable, according to work observation, to leave Kofler preparation as long as possible at high temperatures over the melting point of both components in order to allow the highest melting solid to dissolve in the liquid of the lower melting component, and thus to reduce as far as possible the inaccessible region of the binary phase diagram. In contrast to DCLS, PCA has not only confirmed the distribution of components but also revealed the presence of both FBP polymorphic forms (form I and II), which had not been deduced from the traditional method of optical observation nor from DCLS modelling.

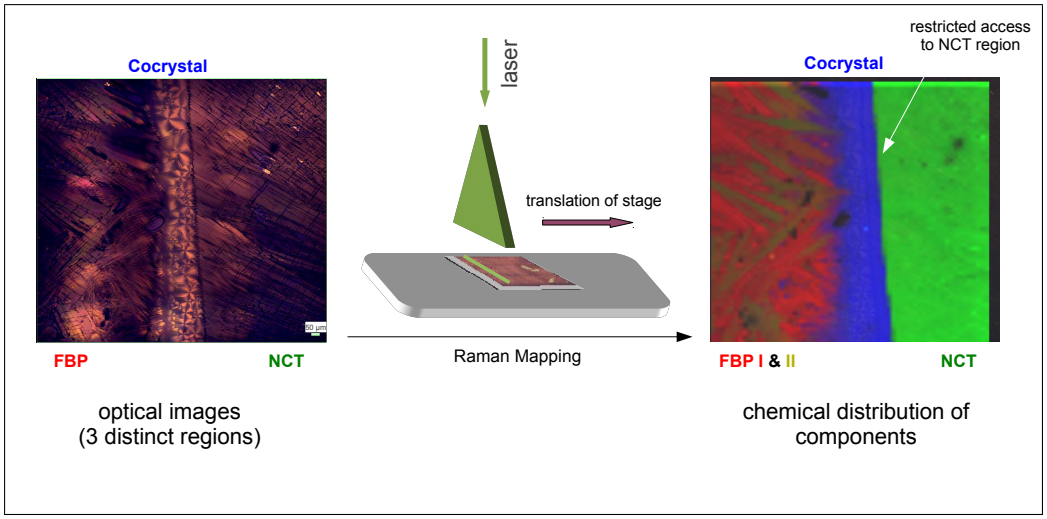

Figure 3.10: Conclusion figure of Kofler melt system.

It is also worth mentioning the sensitivity of screening with respect to the crystalline components which was strongly enhanced by considering the phonon-mode data (30 – 400 cm^{-1}). Raman screening at this region is a highly promising method for investigating *in-situ* crystallisation, polymorphs, co-crystals and solid dosage forms. This is attributed to its significant sensitivity in probing the crystalline structure of molecular compounds.

In conclusion, the use of Raman mapping was advantageous for investigating the nature and composition of phases in Kofler preparation which was nearly impossible in the past. From this work, coupling the hot-stage with Raman microscopy provides new insight into the use of Kofler method to screen co-crystal formation and investigate the composition of ingredients **(fig 3.10)**.

CHAPTER 4

The Study of FBP-NCT Co-crystal Polymorphism

4.1 Abstract

Previous Raman microspectroscopic studies of FBP-NCT Kofler preparation showed the emergence of different crystalline phases of FBP-NCT co-crystal along the zone of mixing over a time of RT storage. Thereupon, the aim was to build a clearer understanding of the solid-state behaviour of FBP-NCT co-crystal, and more specifically investigating the potential presence of FBP-NCT co-crystal polymorphs. Polymorphic screening, in this chapter, was accomplished using classical thermal methods (differential scanning calorimetry and the hot-stage microscopy), and parametric analytical techniques whereby Raman and x-ray diffraction data were collected as a function of temperature (VT-Raman and VT-XRPD experiments). Studies were also supported by the crystal structure of FBP-NCT. The single crystal were grown from a supersaturated solution of solvent-drop ground product of 1:1 FBP-NCT.

4.2 Introduction

Co-crystals have recently gained a great deal of attention in the pharmaceutical context[32,51]. They represent the latest approach in the solid-state field to modify the physicochemical and mechanical properties of single-component materials. Such properties i.e., solubility, stability, hygroscopicity, morphology and flowability, are a matter of importance in the drug development and delivery fields[22,24,26,27,29,69–71,141–145]. The modification of such properties can be achieved by linking the API with various co-crystal formers through non-covalent bonds. Such linkage yields multicomponent systems of specific stoichiometric ratio of interactions and packing forms[48]. The type and the right ratio of interactions, which are mostly dependent on the interaction between complementary functional groups and the structural arrangements of final compound, play an important role in achieving a pharmaceutical co-crystal of the desired properties.

The issue of understanding the right ratio of interactions and the favoured form of crystallisation become a subject of recent interest[107,146,147]. These aspects have been invested to widen the scope of achieving a product with the desired properties; not only by varying co-crystal formers but by investigating the potential polymorphic forms of the API-cocrystal agent[34,51,68,148,149]. However, such diversity in the solid-state forms the API-cocrystal agent can be a hindrance in the drug production and formulation processes if it is uncontrolled i.e., the simultaneous presence of co-crystal polymorphic forms in the final pharmaceutical product. Thus, a sufficient understanding of the potential forms in multicomponent systems, their stability and the transformation process should be built up during the development & manufacturing process[28,123,150–152]. These prospects are important for setting up controlled strategies to achieve co-crystals with the desired drug properties either in their novel or patented forms[153].

Most polymorphic studies were related to single component systems[154,155], however few studies have been very recently employed on molecular complexes such as co-crystal systems[31,134,156–158]. Within the field of polymorphic co-crystals, few researchers showed the feasibility to control the formation and the interconversion between forms using various techniques such as liquid assistant grinding[30,46,99,158–164]. However, very limited work illustrated the usage of thermal techniques coupled with spectroscopic and crystallographic screening to probe the conversion between polymorphic co-crystal forms[116,161,165,166].

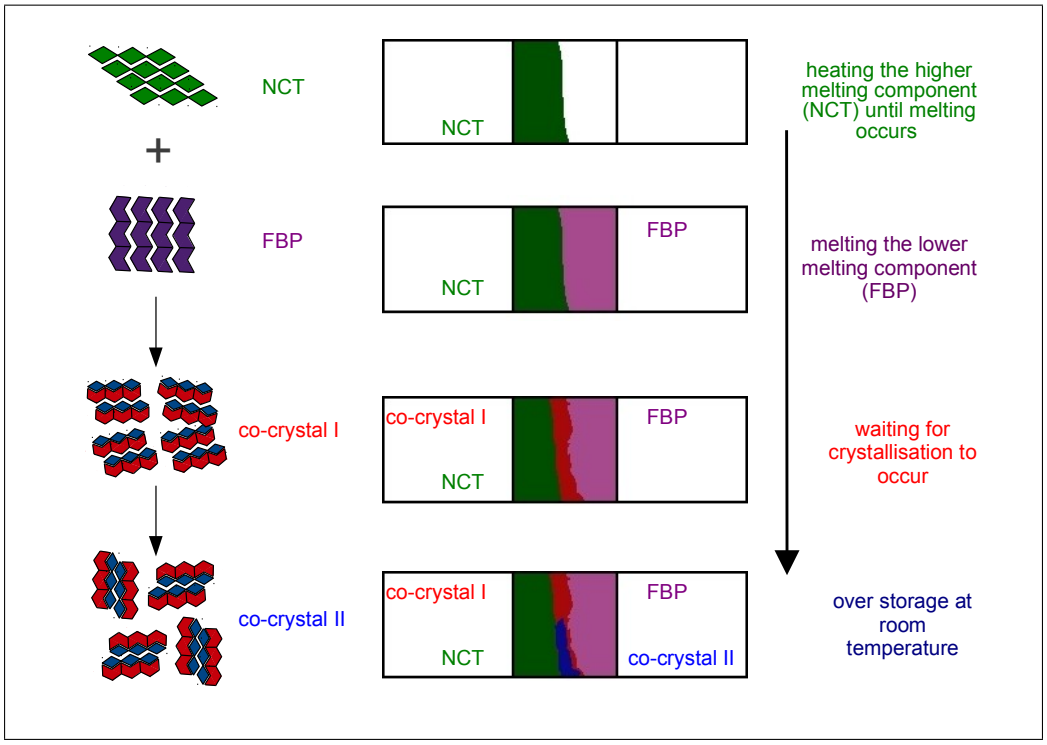

Figure 4.1: Schematic of FBP-NCT Kofler system; co-crystal formation and transformation.

The work presented in this chapter was motivated by an observation of co-existent forms of FBP-NCT co-crystal previously prepared using Kofler method **(fig 4.1)**. Thereby as a part of continuing previous study **(chap 3)** on a model co-crystal system FBP-NCT, a full investigation was performed to characterise FBP-NCT co-crystal polymorphs. Polymorphic screening involved using thermal techniques (DSC and HSM), spectroscopic (Raman spectroscopy), and crystallographic (XRPD) studies. Raman and XRPD

parametric measurements were performed as a function of temperature, and the resulting data were analysed by means of chemometrics (PCA). Finally, the crystal structure of FBP-NCT co-crystal was calculated based on single crystals which were grown in acetonitrile solution.

4.3 Materials and Methods

Materials FBP and NCT were purchased from Sigma-Aldrich (Poole, UK) and used as received. They were confirmed to be of form I crystalline state from XRPD[135,136]. Differential scanning calorimetric scans confirmed their melts to be as in literature (113.55 °C and 128.14 °C, respectively **fig B.3**)[87,137]. The analytical grade acetonitrile solvent (ACN) was supplied by Fisher Scientific (Loughborough, Leicestershire, UK).

4.3.1 Conventional Thermal Screening

DSC Studies:

The thermal behaviour of the starting materials and 1:1 FBP-NCT co-crystal was achieved using DSC Q2000 (TA Instruments, Crawley, West Sussex, UK). Instrumental calibration in relation to the enthalpy and melting temperature were performed on indium, while the heat capacity was calibrated against sapphire.

In the current work, samples of 3 to 4 mg were encapsulated in non-hermetic aluminium T-zero pans. A standard DSC method was adopted, in which samples were heated from 20 °C until 150 °C at a heating rate of 1 °C/min. They were afterwards allowed to cool at room temperature for 24 hours before being reheated again at similar rate. In addition to that, a thermal DSC scanning starting from -35 °C until 150 °C at a heating rate of 1 °C/min was also performed on FBP:NCT melted sample quenched at -35 °C.

Moreover, a modulated DSC method was employed whereas temperature points were oscillated at an amplitude of ± 0.5 °C each 40 sec and the underlying heating rate was set at 1 °C/min. Melted samples were allowed to cool slowly to RT before they were reheated starting from 20 °C until 150 °C.

A series of 13 physical mixed samples of FBP:NCT were used for phase diagram construction. Mixtures were prepared at different mixing molar ratios (0, $\frac{1}{12}$, $\frac{1}{6}$, $\frac{1}{4}$, $\frac{1}{3}$, $\frac{5}{12}$, $\frac{1}{2}$, $\frac{7}{12}$, $\frac{1}{3}$, $\frac{3}{4}$, $\frac{5}{6}$, $\frac{11}{12}$, 1) and screened using DSC. Mixture samples were melted and then allowed to cool at RT for 24 hours after which heating ramps were conducted as previously mentioned in the standard DSC method starting from 20 to 150 °C at a heating rate of 1 °C/min.

HSM Studies:

Thermoscopic investigation on FBP-NCT co-crystal was also observed using PriorLuxMET optical polarised hot-stage microscope (PriorLuxMET, Prior Scientific, Fulbourn, Cambridge, UK), equipped with a Linkam DSC600 heating–freezing stage. The latter is controlled by T95-Linksys temperature programmer and Linksys32 software (Linkam Scientific Instruments Ltd., Tadworth, UK).

FBP-NCT samples were focused through magnifications 4× and 10×. Microscopic images were collected, through CCD camera attached to the microscope, each 2 sec time intervals, using image capture software which is built within Linksys32 package. Thermal scanning profile was set to heat quenched melted 1:1, FBP:NCT over a temperature range of 20 → 130 °C at a 1 °C/min heating rate.

4.3.2 Raman Spectroscopic Screening

A LabRAM HR from HORIBA Jobin Yvon (Villeneuve d'Ascq, France) was exploited to collect Raman spectra from the starting materials and co-crystal preparations. Samples were illuminated using diode-pumped solid-state (DPSS) laser at 532 nm. They were scanned over a spectral range of 20 – 3500 cm^{-1}. Raman

spectra were acquired through an objective of 50× magnification based on an acquisition time of 4 sec per spectrum. Signals were dispersed through grating 600 lines/mm and detected by CCD detector. The Raman system was calibrated before acquiring measurements on a standard silicon (Si) sample after adjusting spectrograph zero position. Raman data were acquired and analysed through LabSpec 5 software.

The LabRAM HR is also supplemented with a XY manual cooling/heating stage (Linkam LTS350) with TMS94 temperature controlling programmer and LNP94 cooling system. These accessories were provided by Linkam Scientific Instruments Ltd (Surrey, UK) and allow for the use of variable temperature (VT)-Raman experiment. VT-Raman experiment was performed on a melted equimolar physical mixture of FBP-NCT. Spectra were collected each 1 °C while heating the sample at a rate of 1 °C/min from -40 → 150 °C. Raman spectra were also acquired through a 50× objective but with an acquisition time of 2 sec/spectrum. Laser focusing was achieved by optimising the intensity of peaks over a range of 1500 - 1600 cm^{-1}. The resulting VT-Raman data were analysed by means of PCA using separate free package designed by the R Foundation for Statistical Computing, R version 2.15.0.

4.3.3 X-ray Diffraction Screening

A Bruker D8 Advance powder diffractometer (Bruker AXS LTD., Coventry, UK) was utilised to collect powder patterns in a Debye-Scherrer geometry. X-ray radiation was generated inside a ceramic X-ray tube from an anode made of copper Cu in Kα_1 spectral line at wavelength λ=1.54059 Å. The diffractometer is equipped with a scintillation detector and Bruker Kristalloflex generator set on a voltage of 40 kV and a current of 40 mA. Samples were loaded in borosilicate glass capillary tubes BGCT with 0.7 mm bore diameters, supplied by CTS Capillary Tube Supplies Ltd UK, and mounted on the goniometer in a preferred orientation. Samples were scanned within 2θ (5 to 45°) at a 0.25 sec/step speed in an increment of 0.0179°. DIFFRACplus software package version 2.3 was used for data acquisition.

The Bruker D8 Advance is provided with a heating-cooling system Cryostream Plus. (Oxford Cryosystems Ltd., Long Hanborough, Oxford, UK), controlled by a Cryopad PC programme for the use of variable temperature x-ray powder diffraction (VT-XRPD) scans. VT-XRPD scans were set as previously mentioned, whereas samples were scanned within 2θ from 5 to 45° at a 0.25 sec/step speed in an increment of 0.0179°, and patterns were acquired each 3 °C from heated samples at a rate of 1 °C/min within the range of 20 → 130 °C.

Single X-ray structure determination:

Single crystals suitable for X-ray structure determination were achieved from solvent screening experiment, where 50 mg of liquid assisted ground FBP-NCT co-crystals were dissolved in 3 ml of acetonitrile (ACN) and left for slow evaporation. A suitable crystal was mounted on Bruker Nonius Smart Apex CCD diffractometer (Bruker AXS LTD., Coventry, UK). X-ray radiation was generated inside a ceramic x-ray tube from an anode made of Mo in Kα spectral line at wavelength λ=0.71073 Å. The diffractometer is equipped with a Bruker Kristalloflex generator set on a voltage of 50 kV and a current of 40 mA, a graphite monochromator, and an Oxford Cryosystem Cryostream (Oxford Cryosystems Ltd., Long Hanborough, Oxford, UK). SMART software was used for collecting frames, indexing reflections, and determining lattice parameters. SAINT programme was used for integration of reflections intensity and scaling. Absorption correction was done in SADABS programme, and SHELXTL software was used for space group determination, structure solution, and least-squares refinements. Structures were solved by direct methods, and non-hydrogen atoms were refined anisotropically. Hydrogen atoms of O−H group were refined from difference fourier maps. Other hydrogen atoms C−H were generated geometrically and allowed to ride on the bound heavy atoms[167].

4.4 Results and Discussion

Kofler preparation of FBP-NCT model system previously screened using Raman mapping technique, showed the formation of co-crystal at the zone of mixing. This was confirmed to be optically and chemically different from parent components (FBP and NCT) **(fig B.1)**[168]. On a prolonged storage at ambient condition, a morphological change in the compound along the middle region was observed; more specifically another phase formed gradually along this region **(fig 4.2)**.

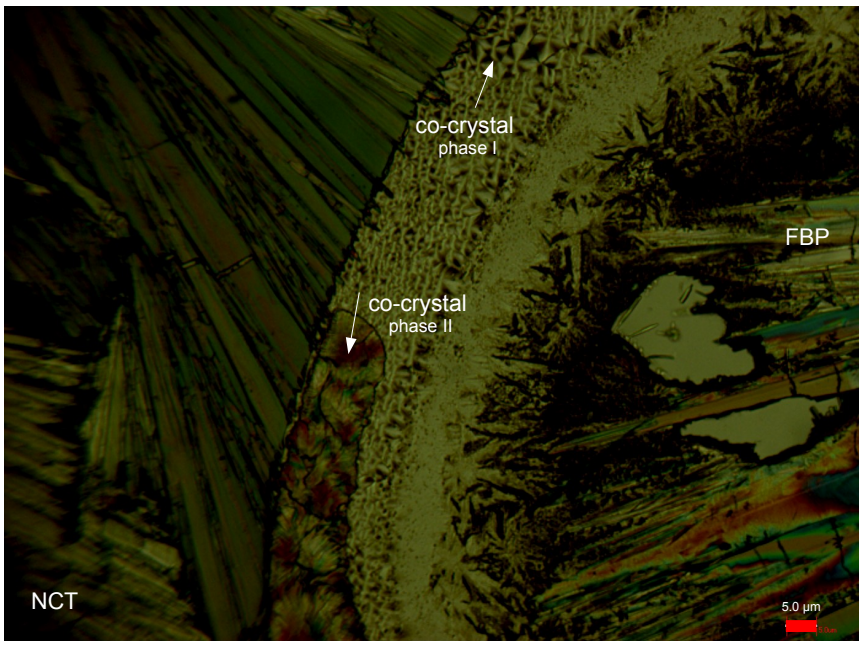

Figure 4.2: Hot-stage microscopic image of FBP-NCT Kofler preparation after a time of storage. Kofler preparation, which originally includes NCT (left) and FBP (right) and the zone of mixing in between (spherulites of co-crystal phase I), showed after a prolonged time of storage another phase (co-crystal phase II) gradually growing in a bottom-top manner along the zone of mixing.

Following such observation, Raman mapping of this preparation was conducted in order to generate a detailed information about formed phases along the zone of mixing. The resulting Raman data were analysed using DCLS analysis* when n=5 **(fig 4.3 a)**. The analysis showed five regions in this preparation corre-

*Similar analysis was performed on FBP-NCT Kofler preparation **(chap 3)** which revealed a distinct distribution of three components within the preparation (FBP, co-crystal, and NCT).

sponding to NCT (left-handed side, green), both FBP forms (I & II) (right-handed side, purple and yellow, respectively), and another region running vertically up the zone of mixing (blue) in addition to co-crystal form I (red). Single Raman spectra were acquired from both morphologically different regions along the zone of

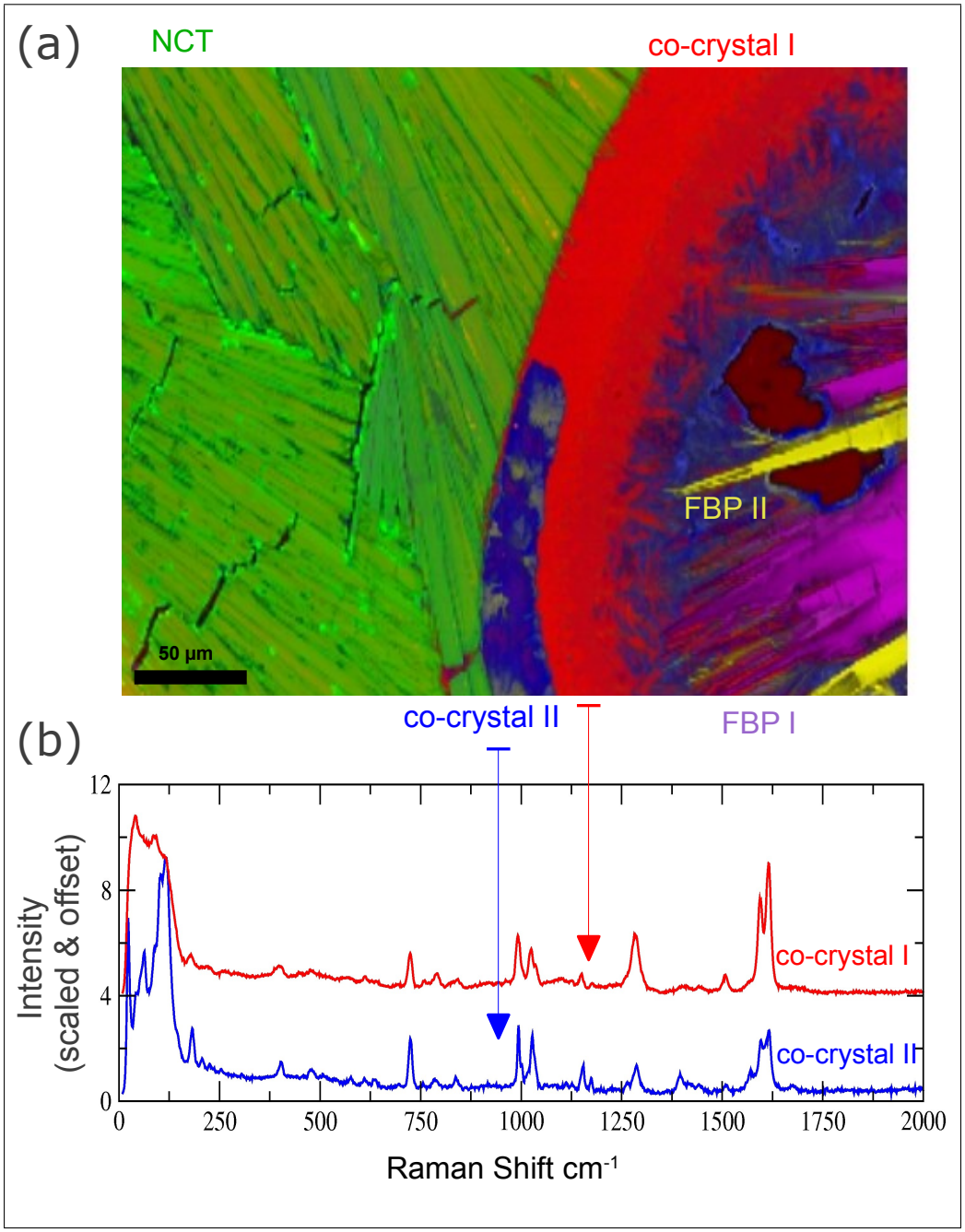

Figure 4.3: Raman spectroscopic analysis of FBP-NCT Kofler preparation over-time of storage using DCLS method (a). The analysis showed the distribution of NCT (green), FBP form I (purple), FBP form II (yellow), and co-crystal form I&II in (red and blue, respectively). The image is accompanied by single Raman spectra acquired from two morphological different regions in the zone of mixing (b); co-crystal form I (red) and co-crystal form II (blue).

mixing **(fig 4.3 b)**. Both spectra confirmed their comparability in the molecular vibrational region but not in the intra-molecular phonon region, which indicated to the likelihood of having polymorphic forms of FBP-NCT co-crystal.

Therefore, the study along the course of this chapter was carried out to investigate the potential of having FBP-NCT co-crystal of different crystalline structures. However, before subjecting FBP-NCT co-crystal to polymorphic screening study, a sensible discussion regarding the stoichiometric ratio of interactions between parent components (FBP and NCT) is worth mentioning. Despite the fact that it is difficult to predict the accurate interaction between synthons, one can estimate the possibility of various interaction between moieties based on the information stored in CSD[169].

From a supramolecular perspective under the crystal engineering protocols for co-crystal formation[45], the interaction between the starting components of co-crystals is facilitated by their complementary functional groups[44,170]. In FBP:NCT case, NCT molecule has got two potential hydrogen-bonding sites (pyridyl and amide groups), while FBP has got one site (carboxylic acid group).

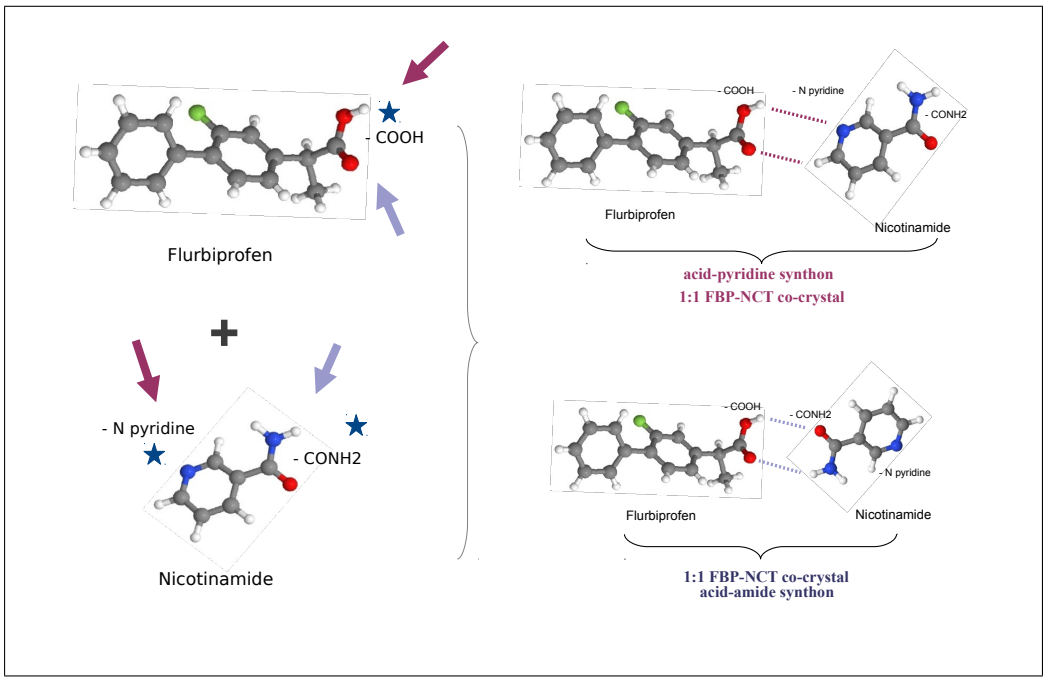

Figure 4.4: Schematic of possible interaction between co-crystal parent components. The structures of supramolecular synthons of FBP-NCT co-crystals with 1:1 stoichiometric ratios were expected to be held; *via* acid-pyridine interaction (a), or *via* acid-amide interaction (b).

The presence of such groups might lead to the formation of two molecular complexes; acid-pyridine FBP-NCT or acid-amide FBP-NCT synthons which in either way can lead to the forming of FBP-NCT co-crystals of 1:1 **(fig 4.4)**. This can also lead the formation of co-crystal at 2:1 molar ratio if both synthons share in holding the interaction between FBP and NCT **(fig B.2)**. Therefore, the possibility of getting different synthons of FBP-NCT co-crystals interacting into two molecular ratios (1:1 or 2:1) exist.

4.4.1 Classical Thermal Studies

DSC Study of FBP-NCT Binary Phase Diagram:

In order to investigate the assumption regarding the stoichiometric ratio of interaction, the binary phase diagram of FBP-NCT was constructed based on fusion method. Starting from the parent components, 13 physical mixtures of both NCT and FBP mixed at different stoichiometric ratios (0, $\frac{1}{12}$, $\frac{1}{6}$, $\frac{1}{4}$, $\frac{1}{3}$, $\frac{5}{12}$, $\frac{1}{2}$, $\frac{7}{12}$, $\frac{1}{3}$, $\frac{3}{4}$, $\frac{5}{6}$, $\frac{11}{12}$, 1), were fused using DSC technique. The changes in the properties of FBP:NCT mixtures as a function of temperature were observed from their first DSC thermal traces which were looked at in order to extract the melting temperatures of corresponding mixtures. Both sets of temperatures (melting temperatures extracted from 2^{nd} DSC scans) were plotted against the molecular ratio of NCT **(fig 4.5)**.

The basic feature in phase diagram should show a decrease in the melting points of either components when both components co-exist as a mixture. This decrease in temperatures last until both components eventually meet at the lowest temperature forming the eutectic mixture. If the latter mixture, which is formed at a specific ratio of mixing, is capable of recrystallisation in a co-crystal phase, then such formation leads to a humped-shape curve emerging from between the melting curves of the starting materials. This new curve refer to the melting points of the new compound (molecular complexes) in the presence of melted mixtures of the starting material at different compositions[42,109]. It is apparent based on that to realise that the formation of FBP-NCT co-crystals from the melt occurs at an

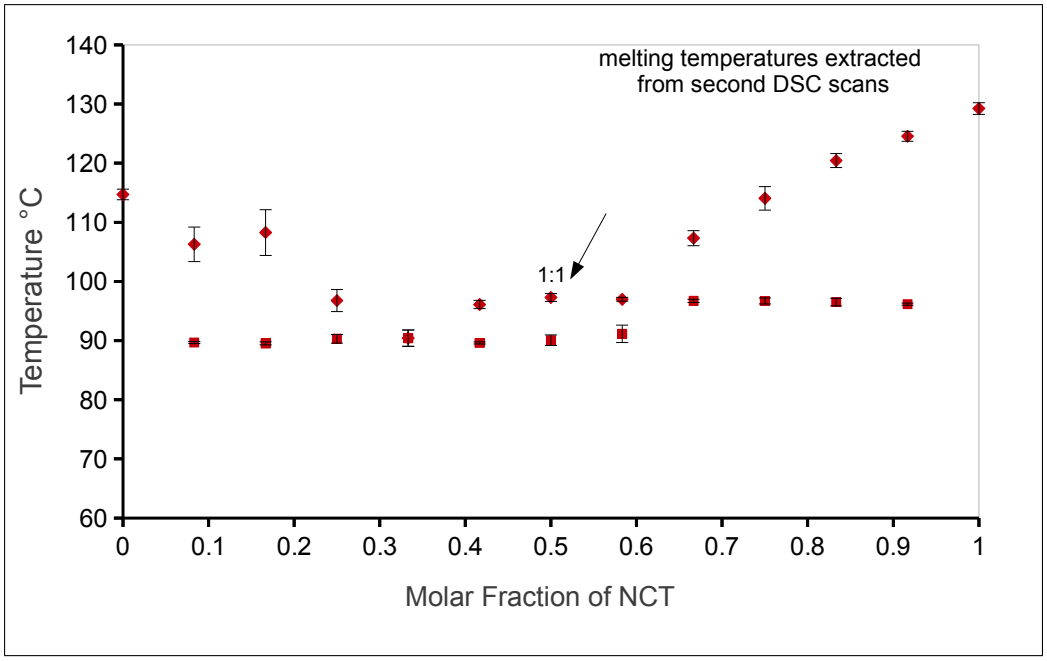

Figure 4.5: Binary phase diagram of FBP-NCT. It shows the potential formation of co-crystal at a ratio of 1:1 (50%), whereas the melting temperatures were extracted from the second DSC scans of melting both FBP and NCT at different molecular ratios.

equimolar ratio of the starting materials only **(fig 4.5, arrow)**. Therefore, the chance of having co-crystal at 2:1 molar ratio of FBP-NCT was excluded and the emphasis was rather to tackle the presence of co-crystal polymorph at 1:1 molar ratio.*

DSC Polymorphic Study of 1:1, FBP-NCT Co-crystal:

Based on the constructed binary phase diagram of FBP:NCT **(fig 4.5)**, only the equimolar physical mixture of FBP and NCT was taken forward for further polymorphism investigation. So to start with, FBP-NCT co-crystal was formed by fusing both FBP and NCT at an equimolar ratio of mixing. The first thermal scanning of both FBP and NCT, 1:1 using standard DSC procedure is shown in **fig 4.6 a**. DSC trace showed two endothermic events; a major one occurred at 97.10 °C, preceded by a small trace of another endothermal event at 89.45 °C **(fig**

*The polymorphism of FBP can complicate the shape of the binary phase diagram of FBP:NCT and mislead the judgements about the right ratio of co-crystal formation using fusion method. For instance, a small portion of phase diagram on left-handed side of **fig 4.5** indicated falsely to co-crystal formation at a ratio of 6:1, FBP:NCT, which is not typical when looking at the structure of FBP and NCT.

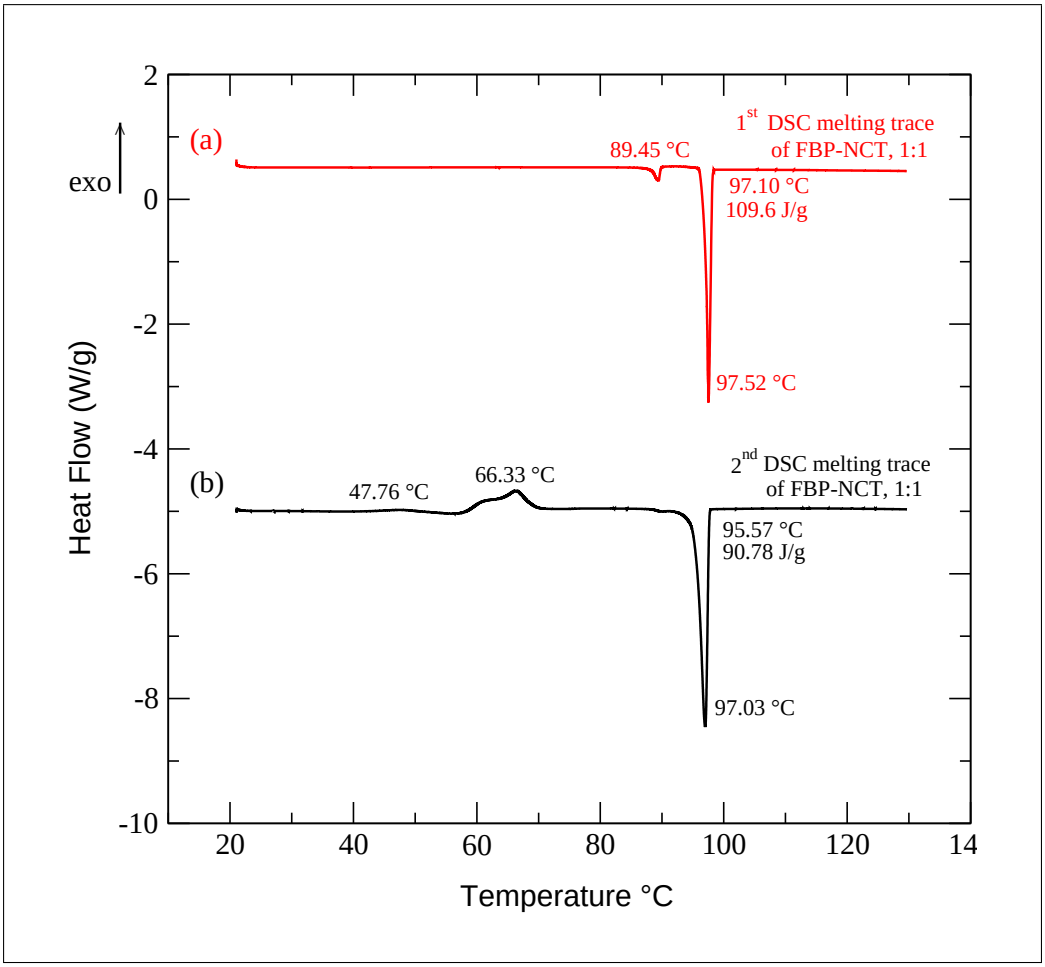

Figure 4.6: DSC scans of 1:1 FBP-NCT physical mixtures. It shows two endothermic events at 89.45 °C and 97.10 °C in (a). Re-heating scan of previously melted FBP:NCT mixture exhibited two exothermic events; one at 47.76 °C and another complex event at (57 to 66 °C), followed by a sharp melting at 95.57 °C as shown in (b).

4.6 a). These melting events were varied from the melting points of the starting materials; 128.17 °C and 113.55 °C of NCT and FBP, respectively **(fig B.3)**.

Thermal re-scanning of 1:1 melted FBP:NCT, which was allowed to cool slowly to RT, was performed to check the reliability of previous observations. The resulting trace **(fig 4.6, b)** showed this time a shallow exothermic one at about 47.76 °C most likely referring to crystallisation event, followed by another complex exothermic event at 66.33 °C, ended by a melting at 95.57 °C.* From the standard DSC procedure, melted FBP-NCT displayed two crystallisation events and one melt.

*The thermal behaviour of 1:1 melted FBP:NCT compound was reproducible when the melted compound was scanned for the third time.

A modulated DSC scanning was run to deconvolute the complexity of crystallisation and separate underlying events at 66.33 °C **(fig B.4)**. This technique provides additional information to standard DSC methods. MDSC heat flow can be separated into two traces; the first signal refers to thermodynamic compound (reverse heat flow), alternatively the second signal indicates the kinetic product (non-reverse heat flow trace). MDSC trace of 1:1 melted FBP:NCT **(fig B.4)** displayed two crystallisation events on the nonreverse heat flow trace (a simple crystallisation event at 47.02 °C and another complex one at 66.94 °C), so this added no further information to the standard DSC outcomes. On the other hand, the information on the reverse heat flow trace gave some clue to the thermal event at 66.94 °C. It revealed a preceding endothermal event at 59.81 °C. This event alerted for considering the presence of another product which co-exists with the main compound. Such assumption can be quite sensible especially when recalling the observation along the zone of mixing in the RT-stored Kofler preparation **(fig 4.2)**.

To rationalise the statement of having co-existence phases of FBP-NCT (a kinetic and thermodynamic products), a decision was made to restrict the degree of freedom within fused FBP-NCT system by applying Ostwald's rule of step changes[171–173]. This can be obtained by entrapping the molecules of melted compound into their glassy state then allowing for successive crystallisation of potential phases *via* slow heating.

Thereupon, the start point should be from the glassy state of material. This phase was achieved by rapidly cooling corresponding melted compound or what so called sample quenching process. Based on that, a quenched melted FBP:NCT, 1:1 mixture was held at -35 °C, followed by a slow heating by means of DSC until the melting occurred.

The thermal DSC trace of rapidly cooled sample is displayed in **fig 4.7**. It revealed the glass transition at -0.13 °C, it also showed a crystallisation at 54.53 °C, followed by a consecutive thermal events encompassing both endothermic and exothermic peaks at 73.16 °C and 75.03 °C respectively, ended by a melt at 96.58 °C. Consequently, six phases appeared on heating quenched melted 1:1, FBP:NCT

compound; glassy state ⟼ supercooled liquid ⟼ crystallisation of solid phase I ⟼ melt I ⟼ recrystallisation of solid phase II ⟼ final melt II. DSC outcomes revealed that the solid phase I underwent an instantaneous rearrangement process once melted (73.16 °C), which has been replaced by another phase at 75.03 °C. The first metastable phase is thought to be the kinetic product, which its presence was difficult to recognise at the beginning of the research work until using quenched method of fusion. The second phase is the more energetically favoured form (the most stable form), and its presence was not much affected when changing the method of sample preparation. Overall, changing the method of thermal scanning enabled to distinguish between the kinetic and thermodynamic solid forms in FBP-NCT system. Thereafter, this method of sample preparation was adopted for the following co-crystal polymorphic studies.

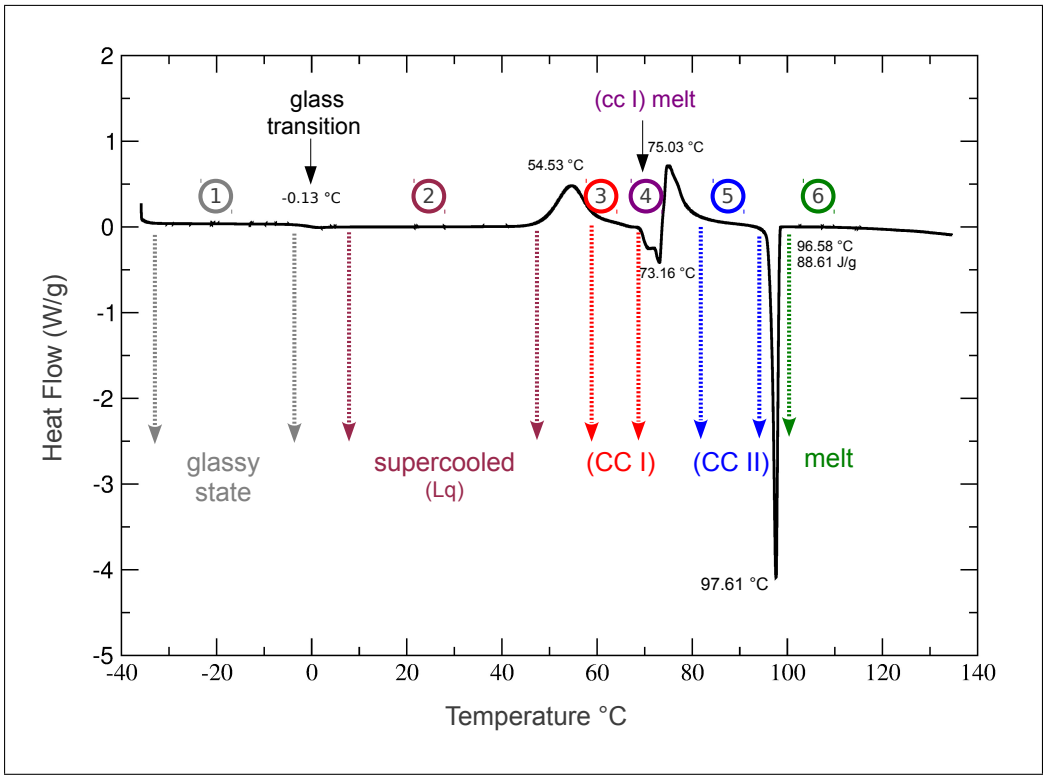

Figure 4.7: Quenched melted 1:1 FBP-NCT mixtures were screened using DSC. The figure displays DSC trace while heating the resulting compounds. Thermal scans were performed over a range of (-35 to 135 °C), which revealed the following events: glass transition (Tg) at -0.13 °C, crystallisation of co-crystal form I (CC I) at 54.53 °C, followed by simultaneous events of (CC I) melting and recrystallisation of co-crystal form II (CC II) at 73.16 °C and 75.03 °C, respectively, finally the melt of (CC II) at 96.58 °C.

HSM Study of 1:1, FBP-NCT Co-crystal:

Earlier thermal DSC observations **(fig 4.7)** were optically explored by means of HSM. This optical tool is quite helpful in understanding the solid-state forms of materials. The combination between microscopic and thermal scanning provides information about the physical changes of materials over heating process. In another word, the physical characterisation as a function of temperature and time can be achieved using such tool.

Thereupon, a sample of quenched melted FBP:NCT, 1:1 was explored by HSM. The resulting photomicroscopic images, snapshot at various temperatures, were selected to show the consecutive transformation events **(fig 4.8)**, which encompassed a series of events;

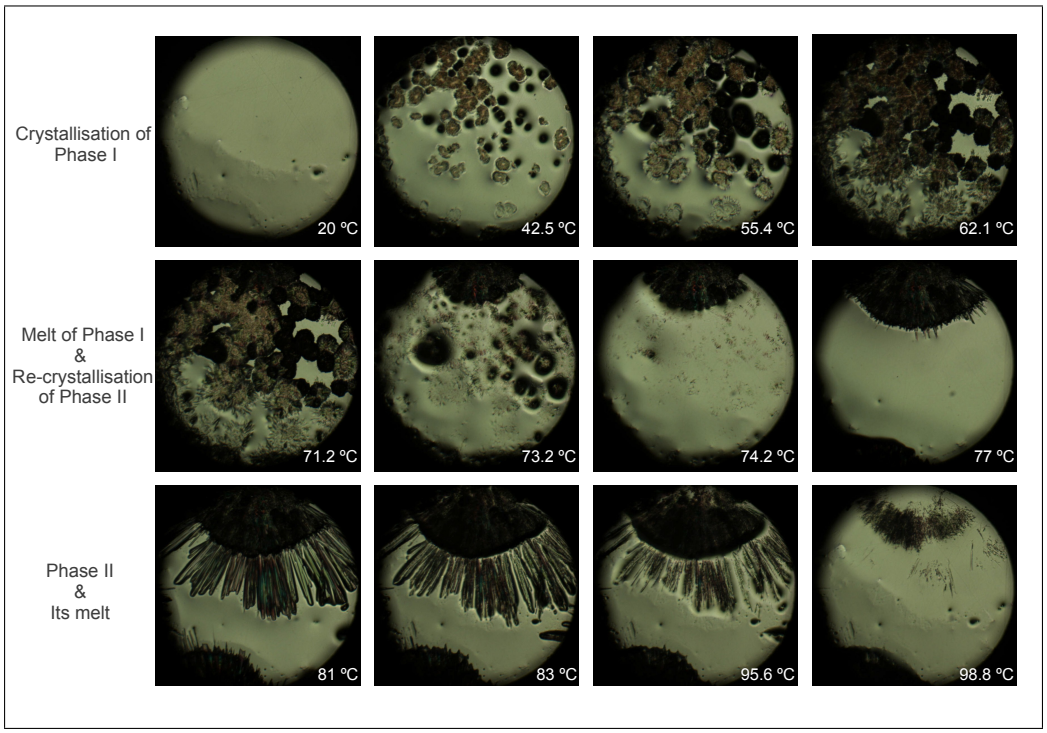

Figure 4.8: Photomicroscopic of melted 1:1 FBP-NCT at various temperatures in the hot-stage microscope experiment. It shows the crystallisation of form I in first row of images, followed by the formation of concomitant forms (the melting of form I and the simultaneous crystallisation of form II) in the second row, finally the melting of form II in the third row.

- **The crystallisation of phase I:** the nucleation of starlike crystals, from amorphous phase (20 °C), occurred at 42.5 °C. The growth of this solid phase became more obvious at 55.4 °C **(fig 4.8, 1^{st} row)**.

- **The simultaneous melt and re-crystalisation:** A careful inspection on first crystallisation, revealed the emergence of small needled crystals from the surrounding parts of starlike crystals, resulting in crystals of a stellar dendrite shape at 62.1 °C. Subsequently at a temperature range of 71.2 °C to 74.2 °C, the melt of stellarlike crystal and the simultaneous crystallisation of needled crystals were noticed **(fig 4.8, 2^{nd} row)**.

- **Phase II and its melt:** The growth of needled crystals occurred at the expense of the starlike crystals which became merely of needled shape above 77.0 °C, and then it started to melt at 95.6 °C **(fig 4.8, 3^{rd} row)**.

Thus, the optical images referred to the following thermal events; amorphous material → solid form I → solid form II → final melt, and such findings tie in nicely with previous DSC findings. Although, the interpretation of DSC and HSM outcomes could be indicative to the formation of concomitant phases, which with the increase of time resolved one phase from the other, yet they can not be definitive. This is because all these observations depend on the physical changes occurred during thermal transitions. Therefore, more investigation was required to unambiguously identify the type of present phases. Studies which probe the intermolecular interactions between FBP and NCT and the crystalline structure of resulting compound, were believed to be essential in polymorphism characterisation; i.e. the use of Raman spectroscopic and x-ray diffraction techniques.

4.4.2 Raman & Diffraction Studies *vs* Heat & Time

Further investigation was conducted by combining similar thermal approaches with spectroscopic and x-ray diffraction techniques. Such strategies are helpful in providing detailed information about the molecular and the crystalline changes while subjecting samples to consecutive heating environment. Again, the main theme of exposing quenched sample to successive heating conditions during Raman and diffraction studies, was to satisfy Ostwald's rule[174]. This rule states that any attempt to crystallise material leads over timescale to the formation of metastable polymorph before isolating the most stable form[171–173].

VT-Raman Studies of Quenched Melted 1:1, FBP:NCT

Considering the VT-Raman data first, Raman spectra which were collected as a function of temperature over a heating range of -40 to 150 °C from a quenched melted 1:1, FBP-NCT sample, are presented in **fig 4.9** and spectra are colour coded in red each 10 °C for the ease of data presentation.

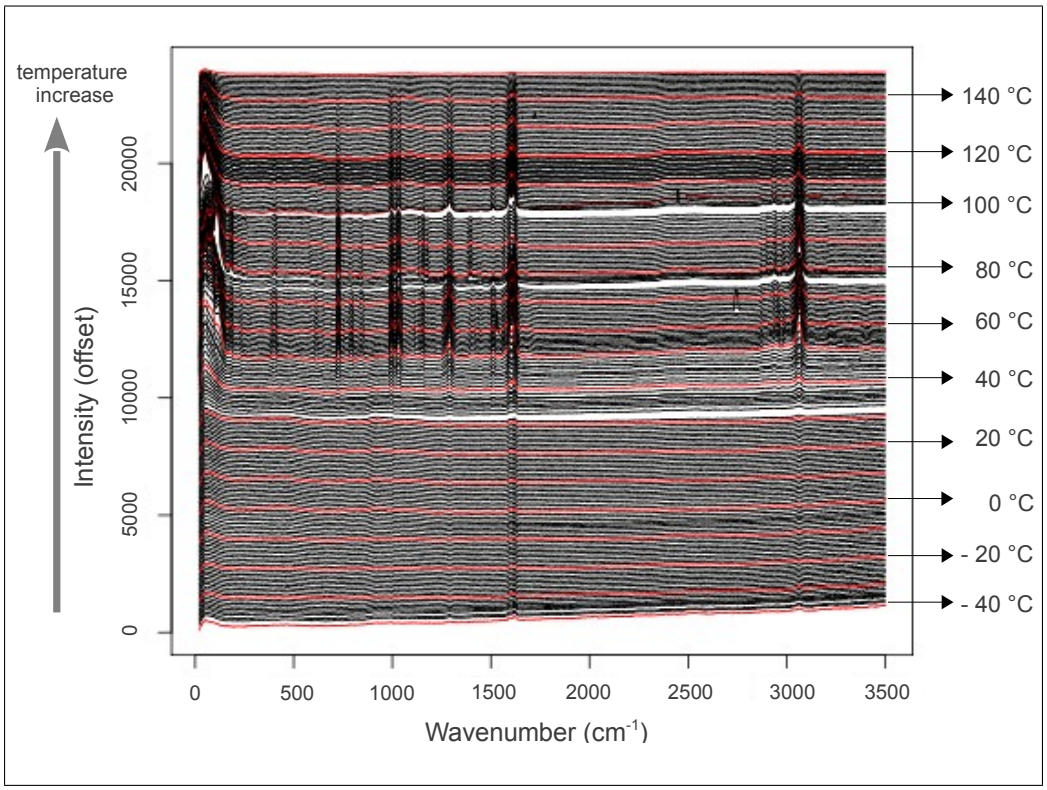

Figure 4.9: VT-Raman raw data of quenched FBP:NCT sample. Spectra are stacked in a bottom-top manner starting from the spectrum collected at -40 °C ended by the one acquired at 150°C. Spectra are mostly colour coded in black apart from those obtained each 10 °C which are colour coded in red for the ease of data showing. The intensity of data are offset and median filtered to get rid of the spikes.

Raman data appeared to be difficult to interpret from the instant visual inspection in **fig 4.9**. Thereafter, the presentation of Raman data was changed using colour contour plot **(fig 4.10 a)**.* Raman data, which consist of three sets of variables (temperatures, Raman intensities, and Raman shift), were simplified by horizontally plotting the intensity of each Raman spectrum as a function

* Phonon data were decided to be explained about in the main body of this thesis[134,175], yet the presentation of VT-Raman data in different wavenumber regions is available in **fig B.5**.

of temperature. The x-axis refers to Raman shift, colours on Z-bar represent scaled Raman intensities, and y-axis refers to temperature points **(fig 4.10 a)**. The resulting plot, currently appears into a 2D form, revealed some noticeable wavenumber bands which were distinct over certain temperature ranges. These bands were correlated with different phases formed over heating process as clearly noticed in **fig 4.10 a**. Despite such apparent transformation between solid-state materials, identifying these phases can not be accurately deduced by eye; and hence the distinction between different spectra of various solid-state forms is not quite straightforward by visual inspection.

To further explore these phases, data were subjected to an automated analysis. PCA was employed to resolve accurately the spectra and the temperatures at which phases were formed without any potential interference. PCA outcomes herein were almost explained based on their scores.

Scores were firstly studied against the changes of temperature. The first three PCs were plotted over a thermal range of -40 $\rightarrow$ 150 °C in **fig 4.10 b**. Investigation within the range of -40 $\rightarrow$ 25 °C, revealed steady changes in the scores as a function of temperature **(fig 4.10 b)**. Nonetheless, the gradual process of transformation over this range of temperature was not continuous and it was rather separated by a barrier point. This points represents the boundary between the brittle glassy state and viscous state. The temperature at which the transformation between the glassy state and supercooled liquid took place is called the glass transition temperature (Tg). Tg is highly influenced by the thermal history of cooled melted sample, specifically the inner state of amorphous phase and its dynamic aggregation state, which generally lead to a less suddenly changes between glassy state and supercooled liquid state as noticed in **fig 4.10 b**. According to VT-Raman data, the small step of change in the scores between the glassy state and viscous state occurred at about -4 °C **(fig 4.10 b)**. When recalling DSC outcomes **(fig 4.7)**, one can realise that Tg can also be deduced, however the occurrence of this event was slightly higher (-0.13 °C). Such variation is quite acceptable when taking into consideration the timelag in recording measurements, and the thermal sensitively of used instruments.

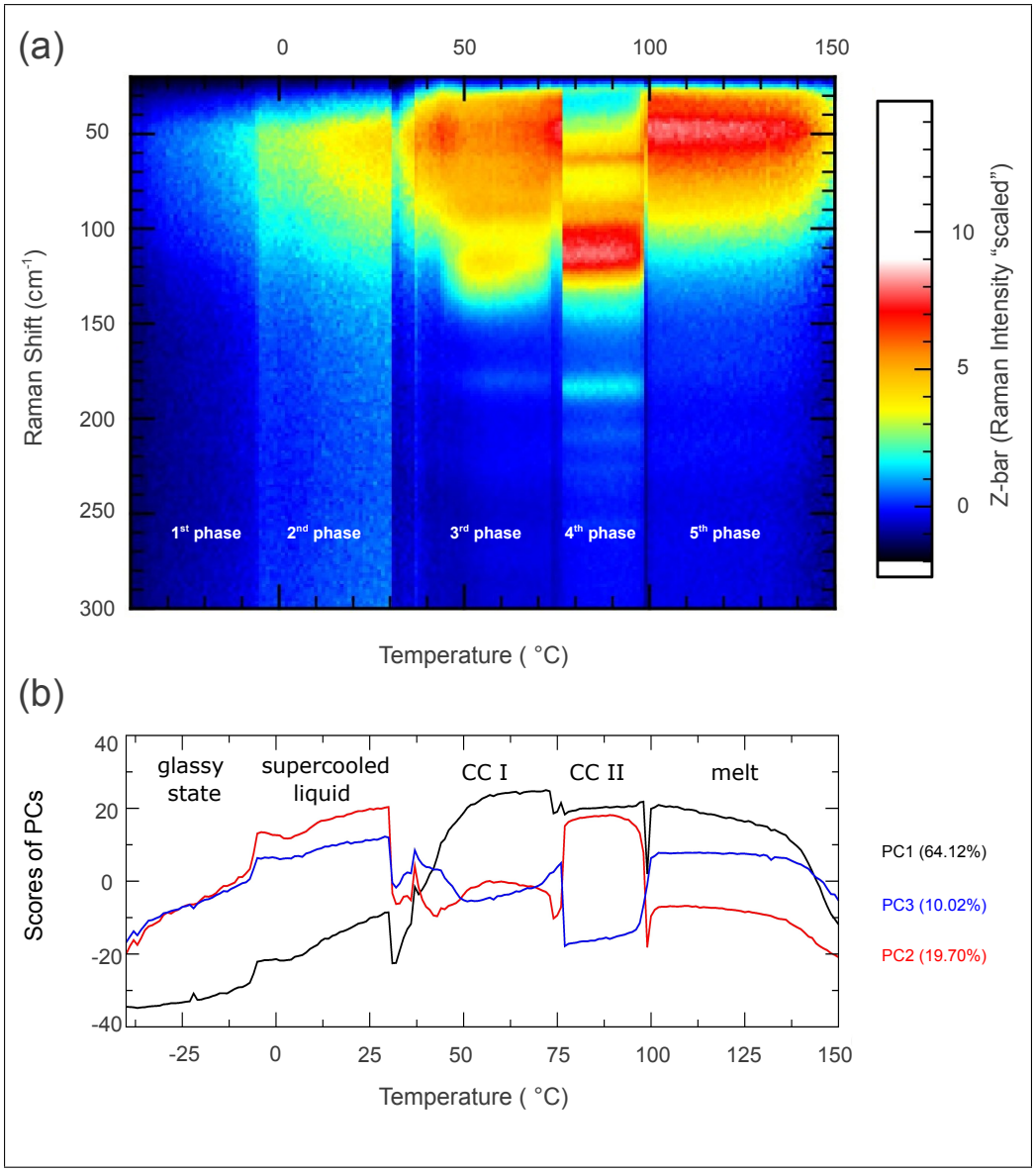

Figure 4.10: VT-Raman analysis of quenched melted FBP:NCT system. Firstly, a 2D plot of VT-Raman data of quenched melted 1:1 FBP-NCT mixtures is shown in (a), whereas the x-axis represents the temperature (°C), y-axis is Raman shift (cm^{-1}), and colours indicate to scaled Raman intensity. Secondly, PCA analysis was performed on VT-Raman data, and in (b) is the resulting PCs scores of the first three PCs as a function of temperature.

The following transition event occurred at about 30 °C which referred to the crystallisation of co-crystal form I. The formation was initiated once the viscous state began to exhibit some molecular kinetic changes represented by a reduction in the free molecular motion of particles, and this was manifested into a sudden change in PCs scores at about 30 °C **(fig 4.10 b)**. The successive formation of such particles led to secondary nuclei and so on until achieving nuclei of suitable size for crystalisation. This resulted in some fluctuations in PC's scores

over a small range of temperature (31 → 37 °C), followed by a steady increase in PCs scores until the formation of co-crystal form I became more prominent (50 → 74 °C).*

The formation of co-crystal form I was followed by the formation of another phase, and this was alluded from the sudden change in the scores at about 77 °C **(fig 4.10 b)**. This abrupt change most likely referred to the transformation to another co-crystal form II before melting occurred at about 100 °C **(fig 4.10 b)**.

Solid-solid transformation between both co-crystal forms was indicated to from the scores of PC2 & PC3 but not from those of PC1. PC1, which represents the majority of data variability (64.12%), showed instead a transition at a preceding temperature (at about 75 °C). Such variability in the scores' behaviour over temperature range of (75 → 77 °C) might highlight the presence of previous thermal event occurring before solid-solid transformation **(fig 4.10 b)**. These findings needed more clarification by studying the PCA scatter plot of VT-Raman data.

Accordingly, the scatter plot of PC1 and PC2 scores was studied as a function of each other **(fig 4.11)**. This is useful in the phase transformation analysis, because the co-ordinate sets (PCs) are defined in terms of the variance of the data, with the first axis (PC1) having the most variance (64.12%) and the second axis (PC2) having the second most of data variation (19.70%). Since different solid-state phases can be distinguished due to their variations in the properties (i.e., the physical properties), including the scores plot can reveal these variations. More specifically herein, it can further clarify and ascertain the behaviour of distinct groups (solid-state phases) which cluster separately over heat and time parameters. Overall, the scatter plot can pinpoint the order of phases with their exact temperature of formation.

Thereupon, the scores' plot (scatter plot) of the first two PCs, generated from the VT-Raman data, is shown in **fig 4.11 a**. Few observations were noticed

* The scenario of achieving some localised co-crystal form I particles followed by the growth of other nuclei among amorphous region caused some topographical changes in the area from which spectra were collected. Raman spectra extracted over temperature range of 31 → 74 °C **(fig B.6)**, supported earlier interpretation regarding the scores of CC I group. These spectra showed a clear formation of CC I after 50 °C **(fig B.6, blue)**.

when looking at the resulting scatter plot **(fig 4.11 a)**;

- There are two well separated clusters from the scatter plot over a temperature range of -40 → 30 °C, although they chemically appeared to be of an amorphous state. Both groups are indicated to as a group (1) in **fig 4.11 a, "black"** and group (2) in **fig 4.11 a, "maroon"**, and their Raman spectra are presented in **4.11 b**. The separation, which occurred at -6 °C, referred to a glass transition temperature, and this was also confirmed from PCA outcomes as a function of temperature **(fig 4.10 b)** and DSC trace presented in **fig 4.7**. Therefore, both groups observed from PCA scatter plot are correlated with a glassy state (group 1) and supercooled liquid state (group 2) of FBP:NCT system, and the transition between both phases occurred at a Tg of -6 °C.

- The third group (3) was noticed from the cluster over a temperature range of 31 → 74 °C **(fig 4.11 a, "red")**, and it is related to co-crystal form I **(fig 4.11 b)**. The scores of CC I do not exhibit a very tight cluster until about 50 °C. This was believed due to the ongoing crystallisation process from amorphous, and this agrees nicely with the tailed trend of CC I scores as a function of temperature **(fig 4.10 b)**.

- Interestingly, the remaining two clusters were noticed over inconsecutive ranges of temperature. The first cluster encompassed two temperature ranges; one over 75 → 77 °C **(fig 4.11 a, "purple")** & another one over 99 → 120 °C **(fig 4.11 a, "green")**. The second cluster appeared over one temperature range (78 → 98 °C) **(fig 4.11 a, "blue")**.

- Having two groups classified in one cluster, 75 → 77 °C **(fig 4.11 a, "purple")** & 99 → 120 °C **(fig 4.11 a, "green")**, might refer to two solid-state groups of comparable chemical features. Consequently, Raman spectra were extracted from temperatures where both groups are classified together **(fig 4.11 b)**. Raman spectral comparison in **fig 4.11 b** revealed that the spectrum acquired at 75 °C looks fairly comparable to the spectrum collected at 99 °C and they both refer to the melt of phases.

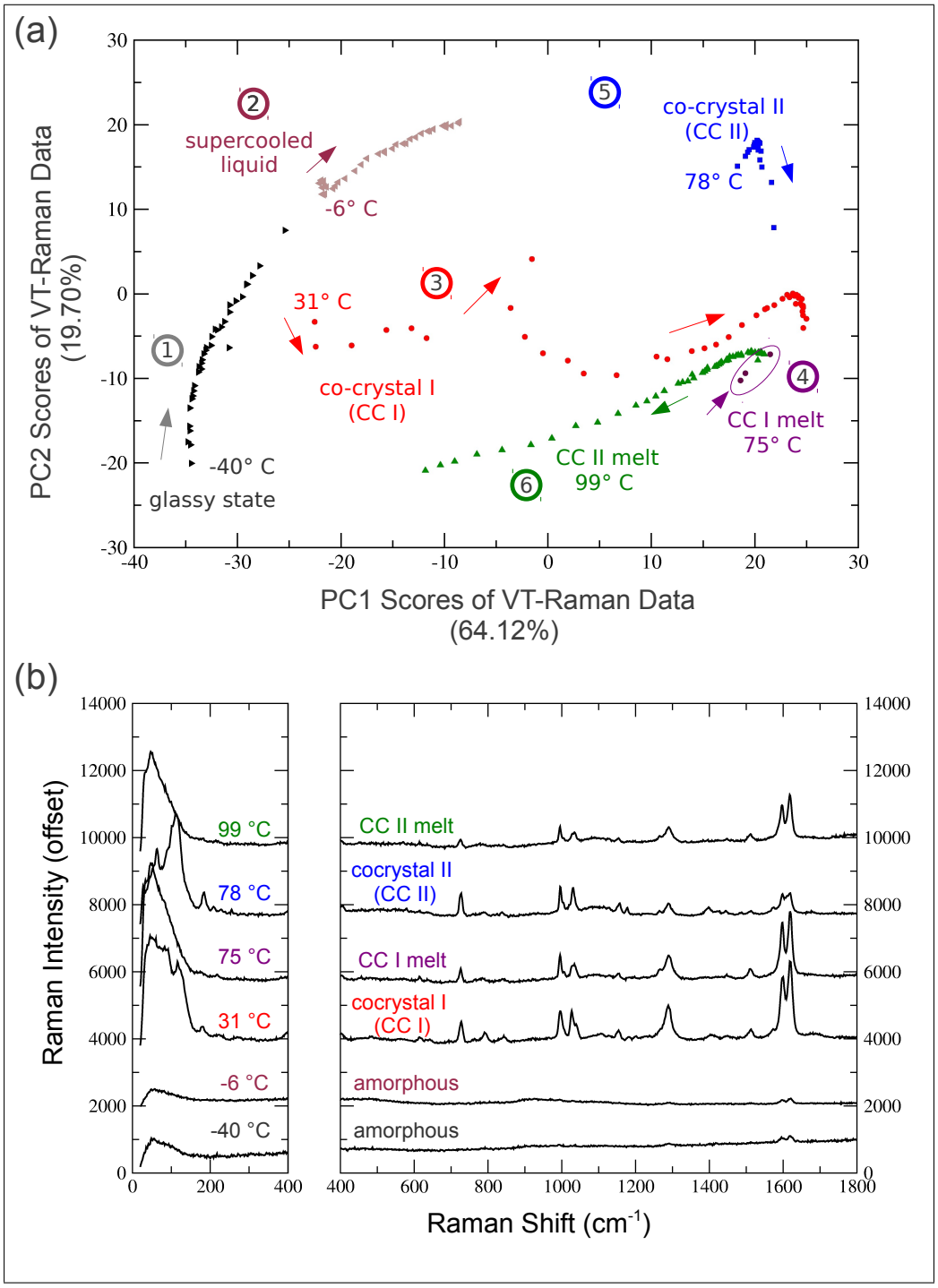

Figure 4.11: VT-Raman data of quenched melted FBP-NCT sample. It shows in (a) the scatter plot of PC1 (64.12%) *vs* PC2 (19.70%). Group of clusters are indicated to by colours and they refer to FBP:NCT glassy state "group 1, black", supercooled liquid "group 2, maroon", CC I "group 3, red", the melt of CC I "group 4, purple", CC II "group 5, blue", and finally the melt of CC II "group 6, green". Corresponding Raman spectra are shown in (b), and they arranged in a bottom-top manner starting from glassy state, supercooled liquid, CC I, CC I melt, CC II, and CC II melt. Spectra are displayed into two regions (phonon and molecular regions).

- Now examining the cluster appeared over a temperature range of 78 → 98 °C **(fig 4.11 a, "blue")**, showed that this solid-state group refer to the formation of CC II **(fig 4.11 b)**. Hence, the formation of CC II started from 78 °C and not 75 °C. Surprisingly, the appearance of CC II does not arise following the crystallisation of CC I group (3) as was assumed from **fig 4.10 b**. This means that the preceding group over a temperature range of 75 → 77 °C which has got the feature of the melt **(fig 4.11 b)** and becomes group (4), refers to the melt of CC I before the recrystallisation in another phase (CC II) group (5). Based on that, the cluster of the final group (6) appeared over a temperature range of 99 → 120 °C **(fig 4.11 a, "green")** and has got the feature of the melt, is related to the melt of CC II.

Overall, the type of group clustering **(fig 4.11 a)** and their representative Raman spectra **(fig 4.11 b)**, confirmed that these groups are related to the glassy state (-40 → -5 °C) ⟼ supercooled liquid (-6 → 30 °C) ⟼ co-crystal form I (CC I) (31 → 74 °C) ⟼ CC I melt (75 → 77 °C) ⟼ co-crystal form II (CC II) (78 → 98 °C) ⟼ CC II melt (99 → 120 °C).*

Recalling consecutive thermal events from the DSC trace **fig 4.7**, and the images obtained from the HSM **(fig 4.8)**, indicated that the melt of CC I was also observed from the VT-Raman experiment. So what was observed from the different behaviour of PC1 as a function of temperature at about 75 °C **(fig 4.10 b)** was an indication to the successful separation between CC I and CC II, and a confirmation that CC II formation does not emerge from a structural rearrangement within CC I compound but rather appeared from a melted FBP-NCT (CC I) phase. A comparable picture occurred to CC I which crystallised from an amorphous state of FBP:NCT (supercooled liquid state).

Correlating Raman outcomes with the HSM and DSC results revealed some slight variability in the occurrence of events. While the onset of transformation events are slightly different, the trend of solid-state transitions according

*The comparison between Raman spectra extracted at 55 and 77 °C, and Raman spectra acquired from FBP and NCT as received, confirmed that these both phases are new compounds (CC I & CC II, respectively) **(fig B.7)**.

to spectroscopic data is similar to those deducted from the HSM and DSC. Such differences in transition temperature resulted from the variation in detection level of chosen technique. For instance, DSC and HSM are considered as bulk analysing techniques while backscattering Raman spectroscopy was used in its single-point screening mode. Besides, the allowance time in VT-Raman experiment compared to HSM and DSC brings earlier observation for the occurrence of thermal events. During VT-Raman experiment, Raman spectra were not acquired constantly over heating process but rather there was a holding time at each temperature degree and this allowed events to occur earlier than expected. There was also a delay occurring after each spectral collection due to the movement of the grating to zero-position, and an autofocus setup which was employed to ensure having the most intense spectrum at each single point. Thereby, such technical issues could offer the molecules of FBP-NCT co-crystal a sufficient time to relax at a lower temperatures in comparable to traditional thermal methods (DSC and HSM). In general, there was a good correlation between HSM & DSC inspection and VT-Raman results. All techniques indicated to phase state transitions corresponded respectively to the crystallisation from amorphous material into co-crystal form I initially before the formation of co-crystal form II.

VT-XRPD Studies of Quenched Melted 1:1, FBP:NCT

XRD is a gold-standard technique in the chemical characterization of unknown materials, and the crystalline determination of their phases. It was employed in such type of work to further identify the crystalline states of FBP-NCT co-crystal materials formed over heating process, and more specifically to verify the polymorphic forms of FBP-NCT system.

This was aimed to be achieved by collecting the x-ray powder patterns from quenched melted 1:1, FBP-NCT sample as a function of temperature. Again, PCA was utilised to analyse variable temperature data of x-ray powder patterns. VT-XRPD data and the outcomes of PCA analysis are displayed in **fig 4.12**. VT-XRPD data were handled similarly as were VT-Raman data.

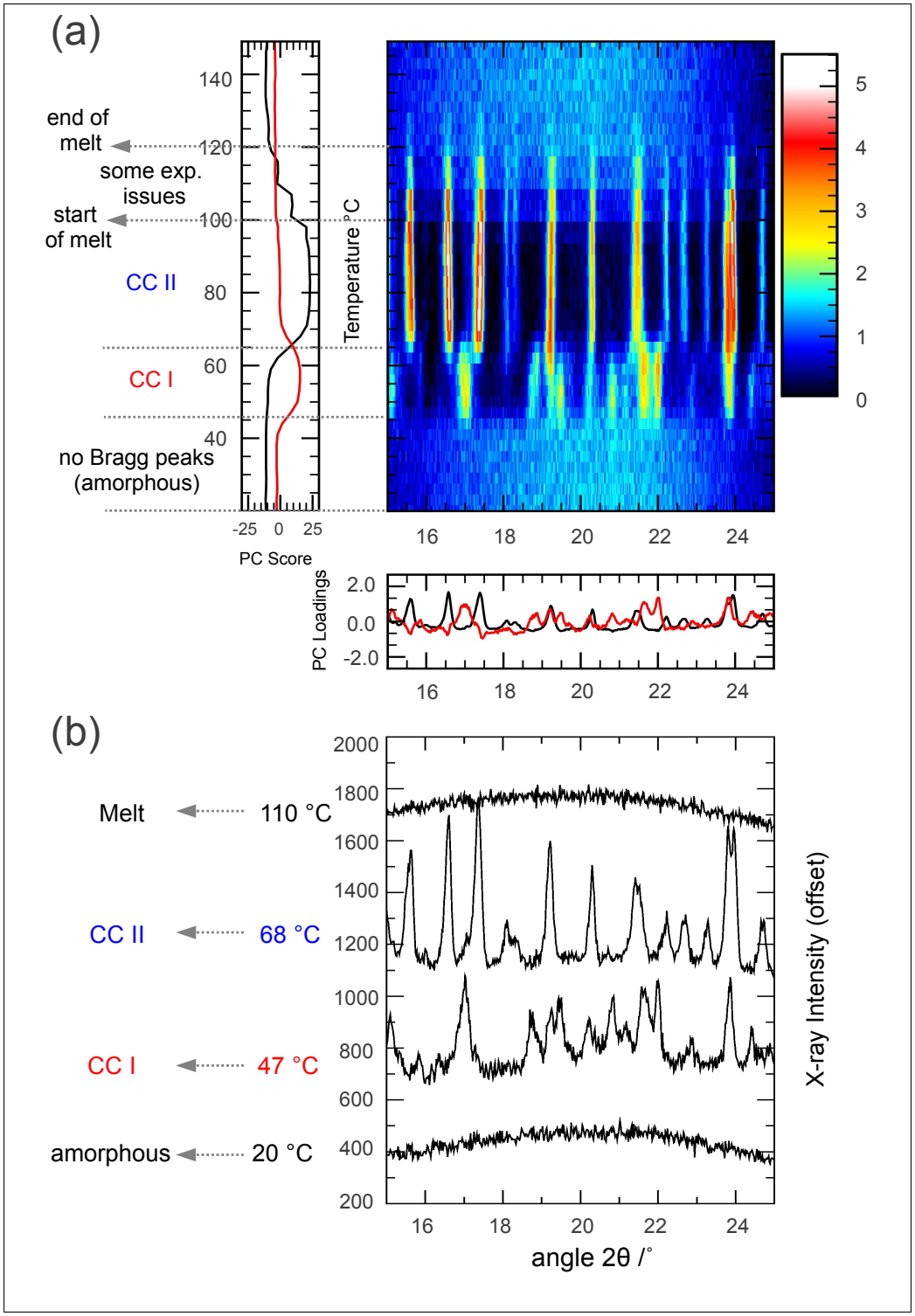

Figure 4.12: VT-XRPD data analysis. (a) is a 2D plot of XRPD data whereas x-axis is $2\theta/°$, y-axis is temperature, and colours represent scaled intensity. The plot is coupled with a plot of PCs scores versus temperature (left-hand side), and the loading plot of the first two PCs (bottom). (b) shows XRPD patterns at the transition temperatures; 20 °C, 47 °C, 68 °C, and 110 °C.

Firstly, the VT-XRPD data are presented into a 2D form **(fig 4.12 a)**, accompanied by PCA outcomes (PCs' scores as a function of temperature on the left-handed side, and PCA loadings plot below). It is quite obvious by looking at the contour plot and PCs score plot **(fig 4.12 a)**, to observe four phases formed over heating process. This was not only checked by eye, but it was also confirmed from x-ray powder patterns collected from FBP:NCT state phases at the transformation temperatures **(fig 4.12 b)**.

PCA outputs from VT-XRPD were in consistent with what was observed earlier using different techniques (Raman spectro), in terms of displaying both FBP-NCT co-crystal forms **(fig B.8)**. However, the number of all presence phases in FBP-NCT system and the onset of thermal events from VT-XRPD varied, and in summary the current XRPD study showed that;

- The initial crystallisation and the final melting started at different temperatures from those observed in VT-Raman experiment; 47 °C and 110 °C (VT-XRPD, **fig 4.12**) *versus* 31 °C and 98 °C (Raman data, **fig 4.10**), respectively.

- The solid/solid transformation occurred in an instantaneous manner without passing through the melt of co-crystal form I. CC I recrystallised in another form CC II, and this happened at 68 °C **(fig 4.12)**.

Such variation in transition temperatures, despite method similarity of sample preparation, could be due to the inequality in the heating environment around the entire sample within the diffractometer. Only the pointed part of the capillary tube was subjected to the heating source, and thus more time should be offered for the sample per temperature degree before the x-ray powder pattern was collected.

However, since the main interest was the polymorphism aspect within FBP-NCT co-crystal system, VT-XPRD outcomes were quite adequate for the comparison purposes between CC I and C II, and the starting components (FBP and NCT) **(fig B.9)**. This comparison showed that not only both forms look different from each other, but they are also different from the starting materials. Thereupon, solid phase appeared from FBP:NCT system are related to different

polymorphic forms of FBP-NCT, and the question left to answer was what is the identify of the crystal structure of FBP-NCT co-crystal.

4.4.3 FBP-NCT Single Crystal X-ray Pattern

The single crystal x-ray diffraction experiment was conducted to identify the crystal structure of co-crystal and to find its relationship with collected powder patterns from the solid-state phases of quenched melted 1:1, FBP:NCT system **(fig 4.12)**.

The crystal structure and the x-ray pattern of 1:1 FBP-NCT co-crystal were confirmed from the single crystal x-ray refinements of the experimental x-ray data. Data were collected from single crystals of liquid-assistant ground FBP:NCT (1:1) grew in ACN solution. The reliability factor (R_{Work}) between experimental diffraction pattern and the crystallographic model of FBP:NCT was equal to 9.72%. The crystal structure of FBP-NCT co-crystal is of a monoclinic lattice system with a space group $P2_1/c$, and a unit cell of four FBP-NCT molecules Z=4 **(fig B.10)**. The parameters of each unit cell are as the following; cell lengths are a=27.473(6) Å, b=5.6443(12) Å, c=11.432(3) Å, cell angles are α=90.00/°, β=92.376(4)/°, γ=90.00/°, and cell volume is V=1771.19 Å^3. The calculations showed, as suggested **(fig 4.4)**, that co-crystal formation is mediated by acid--pyridine heterosynthon **(fig 4.13)**. The chains adopt a zigzag shape supported by NCT amide-amide dimer, and they stack parallel to the crystallographic b-axis **(fig B.11)**.

The x-ray powder pattern was also built, following the calculations of single crystal structure of FBP-NCT co-crystal. The resulting pattern was then compared with the powder patterns of CC I and CC II extracted from VT-XRPD experiment at 47 °C and 68 °C **(fig 4.14)**. It was found that the powder pattern at 68 °C temperatures exhibited a good agreement with calculated pattern based on single x-ray crystal experiment **(fig 4.14, blue *vs* black)**.* Such similarity in x-ray patterns indicated that co-crystal II, which appeared from heating

* Calculated single x-ray pattern was slightly shifted towards the right because the SXD experiment was performed at -180 °C.

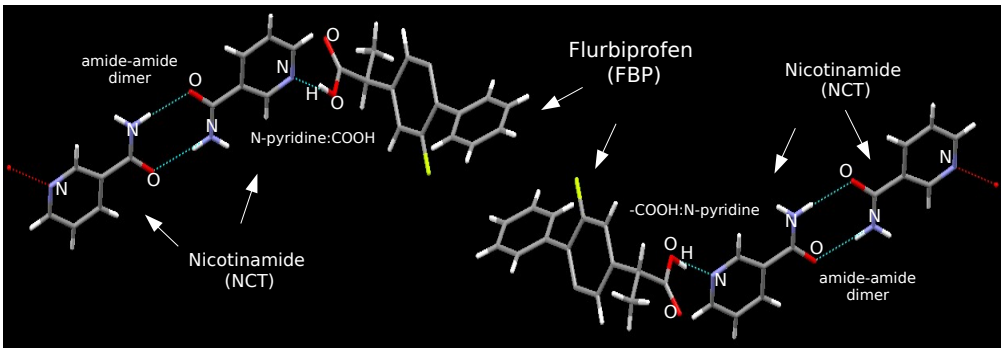

Figure 4.13: Chemical structure of FBP-NCT calculated from single x-ray diffraction (SXD). It shows fragments of the crystal structure of 1:1 FBP-NCT co-crystals viewed along crystallographic (a) direction. It shows the interaction between 1:1 FBP:NCT *via* acid-pyridine synthon and the mediation of NCT amide-amide dimer to support the chains.

quenched melted 1:1, FBP:NCT over 68 °C, has similar crystal structure to the one calculated from the single crystal of FBP-NCT. This means that CC II is 1:1 FBP-NCT co-crystal, whereas hydrogen bonds occur between carboxylic acid:N-pyridine groups and the chains are sustained by NCT amide-amide homosynthons.

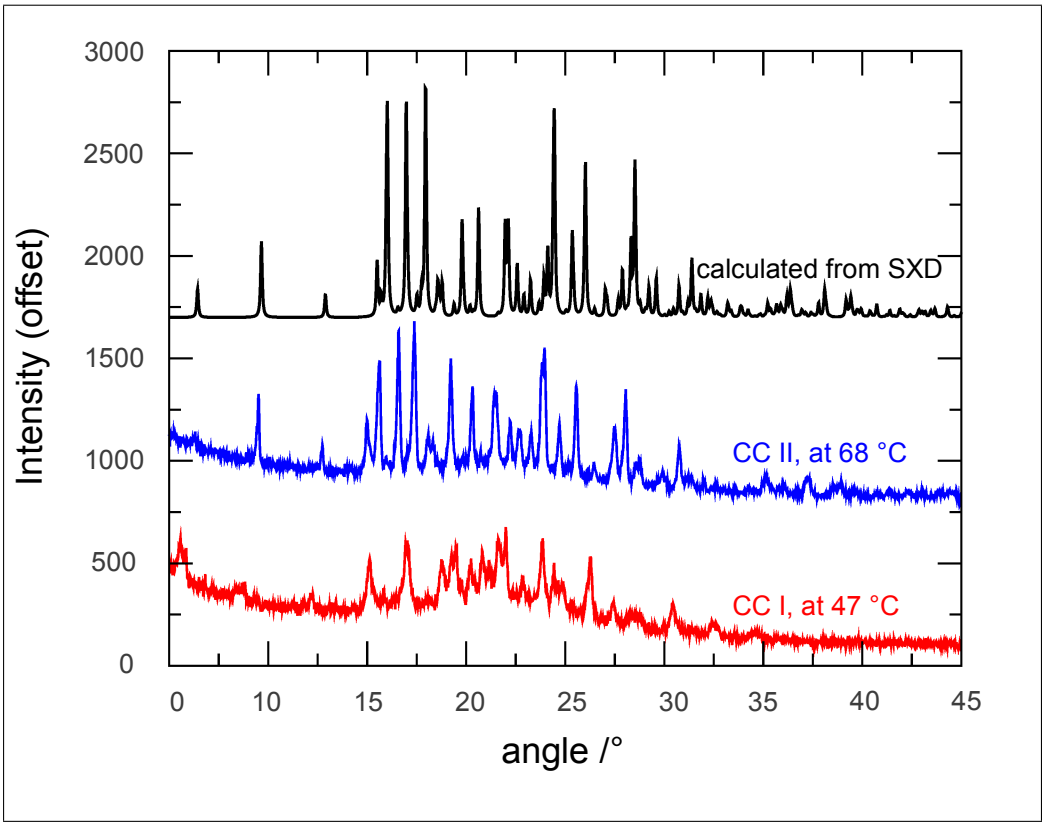

Figure 4.14: XRD studies of FBP-NCT co-crystal forms. It shows calculated pattern from SXD (colour coded in black) in comparison with powder patterns of both CC I (red) and CC II (blue). The patterns of CC I and CC II were extracted from VT-XRPD at 47 °C and 68 °C, respectively.

On the other hand, it is quite noticeable by looking at the powder pattern extracted from VT-XRPD at 47 °C, to observe its pattern differences from the calculated pattern of FBP:NCT single crystal **(fig 4.14, red *vs* black)**. The powder pattern at 47 °C also exhibited different patterns from those of both of the starting materials as mentioned earlier **(fig B.9)**. All of these findings confirm that such solid-state phase, is actually another form of FBP-NCT co-crystal (CC I). * †

4.5 Conclusions

FBP-NCT Kofler melt preparation over a time of storage indicated to polymorphism issue in the co-crystal along the zone of mixing. Therefore, a study was conducted to probe the FBP-NCT solid state forms. The study entailed a proper sample preparation followed by a polymorphic screening procedure. Polymorphic screening involved using traditional thermal techniques (DSC and HSM), and parametric measurement tools such as Raman spectroscopic and x-ray diffraction as a function of time and temperature (VT-Raman & VT-XRPD).

The analysis revealed that all types of phase transformation; glass/viscous, viscous/solid, solid/solid, and solid/liquid, can be clearly distinguished when choosing the right preparation methodology, technique, and data analysis. For instance, methods for producing FBP-NCT phases was optimised by adopting protocol which complies with Ostwald's rule of step changes. Secondly, the use of chemometrics (PCA) to analyse VT data i.e., VT-Raman data enabled to confirm a clear separation of phases from quenched melted 1,1 FBP:NCT; (-40 → -5 °C), (-6 → 30 °C), (31 → 74 °C), (75 → 77 °C), (78 → 98 °C), and (99 → 120 °C); referring respectively to glassy state, supercooled liquid, co-crystal form CC I, the melt of CC I, co-crystal form CC II, finally the melt of CC II. PCA scores as a

*Raman spectra extracted from VT-Raman data at 50 °C was also compared with the spectra collected from FBP-NCT single crystal **(fig B.12)**.

†However, the crystal structure of CC I was not confirmed due to the stability issue of this form, yet XRPD and Raman are considered enough evidents for the characterisation of two polymorphic forms of FBP-NCT co-crystal system.

function of temperature also confirmed such successive transformations between phases at -6 °C, 31 °C, 75 °C, 78 °C, and 99 °C.

Overall, the studies showed that amorphous phase underwent a gradual relaxation over heating which was separated by Tg point. The following ordered crystalline form (co-crystal form I) did not occur suddenly from amorphous phases and this was most likely due to the nucleation and crystallisation process of co-crystal form I at the beginning of transition temperature range (31 → 50 °C). The solid-solid transformation between co-crystal from I & II did happen instantly by rearrangement process, but it was rather mediated by the melt of form I and recrystallisation of second form as was confirmed from DSC and Raman outcomes.

Finally, the VT-XRPD confirmed the presence of two polymorphic forms of FBP-NCT co-crystal. The crystal structure of one of these forms was successful identified and this was supported when the single crystal structure of FBP-NCT co-crystal was calculated (SXD). Although FBP-NCT co-crystals achieved from the fusion methods displayed a presence of transient phase (CC I) before forming the stable form (CC II), such formation can be controlled using the right method of sample preparation.

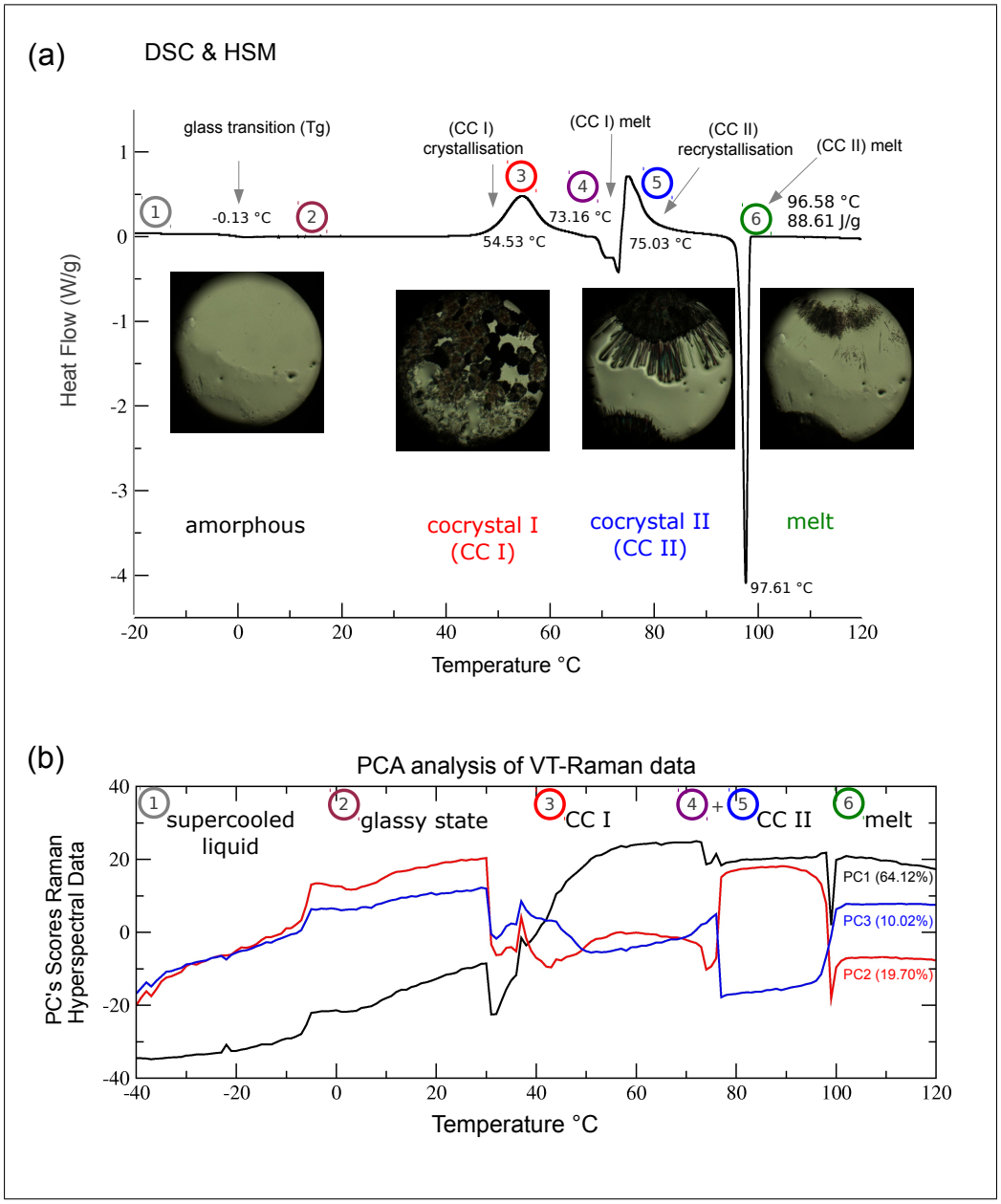

Figure 4.15: Conclusion figure about co-crystal polymorphism studies.

CHAPTER 5

QC Probing of Model Co-crystal Tablets by Transmission Raman

5.1 Abstract

The molecular complexes (co-crystals) were for the first time formulated into pharmaceutical solid form (tablets) using dry-press technique. The resulting tablets were afterwards probed by transmission Raman spectroscopy (TRS). The work presented in this chapter aimed at using pharmaceutical co-crystal in drug formulation (tablets), driven by the fact that such type of molecular complexes are designed to widen the scope of achieving the required physiochemical properties of the APIs. This work was also motivated by the need to find a good analytical tool to screen pharmaceutical preparations; a procedure taken to comply with the FDA call for the QC and good manufacturing processes (GMPs) within the field of pharmaceutical industry. The analytical screening was preceded by a proper experimental design and complemented by choosing suitable statistical methods. Mathematical analysis of TRS data revealed interesting information when compared to the instant eye observation. Such findings were not only related to the distinction based on the chemical contents of tablets (co-crystal *vs* physical mixtures), but also according to the ratio of drug contents (25% *vs* 50%) within the pharmaceutical solid formulations.

5.2 Introduction

Medications can be formulated in various ways according to the required route of application, which is mostly affected by the physicochemical properties of the chosen drug. Drugs could be delivered in simple solutions, emulsions, suspensions, etc, which with a certain level of sterility become suitable for parental injections (internal application) or even ocular administration. Formulations can also be designed for topical use (external application) which can be either aqueous, oily, semi-solid (drops, gels, or ointments) or even a patch type suitable for transdermal application. Apart from these formulations, which are designed to deliver APIs without passing the gastro-intestinal tract (GIT), are the oral dosage forms. Oral dosage forms can be administered either as solutions and suspensions i.e. syrup, or tablet-like solid forms such as pills, tablets, capsules, and buccals.

Unlike intravenous (IV) medications, delivering oral dosage forms does not involve invasive application. Therefore, they are of great acceptance by patients and have been the most popular way for delivering APIs since the nineteenth century[176]. Oral solid dosage forms are again the favourable delivery systems from industrial point of view as they involve less costly techniques and preparations.

In order to prepare such formulations, certain criteria should be considered regarding the solid-state form of the APIs. Ideally, APIs should provide the needed solubility, acceptable stability, low hygroscopicity, a good compatibility with excipients, and finally low cost and minimum process of synthesis without any issue with scaling-up. As mentioned previously **(intro 3.2, 4.2)**, such properties are more likely to be achieved when employing multi-component systems; of which and along the course of this chapter, co-crystal was selected to be formulated in tablet forms and screened for the good manufacturing.

Not only choosing the right state form of the API and selecting the suitable dosage form are crucial during drug development and manufacturing process, but also finding the robust techniques for screening the resulting pharmaceutical preparations is also important in the pharmaceutical industry[73,85,177]. One of the main goals in the industry is to ensure that medications are always provided to

patients with a good homogeneous drug distribution containing the whole pharmaceutical content. Therefore, it is required to find a very reliable, non-destructive, non-invasive, and very rapid analytical tool to validate such standards. Such needs underlay within the framework of deploying a real-time quality control tool in manufacturing and production processes or what is so called PAT[74].

PAT encourages pharmaceutical companies to design, analyse and control manufacturing and production processes *via* in/on-line manner using appropriate analytical techniques[75]. Consequently, vibrational spectral analytical tools are very beneficial to achieve such targets. Vibrational spectrometers such as Raman has been until now considered as a non-invasive, non-destructive techniques, and fast monitoring PAT tool[178–182]. Such instrumentation can be beneficial for the QC and GMPs in the pharmaceutical fields especially when the analysis is coupled with the use of statistics[131,183–185]. The use of Raman spectroscopic technique is not only based on detecting the molecular vibrations which involves stretching and bending of intermolecular interactions but also it probes the phonon excitations (intramolecular interactions) and thus it is beneficial to investigate the emerging phases i.e., polymorphs within pharmaceutical formulations[186].

There are several spectroscopic techniques which utilise Raman scattering radiations, of which two Raman techniques were employed through this research work; the backscattering **(chap 3, 4)** and the transmission Raman modes **(chap 5)**. Backscattering mode was shown to be of beneficial for screening co-crystal preparations and other emerging forms **(chap 3, 4)**. Along the course of this chapter, Raman transmission spectroscopy will be tested on model co-crystal tablets. The main difference between both transmission and backscattering modes is the way photons travel through samples. **Fig 5.1** shows a schematic layout of both transmission and conventional Raman spectroscopy. In Raman transmission mode **(fig 5.1 a)**, photons of the electromagnetic radiations diffuse through the sample and pass the entire volume content to be detected in a forward geometry. Contrary to the transmission Raman spectroscopy, laser light in the conventional backscattering mode **(fig 5.1 b)** is scattered from the surface of the sample and detected in a backward geometry.

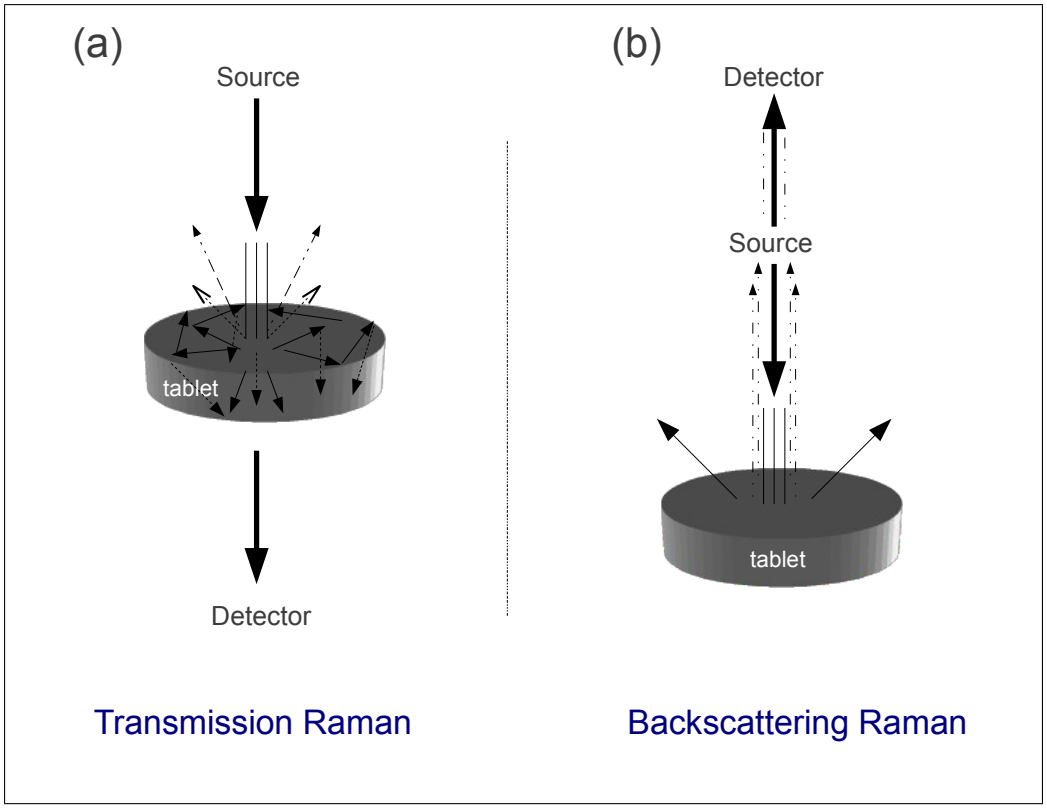

Figure 5.1: Schematic of transmission and backscattering Raman techniques. It shows the experimental layout of both the transmission *vs* the conventional backscattering modes. In transmission mode (a), the electromagnetic light shined on the sample travels ballistically (penetrates and scatters) through the sample of a tablet, then detected in forward geometry. Alternatively in (b), the illuminated laser is scattered from the surface of the sample and detected in a backward geometry.

Taking a decision about using any mode of Raman spectroscopic techniques is related to the real goals the operator wants to achieve, and the experimental design which accordingly leads to a specific data interpretation. For instance, it is feasible through backscattering Raman technique to run either a single point, or even parametric measurements in which vibrational signals are obtained as a function of various factors such as temperature, pressure, and dimensions (XY surface mapping, XYZ three-dimensional mapping herein depth is included)[81,117]. The three-dimensional screening could be performed in consecutive steps; layer by layer (as achieved by backscattering mode), or in one go leading to a bulk screening (as in transmission Raman spectroscopy)[187].

Both Raman modes have proven their well suitability to be employed in the pharmaceutical field. For instance, the backscattering mode is good for

studying the drug distribution within pharmaceutical solid dosage forms.* Nevertheless when choosing to probe the bulk content of pharmaceutical preparations, Raman backscattering mode is not ideal as it is restricted with diluted thinner samples. Such bias in surface layer could be overcome by using transmission Raman spectroscopy which was found to be superior, as it does not probe layer by layer but rather the entire volume content[188,189]. Moreover, it has also been found that the issue of sub-sampling and fluorescence, correlated with the backscattering spectroscopy, could be avoided when using Raman spectroscopy in transmission mode[84]. Hence with a new approach within the vibrational spectroscopic schemes, TRS is useful to overcome the disadvantages accompanied the conventional Raman spectroscopy (backscattering mode) when probing the entire content of pharmaceutical preparations[131].

TRS has been used for characterisating powders of single component content in their loose form[186], or after being concealed in different plastic containers[182]. TRS has also been employed for screening capsules[83,187,188,190] and tablets[84,189,191] of multiple pharmaceutical contents. More importantly, it was also proven to be suitable for probing multi-component systems (complexes) such as co-crystals in their powder form[183], but it has never been tried when complexes exist in pharmaceutical dosage form (capsules or tablets). Therefore, a model co-crystal system FBP-NCT, previously studies in **chap 3, 4**[91,168], was selected as a solid-state form of the API to be prepared in tablet dosage form and later screened by the transmission Raman spectroscopy.

FBP is a part of carboxylated group from the non steroidal anti inflammatory drugs **(5.2 a)** which is used as an analgesic. NCT is a vitamin B3 derivative **(5.2 b)**, listed as a member of GRAS materials[192] and has been used as a co-crystal former[23,91,158]. The co-crystallisation between FBP and NCT was facilitated by liquid-assisting grinding technique[46,159], which resulted in the formation

*Similar observation was noticed when such technique was employed to study the FBP-NCT Kofler melt preparation **(chap 3)**. The outcomes revealed the spatial distribution of components within the preparation and indicated to the polymorphism issue in FBP-NCT co-crystal system.

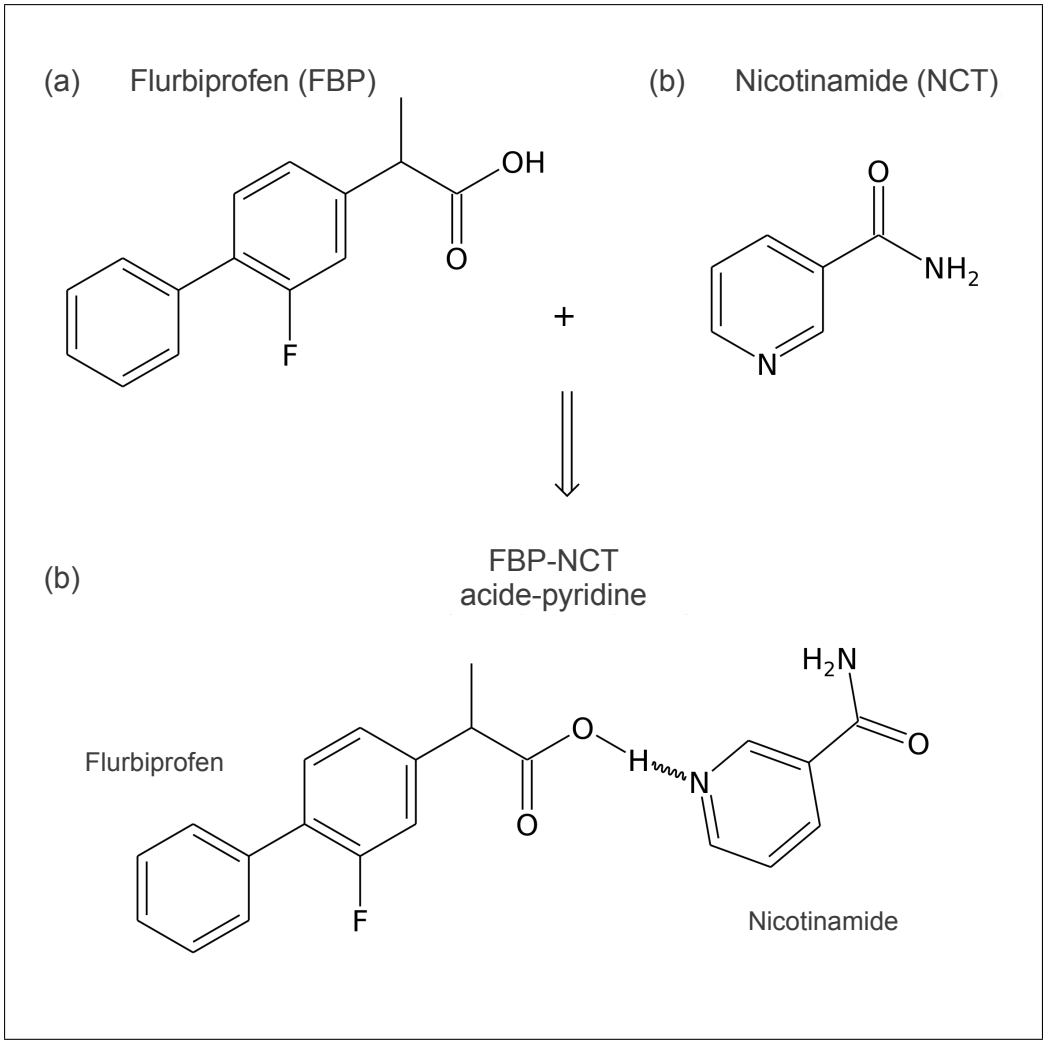

Figure 5.2: Chemical structures of FBP (a), NCT (b), and their co-crystal (c).

of 1:1, FBP-NCT co-crystal **(fig 5.2 c)**.* Realistic formulations of the API (1:1, FBP-NCT co-crystal) was later performed in tablet forms, containing the API and some tableting agents/excipients. Excipients compromised all of the followings; lactose (filling agent), avicel (a direct compression agent), and Mg Stearate (lubricant).

According to knowledge, this is the first time whereas co-crystals are being formulated in tablet dosage form. There are few examples in literature discussing the unintentional emerging of co-crystals between the APIs and excipients, i.e. the formation of co-crystals upon changes in the storage conditions between carbamazepine and nicotinamide in carbamazipine tablets, and between salicylic acid

*Refer to **appx C** regarding Raman and XRD characterisation of FBP-NCT co-crystal formation **(fig C.1)**.

and nicotinamide in aspirin tablets[193]. Nevertheless, there was not any example in literature showing the attempt of formulating co-crystals in solid-dosage form. Screening FBP-NCT co-crystal tablets was performing in parallel with sets of reference tablets containing the physical mixtures of both parent components (FBP and NCT). Tablets were made in two different percentage of drug contents (25% and 50%).

Therefore, the aim was to study two main points. The first one is to investigate whether TRS can distinguish between tablets of identical percentage of composition but different molecular properties i.e., co-crystal *vs* physical mixtures. The second aim is to investigate if TRS can differentiate between tablets of identical molecular properties but different in the ratios of drug contents i.e., co-crystal tablets of 25% ratio *vs* co-crystal tablets of 50% percentage, similarly is the case between the 25% and 50% physical mixture tablets. Overall, the layout of experiments will be of a 2 × 2 matrix; the vertical axis is based on the differences in chemistry (co-crystal *vs* physical mixtures) while the horizontal axis is based on the variation in the ratio of drug contents (25% *vs* 50%).

5.3 Materials and Methods

5.3.1 Preparation of Tablets

FBP-NCT co-crystals were prepared using liquid assisting grinding technique, whereas an equimolar mixture of FBP (243.68 mg) and NCT (123.06 mg) was ball milled for 20 min with a small addition of acetonitrile (30 μL).* The resulting ground powder was then left overnight at RT to allow for any remaining solvent to evaporate. The full conversion of reagents to co-crystal was confirmed using Raman spectroscopy and XRPD techniques **(fig C.1)**.

FBP-NCT co-crystal and their equimolar physical mixture were dry compressed into tablets using single punch press ("F3 tablet press", Manesty, Liv-

*The process was interrupted in between to ensure that the any slurry mixture stuck on the edges was scraped back into the milling jar.

Tablets Type	Tablets no.	Percentage of Ingredients			
		APIs	SDL	Avicel PH-102	Mg Stearate
a) co-crystal & phys mix	9 & 9	25%	44%	30%	1%
b) co-crystal & phys mix	6 & 6	50%	30%	19%	1%

Table 5.3.1: Ingredients compositions and their ratios within co-crystal & physical mixture tablets.

erpool, UK). Tablets were prepared in two different percentages of API content; 25% and 50%. The tableting process was assisted using some filling agents. For example, the binding between ingredients, and the compaction properties, were supported by mixing the entire content with spray dried lactose (SDL)[194], The flowability and disintegration were improved by adding microcrystalline cellulose (avicel PH-102)[195], and finally the adhesion of ingredients during compaction was reduced by using Mg Stearate (lubricant)[196]. The ratios of these agents varied according to the percentage of drug contents within tablets **(tab 5.3.1)**.

For the 25% drug loading tablets, [a) co-crystal & phys mix tablets], the ratio of SDL was 44%, avicel was 30%, and Mg Stearate was 1%. Alternatively, the ratios for the 50% drug loading tables, [b) co-crystal & phys mix tablets], were 30%, 19%, and 1%, respectively. Afterwards, the entire contents of each tablet, regardless to the type of tablets or the percentage of API content, were mixed and fed separately into the hopper*, then dry compressed†. The resulting tablets afterwards were received into vials.

5.3.2 Tablets Screening by TRS

The co-crystal and the physical mixture tablets of 25% and 50% drug content, and their constituent ingredients were then screened using transmission Raman spectrometer TRS100 system (Cobalt Light Systems, Oxfordshire, UK). Tablets were arranged directly in a sample loading tray while the powder ingredients

*To ensure that an even proportion of ingredients exist in all tablets

†Wet granulation was avoided to ensure the stability of co-crystal and their physical mixture during formulation process. The presence of the solvent might cause the collapse of co-crystal into its parent components in co-crystal tablets, or even vice versa forming co-crystals from the starting components in physical mixture tablets.

(co-crystal, FBP, NCT, SDL, avicel, Mg Stearate) were placed first in a quartz pan from which spectra were collected automatically. Tablets samples were illuminated using transmission Raman laser at a wavelength of 830 nm of a 6 mm beam diameter and a laser power of 1 W. Laser power and exposure times varied between referencing powder ingredients. The power was reduced for APIs constituents to be in a range of 0.2 – 0.75 W with an exposure time of 0.1 s for 20 accumulations, whereas laser power was 1.5 W for excipients for longer exposure times 1 – 4 s. The transmitted signal was filtered after being collected slightly off the axis to cut-off the Rayleigh scattering rays. The remaining Raman scattered signal passed to the spectrometer through fibre bundle. The diffracted signal then was detected by the CCD detector which was cooled to -75 °C to minimise the noise added to the spectra because of dark current generation.

Generated data were analysed in a separate free package designed by the R foundation for statistical computing, R version 2.15.0. Data were analysed using two statistical methods; principal component analysis and hierarchical agglomerative clustering. Few preprocessing steps were performed prior to the analysis; scaling and mean-centring.* Spectral data were arranged in a matrix of two dimensions x and y; x column vector represents intensity of each spectrum and y row is a number of total spectra (1024 × 36). Scaling was achieved by dividing each column (numerical vector x) by its standard deviation and then mean-centred by subtracting values in x by its corresponding mean.†

5.4 Results and Discussion

5.4.1 Visual Analysis of Data

Tablets of FBP-NCT co-crystals and their physical mixture, at ratios of 25% and 50% drug contents each, were subjected to TRS. Equally were the starting

*Scaling was applied for the ease of visual comparison. It was also applied along with mean-centring prior to PCA and HAC.

†The effect of baseline subtraction was investigated and provided in the appendix C.

ingredients; FBP, NCT, co-crystal, lactose, Mg Stearate, and avicel. The 30 Raman spectra of 9 tablets of 25% co-crystal + 9 tablets of 25% physical mixture + 6 tablets of 50% co-crystal + 6 tablets of 50% physical mixture, are compared to 6 Raman spectra of the starting ingredients **(fig 5.3)**. The resulting 36 spectra are plotted in two spectral regions; phonon region **(fig 5.3 a)** and molecular region **(fig 5.3 b)**, stacked in a bottom-top manner in the following order; co-crystal tablets 25% → physical mixture tablets 25% → co-crystal tablets 50% → physical mixture tablets 50% → FBP → NCT → co-crystal → lactose → Mg Stearate → avicel.

From an instant inspection and by looking only at the spectral datasets of tablets, **fig 5.3** revealed a similarity between spectra of each dataset, i.e. all nine spectra of co-crystal tablets of 25% drug content are identical. Similarly was the case for spectra from other type of tablets; 25% the physical mixture tablets, spectra of the 50% co-crystal tablets, and those related to the 50% physical mixture tablets. This observation indicates to a good reproducibility in spectral dataset collection.

Hence **fig 5.3**, shows the suitability of choosing one spectrum from each type of tablets to represent the entire datasets. Therefore, singular spectra collected from prepared tablets; co-crystal tables in both percentage of drug contents (25% and 50%) and physical mixture tables in the same drug ratios, are presented in **fig 5.4 a**. Again selected spectra are displayed in two spectral regions; phonon and molecular regions. Further examination in **fig 5.4 a**, revealed alikeness between dataset of co-crystal tablets of different percentage of drug contents (25% and 50%), likewise the situation for datasets of physical mixture tablets at similar ratios **(fig 5.4 a)**. Thereby from a visual examination **(figs 5.3, 5.4 a)**, the main distinction factor between datasets of different types of tablets appeared to be based on differences in chemistry.

Previously selected spectra, which represents dataset of each type of tablets, **(fig 5.4 a)** were moreover compared with the spectra collected from tablets' ingredients; avicel → Mg Stearate → lactose → co-crystal → NCT → FBP **(fig 5.4 b)**. This comparison showed a good compatibility between all spectral datasets of

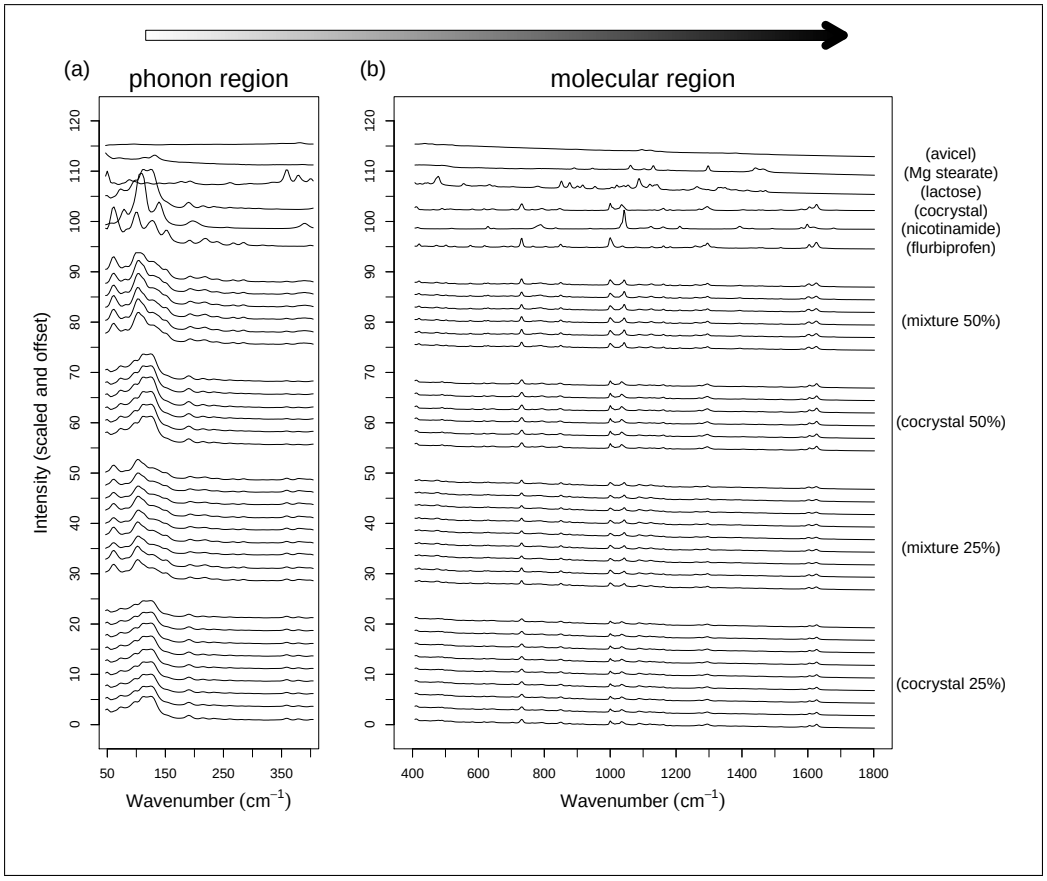

Figure 5.3: Experimental design of TRS data. It shows collected Raman spectra (intensity scaled & offset) of FBP:NCT co-crystal and their equimolar physical mixture tablets with two different percentage of drug contents 25% and 50%. It shows as well spectra of referencing materials. All data are displayed in two spectral regions; phonon (a) and molecular wavenumber region (b). Data are arranged in a bottom-top manner from tablets of lower percentage of drug 25% towards tablets of higher drug content of 50% whereas spectra of co-crystal tablets appear first followed by data of physical mixture tablets. Stacking on the top of such spectra are FBP, NCT, co-crystal, lactose, Mg Stearate, and avicel Raman spectra. Thus, the layout of data becomes as the following; co-crystal 25% (nine spectra) → physical mixture 25% (nine spectra) → co-crystal 50% (six spectra) → physical mixture 50% (six spectra) → FBP → NCT → co-crystal → lactose → Mg Stearate → avicel.

tablets **(fig 5.4 a)** and mainly APIs ingredients (FBP, NCT, co-crystal) but less obviously excipients (lactose, Mg Stearate, avicel) **(fig 5.4 b)**. Among all APIs ingredients, co-crystal **(fig 5.4 b, green)** seemed to be the most dominating feature in the spectra of (25% and 50%) co-crystal tablets **(fig 5.4 a)**. Alternatively, both FBP and NCT spectra (phonon region), colour coded respectively in blue & red **(fig 5.4 b)**, showed some shared information with (25% and 50%) physical mixture tablets only **(fig 5.4 a, box)**.

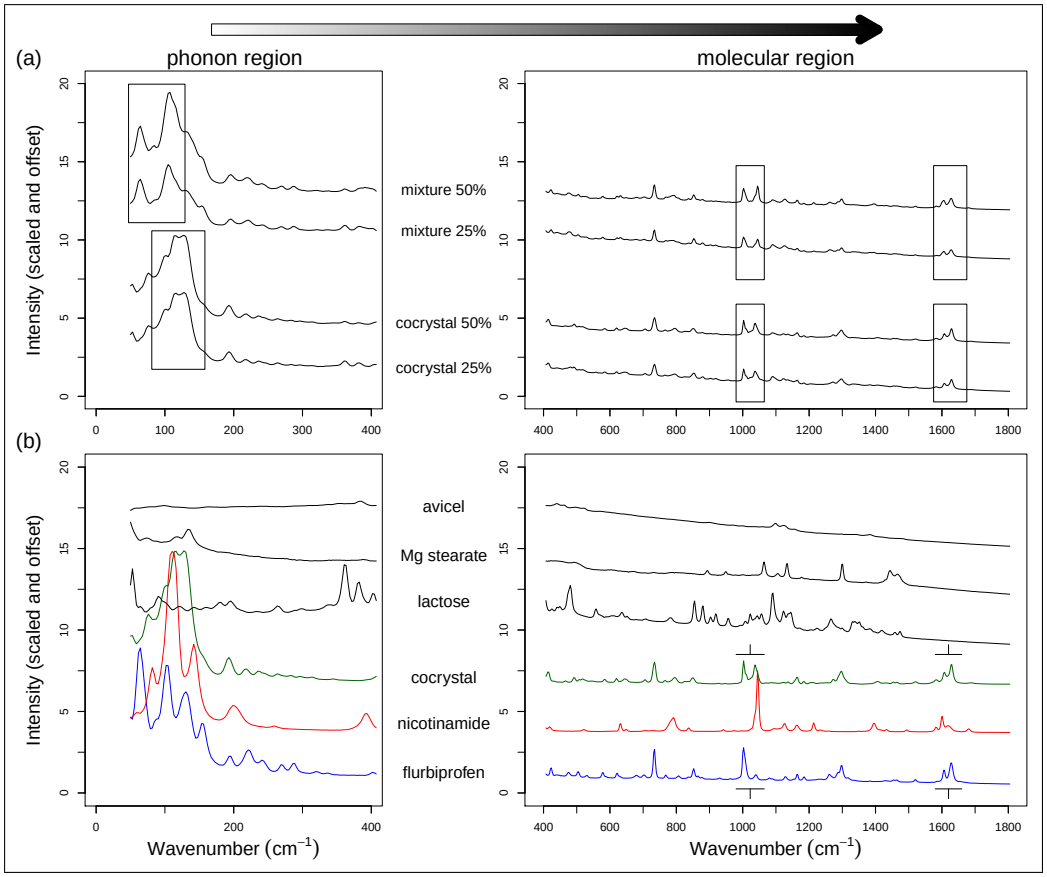

Figure 5.4: Visual inspection of Raman spectral data. It shows in (a) singular spectra collected from prepared tablets; physical mixture and co-crystal tables in their both percentage of drug contents (25% and 50%). These data are displayed in comparison with referencing spectra (b) in a top-bottom arrangement starting with physical mixture 50% (one spectrum) → physical mixture 25% (one spectrum) → co-crystal 50% (one spectrum) → co-crystal 25% (one spectrum) → avicel → Mg Stearate → lactose → co-crystal → NCT → FBP. Again all data (scaled & offset) are displayed in two spectral regions phonon and molecular wavenumber region within which the content of tablets showed some shared chemical features with references as indicated by boxes and segments of lines.

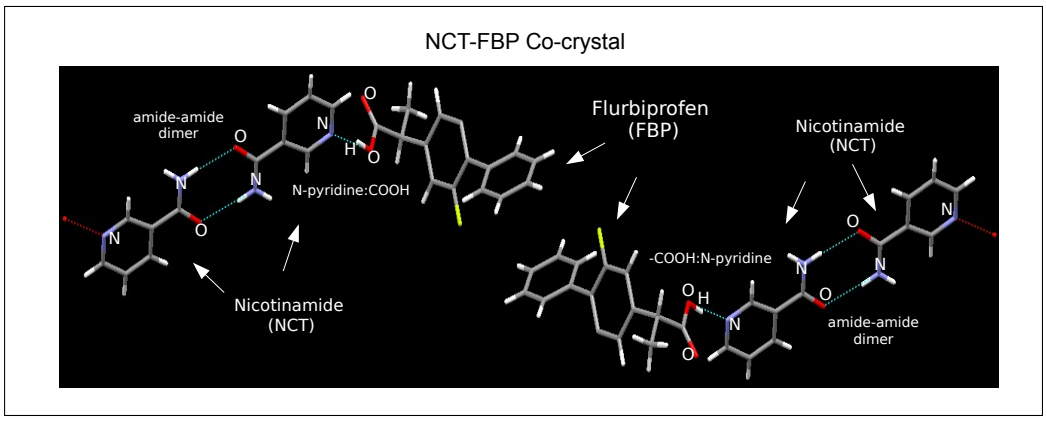

Figure 5.5: Chemical structure of FBP-NCT co-crystal as calculated from SXD.

Contrary to observation within phonon region, the spectra of physical mixture and co-crystal tablets showed comparable similarity with the spectra of all APIs parent ingredients in molecular region. For instance, shared information is quite obvious in two narrowed regions; 900 – 1200 cm^{-1} and 1600 – 1700 cm^{-1} as indicated by boxes in **(fig 5.4 a)** and segments in **(fig 5.4 b)**.

Raman vibrational frequencies within a range of 900 – 1200 cm^{-1} is thought to be related to the rocking of nicotinamide NH_2 group, and to the out-plane deformation of flurbiprofen carbonyle group γ(O–CO–CH3) and FBP $\omega(C–C)_{rings}$ wagging[23,197]. Equally, the chemical features at 1600 – 1700 cm^{-1} correspond to nicotinamide ν(C=O) stretching, and to the symmetric vibrational stretching of flurbiprofen aromatic rings $\nu_s(C–C)_{rings}$[23,197]. Sharing such information is quite meaningful because it refers intuitively to FBP and NCT functional groups **(fig 5.5)**. FBP and NCT complementary groups could serve as potential sites for both FBP and NCT molecular interaction. Therefore, the existence of these features in the datasets of tablets indicates to the presence of both FBP and NCT either in a physical mixture form or co-crystal form; requirements aimed to be achieved when preparing tablets.

5.4.2 Chemometric Analyses

As was alluded earlier from the visual inspection **(fig 5.3)**, the differentiation between components was merely based on the molecular properties of pharmaceutical ingredients (chemistry). Nevertheless, the visual inspection could be subjective and not quite definitive, i.e. the comparability of information between components of different chemistry (physical mixture *vs* co-crystal tablets) in some specific wavenumber regions; regions of molecular interactions 900 – 1200 cm^{-1} and 1600 – 1700 cm^{-1} **(fig 5.4)**. In addition, there was not any new information provided, regarding identical materials of different ratios (25% physical mixture *vs* 50% physical mixture, and 25% co-crystal tablets *vs* 50% co-crystal tablets) **(fig 5.4)**.

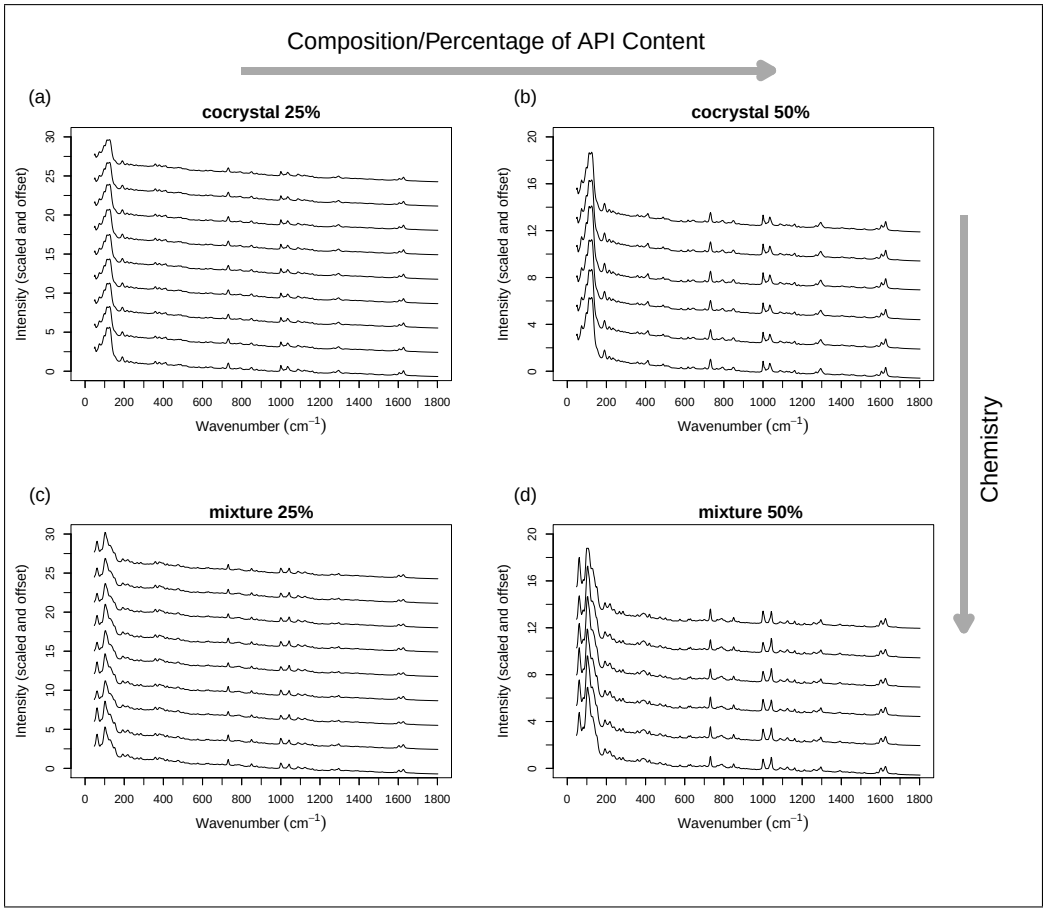

Figure 5.6: Analytical design of co-crystal & physical mixture tablets data. Data of FBP:NCT co-crystal and physical mixture tablets in two different drug contents 25% and 50% are arranged in four panels (a → d). Raman spectra are classified according to their drug ratios (25% (a, c) → 50% (b, d); left → right), and in relation to their chemical content (co-crystal (a, b) → physical mixture (c, d); top → bottom).

Hence, the visual analysis was performed in parallel with unsupervised chemometric methods (PCA & HCA). The spectral datasets of tablets were re-arranged **(fig 5.6)**, before subjecting data to PCA & HCA, prospecting that analysing TRS data with chemometrics might yield interesting outcomes related to the distinction between tablets according to their materials properties (chemistry) and the percentage of drug contents (molecular composition). **Fig 5.6** classifies co-crystal and physical mixture tablets of 25% and 50% drug percentages in four panels (a → d). The effect of drug loading is displayed horizontally (25% *vs* 50%), while the chemical content effect is shown vertically (co-crystal *vs* physical mixture).

Principal Component Analysis:

PCA was used to re-map TRS data, with a minimum interference by operator, into lower spatial dimensions so data becomes simpler to interpret[121]. PCA was applied on variance-scaled and mean-centred data. Only four PCs, covering 97.87% of data variation, were believed to provide sufficient information for the study **(fig C.2)**. Consequently, the rest of PCs were not included as they were considered less informative.* †

The first two PCs were selected for visualising data in 2D subspace of the PCA reduced dimensionality space, whereas the scores of both PCs were plotted against each other, as shown in the scatter plot **(fig 5.7)**. A lot of information could be alluded from the scatter plot especially when choosing two PCs of widely different variations, such as PC1 (66.90%) *vs* PC2 (14.25%). Plotting the scores of such PCs is beneficial in revealing the affiliation of clusters. It is also important to make the distribution of less variable datasets more distinguishable, i.e. revealing more spread out of nearby small clusters. Herein, points within the scatter plot **(fig 5.7)** refer to the spectral datasets acquired from tablets and referencing ingredients. Therefore, **fig 5.7** shows the distribution of PC1 scores against the spread of PC2 scores for similar datasets. Points correspond to 36 spectral datasets; co-crystal 25% (9 points, empty diamond), co-crystal 50% (6 points, crossed diamond), physical mixture 25% (9 points, (X) square), physical mixture 50% (6 points, crossed square), FBP (one point, blue square), NCT (one point, red triangle), co-crystal spectrum (one point, green plus), lactose (one point, maroon asterisk), Mg Stearate (one point, grey cross), and avicel (one point, crossed circle).

Now by looking at the scatter plot **(fig 5.7)**, the first eye catching observation is the presence of four distinct clusters, which are related to the following

*__Fig C.2__ shows a clear cut-off in PCs variations at PC6 after which the changes in PC variations become very steady.

†More information about the loading of PCs are listed in the **appx C**. The loadings of PC4 & PC5 revealed repetitive information to those exist in the first four PCs, therefore only the first four PCs were believed to be sufficient.

datasets; the physical mixture tablets of 25%, and 50% drug contents, another two sets linked to their co-crystal tablets of similar ratios (25%, and 50%). The scores of four datasets are almost located in different quadrants of the scatter plot **(fig 5.7)** which also displays a separate distribution of other six points, referring to the ingredients of tablets (excipients and APIs). Data points which correlate with excipients (lactose, Mg Stearate and avicel), distribute apart from those correspond to APIs (FBP, NCT, and co-crystal).

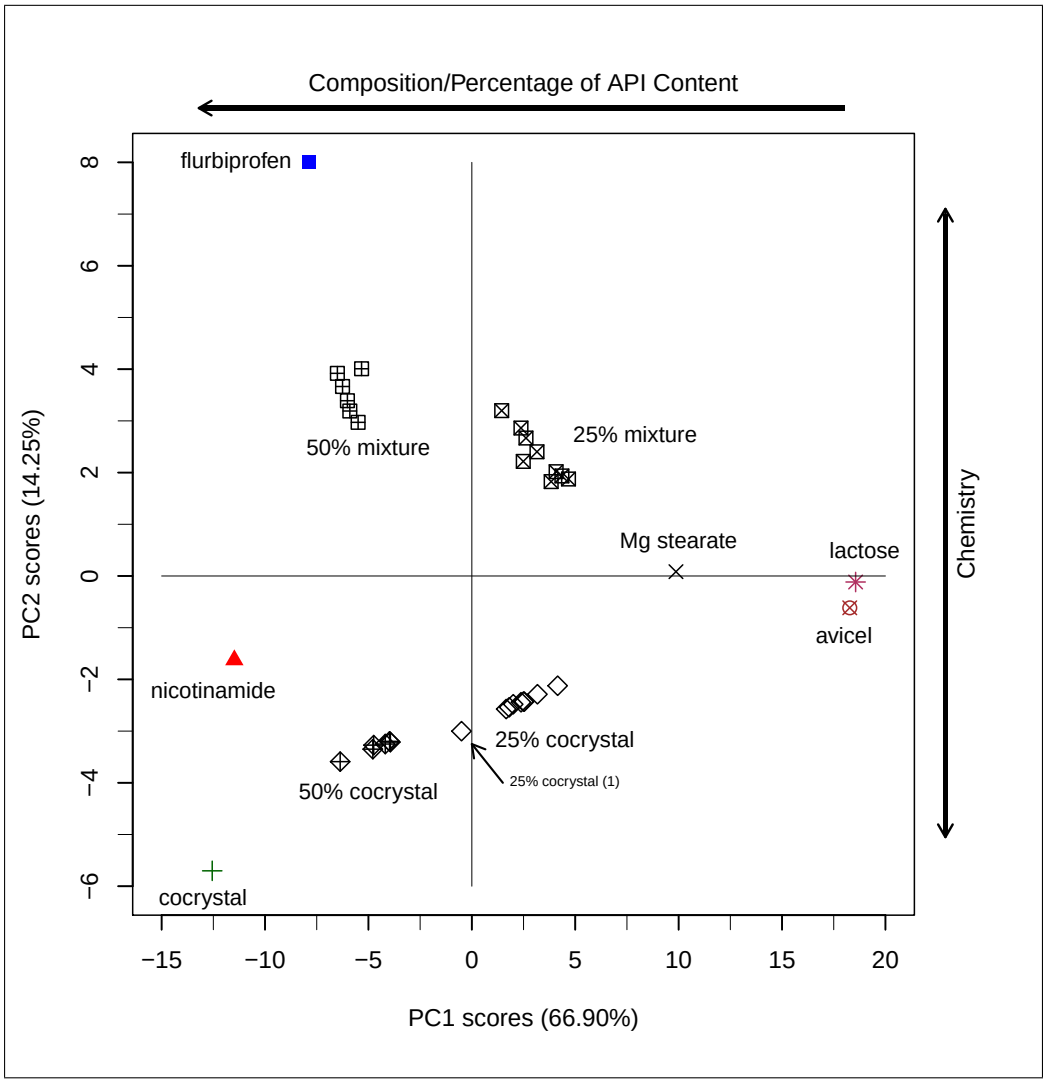

Figure 5.7: Scatter plot of principal components 1 *vs* 2. The plot shows the scatter of PC2 (14.25%) scores against those of PC1 (66.90%). The differences in chemistry (drug contents) appears to be clearer on PC2. On the other hand, PC1 reveals the variation in tablets with different ratio of contents (25% and 50%). Shapes and colour codes: black squares and diamond=tablets data, dark grey cross=Mg Stearate reference spectrum, blue filled square=FBP reference spectrum, red filled triangle=NCT reference spectrum, dark green plus=co-crystal reference spectrum, maroon asterisk=lactose reference spectrum, and brown crossed circle=avicel reference spectrum.

Detailed observations were revealed when examining, in a counterclockwise manner, the four quadrants of the scatter plot **(fig 5.7)**;

- The first quadrant encompasses the physical mixture tablets of 25% drug loading. Therefore, 25% physical mixture tablets are expected to have positive loadings on both PC1 and PC2.
- The second quadrant accommodate the 50% physical mixture tablets plus FBP reference. Consequently, both of the 50% physical mixture tablets and FBP reference are negatively loaded on PC1 while positively projected on PC2.
- Thus, the first and second quadrants compromise physical mixture tablets of both 25% and 50% ratios. More specifically, the 25% (+ on PC1), and the 50% (− on PC1) physical mixture tablets appeared to be well distributed along PC1 axis but not on PC2.
- The third quadrant contains the 50% co-crystal tablets along with the references of NCT and co-crystal, so this means all of them are negatively loaded on both PC1 and PC2.
- The fourth quadrant includes most of the 25% co-crystal tablets*† so for most of the 25% co-crystal tablets, data are positively projected on PC1 but negatively loaded on PC2.
- Thus, the third and fourth quadrants enclosed co-crystal tablets of both 25% and 50% ratios. The 25% (+ on PC1) and the 50% (− on PC1) co-crystal tablets seemed as well to be spread out along PC1 axis but not on PC2.

*Out of 9 spectra of the 25% co-crystal tablets, only the first spectrum is located slightly further from the rest of the dataset. The 25% co-crystal tablet no.1, is in between the clusters of both the 25% and 50% co-crystal tablets; indicated to by an arrow in **fig 5.7**.

†Refer to **appx C** for further details about the spectra of the 25% co-crystal tablets.

- The first and second quadrants contains physical mixture tablets of both 25% and 50% ratios, while the third and fourth quadrants encompasses co-crystal tablets of similar ratios. Thereby, physical mixture and co-crystal tablets appeared to be well separated along PC2 but not PC1.

- As for the excipients, all of lactose, avicel, and Mg Stearate appeared to have noticeable positive loadings on PC1 compared to PC2. Excipients' projections on PC2 are very minimum. More specifically, the loadings of lactose and avicel are slightly negative while those of Mg Stearate is to some extent positive on PC2. More importantly, nevertheless, is the location of excipients. Lactose, avicel, and Mg Stearate are localised nearby tablets of lower drug content. They are between the clusters of both the 25% co-crystal and the 25% physical mixture tablets.

- Alternatively, API references (FBP, NCT, and co-crystal) are positioned nearby tablets of a higher drug content 50% (second and third quadrants). For instance, FBP is localised in the same quadrant (second) of the 50% mixture tablets, while NCT and co-crystal are in the third quadrant close to the 50% co-crystal tablets.

To further support previous assumptions about dataset distribution, more inspection was performed on PC loadings. The first and second PCs were checked out for any related chemical information.* The investigation of PCs loadings was performed in comparison with reference Raman spectra of tablets' ingredients; in both phonon (40–400 cm^{-1}) and higher wavenumber regions (400–1800 cm^{-1}) **(fig 5.8)**, and within a range of 40-600 cm^{-1} **(fig 5.9)**.

The reference spectra of tablets' ingredients (FBP, NCT, lactose, Mg Stearate, and avicel) exhibited some positive and negative projections on PC1, such similarity is indicated to by boxes **(fig 5.8)**. Spectra of negative loadings are arranged below PC1 while the one of positive loadings is above. Therefore, the layout of the spectra and loading becomes as following; bottom → top: NCT (red,

*Refer to **appx C** for further information related to the loadings of PCs **(figs C.3, C.4, C.5, C.6, C.7, C.8)**.

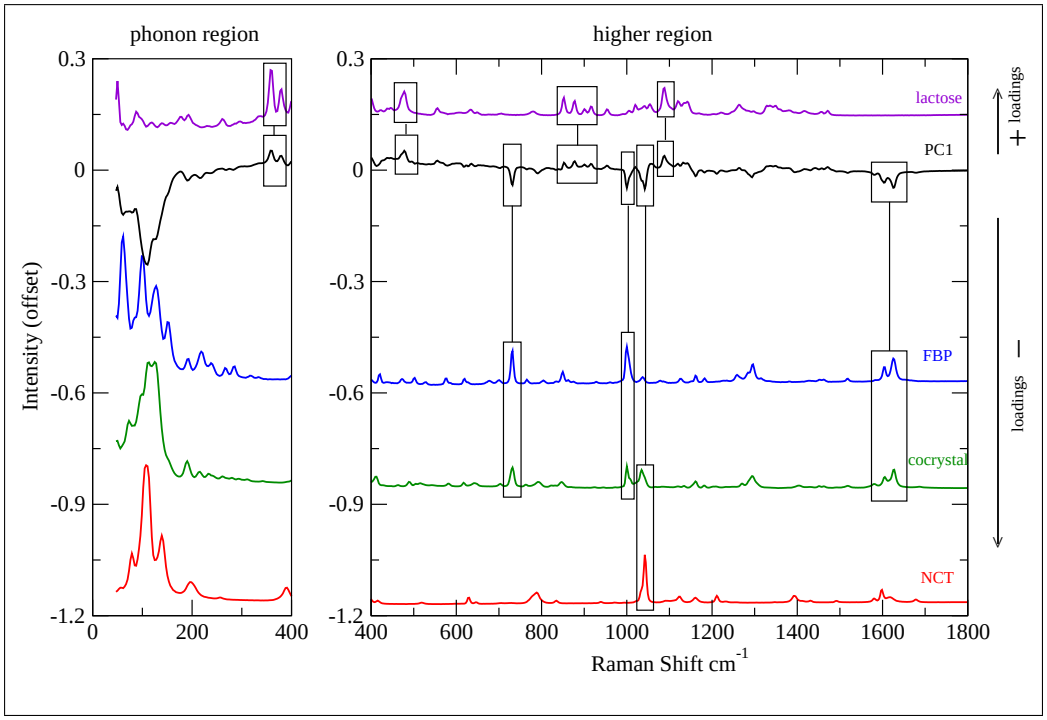

Figure 5.8: PC1 loadings in comparison with referencing Raman spectra of tablets' ingredients. Spectra and PC1 loading are arranged in a bottom-top manner; NCT (red), co-crystal (green), FBP (blue), PC1 (black), lactose (maroon). Below PC1 are spectra of negative drug loadings (NCT, co-crystal, and FBP) while the one above PC1 is of positive drug loadings (lactose). Spectra of tablets' ingredients were scaled by 1/20 for sake of clear presentation.

−), co-crystal (green, −), FBP (blue, −), PC1 loadings (black), lactose (maroon, +) **(fig 5.8)**. Thus, PCA statistical outcomes appeared to contain meaningful chemical information as supported by PC1 loadings. This ties nicely with the scatter plot **fig 5.7** whereas all APIs ingredients; FBP (2^{nd} quadrant), NCT and co-crystal (3^{rd} quadrant) are negatively projected on PC1 axis.

As for PC2, only FBP spectrum was found to exhibit some positive loadings on PC2 within the wavenumber range of 40–600 cm^{-1} **(fig 5.9, boxes)**. Hence, the spectrum of FBP (blue, +) was arranged above PC2 loadings (black) **(fig 5.9)**. Again such observation correlates well with the positive projection of FBP (2^{nd} quadrant) on PC2 axis **(fig 5.7)**.

Overall, interesting findings were discovered by looking into some of PC loadings and the clusters of all datasets **(figs 5.7, 5.8, 5.9)**; tablets of physical mixture 25%, physical mixture 50%, co-crystal 25%, co-crystal 50%, APIs, and excipients. Firstly, more information were deduced in regards to the ingredients of tablets (APIs and excipients), more specifically the sensible nearby localisation

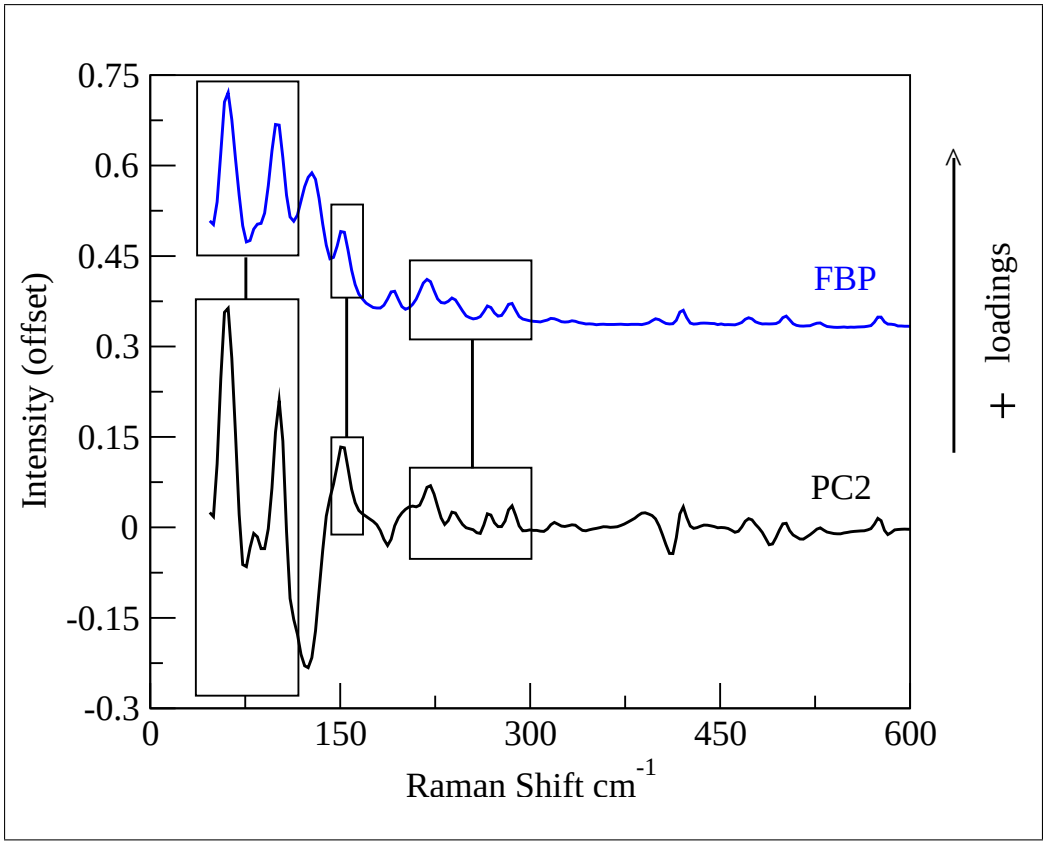

Figure 5.9: PC2 loadings in comparison with reference Spectra Raman spectra of FBP. The spectrum of FBP (blue) which has positive loadings on PC2 is arranged above PC2 loading (black). FBP spectrum was scaled by 1/20 for presentational purpose.

of components with comparable volume content. For instance, APIs localise close to tablets of higher drug content (50%) leaving excipients among tablets of lower drug content (25%). Secondly, the ready separation between tablets of different drug loading (25% and 50%) was noticed from data projections along the axis of PC with a higher variation (PC1, 62.82%). In another word, co-crystal tablets of 25% and 50% drug contents are well apart base on their projection on PC1. Similarly was the case of physical mixture tablets of 25% and 50% drug contents. Thereby, PC1 can be called herein the axis of composition **(fig 5.7)**. Alternatively, the differentiation according to chemistry was clearer on the axis of PC with a lower variation (PC2, 14.25%), i.e. tablets of various drug contents (co-crystal *vs* physical mixture tablets) are separated along PC2 (14.25%) rather than along PC1 (62.82%). Thus, PCs can be called herein the axis of chemistry **(fig 5.7)**.

Hierarchical Agglomerative Clustering:

Earlier interesting conclusion about data distribution, drawn from the scatter plot **(fig 5.7)** and the study of PCA loadings **(figs 5.8, 5.9)**, were carefully examined and clarified by means of cluster analysis (HAC analysis in specific). The distribution of datasets is affected by the degree of similarity and dissimilarity which could be calculated in various ways, however the most related method to PCA for measuring data similarity is Euclidean method[121]. Therefore, Euclidean method was the method of choice herein to work out the distance between similar pairs which later were linked in a bottom-top manner using Ward's agglomeration method HAC.

HAC analysis was performed on intensity scaled data **(5.10)**.* Data compromise 36 sets related to tablets of all drug contents (30 spectra)†, and tablets' individual ingredients (6 spectra)‡. Moreover, HAC analysis was performed in three wavenumber regions; the entire Raman region **(figs 5.10 a)**, phonon region < 400 cm^{-1} **(figs 5.10 b)**, and higher molecular region > 400 cm^{-1} **(figs 5.10 c)**. The resulting linked data of the HAC analysis, performed in the three wavenumber regions, were framed in boxes respectively coloured in green, red, and blue. Now by looking at the HAC outcomes **(fig 5.10)**, when analysis was performed on intensity scaled data only without baseline correction preprocessing, some interesting observations are noticed;

1. The first dendrogram **(fig 5.10 a, green)**, which refers to HAC analysis within the entire wavenumber region, displayed the followings;

    - The first level of clustering interestingly revealed the loading-based distinction between datasets. In another word, the main two branches

* The effect of baseline correction on such analysis is presented in **appx C (figs C.9, C.10, C.11, 5.11, C.12, C.13, C.14, C.15, C.16)**.

†30 tablets spectra: 25% co-crystal loading (9 spectra), 25% physical mixture loading (9 spectra), 50% co-crystal loading (6 spectra), and 50% physical mixture loading (6 spectra).

‡6 references spectra: FBP, NCT and their co-crystal, lactose, Mg Stearate and avicel.

of the dendrogram captured the 50% drug content tablets against tablets of the 25% drug ratios. Within tablets of the higher drug content (50%) categorised API ingredients (FBP, NCT, and their co-crystal), whereas they were excipients (lactose, avicel, and Mg Stearate) which localised within tablets of the lower drug content (25%).

- More specifically (levels down) in the 50% drug ratio branch, all of API references (FBP, NCT, and their co-crystal) are classified within the same sub-branch of the 50% physical mixture tablets away from the sub-branch of co-crystal tablets of 50% ratio. From the APIs, only FBP was directly linked to the 50% physical mixture tablets while the rest of APIs (NCT and co-crystal) are paired one level above.
- On the 25% drug ratio branch (levels down), excipients were linked together in a separate sub-branch from the one which holds both of co-crystal and physical mixture tablet sets of the 25% drug ratio. The latter by its turn sub-classified into two categories; co-crystal tablets of 25% ratio and physical mixture tablets of similar percentage.
- Hence, the chemistry based distinction between datasets can be alluded by another look at secondary levels of clustering. For instance, the differentiation between co-crystal and physical mixture tablets was mainly noticed one branch below both main branches (drug loading-based branches).

2. The second dendrogram **(fig 5.10 b, red)**, which refers to HAC analysis within the phonon region, revealed comparable observations to those deduced from the first dendrogram (entire wavenumber region). There are however some minor changes related to the way the APIs were sub-classified with tablets of higher drug percentages (50%), i.e. only FBP was paired with physical mixture tablets (50%) leaving co-crystal and NCT references to be linked with co-crystal tablets of similar ratio.

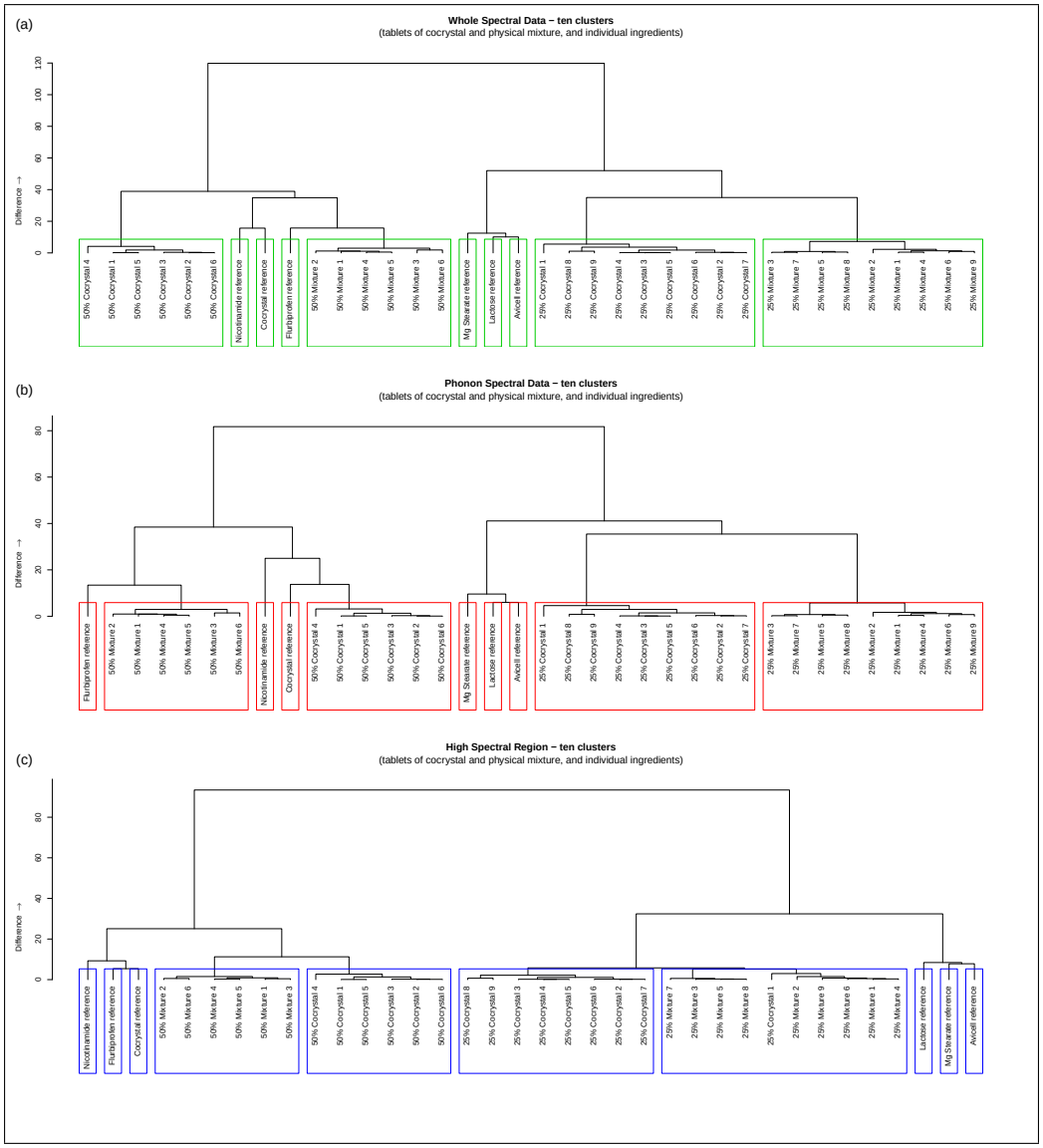

Figure 5.10: HAC dendrograms in 3 regions (scaled only). Dendrograms are calculated on intensity scaled data without baseline correction from the entire wavenumber region (a), phonon region (b), and molecular region (c). The analysis was based on measuring the similarity between data using the Euclidean method. Data were then linked using ward agglomeration method. Similar clusters were framed in boxes and colour coded in green, red, and blue in the three panels, respectively.

3. Finally, the third dendrogram **(fig 5.10 c, blue)** which refers to HAC analysis within the higher wavenumber or molecular region. The dendrogram revealed very comparable outcomes to the analysis performed on the entire wavenumber region **(fig 5.10 a)**, apart from the classification of the first tablet of the 25% co-crystal ratio. The latter localised among the 25% physical mixture tablets. Such classification **(fig C.12 a, arrow)** was justified when looking at the spectra of 25% co-crystal tablets. Data of

25% co-crystal tablets exhibited noticeable background **(fig C.12 b)** which seemed to affect HAC outcomes **(fig 5.10 c, blue)**. Therefore, HAC analysis performed after subjecting datasets to baseline correction preprocessing, resulted in a sensible classification of the first tablet of the 25% co-crystal loading **(fig 5.11)**.*

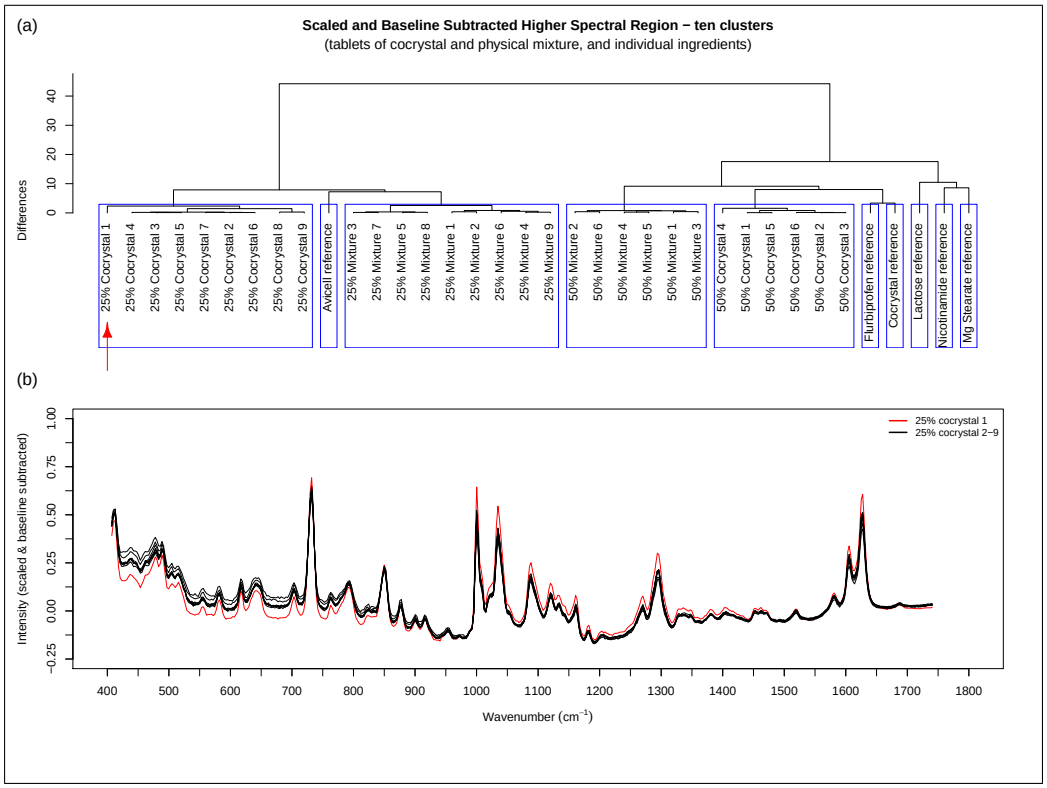

Figure 5.11: Statistical pre-treatment effects on molecular data, Dendrogram (a) *vs* Spectra of 25% co-crystal (b). Data herein are intensity scaled and baseline subtracted before performing cluster analysis. Tablet number 1 from the 25% co-crystal content is referred to by red arrow in dendrogram plot (a) while its spectrum is coloured in red (b). The rest of 25% co-crystal tablets data are in black (b).

Overall, HAC and PCA showed the main structure of datasets which is defined by the percentage of drug contents and not by chemistry, contrary to visual inspection which indicated the chemistry differences between datasets. Such outcomes could be justified based on the tendency of visual inspection to be subjective which leads mostly to incomplete story. HAC outcomes clarified PCA observations such as revealing the distinction between all datasets regardless to

*HAC analysis was performed on intensity scaled and baseline corrected data within the entire Raman region, phonon, and molecular region **(fig C.13)**.

their composition and contents. Besides to the way the references (tablets' ingredients) were categorised which seems to be intuitively sensible. For instance, APIs classified with tablets of higher drug contents, contrary to excipients which tend to cluster with tablets of lower drug content. Hence, the differentiation between tablets of different content, observed by visual inspection, was supported by chemometrics. This was in opposite to the distinction between different percentage of identical drug contents which was not at all alluded from visual examination **(figs 5.3 & 5.4)**, until PCA and HAC were employed **(fig 5.7, 5.10)**. Thereby, the distinctions between tablets' ingredients regardless to their contents and percentages were feasible from the parallel usage of both visual and chemometric analysis.

5.5 Conclusion

Interesting information related to drug development and manufacturing were revealed by using the new approach within vibrational spectroscopic schemes TRS, in a couple with unsupervised statistical analysis (PCA and HAC). This was tested for the first time on FBP-NCT co-crystal oral dosage form. The study displayed a clear distinction between components of different chemical identities from the visual inspection which was later clarified by statistical analysis. The latter analyses (PCA and HAC) also differentiate between identical components of various percentage of loadings. Therefore, the use of such analytical tool can be of a great benefit for the quality control and the good manufacturing processes in the pharmaceutical field.

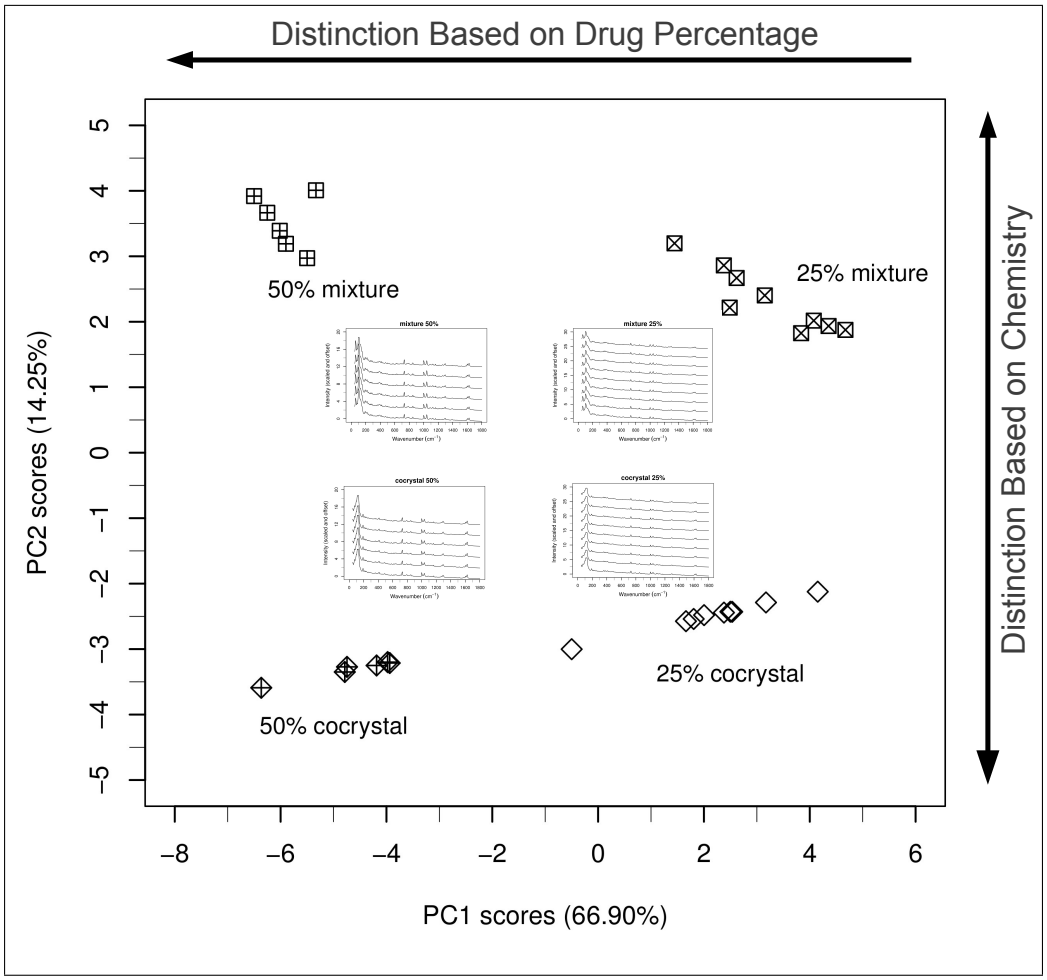

Figure 5.12: Conclusion figure of Screening Model Co-crystal Tablets by TRS.

CHAPTER 6

General Discussion & Conclusion

The work presented earlier described screening model co-crystal system starting from preparation until formulation using various methodologies and analytical tools. Based on previous work done by Berry *et al.*[91] and Shing *et al.*[86], flurbiprofen-nicotinamide co-crystal was selected as a model system for this work. The co-crystallisation mostly involved friendly environment methodologies such as Kofler fusion method and mechanochemical co-grinding. The resulting materials from grinding method were formulated in tablet dosage form. The screening of preparations was mostly performed using rapid and non-destructive analytical tools.

For instance, the work presented in **chap 3** handled the use of Kofler preparations to study binary systems which are generally difficult to prepare using traditional methods (i.e., evaporation from solution). Kofler preparation are traditionally assessed using the hot-stage microscopy[91]. One of the main objectives of this work was to develop a detailed protocol for screening Kofler preparations at room temperature using Raman spectroscopy. Raman spectroscopy yielded valuable chemical and physical insights into components, and the sensitivity of screening was strongly enhanced when considering low wavenumber region, which probes the crystalline structure of components[198]. In this chapter the new co-crystal phase and another polymorphic form of FBP were identified by means of statistical analysis PCA and DCLS. In addition, a refinement was made regarding the prediction of binary phase diagram from Kofler melt. It was shown that the

composition gradient is not linear as a function of position as had been traditionally presumed. Hence, this protocol provided additional information which might advance the field of co-crystal screening. An overall summary for the work presented in this chapter is displayed in **fig 6.1**.

A continuing study on FBP-NCT Kofler preparation was shown in **chap 4**. Such system which already consisted of NCT and FBP holding at the interface FBP-NCT co-crystal form I[168], was accompanied on prolonged storage at ambient condition by a co-crystal form II running along the zone of mixing. The phenomenon of drug polymorphism whether it is single or multi-component systems is of an impact on the quality of drug production if it is not understood. Thereby, a sufficient understanding of the transformation process between forms was explored. Accordingly, the FBP-NCT co-crystal polymorphism was investigated. It was found that the preparation of co-crystal sample suitable for polymorphism study was achievable when adopting Ostwald's rule of step changes protocol. Henceforth, a quenched equimolar mixture of FBP:NCT was prepared and investigated using;

- DSC as initial thermal scanning helped in optimising methods of preparation and this was also confirmed optically when using polarised thermo-microscopy (HSM).
- VT-Raman accompanied with PCA as a clustering technique provided a clear identification of all FBP-NCT phases; amorphous → co-crystal form I → the melt of CC I → co-crystal form II → melt.
- Alternatively in VT-XRPD, analysis showed only four phases instead of five (amorphous → co-crystal form I → co-crystal form II → melt), despite the similarity in sample preparation. In another word, solid/solid transformation was picked up and this was more likely due to some technical issues (uneven heating atmosphere surrounding the sample), which resulted in the rearrangement between co-crystal forms.

- It was also found from VT-XRPD that the transformation led to the stable form which matched well with the calculated powder pattern based on single x-ray crystal experiment.

- Regarding the crystal structure determination, the crystal structure of one form was determined. It was found that the interaction between FBP:NCT occurs in an equimolar ratio *via* pyridine-carboxylic acid heterosynthon, separated by amid-amid dimer.

In summary, the thermal screening (DSC and HSM), Raman spectroscopy, and diffraction methods (XRPD) displayed the presence of a metastable form in FBP-NCT co-crystal system before forming the stable form 1:1. An overall summary for this study is presented in **fig 6.2**.

Finally in **chap 5**, FBP-NCT co-crystal prepared using LAG method was formulated in tablets form for the first time. It was demonstrated that co-crystal and not individual API exists within formulation. Moreover and by using analytical tool sensitive to solid-state substances (transmission Raman spectroscopy), a distinction was made between formulations containing FBP-NCT co-crystals and those containing co-crystal parent components. It was also proved that a distinction based on the ratio of drug composition, not only the chemistry was feasible using chemometric tools (PCA and cluster analysis). A summary illustrating this study is shown in **fig 6.3**.

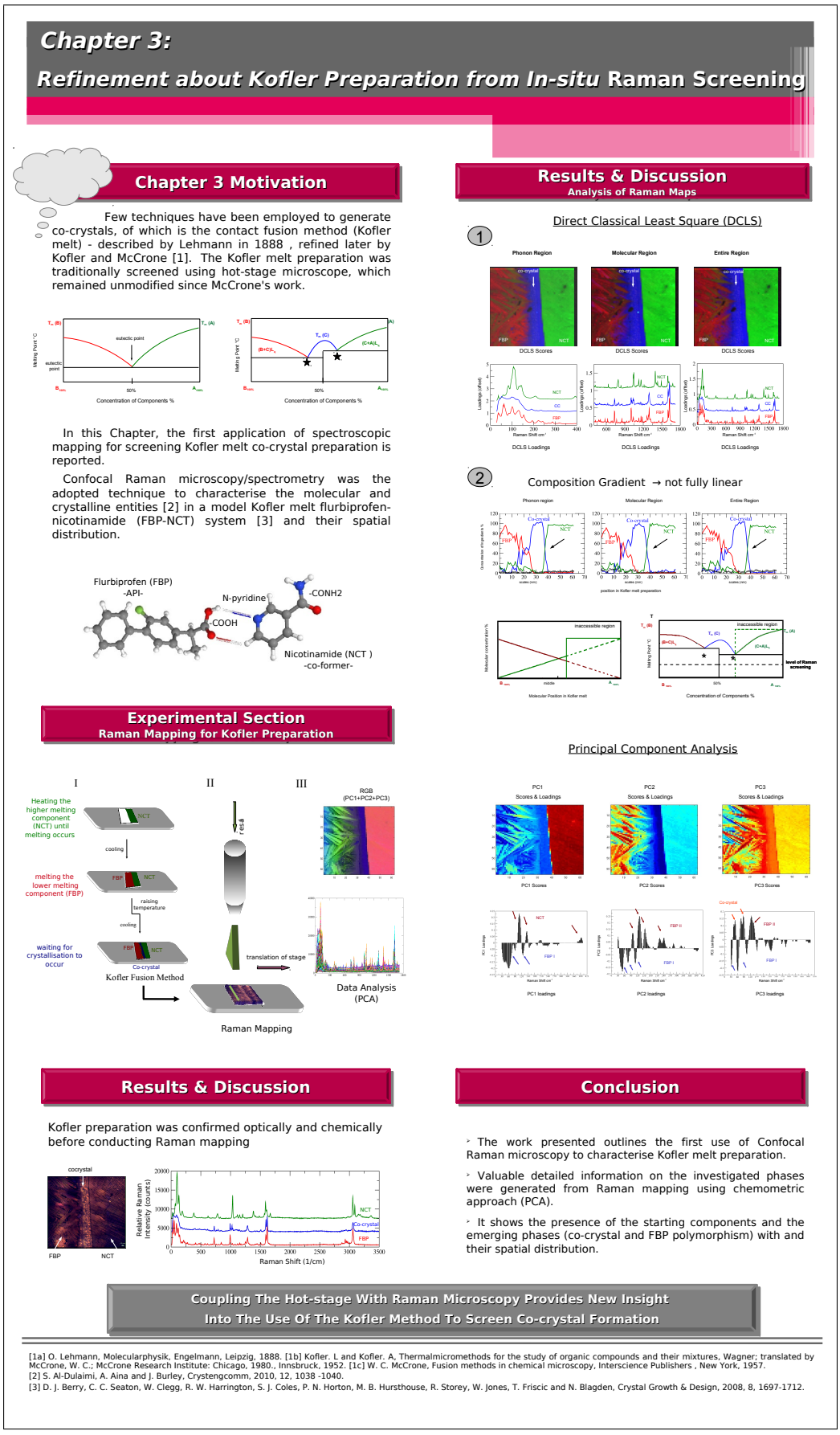

Figure 6.1: Summary card of research work in chapter 3.

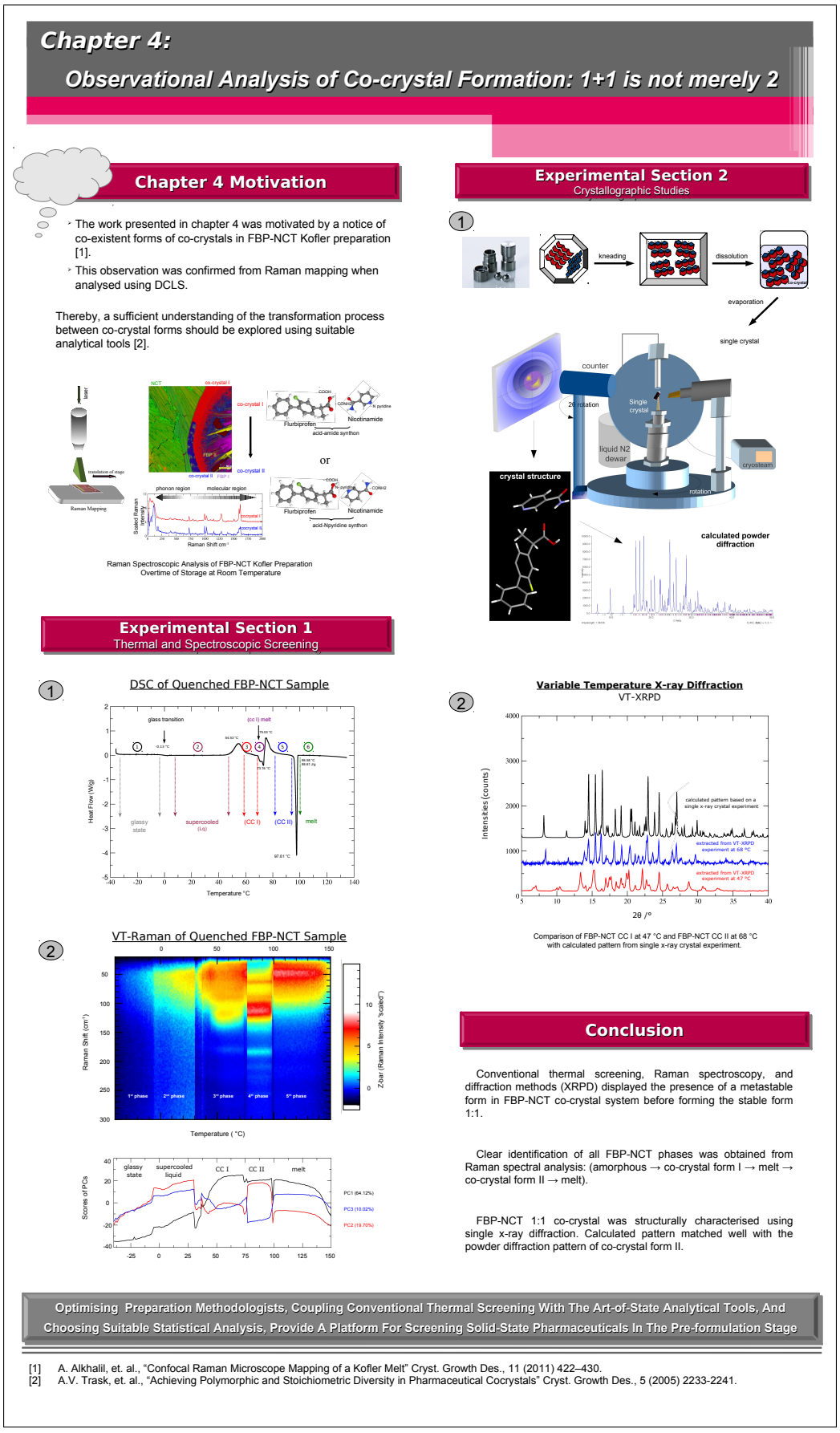

Figure 6.2: Summary card of research work in chapter 4.

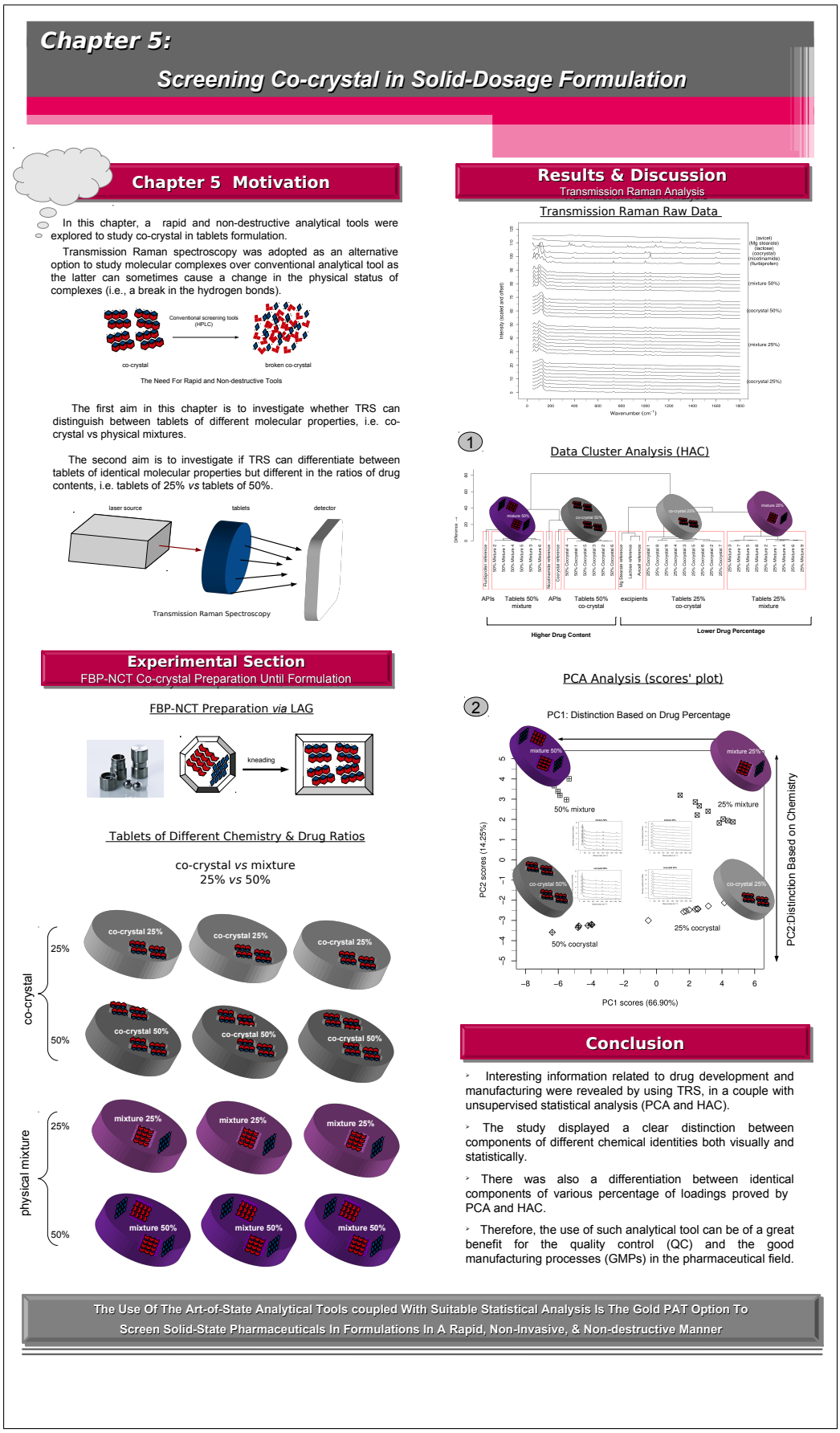

Figure 6.3: Summary card of research work in chapter 5.

APPENDIX A

Supplementary Info Part-I

Confocal Raman Mapping of Kofler Co-crystal System

It can be seen from **(fig A.1 a,b)** that both sampling points of NCT and FBP respectively, located in the peripheral regions of the mapped areas, exhibit similar chemical behaviour to the parent components prepared separately under similar conditions. Interestingly, this was also the case of the spectrum at the zone of mixing when compared to the spectra of a melted equimolar mixture of FBP and NCT **(fig A.1 c)**.

Different ratios of FBP and NCT mixtures (1:1, 2:1, and 1:2) were prepared under Kofler condition, of which only (1:1) was capable of forming their co-crystal. Fusing an equimolar FBP:NCT mixture exhibited similar optical **(fig A.2)** and chemical features **(fig A.1 c)** to the one extracted from the zone of mixing.

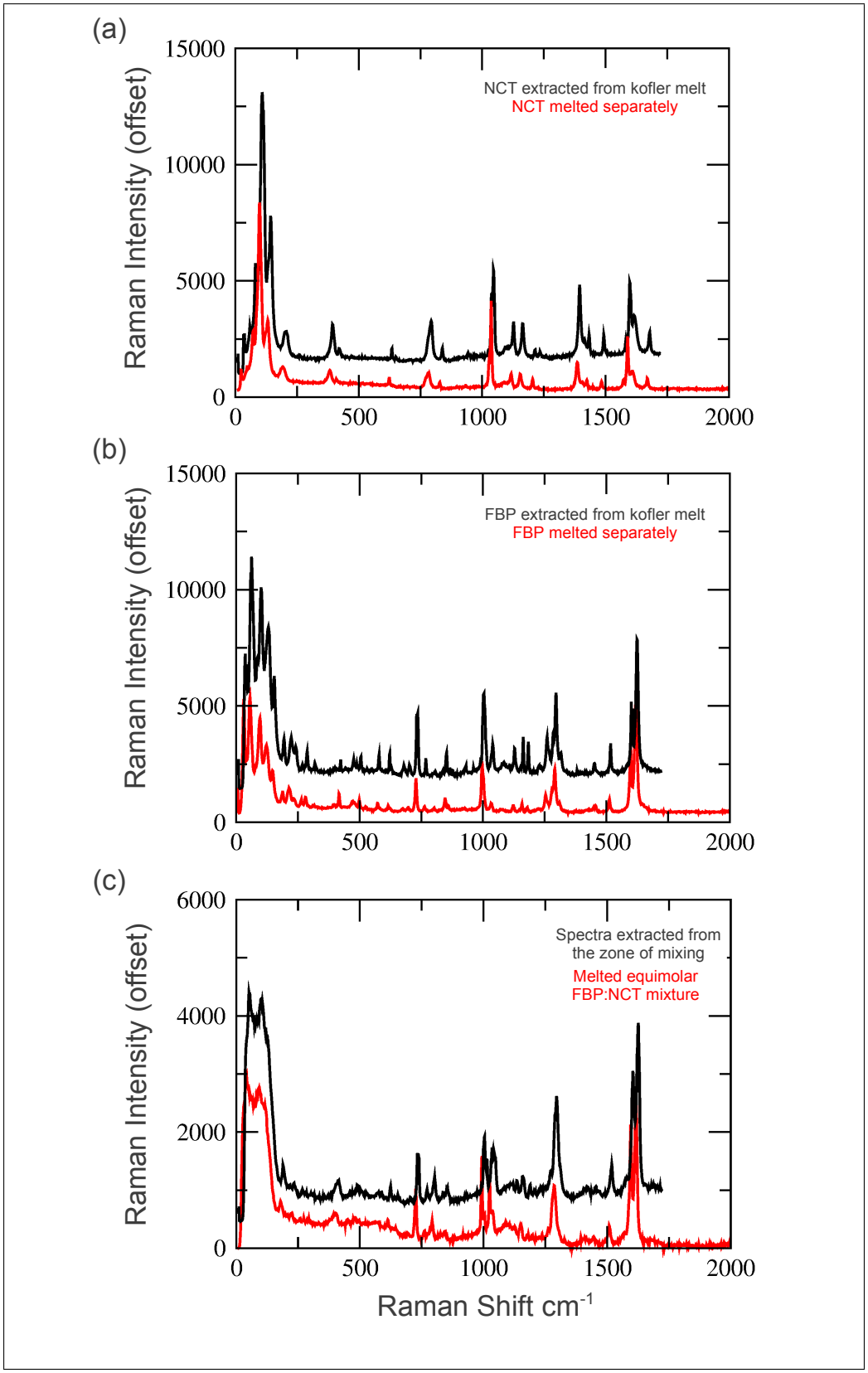

Figure A.1: Raman spectra of NCT, FBP, and co-crystal, from pure samples and from the Kofler melt; (a) is a comparison of separately melted NCT with that at the NCT side in Kofler preparation (right), (b) is a comparison of separately melted FBP with that at the FBP side in Kofler preparation (left), while (c) is a comparison of an equimolar melted preparation of FBP and NCT with material at the zone of mixing in Kofler preparation (in between).

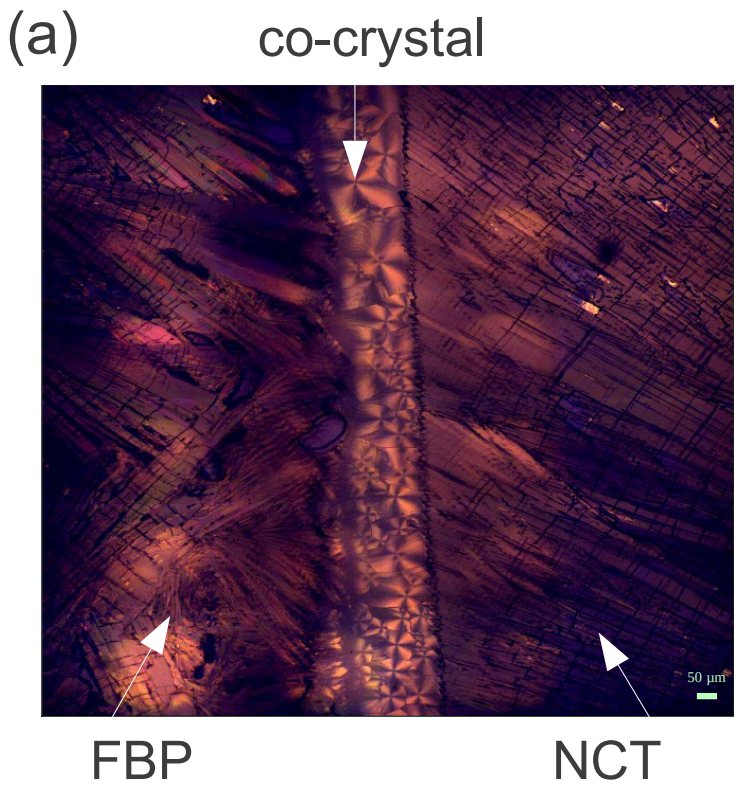

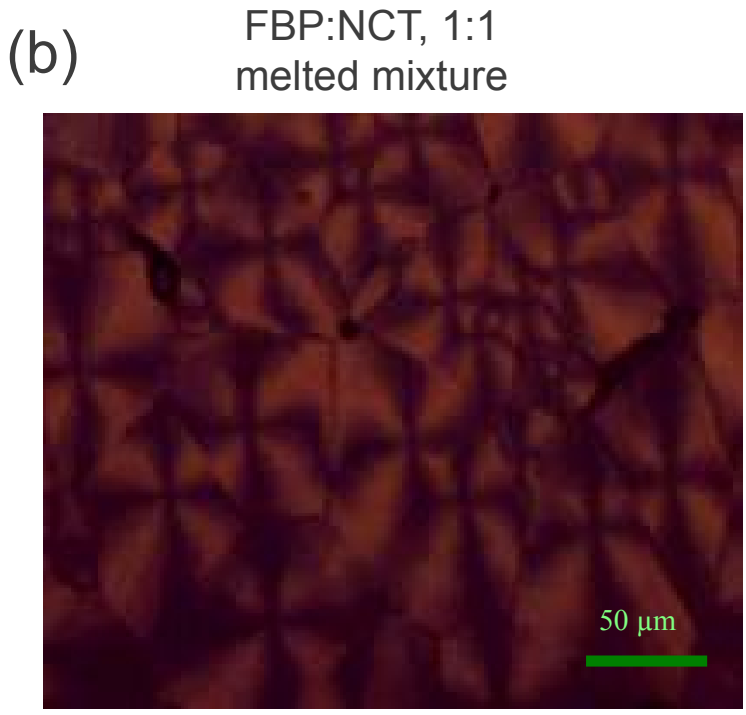

Figure A.2: Morphological similarity between the area of the zone of mixing in Kofler melt (a) and melted equimolar FBP:NCT mixture (b) as confirmed optically.

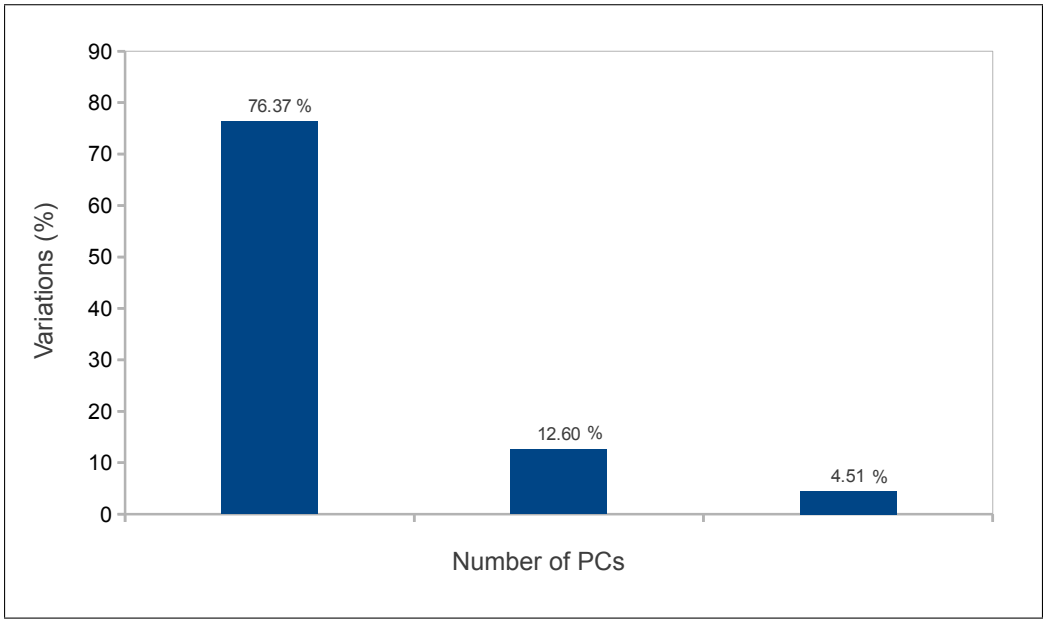

Figure A.3: Scree plots of the first three principal components. It shows that they are assigned $> 93\%$ of the whole PCs' variations.

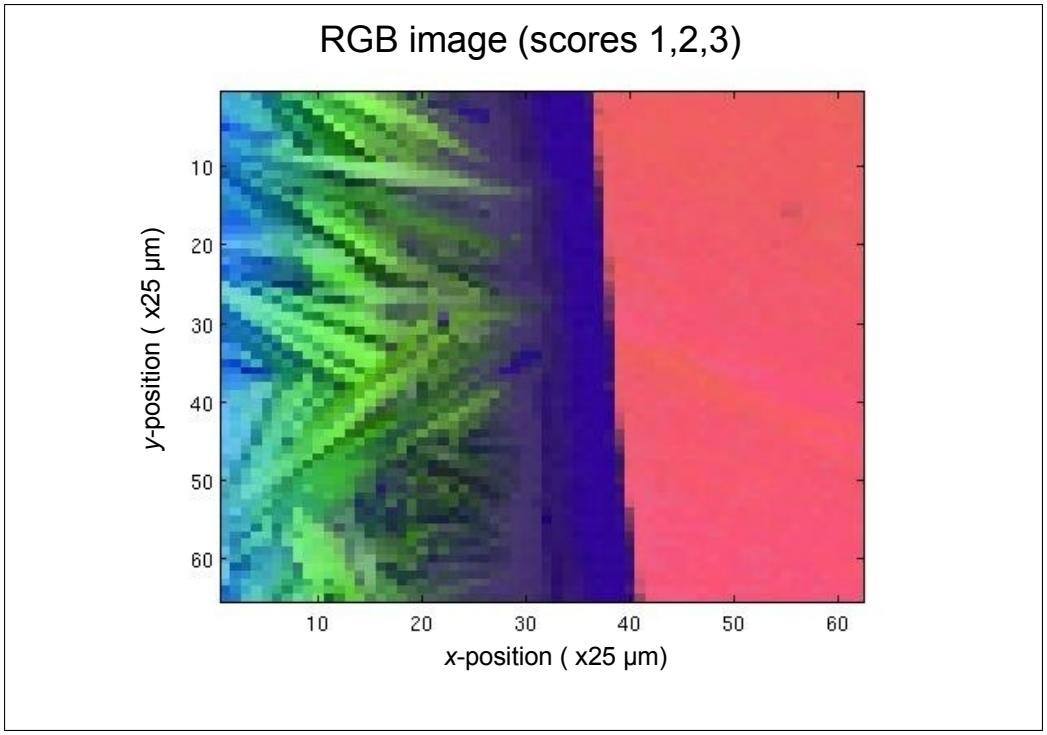

Figure A.4: RGB colour-map image created by overlapping the first three PCs (being assigned by the anticipated/unexpected compounds and having variances of $> 93\%$) **(fig A.3)**. This demonstrates the localization of the components in three regions, which was also noticed form DCLS scores at n=3 **(fig 3.5)**.

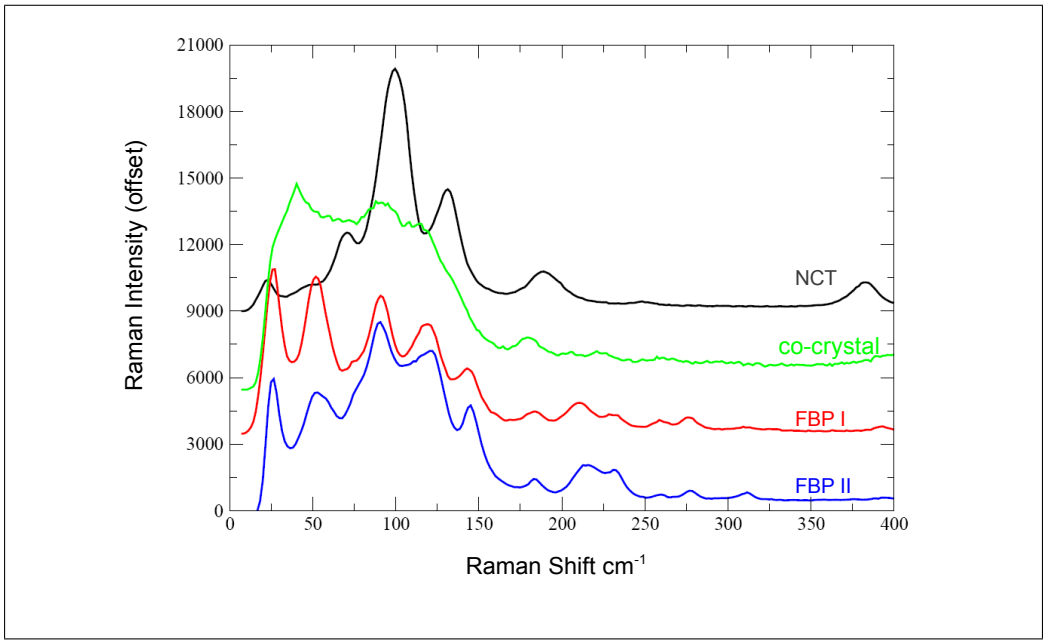

Figure A.5: Raman spectra of Kofler components stacked in a top-bottom manner; NCT (black), co-crystal (green), FBP I (red), and FBP II (blue). They are used as references for the advantage of comparison with PCs loadings **(fig 3.9, bottom images)**

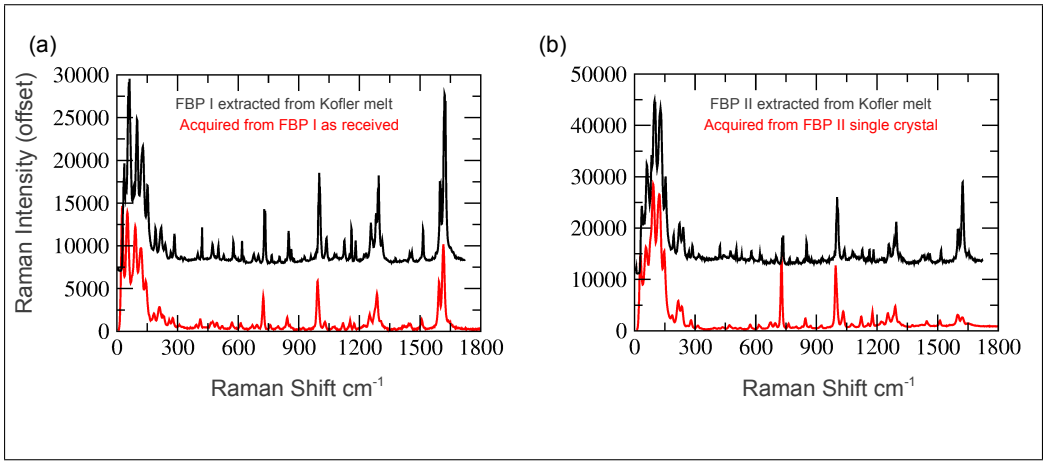

Figure A.6: Comparison of Raman spectra of pure FBP form I and II (red), and spectra extracted from mapping (black). (a) is a comparison of FBP I with that extracted from Kofler mapping, while (b) is a comparison of FBP II acquired from single crystal (obtained from solution) with that extracted from FBP area in Kofler mapping.

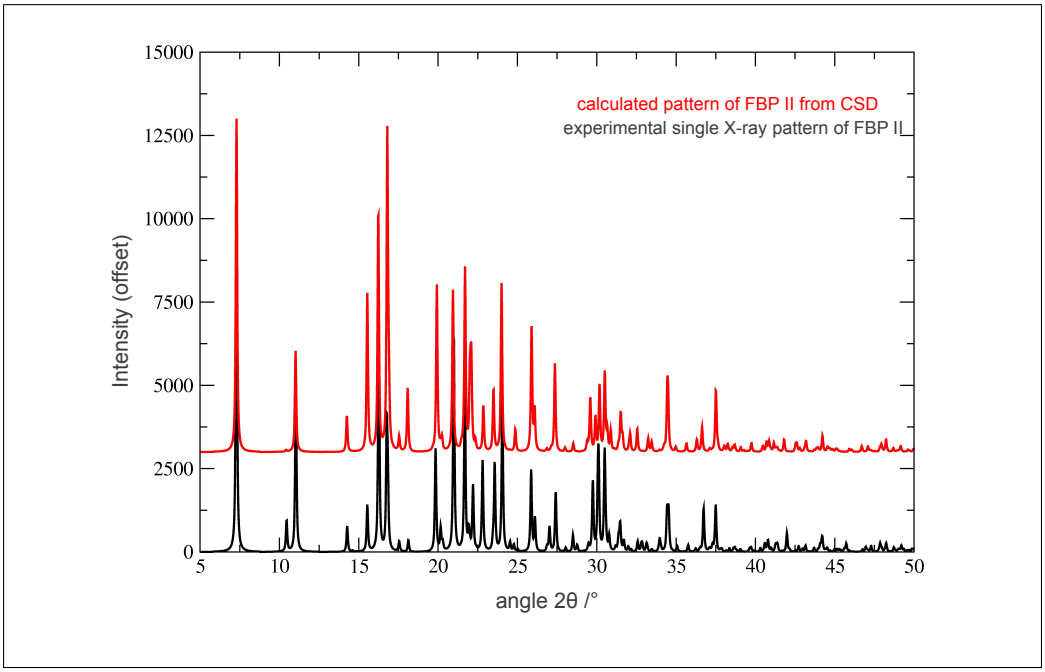

Figure A.7: Comparison of X-ray pattern of calculated FBP form II of a ref-code (FLUBIP01) (red) *vs* the experimental single x-ray pattern of FBP (black) obtained spontaneously from acetonitrile solution in attempt to get FBP-NCT co-crystal form.

APPENDIX B

Supplementary Info Part-II

The Study of FBP-NCT Co-crystal Polymorphism

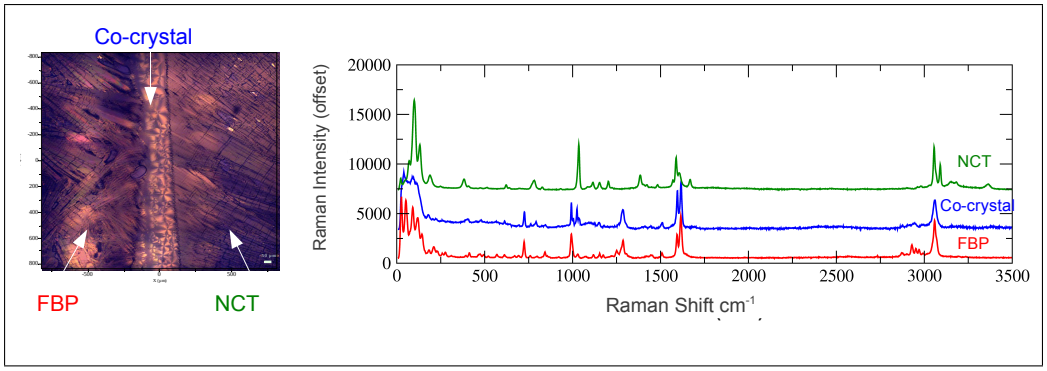

Figure B.1: Raman microspectroscopic studies of FBP-NCT Kofler preparation. Shown in (a) is Kofler preparation after cooling which includes two peripheral regions, FBP (left) and NCT (right), and the zone of mixing in between, all are indicated by arrows. In (b) is Raman spectra of NCT (green), co-crystal (blue), and FBP (red), all are arranged in a top-bottom manner.

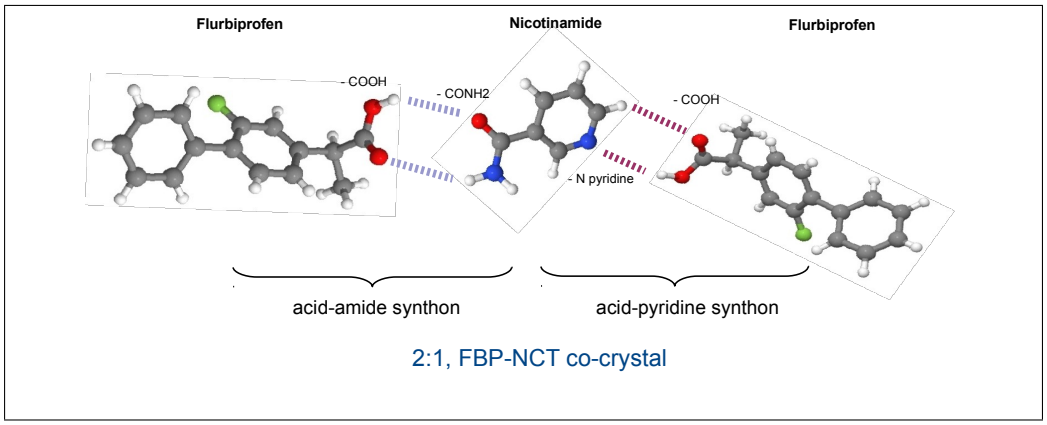

Figure B.2: Schematic structure of 2:1, FBP-NCT supramolecular synthon. The interaction is expected to be facilitated *via* both acid-pyridine and acid-amide synthons.

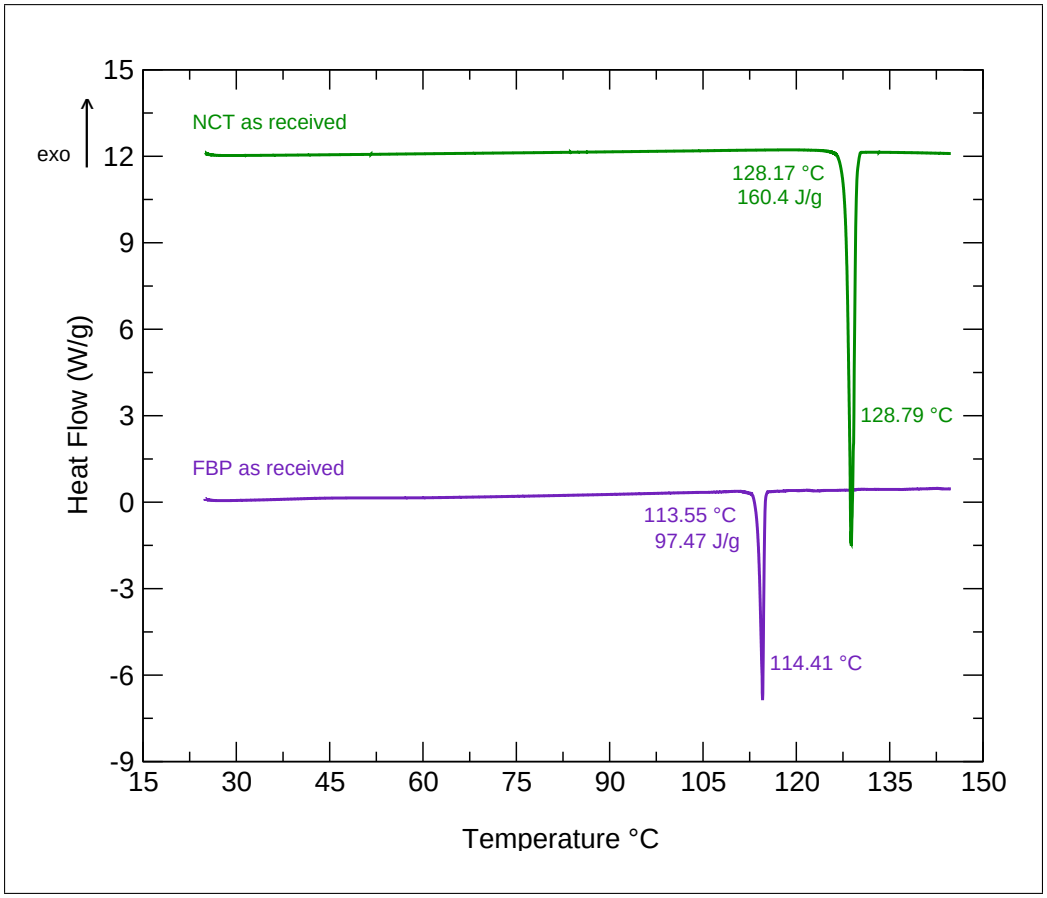

Figure B.3: DSC scanning of co-crystal parent components screened as received. It shows the thermal traces of NCT at the top (green) and FBP at the bottom (purple).

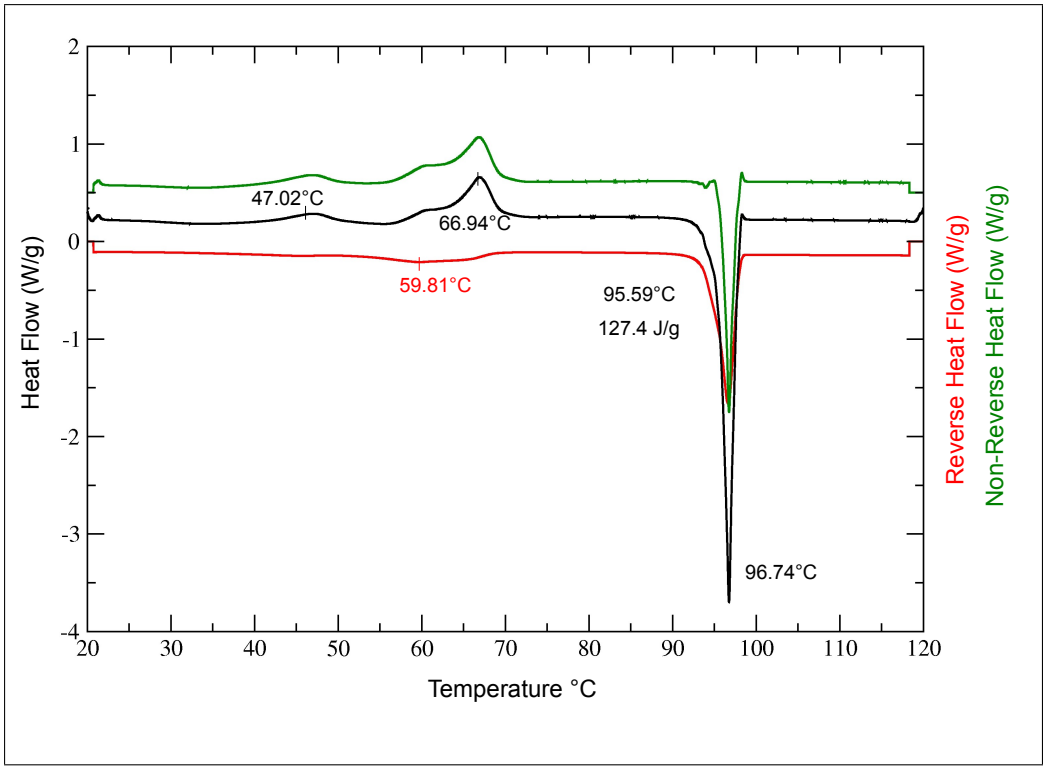

Figure B.4: Modulated DSC of solidified melted equimolar mixture of FBP-NCT. It is separated in a top-bottom manner to a non-reverse heat flow trace at the top (green), the whole heat flow trace in the middle (black), and a reverse heat flow trace at the bottom (red). The heat flow trace shares with the non-reverse heat trace similar thermal information. Both display two exothermic events at 47.02 °C and 66.94 °C, and one endothermic event at 95.59 °C. On the other hand, the reverse heat flow shows two endothermic peaks only.

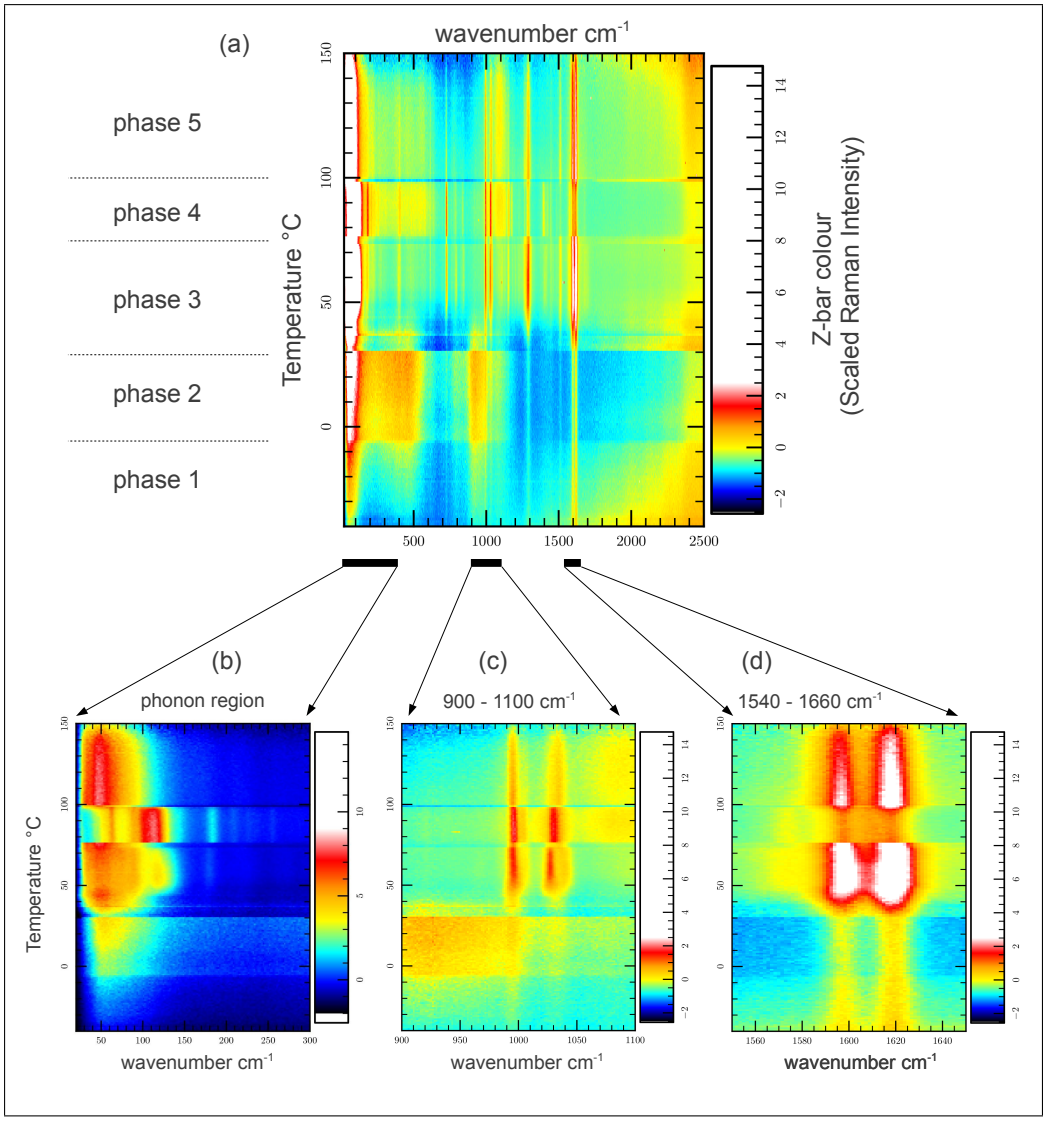

Figure B.5: VT-Raman raw data into 2D presentation. A 2D plot of the entire VT-Raman data of quenched melted 1:1 FBP-NCT mixtures is shown in (a). Below are 3 sub-plots of VT data at narrower wavenumber regions; (b) phonon mode, (c) 900 - 1100 cm^{-1}, (d) 1540 - 1660 cm^{-1}. In all these plots, the x-axis represents Raman shift (cm^{-1}), y-axis is temperature (°C), and colours indicate to scaled Raman intensity.

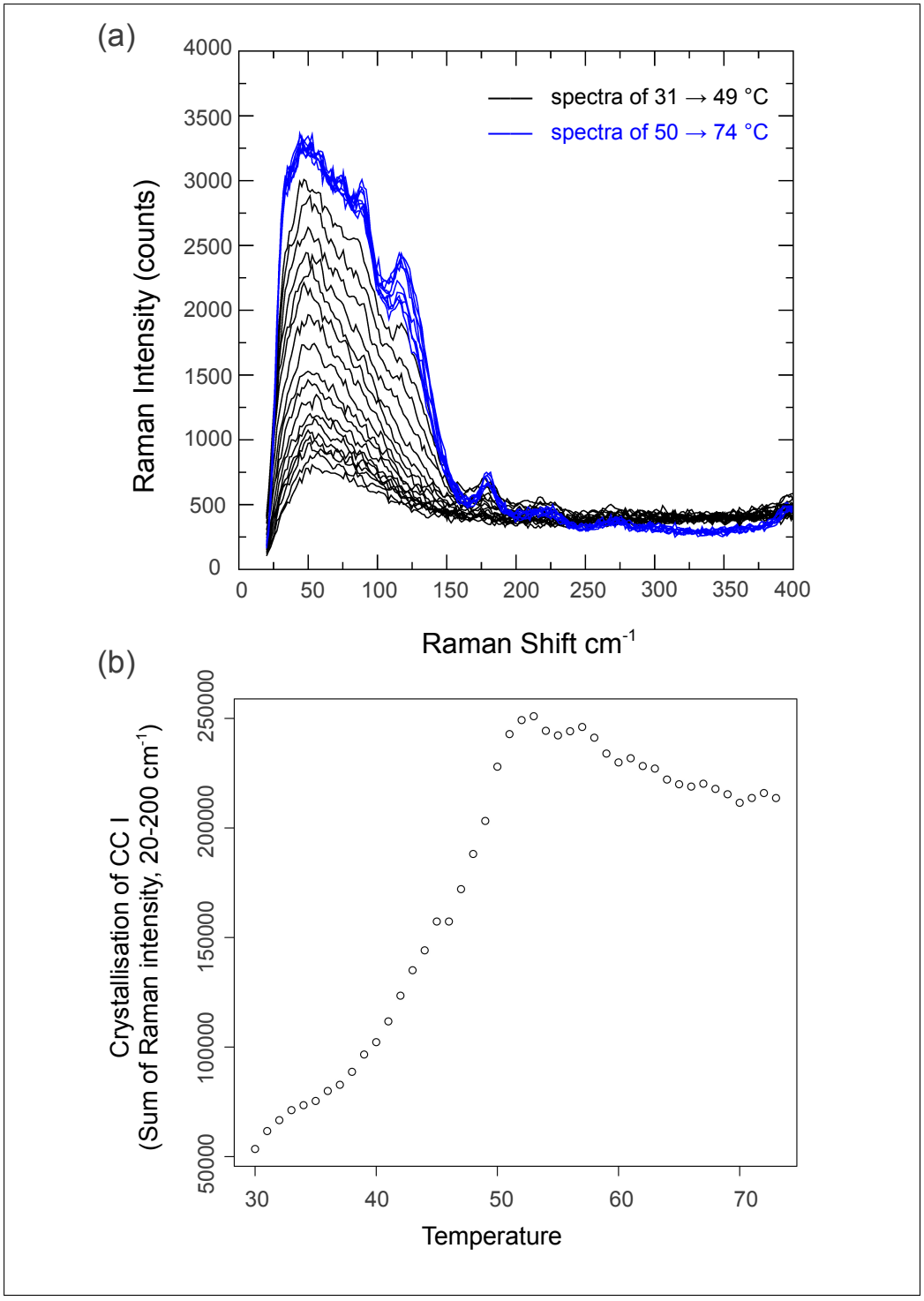

Figure B.6: The Crystallisation of CC I is explained by the variation in the intensity of CC I spectra. Phonon Raman spectra at a temperature range of 31 → 74 °C, which correlate with the group of co-crystal form I **(fig 4.10 b)**, are displayed in (a) with no offset between data. Highlighted in black are spectra at a temperature range of 31 → 49 °C (bottom sets of spectra), while the ones in blue were collected over a temperature range of 50 → 74 °C (top sets of spectra). In (b) is the crystallisation behaviour of CC I, whereas the intensities of phonon Raman spectra (20 → 200 cm^{-1}) are plotted as a function of temperature range of 31 → 74 °C.

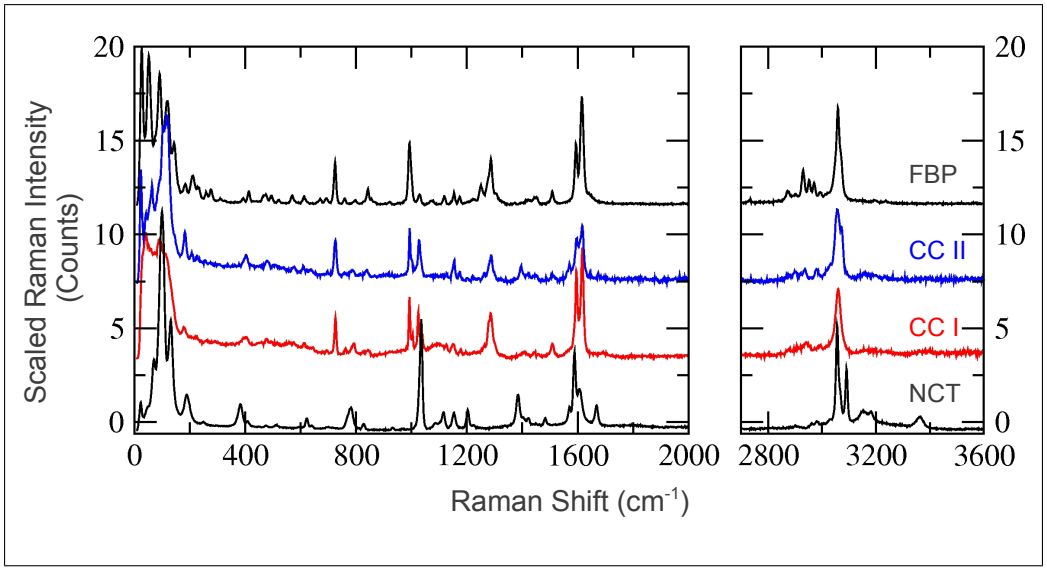

Figure B.7: Raman comparison between co-crystals & the starting components. Raman spectra extracted at 50 °C (CC I, bottom-middle in red) and 70 °C (CC II, top-middle in blue) from VT-Raman data of quenched melted 1:1, FBP:NCT, in comparison with Raman spectra acquired from FBP (top black) and NCT (bottom black) as received.

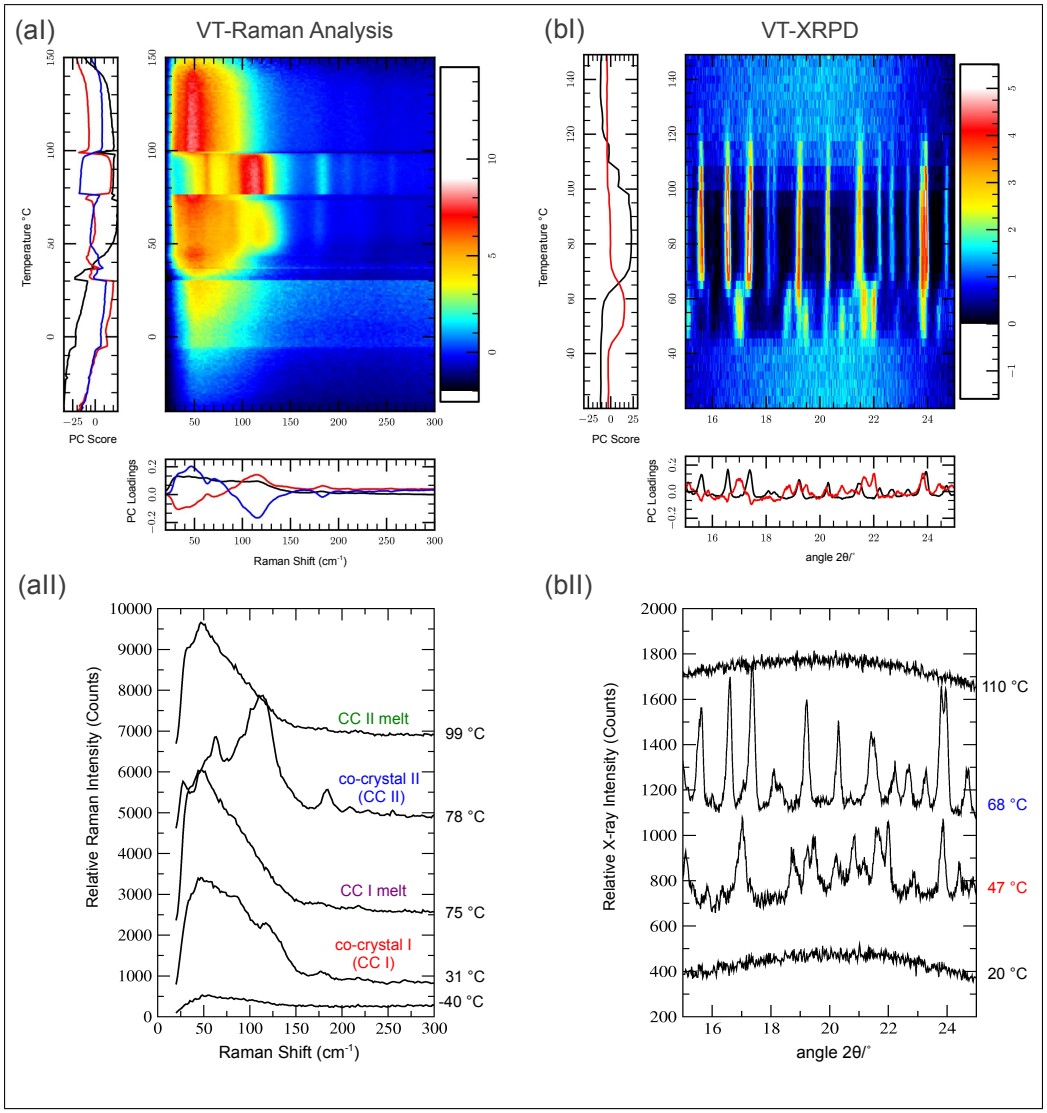

Figure B.8: A comparison between VT-Raman *vs* VT-XRPD data. VT-Raman data are shown in (aI & aII) while VT-XRPD are displayed in (bI & bII). Data are shown into 2D form, whereas y-axis is temperature, x-axis is wavenumber in (aI) and angle in (b1), and scaled intensities are represented in Z-bar colours. Both plots (aI & bI) are coupled with a sub plot (left-hand side) of PCs scores versus temperature, and another one at the bottom for the loading of the first two PCs. In aII & bII respectively, are Raman spectra and XRPD patterns collected at transition temperatures as alluded from each technique.

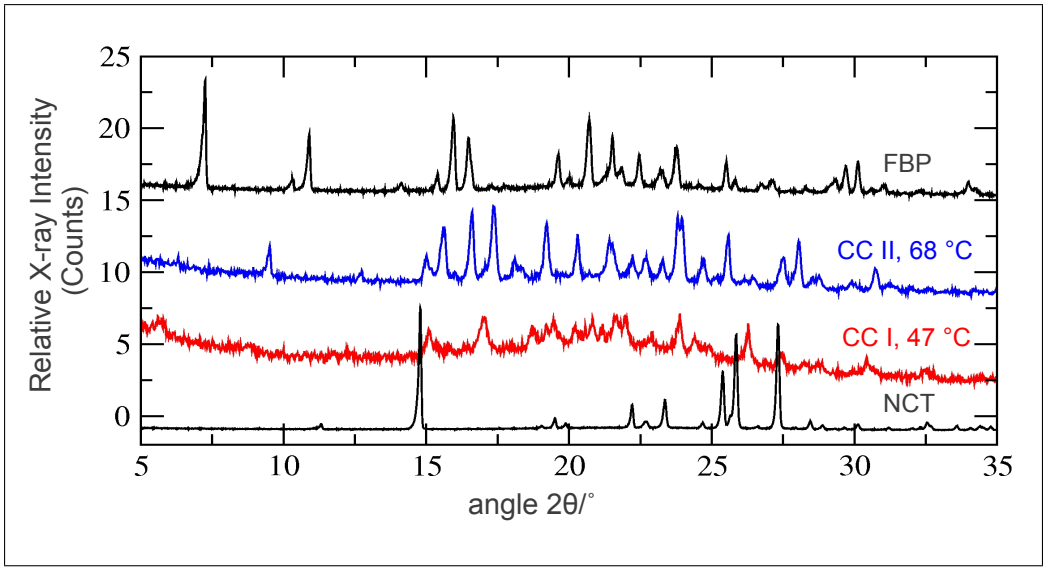

Figure B.9: XRPD comparison between co-crystals & the starting components. Powder patterns extracted at 47 °C (CC I, bottom-middle in red) and 68 °C (CC II, top-middle in blue) from VT-XRPD data of quenched melted 1:1, FBP:NCT, in comparison with powder patterns collected from FBP (top black) and NCT (bottom black) as received.

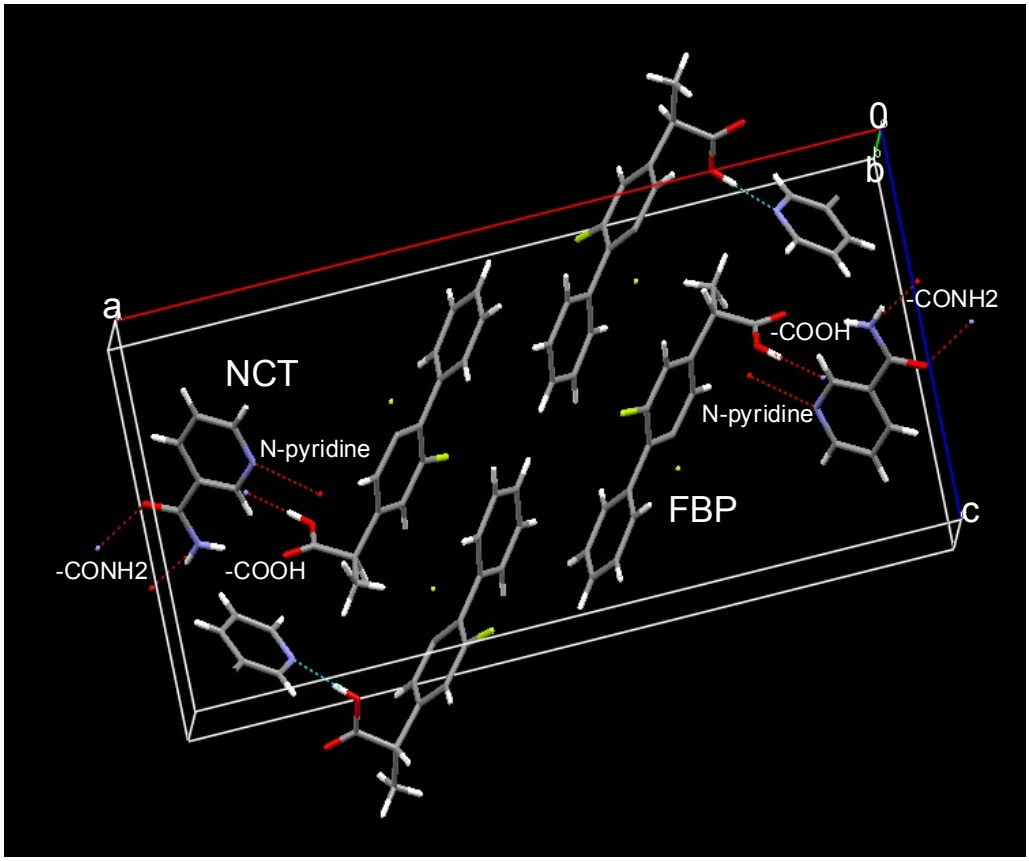

Figure B.10: SXD unit cell of the crystal structure of FBP-NCT co-crystal. It shows four molecules in each unit cell. The interacting between FBP and NCT occurred through acid-pyridine hydrogen bonds.

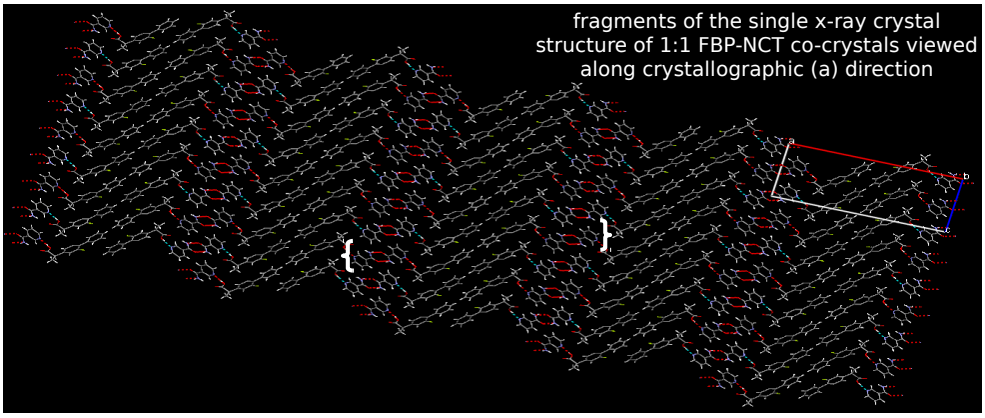

Figure B.11: Fragments of the crystal structure of 1:1 FBP-NCT co-crystals viewed along crystallographic (a) direction. It displays the zigzag shape which is supported by NCT amid-amide dimer.

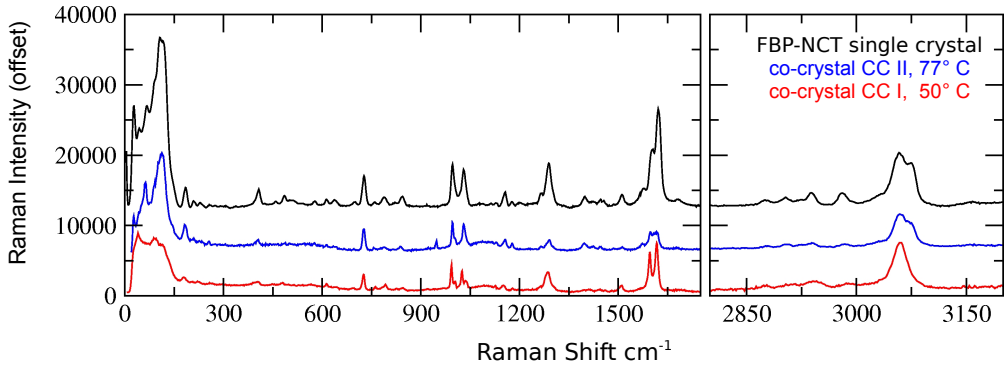

Raman spectrum extracted from VT-Raman experiment of quenched melted 1:1, FBP:NCT mixture above 77 °C was in a good agreement with the spectrum acquired from FBP-NCT single co-crystal **(fig B.12)**. Nevertheless, this was not the case of the spectrum extracted from the compound formed above 31 °C. Thus, keeping the 1:1 melted FBP-NCT mixture above 77 °C leads to the formation of 1:1 FBP-NCT co-crystal.

Figure B.12: VT-Raman spectra *vs* spectra of FBP-NCT single crystal. It shows a comparison between Raman spectra extracted from VT-Raman data at 50 °C (bottom in red) and 77 °C (middle in blue), which correlate with CC I and CC II respectively, *versus* Raman spectrum acquired from FBP-NCT single crystal (top in black).

APPENDIX C

Supplementary Info Part-III

QC Probing of Model Co-crystal Tablets by TRS

Characterisation of Co-crystal Prepared by LAG

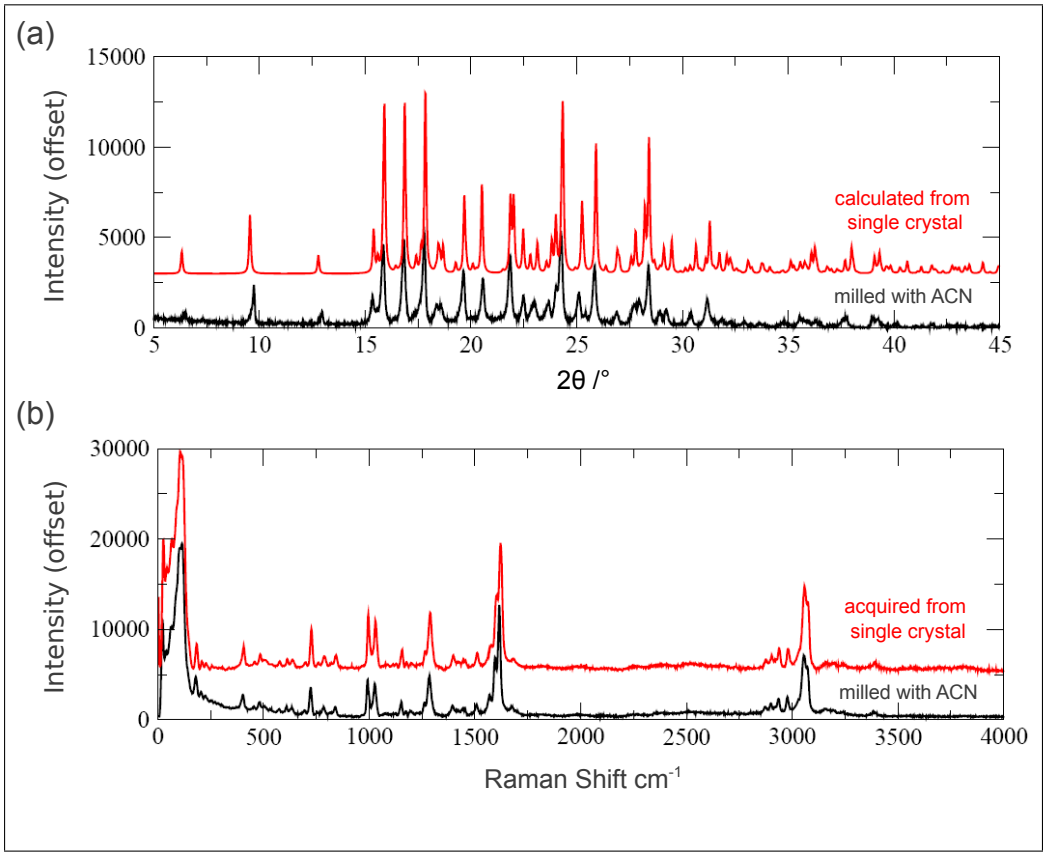

Figure C.1: Raman (a) and XRPD (b) characterisation of co-crystal prepared by LAG (milling with ACN).

The Variations of Principal Components (screeplot)

The variations of 10 PCs are shown in the chart of **fig C.2**, and their accumulative values in the table below **fig C.2**. It is quite obvious from the table in **fig C.2** to notice that the first six PCs covers most of the variations. **Fig C.2** shows a clear cut-off in PCs variations at PC6 after which the change in the variations becomes very steady. That is why only six PCs will be included for PCA analysis as the rest are considered less informative.

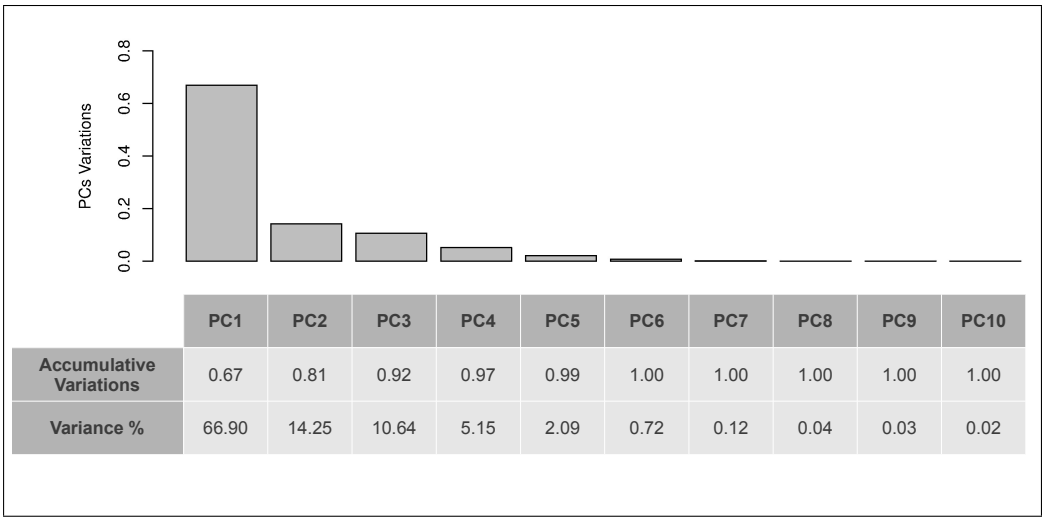

	PC1	PC2	PC3	PC4	PC5	PC6	PC7	PC8	PC9	PC10
Accumulative Variations	0.67	0.81	0.92	0.97	0.99	1.00	1.00	1.00	1.00	1.00
Variance %	66.90	14.25	10.64	5.15	2.09	0.72	0.12	0.04	0.03	0.02

Figure C.2: PCA scree plot of tablets data. It shows the variations of ten components. The selection of six components is considered as sufficient to represent the whole real data as supported from the bottom table

Further inspection was performed on the first 6 PCs' loadings **(figs C.3, C.4, C.5, C.6, C.7, C.8)**. A step was needed to check the suitability of including PCs with meaningful chemical information and excluding ones that bear either noise or repetitive information.

The loadings of PC1 which accounts for 60.90% of data variance **(fig C.3, top)** was plotted in comparison with Raman spectra of tablets' ingredients **(fig C.3, below)**. The comparison was shown in both phonon (40–400 cm^{-1}) and higher wavenumber region (400–1800 cm^{-1}). PC1 loadings showed some resembling features to Raman spectra of tablets' ingredients; in their positive values with lactose, and negative values with co-crystal **(fig C.3)**. Similar inspection was done on the loadings of other PCs. PC2 shows shared information with FBP only **(fig C.4)**, PC3 shared features with NCT and co-crystal **(fig C.5)**, PC4 shares information with lactose and Mg Stearate **(fig C.6)**. PC4 also has got slight negative background which could be referring to avicel **(fig C.6)**.

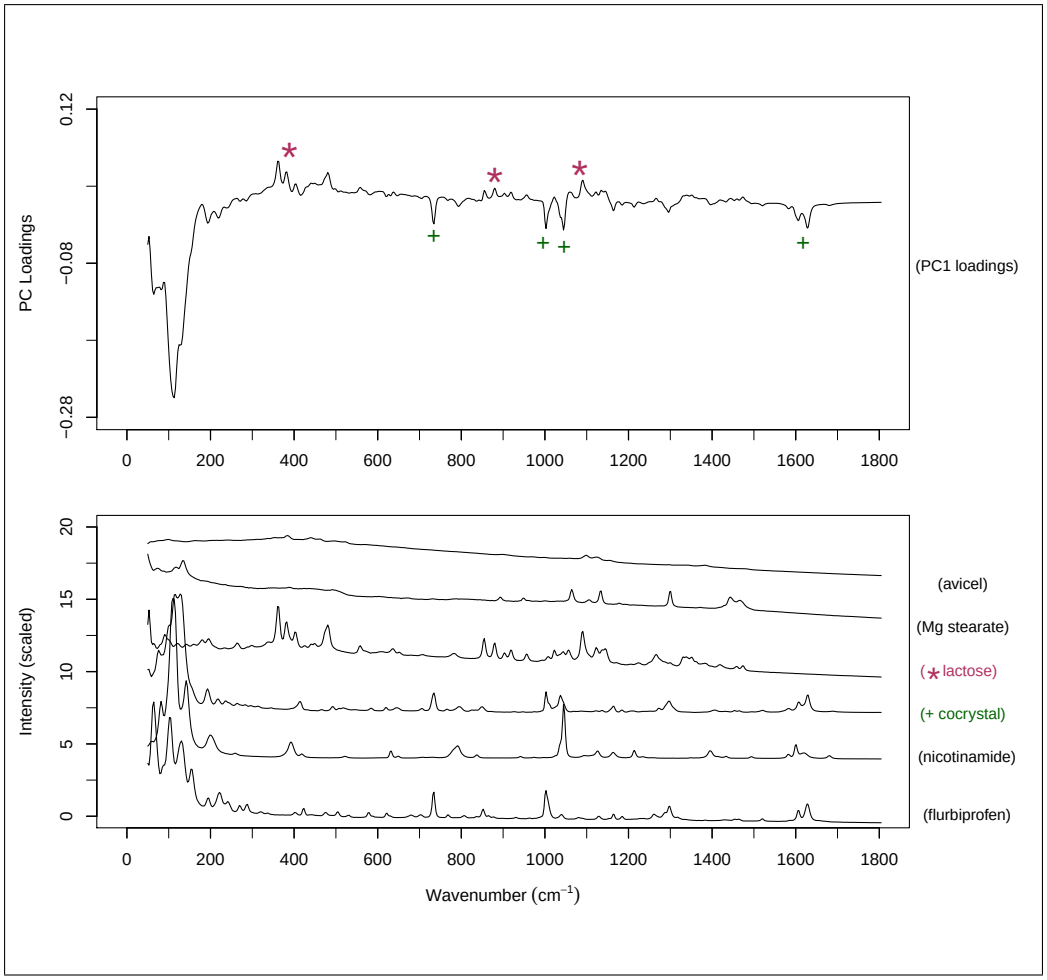

Figure C.3: The loadings of PC1 in comparison with referencing spectra. PC1 loadings is shown in (a) while Raman spectra of references are in (b). Spectra in (b) are arranged in a bottom-top manner starting from FBP, NCT, co-crystal (green), lactose (maroon), Mg Stearate, and avicel. Shared information between PC1 and references are indicated to by signs; green plus and maroon star signs referred to co-crystal and lactose, respectively.

There are some repetitive information projected on PC5 **(fig C.7)** and PC6 **(fig C.8)**. For example, lactose was projected on PC5 **(fig C.7)** as well as on PC2 and PC4. Equally was the case for FBP which was projected on both PC6 **(fig C.8)** and PC2. Accordingly, only the first four PCs are believed to represent the whole data; both PC5 and PC6 provide redundant information.

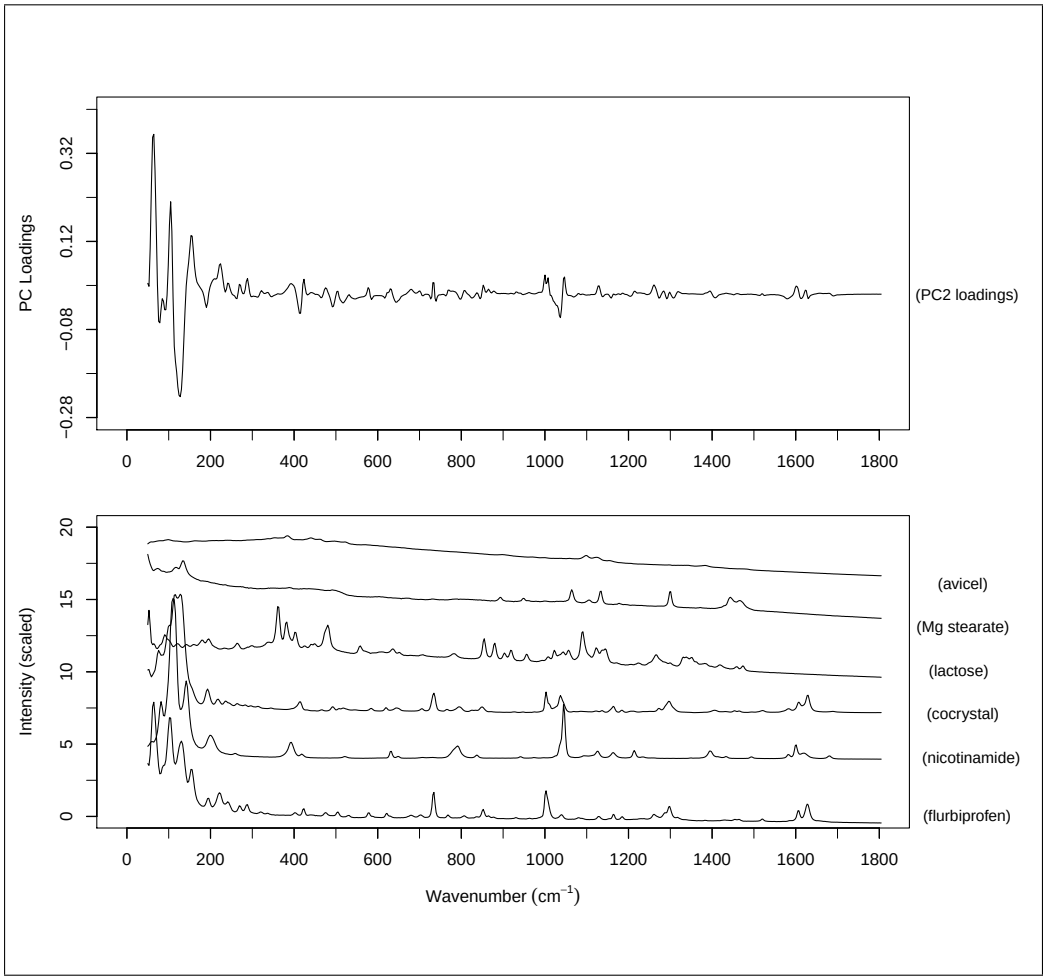

Figure C.4: The loadings of PC2 in comparison with referencing spectra. PC2 loadings is shown in (a) while Raman spectra of references are in (b). Spectra in (b) are arranged in a bottom-top manner starting from FBP, NCT, co-crystal, lactose, Mg Stearate, and avicel. PC2 shared some information mainly with FBP spectrum in the region 40–600 cm^{-1} **(fig 5.9)**.

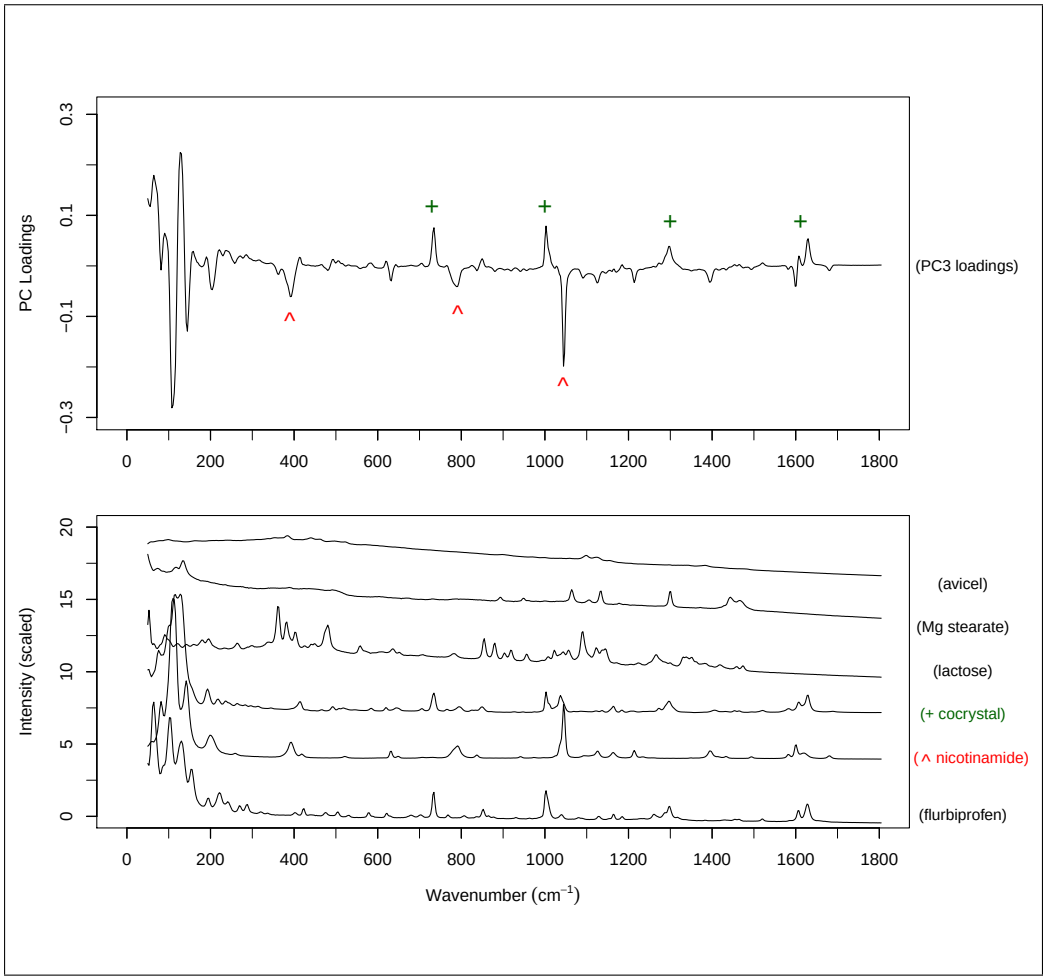

Figure C.5: The loadings of PC3 in comparison with referencing spectra. PC3 loadings is shown in (a) while Raman spectra of references are in (b). Spectra in (b) are arranged in a bottom-top manner starting from FBP, NCT (red), co-crystal (green), lactose, Mg Stearate, and avicel. Shared information between PC3 and references are indicated to by signs; green plus and red headarrow signs referred to co-crystal and NCT, respectively.

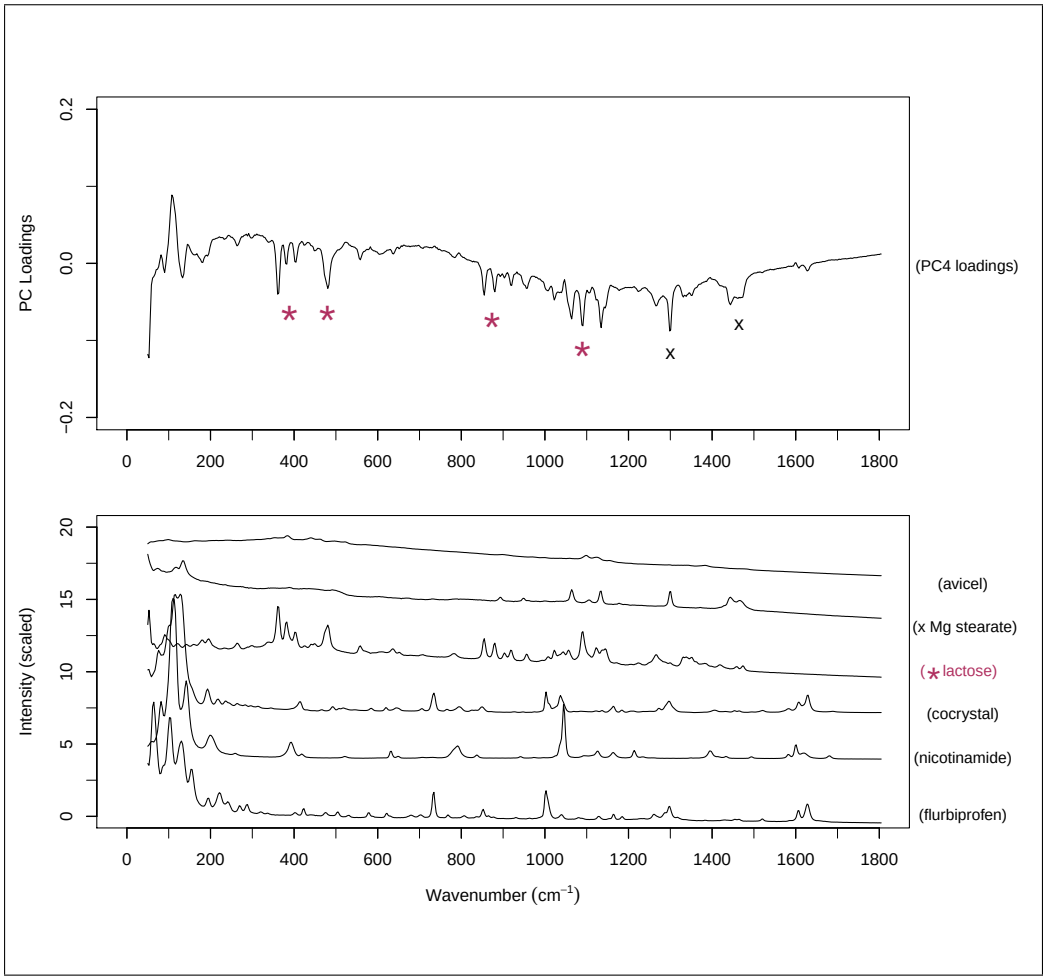

Figure C.6: The loadings of PC4 in comparison with referencing spectra. PC4 loadings is shown in (a) while Raman spectra of references are in (b). Spectra in (b) are arranged in a bottom-top manner starting from FBP, NCT, co-crystal, lactose (maroon), Mg Stearate (X), and avicel. Shared information between PC4 and references are indicated to by signs; maroon star and black X signs referred to lactose and Mg Stearate, respectively.

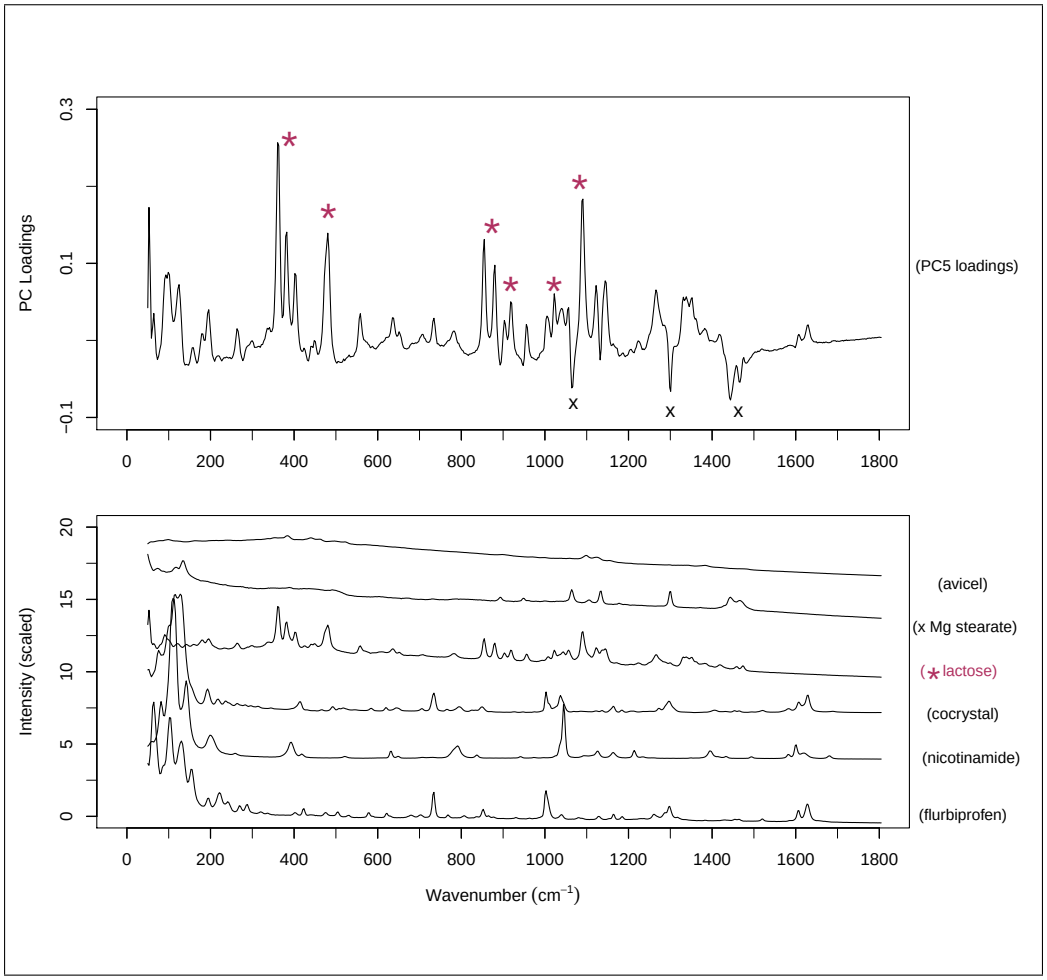

Figure C.7: The loadings of PC5 in comparison with referencing spectra. PC5 loadings is shown in (a) while Raman spectra of references are in (b). Spectra in (b) are arranged in a bottom-top manner starting from FBP, NCT, co-crystal, lactose (maroon), Mg Stearate (X), and avicel. Shared information between PC5 and references are indicated to by signs; maroon star and, black (X) signs referred to lactose and Mg Stearate, respectively.

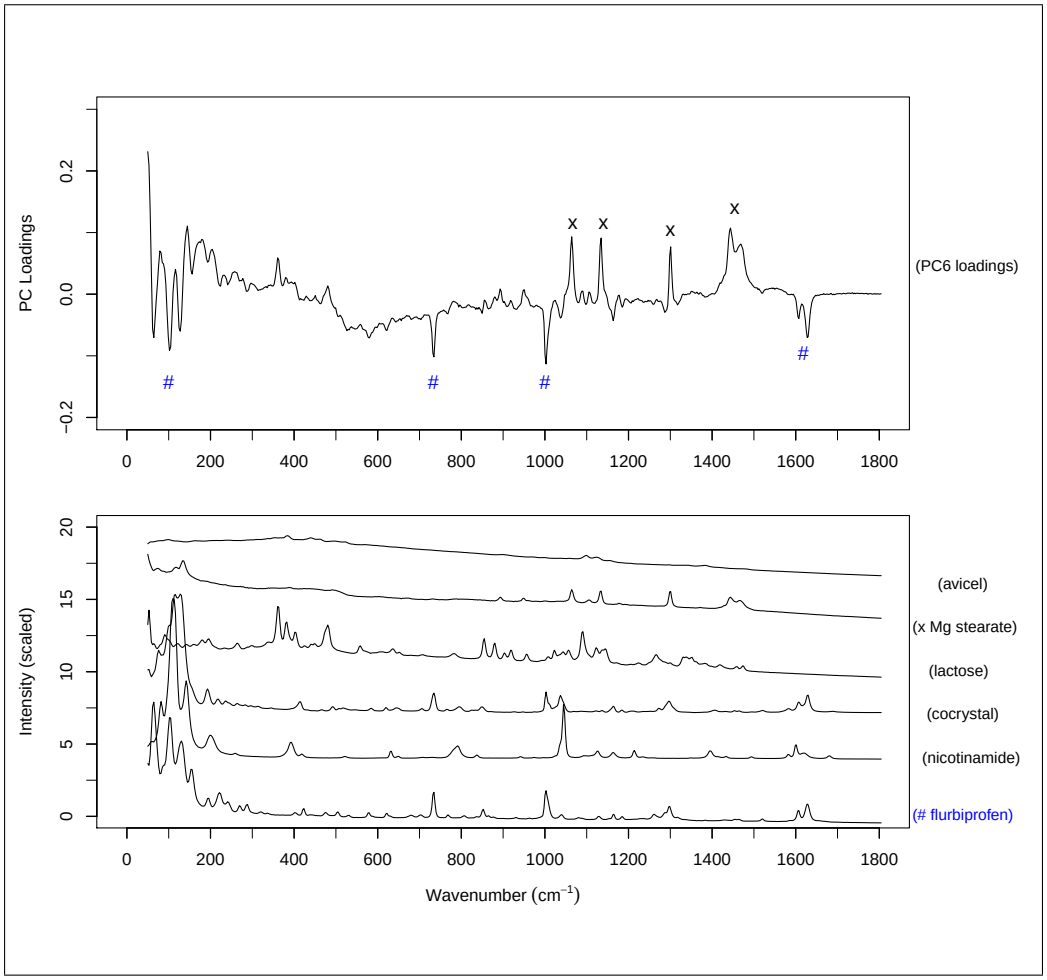

Figure C.8: The loadings of PC6 in comparison with referencing spectra. PC6 loadings is shown in (a) while Raman spectra of references are in (b). Spectra in (b) are arranged in a bottom-top manner starting from FBP (blue), NCT, co-crystal, and lactose, Mg Stearate, and avicel. Shared information between PC6 and references are indicated to by signs; blue (#) and black (X) signs referred to FBP and Mg Stearate, respectively.

The Effect of Baseline Correction on the 25% Co-crystal Tablets Data

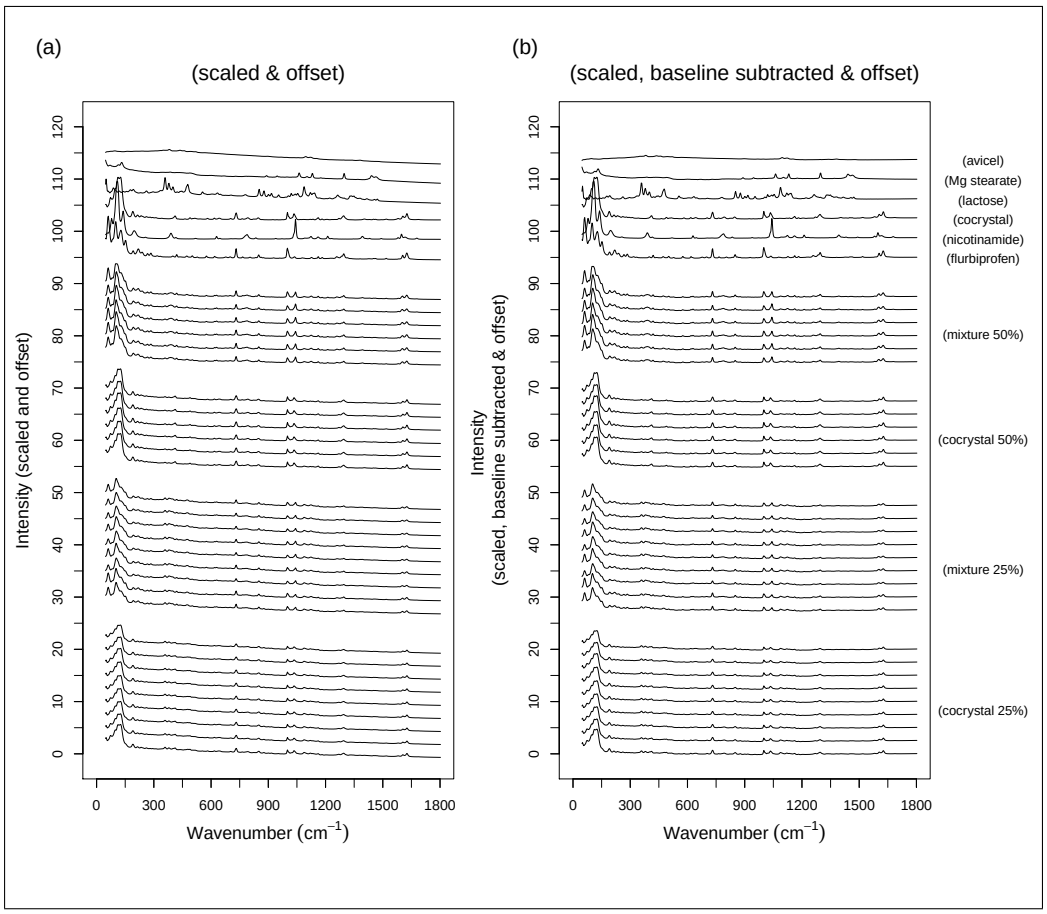

Figure C.9: TRS data comparison: un-treated *vs* treated. Data are intensity scaled and offset in (a) adding to such preprocessing, data are baseline subtracted in (b).

No major changes was observed when the background correction was done on datasets **(fig C.9 a, b)**. However, it was quite obvious, by looking at the spectra of the 25% co-crystal tablets **(fig C.10)**, to observe the considerably high background below all of the spectra. It is also noticeable that 8 of the spectra are very similar to each other (colour coded in black, **fig C.10**), apart from spectrum no.1 (colour coded in red, **fig C.10**) which was slightly different. This spectrum referred to the first 25% co-crystal tablet.* Such an observation justifies the inhomogeneous distribution of 25% co-crystal tablet datasets when subjected to chemometric (indicated to by an arrow in the scatter plot, **fig 5.7**). Consequently, the baseline correction was performed on the spectra of the 25% co-crystal tablet (**fig C.11**). **Fig C.11** shows an improvement in the degree of comparability between such spectra.

*all spectra were normalised to minimise as possible the effect of variable intensities on chemometric analysis.

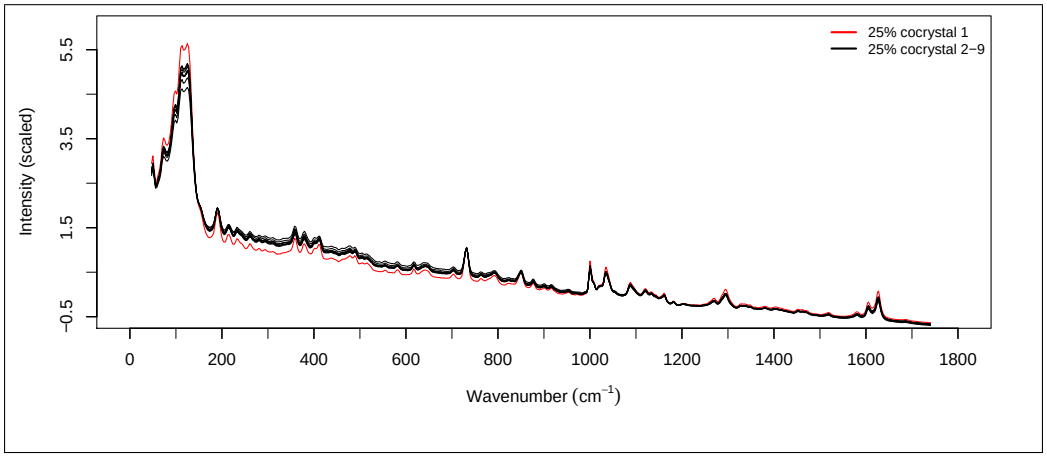

Figure C.10: TRS spectra of 25% co-crystal tablets scaled.

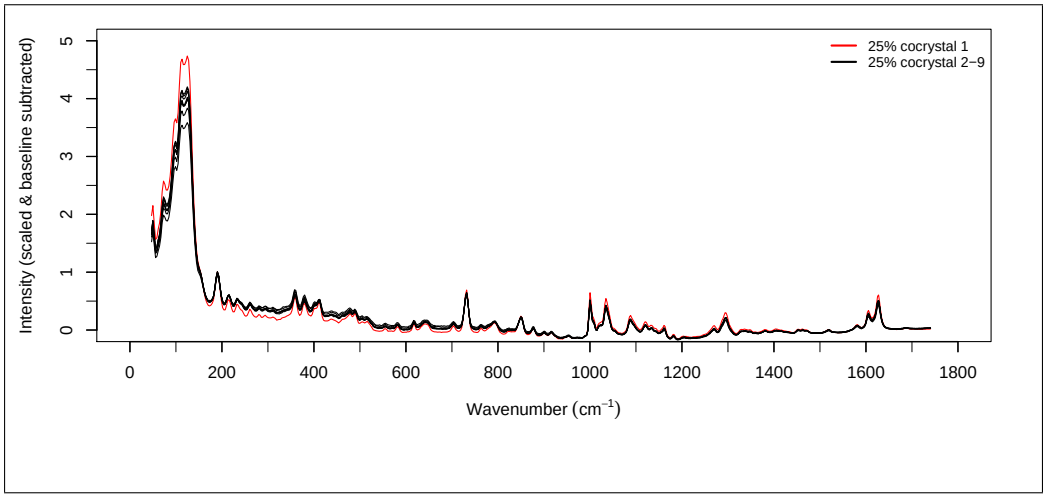

Figure C.11: TRS spectra of 25% co-crystal tablets scaled and baseline subtracted.

The Effect of Baseline Corrected Data on HAG Analysis

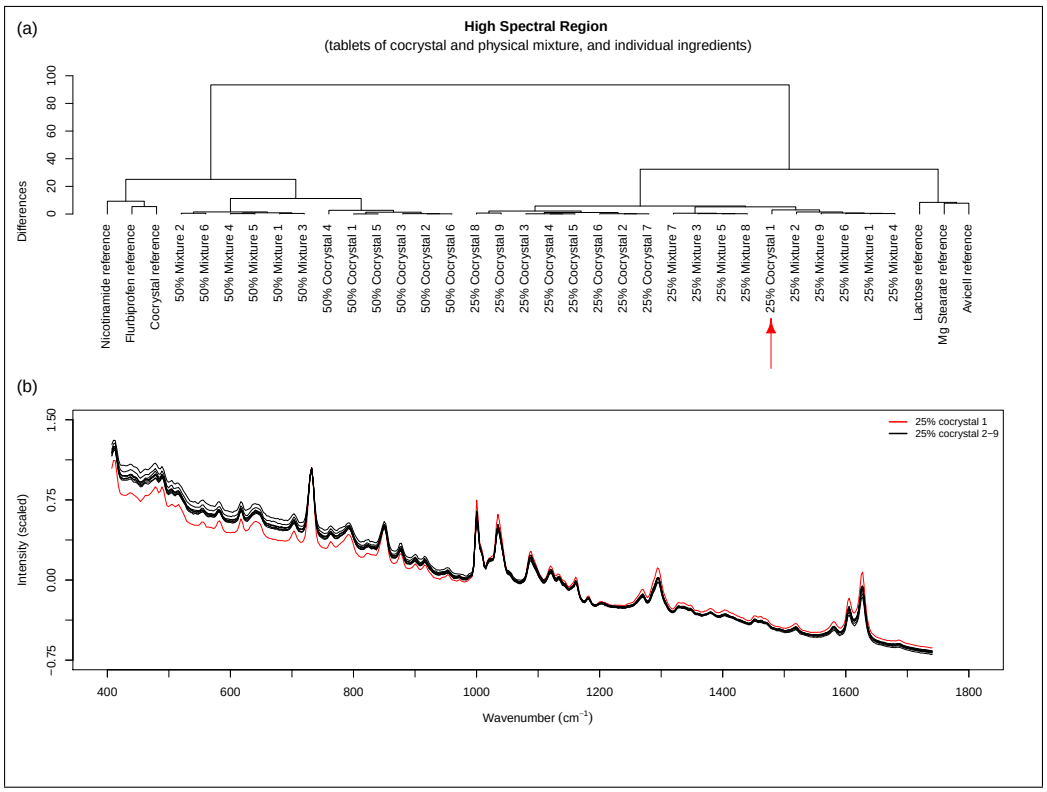

Figure C.12: Molecular spectral data, dendrogram (a) *vs* spectra of 25% co-crystal (b). Tablet number 1 from the 25% co-crystal content is referred to by red arrow in dendrogram plot (a) and its spectrum is also coloured in red (b). The rest of 25% co-crystal tablets data are in black.

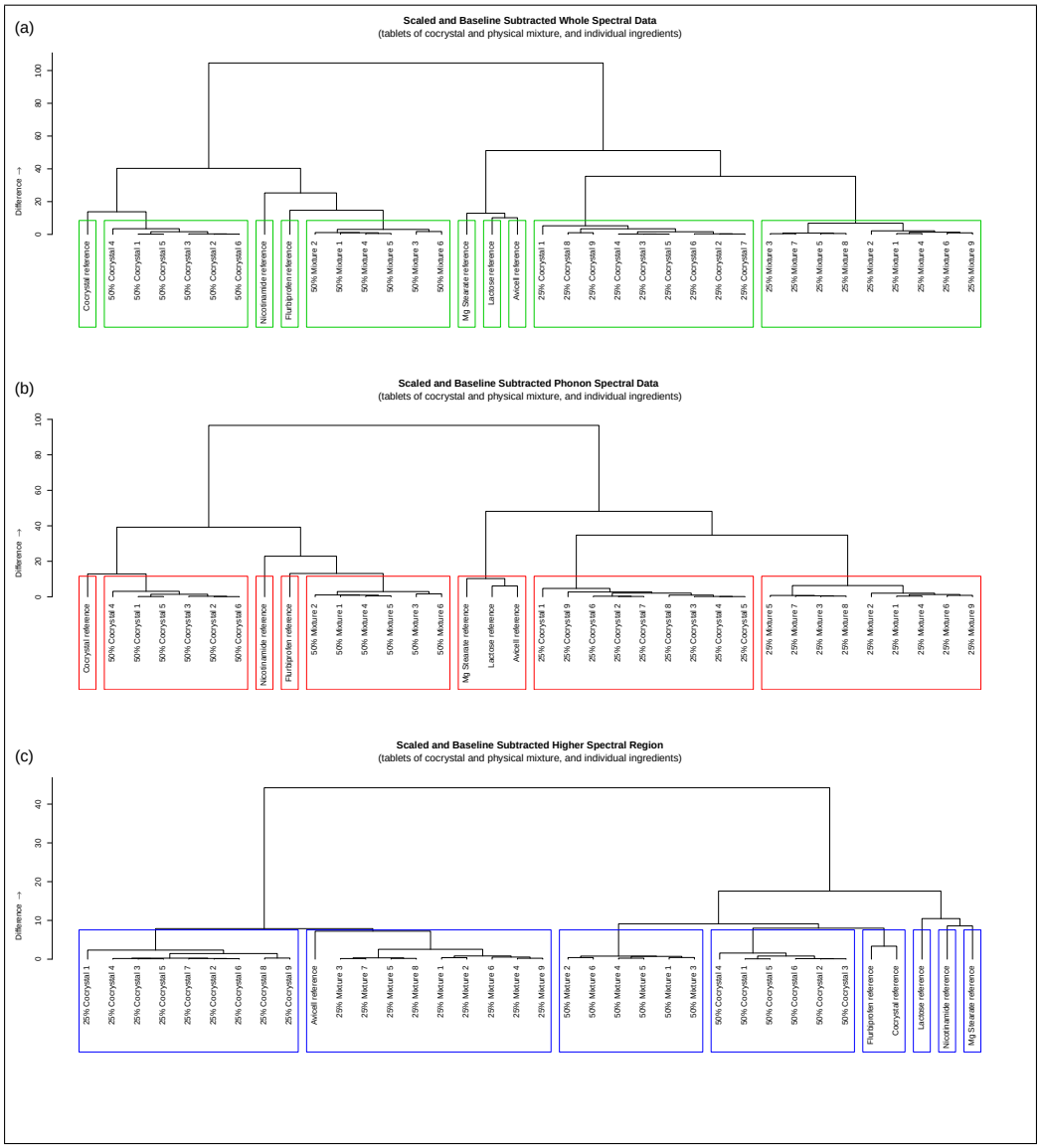

Figure C.13: HAC dendrograms in 3 Raman regions (treated). Dendrograms are calculated on intensity scaled and baseline corrected data from the entire wavenumber region (a), phonon region (b), and molecular region (b). The analysis was based on measuring the similarity between data using the Euclidean method. Data were then linked using ward agglomeration method. Similar linked clusters were framed in boxes and colour coded in green, red, and blue in the three panels, respectively.

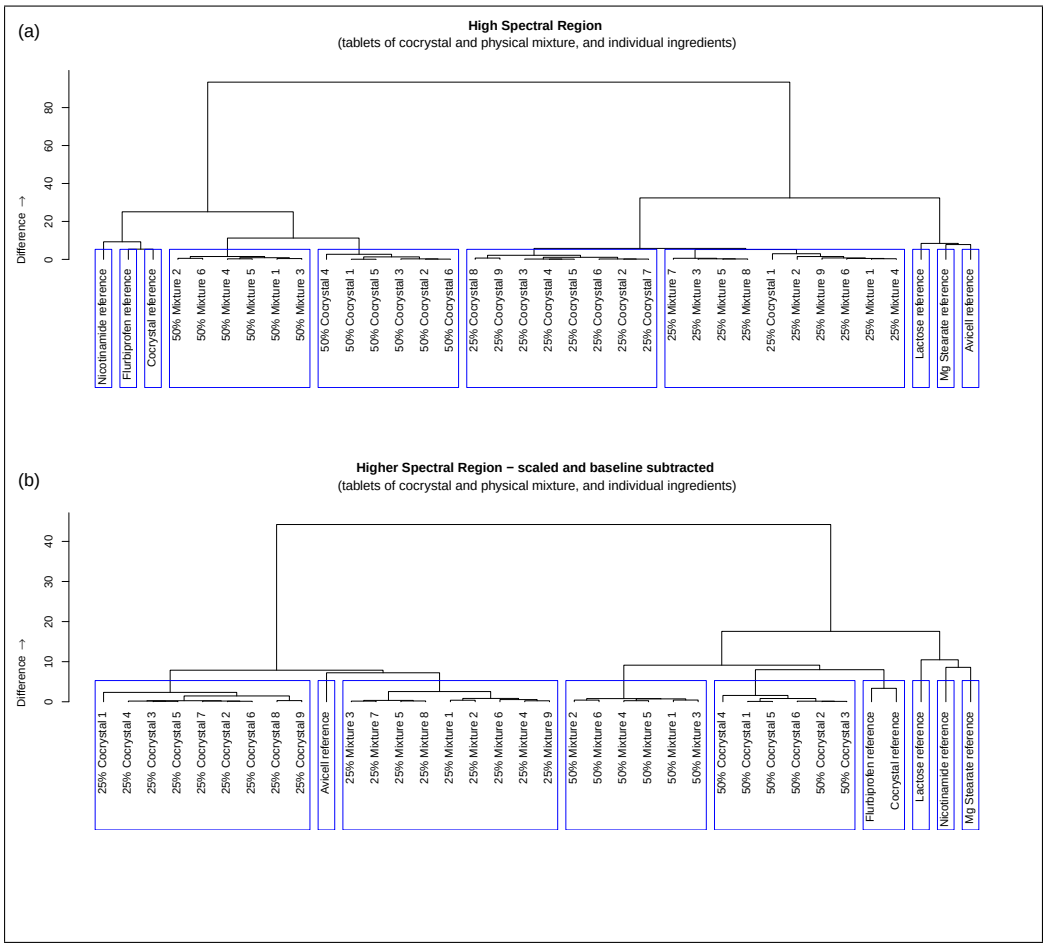

Figure C.14: Dendrogram comparison of Raman data scaled (a) *vs* scaled and baseline subtracted (b) in the molecular region (400-2000 cm^{-1}).

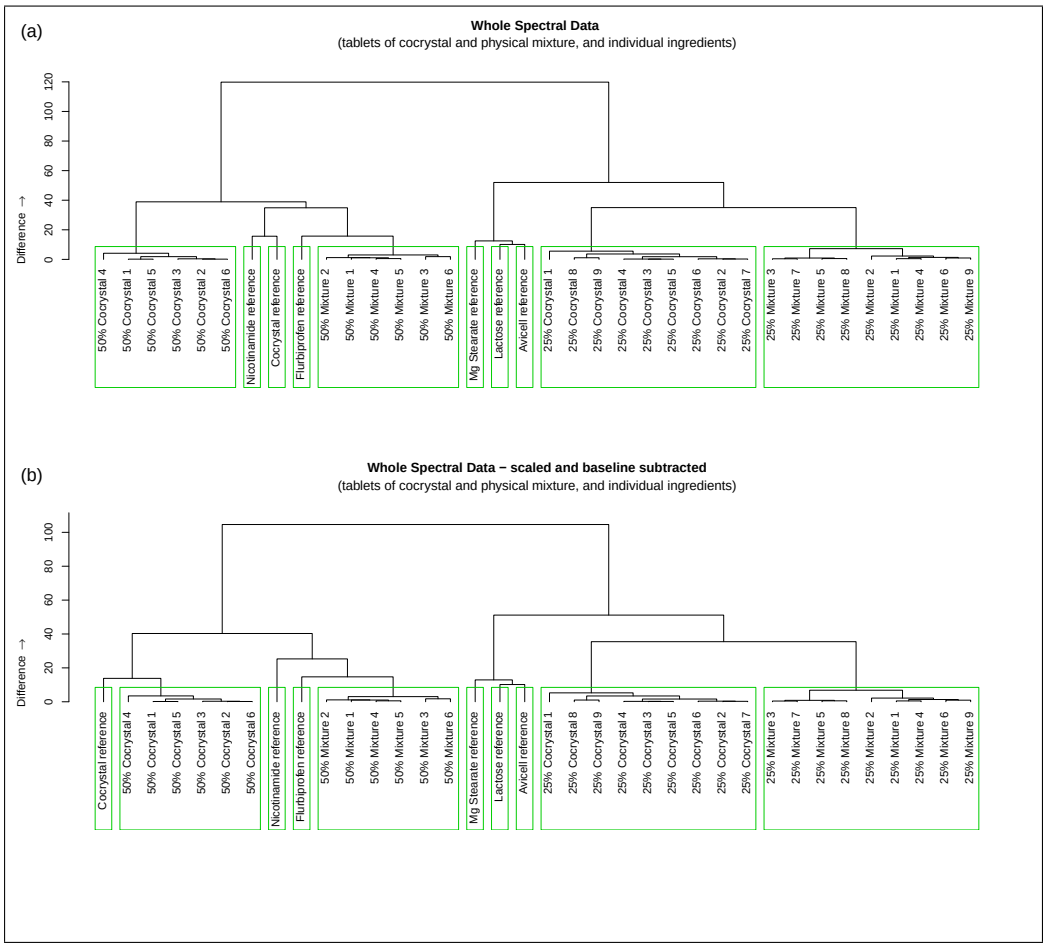

Figure C.15: Dendrogram comparison of Raman data scaled (a) *vs* scaled and baseline subtracted (b) in the region of 30-2000 cm^{-1}.

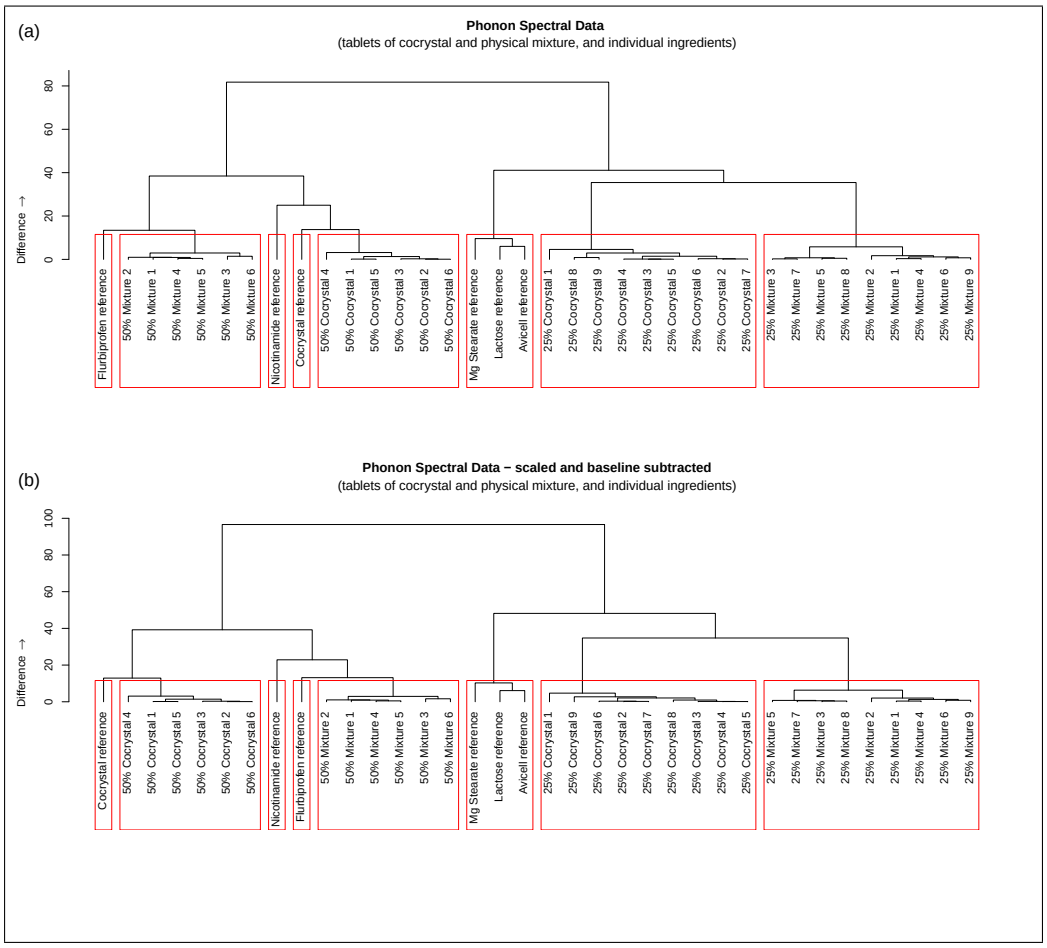

Figure C.16: Dendrogram comparison of Raman data scaled (a) *vs* scaled and baseline subtracted (b) in the phonon region (30-400 cm^{-1}).

Bibliography

[1] "Improving Global Health through Pharmaceutical Innovation". URL http://www.ifpma.org/fileadmin/content/Publication/IFPMA_Innovation_A5-PRweb.pdf.

[2] Munos B., "Lessons from 60 years of pharmaceutical innovation". *Nature Reviews Drug Discovery* 8(12), **2009**, pp. 959–968.

[3] "2011 profile pharmaceutical industry". URL http://www.phrma.org/track-pdf.php?q=/sites/default/files/159/phrma_profile_2011_final.pdf.

[4] "The market for contract analytical and development services". URL http://www.pharmsource.com/wp-content/uploads/2009/11/pharmsource_the_market_contract_dev_services.pdf.

[5] Giaccotto C., Santerre R., and Vernon J., "Drug prices and research and development investment behavior in the pharmaceutical industry". *Journal of Law & Economics* 48(1), **2005**, pp. 195–214.

[6] DiMasi J., Hansen R., and Grabowski H., "The price of innovation: new estimates of drug development costs". *Journal of Health Economics* 22(2), **2003**, pp. 151–185.

[7] Cockburn I.M., "Is the pharmaceutical industry in a productivity crisis?" In: Jaffe, AB and Lerner, J and Stern, S, ed., "Innovation Policy and the Economy 7", *Innovation Policy and the Economy*, vol. 7, **2006**, pp. 1–32.

[8] Pammolli F., Magazzini L., and Riccaboni M., "The productivity crisis in pharmaceutical R&D". *Nature Reviews Drug Discovery* 10(6), **2011**, pp. 428–438.

[9] "The pharmaceutical market outlook to 2015, implementing innovative, long-term strategies for sustainable future grow". URL http://www.globalbusinessinsights.com/content/rbhc0137t.pdf.

[10] "The innovative medicines initiative (imi) research agenda". URL http://www.imi.europa.eu/sites/default/files/uploads/documents/imi-gb-006v2-15022008-research-agenda_en.pdf.

[11] "Research and Development to Meet Health Needs in Developing Countries: Strengthening Global Financing and Coordination". URL http://www.who.int/phi/CEWG_Report_5_April_2012.pdf.

[12] Manallack D.T., "The acid-base profile of a contemporary set of drugs: implications for drug discovery". *SAR and QSAR in Environmental Research* 20(7-8), **2009**, pp. 611–655.

[13] Manallack D., "The pka distribution of drugs: Application to drug discovery". *Perspect Medicin Chem* 1, **2008**, pp. 25–38, URL http://ukpmc.ac.uk/abstract/MED/19812734.

[14] Leeson P.D., St-Gallay S.A., and Wenlock M.C., "Impact of ion class and time on oral drug molecular properties". *MedChemComm* 2(2), **2011**, pp. 91–105.

[15] Vieth M., Siegel M., Higgs R., Watson I., Robertson D., Savin K., Durst G., and Hipskind P., "Characteristic physical properties and structural fragments of marketed oral drugs". *Journal of Medicinal Chemistry* 47(1), **2004**, pp. 224–232.

[16] Hughes J.D., Blagg J., Price D.A., Bailey S., DeCrescenzo G.A., Devraj R.V., Ellsworth E., Fobian Y.M., Gibbs M.E., Gilles R.W., Greene N., Huang E., Krieger-Burke T., Loesel J., Wager T., Whiteley L., and Zhang Y., "Physiochemical drug properties associated with in vivo toxicological outcomes". *Bioorganic & Medicinal Chemistry Letters* 18(17), **2008**, pp. 4872 – 4875.

[17] Peters J.U., Schnider P., Mattei P., and Kansy M., "Pharmacological Promiscuity: Dependence on Compound Properties and Target Specificity in a Set of Recent Roche Compounds". *ChemMedChem* 4(4), **2009**, pp. 680–686.

[18] Davis A. and Riley R., "The impact of physical organic chemistry on the control of drug-like properties". In: Flower, DR, ed., "Drug Design: cutting Edge Approaches", No. 279 in Royal Society of Chemistry Special Publications, **2002**, pp. 106–123.

[19] Gleeson M.P., "Generation of a set of simple, interpretable admet rules of thumb". *Journal of Medicinal Chemistry* 51(4), **2008**, pp. 817–834.

[20] Smith D., Jones B., and Walker D., "Design of drugs involving the concepts and theories of drug metabolism and pharmacokinetics". *Medicinal Research Reviews* 16(3), **1996**, pp. 243–266.

[21] Berellini G., Springer C., Waters N.J., and Lombardo F., "In silico prediction of volume of distribution in human using linear and nonlinear models on a 669 compound data set". *Journal of Medicinal Chemistry* 52(14), **2009**, pp. 4488–4495.

[22] Karki S., Friščić T., Fábián L., Laity P.R., Day G.M., and Jones W., "Improving mechanical properties of crystalline solids by cocrystal formation: New compressible forms of paracetamol". *Advanced Materials* 21(38-39).

[23] Lu J. and Rohani S., "Preparation and characterization of theophylline−nicotinamide cocrystal". *Organic Process Research & Development* 13(6), **2009**, pp. 1269–1275.

[24] Trask A., Motherwell W., and Jones W., "Pharmaceutical cocrystallization: Engineering a remedy for caffeine hydration". *Crystal Growth & Design* 5(3), **2005**, pp. 1013–1021.

[25] Rager T. and Hilfiker R., "Stability Domains of Multi-Component Crystals in Ternary Phase Diagrams". *Zeitschrift Fur Physikalische Chemie-international Journal of Research In Physical Chemistry & Chemical Physics* 223(7), **2009**, pp. 793–813.

[26] Basavoju S., Bostrom D., and Velaga S.P., "Indomethacin-saccharin cocrystal: Design, synthesis and preliminary pharmaceutical characterization". *Pharmaceutical Research* 25(3), **2008**, pp. 530–541.

[27] Cherukuvada S., Babu N.J., and Nangia A., "Nitrofurantoin-p-aminobenzoic acid cocrystal: Hydration stability and dissolution rate studies". *Journal of Pharmaceutical Sciences* 100(8), **2011**, pp. 3233–3244.

[28] Rahman Z., Agarabi C., Zidan A.S., Khan S.R., and Khan M.A., "Physicomechanical and stability evaluation of carbamazepine cocrystal with nicotinamide". *AAPS PharmSciTech* 12(2), **2011**, pp. 693–704.

[29] Bolton O. and Matzger A.J., "Improved stability and smart-material functionality realized in an energetic cocrystal". *Angewandte Chemie International Edition* 50(38).

[30] Chieng N., Hubert M., Saville D., Rades T., and Aaltonen J., "Formation kinetics and stability of carbamazepine−nicotinamide cocrystals prepared

by mechanical activation". *Crystal Growth & Design* 9(5), **2009**, pp. 2377–2386.

[31] Babu N.J., Reddy L.S., Aitipamula S., and Nangia A., "Polymorphs and polymorphic cocrystals of temozolomide". *Chemistry - An Asian Journal* 3(7), **2008**, pp. 1122–1133.

[32] Shan N. and Zaworotko M.J., "The role of cocrystals in pharmaceutical science". *Drug Discovery Today* 13(9-10), **2008**, pp. 440–446.

[33] Feynman R.P., "There's plenty of room at the bottom", **1960**, URL http://resolver.caltech.edu/CaltechES:23.5.1960Bottom.

[34] Vishweshwar P., McMahon J., Bis J., and Zaworotko M., "Pharmaceutical co-crystal". *Journal of Pharmaceutical Sciences* 95(3), **2006**, pp. 499–516.

[35] Morissette S.L., Örn Almarsson, Peterson M.L., Remenar J.F., Read M.J., Lemmo A.V., Ellis S., Cima M.J., and Gardner C.R., "High-throughput crystallization: polymorphs, salts, co-crystals and solvates of pharmaceutical solids". *Advanced Drug Delivery Reviews* 56(3), **2004**, pp. 275 – 300.

[36] McCrone W., Polymorphism. In: Physics and Chemistry of the Organic Solid State, vol. 2. Interscience Publishers, London, **1965**.

[37] Wöhler and Liebig, "Untersuchungen über das radikal der benzoesäure". *Annalen der Pharmacie* 3(3), **1832**, pp. 249–282.

[38] Wöhler F., "Untersuchungen über das chinon". *Justus Liebigs Annalen der Chemie* 51(2), **1844**, pp. 145–163.

[39] Buck J.S. and Ide W.S., "Mixed bezoins. vi further examples of reversibility. the formation of addition compounds". *Journal of the American Chemical Society* 53(7), **1931**, pp. 2784–2787.

[40] Anderson J., "Structure of organic molecular compounds". *Nature* 140, **1937**, pp. 583–584.

[41] Etter M., Kress R., Bernstein J., and Cash D., "Solid-state chemistry and structures of a new class of mixed dyes. cyanine-oxonol". *Journal of the American Chemical Society* 106(23), **1984**, pp. 6921–6927.

[42] Kitaĭgorodskiĭ A.I., Mixed crystals. New York, **1984**.

[43] Desiraju G., "Supramolecular synthons in crystal engineering - a new organic synthesis". *Angewandte Chemie International Edition in English* 34(21), **1995**, pp. 2311–2327.

[44] Krautscheid H., "Frontiers in crystal engineering. herausgegeben von edward r. t. tiekink und jagadese vittal." *Angewandte Chemie* 119(14).

[45] Vishweshwar P., McMahon J.A., and Zaworotko M.J., Crystal Engineering of Pharmaceutical Co-crystals. John Wiley & Sons, Ltd.

[46] Friscic T., Childs S.L., Rizvi S.A.A., and Jones W., "The role of solvent in mechanochemical and sonochemical cocrystal formation: a solubility-based approach for predicting cocrystallisation outcome". *CrystEngComm* 11, **2009**, pp. 418–426.

[47] Blagden N., de Matas M., Gavan P.T., and York P., "Crystal engineering of active pharmaceutical ingredients to improve solubility and dissolution rates". *Advances Drug Delivery Reviews* 59(7), **2007**, pp. 617–630.

[48] Aakeroy C., "Crystal engineering: Strategies and architectures". *Acta Crystallographica Section B-Structural Science* 53(Part 4), **1997**, pp. 569–586.

[49] Etter M.C., "Hydrogen bonds as design elements in organic chemistry". *The Journal of Physical Chemistry* 95(12), **1991**, pp. 4601–4610.

[50] Peterson M.L., Collier E.A., Hickey M.B., Guzman H., and Almarsson O., Multi-Component Pharmaceutical Crystalline Phases: Engineering for Performance. John Wiley & Sons, Ltd.

[51] Almarsson O. and Zaworotko M., "Crystal engineering of the composition of pharmaceutical phases. do pharmaceutical co-crystals represent a new path to improved medicines?" *Chemical Communications* (17), **2004**, pp. 1889–1896.

[52] Desiraju G.R., "Crystal and co-crystal". *CrystEngComm* 5, **2003**, pp. 466–467.

[53] Dunitz J.D., "Crystal and co-crystal: a second opinion". *CrystEngComm* 5, **2003**, pp. 506–506.

[54] Aakeroy C.B. and Salmon D.J., "Building co-crystals with molecular sense and supramolecular sensibility". *CrystEngComm* 7, **2005**, pp. 439–448.

[55] Desiraju G., "Crystal engineering: Outlook and prospects". *Current Science* 81(8), **2001**, pp. 1038–1042.

[56] Blagden N., Berry D.J., Parkin A., Javed H., Ibrahim A., Gavan P.T., De Matos L.L., and Seaton C.C., "Current directions in co-crystal growth". *New J. Chem.* 32, **2008**, pp. 1659–1672.

[57] Childs S.L., Stahly G.P., and Park A., "The salt−cocrystal continuum: the influence of crystal structure on ionization state". *Molecular Pharmaceutics* 4(3), **2007**, pp. 323–338.

[58] Laurence C. and Berthelot M., "Observations on the strength of hydrogen bonding". *Perspectives in Drug Discovery and Design* 18, **2000**, pp. 39–60.

[59] Fox S.H. and Fox S.H., "Nicotinamide- ascorbic acid", **1947**, URL http://www.google.com/patents/US2433688.

[60] Zellner H. and Zellner H., "Anti-inflammatory therapy with purine molecular compounds", **1961**, URL http://www.google.com/patents/US2994640.

[61] Childs S.L.U., "Cocrystallization", **2008**, URL http://www.patentlens.net/patentlens/patent/US_7452555/en/.

[62] Brittain H.G., ed., Polymorphism in Pharmaceutical Solids. 1st ed., Informa Healthcare, **1999**.

[63] Karki S., Friscic T., Jones W., and Motherwell W.D.S., "Screening for pharmaceutical cocrystal hydrates via neat and liquid-assisted grinding". *Molecular Pharmaceuticals* 4(3), **2007**, pp. 347–354.

[64] Jayasankar A., Roy L., and Rodriguez-Hornedo N., "Transformation Pathways of Cocrystal Hydrates When Coformer Modulates Water Activity". *Journal of Pharmaceutical Sciences* 99(9), **2010**, pp. 3977–3985.

[65] Park A., Chyall L.J., Dunlap J., Schertz C., Jonaitis D., Stahly B.C., Bates S., Shipplett R., and Childs S., "New solid-state chemistry technologies to bring better drugs to market: knowledge-based decision making". *Expert opinion on drug discovery* 2(1), **2007**, pp. 145–154.

[66] K S. and Ito K., "Studies on molecular compounds of organic medicals .i. dissolution behavior of molecular compound of sulfanilamide and sulfathiazole" .

[67] Krantz J., Holbert J., Iwamoto H., and Carr C., "Sodium theophylline glycinate". *Journal of the American Pharmaceutical Association-Scientific edition* 36(8), **1947**, pp. 248–250.

[68] Jones W., Motherwell S., and Trask A.V., "Pharmaceutical cocrystals: An emerging approach to physical property enhancement". *MRS BULLETIN* 31(11), **2006**, pp. 875–879.

[69] Schultheiss N. and Newman A., "Pharmaceutical cocrystals and their physicochemical properties". *Crystal Growth & Design* 9(6), **2009**, pp. 2950–2967.

[70] Childs S., Chyall L., Dunlap J., Smolenskaya V., Stahly B., and Stahly G., "Crystal engineering approach to forming cocrystals of amine hydrochlorides with organic acids. molecular complexes of fluoxetine hydrochloride with benzoic, succinic, and fumaric acids". *Journal of the american chemical society* 126(41), **2004**, pp. 13 335–13 342.

[71] Hickey M.B., Peterson M.L., Scoppettuolo L.A., Morrisette S.L., Vetter A., Guzman H., Remenar J.F., Zhang Z., Tawa M.D., Haley S., Zaworotko M.J., and Almarsson O., "Performance comparison of a co-crystal of carbamazepine with marketed product". *European journal of pharmaceutics and biopharmaceutics* 67(1), **2007**, pp. 112–119.

[72] "WHO Medicines Strategy 2008-2013". URL http://www.who.int/medicines/publications/WHOMedicinesStrategydraft.pdf.

[73] Bondi Jr. R.W. and Drennen III J.K., "5 - Quality by Design and the importance of PAT in QbD". In: S. Ahuja and S. Scypinski, eds., "Handbook of Modern Pharmaceutical Analysis", *Separation Science and Technology*, vol. 10, Academic Press, **2011**, pp. 195 – 224.

[74] "About the center for drug evaluation and research - OPS process analytical technology - (PAT) initiative", **2009**.

[75] "Guidance for industry PAT — a framework for innovative pharmaceutical development, manufacturing, and quality assurance", **2004**, URL http://www.fda.gov/downloads/drugs/guidancecomplianceregulatoryinformation/guidances/ucm070305.pdf.

[76] Workman Jr. J., "Review of near-infrared and infrared spectroscopy". In: "The Handbook of Organic Compounds: Methods and interpretations", Burlington: Academic Press, **2001**, pp. 79 – 129.

[77] Roggo Y., Chalus P., Maurer L., Lema-Martinez C., Edmond A., and Jent N., "A review of near infrared spectroscopy and chemometrics in pharmaceutical technologies". *Journal of Pharmaceutical and Biomedical Analysis* 44(3), **2007**, pp. 683 – 700.

[78] Luypaert J., Massart D.L., and Vander Heyden Y., "Near-infrared spectroscopy applications in pharmaceutical analysis". *Talanta* 72(3), **2007**, pp. 865 – 883.

[79] Reich G., "Near-infrared spectroscopy and imaging: Basic principles and pharmaceutical applications". *Advanced Drug Delivery Reviews* 57(8), **2005**, pp. 1109 – 1143.

[80] Ramalingam S., Periandy S., Govindarajan M., and Mohan S., "FT-IR and FT-Raman vibrational spectra and molecular structure investigation of nicotinamide: A combined experimental and theoretical study". *Spectrochimica Acta Part A: Molecular and Biomolecular Spectroscopy* 75(5), **2010**, pp. 1552 – 1558.

[81] Alkhalil A., Nanubolu J.B., and Burley J.C., "Analysis of phase transitions in molecular solids: quantitative assessment of phonon-mode vs intramolecular spectral data". *Royal Society of Chemistry Advances* 2, **2012**, pp. 209–216.

[82] Izake E.L., "Forensic and homeland security applications of modern portable Raman spectroscopy". *Forensic Science International* 202(1–3), **2010**, pp. 1 – 8.

[83] Hargreaves M.D., Macleod N.A., Smith M.R., Andrews D., Hammond S.V., and Matousek P., "Characterisation of transmission Raman spectroscopy for rapid quantitative analysis of intact multi-component pharmaceutical capsules". *Journal of Pharmaceutical and Biomedical Analysis* 54(3), **2011**, pp. 463 – 468.

[84] McGoverin C.M., Hargreaves M.D., Matousek P., and Gordon K.C., "Pharmaceutical polymorphs quantified with transmission Raman spectroscopy". *Journal of Raman Spectroscopy* .

[85] Stephenson G.A., Forbes R.A., and Reutzel-Edens S.M., "Characterization of the solid state: quantitative issues". *Advanced Drug Delivery Reviews* 48(1), **2001**, pp. 67 – 90.

[86] Chow S., Chen M., Shi L., Chow A., and Sun C. .

[87] Henck J. and Kuhnert-Brandstatter M., "Demonstration of the terms enantiotropy and monotropy in polymorphism research exemplified by flurbiprofen". *Journal of Pharmaceutical Sciences* 88(1), **1999**, pp. 103–108.

[88] Varma M.M. and Pandi J.K., "Dissolution, solubility, xrd, and dsc studies on flurbiprofen-nicotinamide solid dispersions." *Drug Development & Industrial Pharmacy* 31(4/5), **2005**, pp. 417 – 423.

[89] Oberoi L.M., Alexander K.S., and Riga A.T., "Study of interaction between ibuprofen and nicotinamide using differential scanning calorimetry, spectroscopy, and microscopy and formulation of a fast-acting and possibly better ibuprofen suspension for osteoarthritis patients". *Journal of Pharmaceutical Sciences* 94(1).

[90] Frost D.V., "The effect of nicotinamide on the solubility of riboflavin in water". *Journal of the American Chemical Society* 69(5), **1947**, pp. 1064–1065.

[91] Berry D.J., Seaton C.C., Clegg W., Harrington R.W., Coles S.J., Horton P.N., Hursthouse M.B., Storey R., Jones W., Friscic T., and Blagden N., "Applying hot-stage microscopy to co-crystal screening: A study of nicotinamide with seven active pharmaceutical ingredients". *Crystal Growth & Design* 8(5), **2008**, pp. 1697–1712.

[92] Blagden N., Berry D.J., Parkin A., Javed H., Ibrahim A., Gavan P.T., De Matos L.L., and Seaton C.C., "Current directions in co-crystal growth". *New Journal of Chemistry* 32(10), **2008**, pp. 1659–1672.

[93] Childs S.L., Rodriguez-Hornedo N., Reddy L.S., Jayasankar A., Maheshwari C., McCausland L., Shipplett R., and Stahly B.C., "Screening strategies based on solubility and solution composition generate pharmaceutically acceptable cocrystals of carbamazepine". *CrystEngComm* 10, **2008**, pp. 856–864.

[94] Rager T. and Hilfiker R., "Cocrystal formation from solvent mixtures". *Crystal Growth & Design* 10(7), **2010**, pp. 3237–3241.

[95] Porter III W.W., Elie S.C., and Matzger A.J., "Polymorphism in carbamazepine cocrystals". *Crystal Growth & Design* 8(1), **2008**, pp. 14–16.

[96] Fleischman S., Kuduva S., McMahon J., Moulton B., Walsh R., Rodriguez-Hornedo N., and Zaworotko M., "Crystal engineering of the composition of pharmaceutical phases: Multiple-component crystalline solids involving carbamazepine". *Crystal Growth & Design* 3(6), **2003**, pp. 909–919.

[97] Tiekink E.R.T. and Vittal J., eds., Frontiers in Crystal Engineering. 1st ed., Wiley, **2006**.

[98] Zhang G.G.Z., Henry R.F., Borchardt T.B., and Lou X., "Efficient co-crystal screening using solution-mediated phase transformation". *Journal of Pharmaceutical Sciences* 96(5), **2007**, pp. 990–995.

[99] Trask A. and Jones W., "Crystal engineering of organic cocrystals by the solid-state grinding approach". In: Toda, F, ed., "Organic Solid State Reactions", *Topics in Current Chemistry*, vol. 254, **2005**, pp. 41–70.

[100] Ibrahim A.Y., Forbes R.T., and Blagden N., "Spontaneous crystal growth of co-crystals: the contribution of particle size reduction and convection mixing of the co-formers". *CrystEngComm* 13, **2011**, pp. 1141–1152.

[101] Chadha R., Saini A., Arora P., and Bhandari S., "Pharmaceutical Cocrystals: A Novel Approach for Oral Bioavailability Enhancement of Drugs". *Critical Reviews in Therapeutic Drug Carrier Systems* 29(3), **2012**, pp. 183–218.

[102] Friscic T., Fabian L., Burley J.C., Reid D.G., Duer M.J., and Jones W., "Exploring the relationship between cocrystal stability and symmetry: is wallach's rule applicable to multi-component solids?" *Chem. Commun.* , **2008**, pp. 1644–1646.

[103] Kaupp G., "Waste-free large-scale syntheses without auxiliaries for sustainable production omitting purifying workup". *CrystEngComm* 8, **2006**, pp. 794–804.

[104] Kaupp G., Schmeyers J., and Hangen U., "Anisotropic molecular movements in organic crystals by mechanical stress". *Journal of Physical Organic Chemistry* 15(6), **2002**, pp. 307–313.

[105] Kaupp G., "Mechanochemistry: the varied applications of mechanical bond-breaking". *CrystEngComm* 11, **2009**, pp. 388–403.

[106] Friscic T. and Jones W., "Recent advances in understanding the mechanism of cocrystal formation via grinding". *Crystal Growth & Design* 9(3), **2009**, pp. 1621–1637.

[107] Trask A.V., van de Streek J., Motherwell W.D.S., and Jones W., "Achieving polymorphic and stoichiometric diversity in cocrystal formation: importance of solid-state grinding, powder x-ray structure determination, and seeding". *Crystal Growth & Design* 5(6), **2005**, pp. 2233–2241.

[108] Linol J. and Coquerel G., "Simplification of the landscape under high energy milling of molecular solids exhibiting polymorphism." In: Lomello, M and Beauquis, S and Durand, C and Galez, PH, ed., "XXXV JEEP - 35th Conference on Phase Equilibria", **2009**.

[109] Raymond E. Davis Keith A. Lorimer M.A.W. and Rivers J.H., "Studies of phase relationships in cocrystal systems".

[110] McCrone W.C., "Fusion methods vs. kofler-mikro-methoden". *Microchimica Acta* 38, pp. 476–486.

[111] Kofler L.; Kofler A., Thermal Micromethods for the Study of Organic Compounds and Their Mixtures. Innsbrook: Wagner, **1952**, translated by McCrone, W. C.; McCrone Research Institute: Chicago, 1980.

[112] Bailey C.W., Bright J.R., and Jasper J.J., "A study of the binary system nicotinamide—ascorbic acid". *Journal of the American Chemical Society* 67(7), **1945**, pp. 1184–1186.

[113] "Melt Crystallization & wash column separation". URL http://www.isup2008.org/presentations/Conference_2/VanderSteen_RPM.pdf.

[114] Detoisien T., Arnoux M., Taulelle P., Colson D., Klein J.P., and Veesler S., "Thermal analysis: A further step in characterizing solid forms obtained by screening crystallization of an api". *International Journal of Pharmaceutics* 403(1–2), **2011**, pp. 29 – 36, URL http://www.sciencedirect.com/science/article/pii/S0378517310007787.

[115] Storey R.A. and Ymén I., eds., Solid State Characterization of Pharmaceuticals. Wiley-Blackwell, **2011**.

[116] Seefeldt K., Miller J., Alvarez-Nunez F., and Rodriguez-Hornedo N., "Crystallization pathways and kinetics of carbamazepine-nicotinamide cocrystals from the amorphous state by in situ thermomicroscopy, spectroscopy and calorimetry studies". *Journal of Pharmaceutical Sciences* 96(5), **2007**, pp. 1147–1158.

[117] Watson D.G., Pharmaceutical analysis: a textbook for pharmacy students and pharmaceutical chemists. Elsevier/Churchill Livingstone, **2005**.

[118] McCreery R.L., Raman Spectroscopy for Chemical Analysis. 1st ed., Wiley-Interscience, **2000**.

[119] Ekins S., Pharmaceutical Applications of Raman Spectroscopy. 1st ed., Wiley-Interscience, **2007**.

[120] Barnett N.W., Chemometrics in Analytical Spectroscopy. 2nd ed., RSC Analytical Spectroscopy Series, The Royal Society of Chemistry, **2004**.

[121] Jolliffe I.T., Principal component analysis. Springer, **2002**.

[122] Lu E., Rodriguez-Hornedo N., and Suryanarayanan R., "A rapid thermal method for cocrystal screening". *CrystEngComm* 10, **2008**, pp. 665–668.

[123] Morissette S.L., Örn, Peterson M.L., Remenar J.F., Read M.J., Lemmo A.V., Ellis S., Cima M.J., and Gardner C.R., "High-throughput crystallization: polymorphs, salts, co-crystals and solvates of pharmaceutical solids". *Advanced Drug Delivery Reviews* 56(3), **2004**, pp. 275 – 300.

[124] Chiarella R.A., Davey R.J., and Peterson M.L., "Making co-crystalsthe utility of ternary phase diagrams". *Crystal Growth & Design* 7(7), **2007**, pp. 1223–1226.

[125] McCrone W.C., Fusion Methods in Chemical Microscopy. Interscience Publishers, Inc., New York, **1957**.

[126] McCrone W.C., "Application of fusion methods in chemical microscopy". *Analytical Chemistry* 21(4), **1949**, pp. 436–441.

[127] McCrone W.C., "Chemical microscopy". *Analytical Chemistry* 26(1), **1954**, pp. 42–49.

[128] Lehmann O., Molecularphysik. Leipzig: Engelmann, **1888**.

[129] McNamara D.P., Childs S.L., Giordano J., Iarriccio A., Cassidy J., Shet M.S., Mannion R., O'Donnell E., and Park A., "Use of a glutaric acid cocrystal to improve oral bioavailability of a low solubility api". *Pharmaceutical Research* 23(8), **2006**, pp. 1888–1897.

[130] Kuhnert-Brandstätter M., "The status and future of chemical microscopy". *Pure and Applied Chemistry* 10, **1965**, pp. 133–144.

[131] Matousek P. and Morris M.D., eds., Emerging Raman Applications and Techniques in Biomedical and Pharmaceutical Fields. 1st ed., Springer, **2010**.

[132] Day G., Zeitler J., Jones W., Rades T., and Taday P., "Understanding the influence of polymorphism on phonon spectra: Lattice dynamics calculations and terahertz spectroscopy of carbamazepine". *Journal of Physical Chemistry B* 110(1), **2006**, pp. 447–456.

[133] Al-Dulaimi S., Aina A., and Burley J., "Rapid polymorph screening on milligram quantities of pharmaceutical material using phonon-mode Raman spectroscopy". *CrystEngComm* 12, **2010**, pp. 1038–1040.

[134] Brillante A., Bilotti I., Della Valle R.G., Venuti E., and Girlando A., "Probing polymorphs of organic semiconductors by lattice phonon Raman microscopy". *CrystEngComm* 10, **2008**, pp. 937–946.

[135] Batsanov A. S.; Howard J.A.K. *Private Communication* , **2005**, (cited in Cambridge Structural Database).

[136] Miwa Y., Mizuno T., Tsuchida K., Taga T., and Iwata Y., "Experimental charge density and electrostatic potential in nicotinamide". *Acta Crystallographica Section B* 55(1), **1999**, pp. 78–84.

[137] Hino T., Ford J., and Powell M., "Assessment of nicotinamide polymorphs by differential scanning calorimetry". *Thermochimica Acta* 374(1), **2001**, pp. 85–92.

[138] Clark D. and Sasic S., "Chemical images: Technical approaches and issues". *Cytometry Part A* 69A(8), **2006**, pp. 815–824.

[139] Grzesiak A.L. and Matzger A.J., "New form discovery for the analgesics flurbiprofen and sulindac facilitated by polymer-induced heteronucleation". *Journal of Pharmaceutical Sciences* 96(11), **2007**, pp. 2978–2986.

[140] Lacoulonche F., Chauvet A., and Masse J., "An investigation of flurbiprofen polymorphism by thermoanalytical and spectroscopic methods and a study of its interactions with poly-(ethylene glycol) 6000 by differential scanning calorimetry and modelling". *International Journal of Pharmaceutics* 153(2), **1997**, pp. 167–179.

[141] Babu N.J. and Nangia A., "Solubility advantage of amorphous drugs and pharmaceutical cocrystals". *Crystal Growth & Design* 11(7), **2011**, pp. 2662–2679.

[142] Bethune S.J., Schultheiss N., and Henck J.O., "Improving the poor aqueous solubility of nutraceutical compound pterostilbene through cocrystal formation". *Crystal Growth & Design* 11(7), **2011**, pp. 2817–2823.

[143] Sun C.C. and Hou H., "Improving mechanical properties of caffeine and methyl gallate crystals by cocrystallization". *Crystal Growth & Design* 8(5), **2008**, pp. 1575–1579.

[144] Yadav A.V., Shete A.S., Dabke A.P., Kulkarni P.V., and Sakhare S.S., "Co-Crystals: a novel approach to modify physicochemical properties of active pharmaceutical ingredients". *Indian Journal of Pharmaceutical Sciences* 71(4), **2009**.

[145] Trask A.V., Motherwell W.D.S., and Jones W., "Pharmaceutical cocrystallization: engineering a remedy for caffeine hydration". *Crystal Growth & Design* 5(3), **2005**, pp. 1013–1021.

[146] Issa N., Karamertzanis P.G., Welch G.W.A., and Price S.L., "Can the formation of pharmaceutical cocrystals be computationally predicted? i. comparison of lattice energies". *Crystal Growth & Design* 9(1), **2009**, pp. 442–453.

[147] Blagden N. and Davey R.J., "Polymorph selection: challenges for the future?" *Crystal Growth & Design* 3(6), **2003**, pp. 873–885.

[148] Schultheiss N., Bethune S., and Henck J.O., "Nutraceutical cocrystals: utilizing pterostilbene as a cocrystal former". *Crystengcomm* 12(8), **2010**, pp. 2436–2442.

[149] Cruz-Cabeza A.J., Day G.M., and Jones W., "Towards Prediction of Stoichiometry in Crystalline Multicomponent Complexes". *Chemistry-A European Journal* 14(29), **2008**, pp. 8830–8836.

[150] Peterson M.L., Hickey M.B., Zaworotko M.J., and Almarsson O., "Expanding the scope of crystal form evaluation in pharmaceutical science". *Journal of Pharmacy and Pharmaceutical Sciences* 9(3), **2006**, pp. 317–326.

[151] Sarma B., Chen J., Hsi H.Y., and Myerson A., "Solid forms of pharmaceuticals: Polymorphs, salts and cocrystals". *Korean Journal of Chemical Engineering* 28, pp. 315–322.

[152] "A novel multifunctional pharmaceutical excipient: Modification of the permeability of starch by processing with magnesium silicate". *International Journal of Pharmaceutics* 411(1–2), **2011**, pp. 18 – 26.

[153] Trask A.V., "An overview of pharmaceutical cocrystals as intellectual property". *Molecular Pharmaceutics* 4(3), **2007**, pp. 301–309.

[154] "An overview of recent studies on the analysis of pharmaceutical polymorphs". *Journal of Pharmaceutical and Biomedical Analysis* 55(4), **2011**, pp. 618 – 644.

[155] Desiraju G.R., "Polymorphism: The same and not quite the same". *Crystal Growth & Design* 8(1), **2008**, pp. 3–5.

[156] Aitipamula S., Chow P.S., and Tan R.B.H., "Polymorphs and solvates of a cocrystal involving an analgesic drug, ethenzamide, and 3,5-dinitrobenzoic acid". *Crystal Growth & Design* 10(5), **2010**, pp. 2229–2238.

[157] Stahly G.P., "Diversity in single- and multiple-component crystals. the search for and prevalence of polymorphs and cocrystals". *Crystal Growth & Design* 7(6), **2007**, pp. 1007–1026.

[158] Ueto T., Takata N., Muroyama N., Nedu A., Sasaki A., Tanida S., and Terada K., "Polymorphs and a hydrate of furosemide-nicotinamide 1:1 cocrystal". *Crystal Growth & Design* 12(1), **2012**, pp. 485–494.

[159] Strobridge F.C., Judas N., and Friscic T., "A stepwise mechanism and the role of water in the liquid-assisted grinding synthesis of metal-organic materials". *CrystEngComm* 12, **2010**, pp. 2409–2418.

[160] Jayasankar A., Somwangthanaroj A., Shao Z., and Rodríguez-Hornedo N., "Cocrystal formation during cogrinding and storage is mediated by amorphous phase". *Pharmaceutical Research* .

[161] Halasz I., Rubcic M., Uzarevic K., Dilovic I., and Mestrovic E., "The cocrystal of 4-oxopimelic acid and 4,4[prime or minute]-bipyridine: polymorphism and solid-state transformations". *New J. Chem.* 35, **2011**, pp. 24–27.

[162] Cheung E.Y., Kitchin S.J., Harris K.D.M., Imai Y., Tajima N., and Kuroda R., "Direct structure determination of a multicomponent molecular crystal prepared by a solid-state grinding procedure". *Journal of the American Chemical Society* 125(48), **2003**, pp. 14 658–14 659.

[163] Aitipamula S., Chow P.S., and Tan R.B.H., "Dimorphs of a 1 : 1 cocrystal of ethenzamide and saccharin: solid-state grinding methods result in metastable polymorph". *CrystEngComm* 11, **2009**, pp. 889–895.

[164] Jayasankar A., Somwangthanaroj A., Shao Z.J., and Rodriguez-Hornedo N., "Cocrystal formation during cogrinding and storage is mediated by amorphous phase". *Pharmaceutical Research* 23(10), **2006**, pp. 2381–2392.

[165] Buanz A.B.M., Parkinson G.N., and Gaisford S., "Characterization of carbamazepine-nicatinamide cocrystal polymorphs with rapid heating dsc and xrpd". *Crystal Growth & Design* 11(4), **2011**, pp. 1177–1181.

[166] Friscic T. and MacGillivray L.R., "Engineering cocrystal and polymorph architecture via pseudoseeding". *Chem. Commun.* , **2009**, pp. 773–775.

[167] Sheldrick G.M., "A short history of *SHELX*". *Acta Crystallographica Section A* 64(1), **2008**, pp. 112–122.

[168] Alkhalil A., Nanubolu J.B., Roberts C.J., Aylott J.W., and Burley J.C., "Confocal Raman microscope mapping of a kofler melt" .

[169] Bondw A.D., The Role of the Cambridge Structural Database in Crystal Engineering. John Wiley & Sons, Ltd.

[170] Tiekink E.R.T., Crystal Engineering. John Wiley & Sons, Ltd.

[171] Threlfall T., "Structural and thermodynamic explanations of ostwald's rule". *Organic Process Research & Development* 7(6), **2003**, pp. 1017–1027.

[172] Burley J.C., "A new method for rapid, reliable and effective polymorph screening". *Journal of Pharmacy and pharmacology* 59(1), **2007**.

[173] Zimmermann H.W., "Ostwald's rule and the principle of the shortest way". *Zeitschrift Fur Physikalische Chemie-International Journal of Research in Physical Chemistry & Chemical Physics* 224(6), **2010**, pp. 929–934.

[174] Ostwald W., "Studien über die bildung und umwandlung fester körper. 1. abhandlung: Übersättigung und Überkaltung". *Zeitschrift für Physikalische Chemie* 22, **1897**, p. 289–330.

[175] Brillante A., Della Valle R., Farina L., Girlando A., Masino M., and Venuti E., "Raman phonon spectra of pentacene polymorphs". *Chemical Physics Letters* 357(1-2), **2002**, pp. 32–36.

[176] Gibson M., Pharmaceutical Preformulation and Formulation: A Practical Guide from Candidate Drug Selection to Commercial Dosage Form. Interpharm Press, **2001**.

[177] Kar A., Pharmaceutical Drug Analysis. New Age International, **2007**.

[178] Matousek P., Thorley F., Chen P., Hargreaves M., Tombling C., Loeffen P., Bloomfield M., and Andrews D., "Emerging Raman techniques for rapid noninvasive characterization of pharmaceutical samples and containers". *Spectroscopy* 26(3), **2011**, pp. 44–51.

[179] Beer T.D., Bodson C., Dejaegher B., Walczak B., Vercruysse P., Burggraeve A., Lemos A., Delattre L., Heyden Y.V., Remon J., Vervaet C., and Baeyens W., "Raman spectroscopy as a process analytical technology (pat) tool for the in-line monitoring and understanding of a powder blending process". *Journal of Pharmaceutical and Biomedical Analysis* 48(3), **2008**, pp. 772 – 779.

[180] Beer T.D., Burggraeve A., Fonteyne M., Saerens L., Remon J., and Vervaet C., "Near infrared and Raman spectroscopy for the in-process monitoring of pharmaceutical production processes". *International Journal of Pharmaceutics* 417(1–2), **2011**, pp. 32 – 47.

[181] De Beer T.R.M., Baeyens W.R.G., Ouyang J., Vervaet C., and Remon J.P., "Raman spectroscopy as a process analytical technology tool for the understanding and the quantitative in-line monitoring of the homogenization process of a pharmaceutical suspension". *Analyst* 131, **2006**, pp. 1137–1144.

[182] Eliasson C., Macleod N., and Matousek P., "Non-invasive detection of powders concealed within diffusely scattering plastic containers". *Vibrational Spectroscopy* 48(1), **2008**, pp. 8 – 11.

[183] Elbagerma M.A., Edwards H.G.M., Munshi T., Hargreaves M.D., Matousek P., and Scowen I.J., "Characterization of new cocrystals by Raman spectroscopy, powder X-ray diffraction, differential scanning calorimetry, and transmission Raman spectroscopy". *Crystal Growth & Design* 10(5), **2010**, pp. 2360–2371.

[184] Schrader B., Infrared and Raman Spectroscopy. John Wiley & Sons, **2008**.

[185] Schrader B. and G. B., "Die intensitat des Ramanspektrums polykristalliner substanzen .I. strahlungsbilanz von substanz und probenanordnung". *Zeitschrift fur Analytische Chemie Fresenius* , **1967**, pp. 225–230.

[186] Aina A., Hargreaves M.D., Matousek P., and Burley J.C., "Transmission Raman spectroscopy as a tool for quantifying polymorphic content of pharmaceutical formulations". *Analyst* 135, **2010**, pp. 2328–2333.

[187] Eliasson C., Macleod N.A., Jayes L.C., Clarke F.C., Hammond S.V., Smith M.R., and Matousek P., "Non-invasive quantitative assessment of the content of pharmaceutical capsules using transmission Raman spectroscopy". *Journal of Pharmaceutical and Biomedical Analysis* 47(2), **2008**, pp. 221 – 229.

[188] Buckley K. and Matousek P., "Recent advances in the application of transmission Raman spectroscopy to pharmaceutical analysis". *Journal of Pharmaceutical and Biomedical Analysis* 55(4), **2011**, pp. 645 – 652.

[189] Burley J.C., Alkhalil A., Bloomfield M., and Matousek P., "Transmission Raman spectroscopy for quality control in model cocrystal tablets". *Analyst* 137, **2012**, pp. 3052–3057.

[190] Matousek P. and Parker A.W., "Non-invasive probing of pharmaceutical capsules using transmission Raman spectroscopy". *Journal of Raman Spectroscopy* 38(5), **2007**, pp. 563–567, URL http://dx.doi.org/10.1002/jrs.1688.

[191] Matousek P. and Parker A.W., "Bulk Raman analysis of pharmaceutical tablets". *Applied Spectroscopy* 60(12), **2006**, pp. 1353–1357.

[192] "Database of select committee on GRAS substances (SCOGS) reviews". URL http://www.accessdata.fda.gov/scripts/fcn/fcnDetailNavigation.cfm?rpt=scogsListing&id=221.

[193] Arora K.K., Tayade N.G., and Suryanarayanan R., "Unintended water mediated cocrystal formation in carbamazepine and aspirin tablets". *Molecular Pharmaceutics* 8(3), **2011**, pp. 982–989.

[194] Gunsel W. and Lachman L., "Comparative evaluation of tablet formulations prepared from conventionally processed and spray-dried lactose". *Journal of Pharmaceutical Sciences* 52(2), **1963**, pp. 178–&.

[195] Bastos M.d.O., Friedrich R.B., and Beck R.C.R., "Effects of filler-binders and lubricants on physicochemical properties of tablets obtained by direct compression: A 2(2) factorial design". *Latin American Journal of Pharmacy* 27(4), **2008**, pp. 578–583.

[196] Jr. M.J.M. and Çelik M., "The effects of lubrication on the compaction and post-compaction properties of directly compressible maltodextrins". *International Journal of Pharmaceutics* 144(1), **1996**, pp. 1 – 9.

[197] Sagdinc S. and Pir H., "Spectroscopic and DFT studies of flurbiprofen as dimer and its Cu(ii) and Hg(ii) complexes". *Spectrochimica Acta Part A: Molecular and Biomolecular Spectroscopy* 73(1), **2009**, pp. 181 – 194.

[198] Pelletier M.J., Analytical Applications of Raman Spectroscopy. 1st ed., Blackwell Publishing, **1999**.